














Lea Lee first author 1974-1995 Pungor Hlady Herron Voss Jhon Shim Kopecek Kopeckova

ck View Arrange By Action Share Edit Tags

me	^	Date Modified	Size	Kind
 Lea 1992 AFM Proteins U mica pungor hlady herron voss.pdf		Oct 12, 2006, 7:07 PM	2.5 MB	PDF D
 Lea 1993 AFM Steric Force ACS Colloid Bk hlady.pdf		Oct 12, 2006, 7:13 PM	2.8 MB	PDF D
 Lea 1994 AFM PEG SiN hlady.pdf		Oct 12, 2006, 7:21 PM	2.2 MB	PDF D
 Lee H B 1974 Water in Gels II. Proton P...mer Preprints ACS Jhon-compressed.pdf		Nov 14, 2018, 1:44 PM	627 KB	PDF D
 Lee HB 1972 Polymer Preprints Radiation Graft HEMA Shim .pdf		Nov 12, 2018, 8:33 AM	998 KB	PDF D
 Lee HB 1975 Water in Gels I Jhon.pdf		Oct 15, 2006, 4:06 PM	1.1 MB	PDF D
 Lee JH 1988 Polymer Surface Dynamics Bk block surfactants.pdf		Oct 12, 2006, 9:13 PM	2.2 MB	PDF D
 Lee JH 1989 PEO Surfactants Protein Resist kopecek.pdf		Feb 21, 2015, 8:56 AM	2.9 MB	PDF D
 Lee JH 1989 Surfaces I Korean.pdf		Oct 15, 2006, 10:36 AM	1.8 MB	PDF D
 Lee JH 1989 Surfaces II Korean.pdf		Oct 15, 2006, 10:52 AM	1.4 MB	PDF D
 Lee JH 1990 Surface Supersurfactants kopeckova kopecek.pdf		Oct 12, 2006, 9:33 PM	3 MB	PDF D
 Lee JH 1995 PEO Blood Review h b lee.pdf		Oct 12, 2006, 8:53 PM	6.2 MB	PDF D
 Lee Jin Ho 1987 PEO Block Surfactants Protein-Resistant PMSE ACS Kopecek.pdf		Nov 14, 2018, 1:36 PM	492 KB	PDF D

## Manipulation of Proteins on Mica by Atomic Force Microscopy

A. S. Lea,<sup>†</sup> A. Pungor,<sup>†</sup> V. Hlady,<sup>†,‡</sup> J. D. Andrade,<sup>\*,†</sup> J. N. Herron,<sup>§</sup> and E. W. Voss, Jr.<sup>||</sup>

Departments of Bioengineering and of Pharmaceutics, University of Utah, Salt Lake City, Utah 84112, and Department of Microbiology, University of Illinois, Urbana, Illinois 61801

Received March 1, 1991. In Final Form: June 25, 1991

The atomic force microscope was used to image adsorption of a monoclonal IgM on mica in real time. Under the smallest possible force we could achieve ( $<4$  nN), the cantilever tip behaved as a molecular broom and was observed to orient protein aggregates in strands oriented perpendicularly to the facet of the cantilever tip. Rotating the scan direction preserved the orientational relationship, as seen by the formation of rotated strands. When the applied force was increased, the distance between the strands increased, indicating the amount of protein that can be swept depends on the applied force. The effect of scanning increased the apparent surface coverage of IgM. Manipulation of a deposited fibrinogen layer with a 4-nN repulsive force was observed only after tens of minutes, but not to the extent that strands formed, indicating a greater adhesion between the fibrinogen and mica than between IgM and mica. With an applied repulsive force of 30 nN, fibrinogen strands formed and the protein was manipulated to produce the block letter U. At a much higher repulsive force, the entire scanning area was swept clean.

### Introduction

The ability of the atomic force microscope (AFM) to image nonconductors in both air and aqueous environments has enabled it to be used as a research instrument for the biological community. Already, it has been used to observe nucleic acids,<sup>1-4</sup> lipid assemblies,<sup>2-4</sup> proteins,<sup>4-10</sup> and even entire cell surfaces.<sup>10-13</sup>

The amount of AFM work in the biological area is currently small, but expanding rapidly. Unfortunately, most of the published studies merely report the observation of various structures on surfaces and do not address the issue of perturbation of the observed system by the AFM cantilever tip.

In a previous study, we had observed the adsorption of a monoclonal IgG from solution onto mica.<sup>6</sup> We hypothesized that the IgG ridges were a consequence of the protein being swept across the surface by the scanning probe. Since then, we have been focusing our efforts on observing real time adsorption of proteins in a system in which perturbation by the scanning probe is minimal. We found, however, protein manipulation so prevalent that an unperturbed observation of the adsorption process would not be easily attainable. We decided to investigate how manipulation by the cantilever tip can be used to determine interactions between the tip and protein and between protein and substrate. The results of this study demonstrate that the cantilever not only has a profound effect on adsorption processes, but also may be used to manipulate molecules into desired patterns or shapes.

To study the effects of scanning the cantilever tip on protein adsorption processes, we followed the adsorption of an IgM on mica. The rationale for using IgM in these experiments was that, due to the limited resolving power of the AFM, the protein needed to be large and have a distinct molecular shape in order to observe individual proteins. IgM has a molecular weight of 900 kDa and its tertiary structure when viewed by electron microscopy resembles a five-pointed star.<sup>14</sup> The IgM is a mouse monoclonal antifluorescyl antibody (clone 18-2-3).<sup>15-17</sup> This particular IgM is a cryoglobulin that disaggregates, producing individual pentamers, when fluorescein is bound or when the ionic strength exceeds 0.3 M. All IgM work in this study is with the fluorescein-bound, disaggregated form. The association constant for the antigen is  $(2-3) \times 10^{10} \text{ M}^{-1}$ , which is unusually large for an IgM.

### Experimental Section

The atomic force microscope used is a commercial one (Digital Instruments) that incorporates optical beam deflection<sup>18</sup> for sensing cantilever motion. The cantilevers (Park Scientific), with

\* To whom correspondence should be addressed.

<sup>†</sup> Department of Bioengineering, University of Utah.

<sup>‡</sup> On the leave of absence from "Ruder Boskovic" Institute, Zagreb, Croatia, Yugoslavia.

<sup>§</sup> Department of Pharmaceutics, University of Utah.

<sup>||</sup> University of Illinois.

(1) Lindsay, S. M.; Nagahara, L. A.; Thundat, T.; Knipping, U.; Rill, R. L.; Drake, B.; Prater, C. B.; Weisenhorn, A. L.; Gould, S. A. C.; Hansma, P. K. *J. Biomol. Struct. Dyn.* 1989, 7, 279.

(2) Weisenhorn, A. L.; Hansma, H. G.; Gaub, H. E.; Sinsheimer, R. L.; Gould, S. A. C.; Hansma, P. K. *Proceedings of STM '90*, Baltimore, MD.

(3) Hansma, P. K.; Elings, V. B.; Marti, O.; Bracker, C. E. *Science* 1988, 242, 209.

(4) Egger, M.; Ohnesorge, F.; Weisenhorn, A. L.; Heyn, S. P.; Drake, B.; Prater, C. B.; Gould, S. A. C.; Hansma, P. K.; Gaub, H. E. *J. Struct. Biol.* 1990, 103, 89.

(5) Drake, B.; Prater, C. B.; Weisenhorn, A. L.; Gould, S. A. C.; Albrecht, T. R.; Quate, C. F.; Cannell, D. S.; Hansma, H. G.; Hansma, P. K. *Science* 1989, 243, 1586.

(6) Lin, J. N.; Drake, B.; Lea, A. S.; Hansma, P. K.; Andrade, J. D. *Langmuir* 1990, 6, 509.

(7) Weisenhorn, A. L.; Hansma, P. K. *Proceedings of the Applied Physical Society Meeting*, Pittsburgh, PA, 1990.

(8) Edstrom, R. D.; Meinke, M. H.; Yang, X.; Yang, R.; Elings, V.; Evans, D. F. *Biophys. J.* 1990, 58, 1437.

(9) Marchant, R. E.; Lea, A. S.; Andrade, J. D.; Brockenstedt, P.; Ginsburg, D. submitted to *J. Colloid Interface Sci.*

(10) Butt, H.-J.; Hansma, P. K. *Proceedings of STM '90*, Baltimore, MD.

(11) Gould, S. A. C.; Drake, B.; Prater, C. B.; Weisenhorn, A. L.; Manne, S.; Hansma, H. G.; Hansma, P. K.; Massie, J.; Longmire, M.; Elings, V.; Northern, B. D.; Mukerjee, B.; Patterson, C. M.; Stoeckenius, W.; Albrecht, T. R.; Quate, C. F. *J. Vac. Sci. Technol.* 1990, A8, 369.

(12) Worcester, D. L.; Miller, R. G.; Bryant, P. J. *J. Microsc.* 1988, 152, 817.

(13) Horber, J. K. H.; Haberle, W.; Binnig, G. *Proceedings of STM '90*, Baltimore, MD.

(14) Davis, A. C.; Shulman, M. J. *Immunol. Today* 1989, 10, 118.

(15) Ballard, D. W.; Kranz, D. M.; Voss, E. W. Jr. *Proc. Natl. Acad. Sci. U.S.A.* 1983, 80, 5071.

(16) Swanson, S. M.; Dombrink-Kurtzman, M. A.; Voss, E. W. Jr. *Mol. Immunol.* 1988, 25, 545.

(17) Dombrink-Kurtzman, M. A.; Johnson, L. S.; Riordan, G. S.; Bedzyk, W. D.; Voss, E. W. Jr. *J. Biol. Chem.* 1989, 264, 4513.



spring constants of 0.37 and 0.064 N/m, were microfabricated from silicon nitride and have a 600-Å vapor-deposited, gold-chromium layer.

To conduct the IgM adsorption experiment, mica was first imaged under pH 8.0 phosphate buffer saline (PBS) in a fluid cell. The PBS was then exchanged for a 20  $\mu\text{g/mL}$  IgM solution in pH 8.0 PBS. We decided to operate at pH 8.0, the isoelectric point of the IgM clone, where adsorption of the protein would be the greatest, due to decreased electrostatic repulsion. A very small area was initially scanned in order to minimize the effect of the cantilever tip on the adsorbing protein while the applied force was being minimized.<sup>19</sup> Once the force was minimized, the scan area was increased to 3000 nm by 3000 nm and the adsorption process was observed using constant-force mode (4 nN). After 12 min of continuous scanning a 3000 nm by 3000 nm area, the scan size was increased to 9700 nm by 9700 nm. Scanning of this larger area was continued in constant-height mode.

The influence of the tip on the protein adsorption process was investigated by scanning the same 1700 nm by 1700 area in the constant-height mode at three different applied forces: 8, 12, and 14 nN. IgM was allowed to adsorb on mica from a 20  $\mu\text{g/mL}$  pH 8.0 PBS solution for 13.5 min. Then three images were taken consecutively, beginning at low force and ending with high force, and each was taken after three successive scans of 1700 nm by 1700 nm areas, with the first scan being from bottom to top.

An experiment in which adsorbed protein was intentionally manipulated into a desired shape was conducted using fibrinogen (65% clottable human sample, U.S. Biochemical Corp., Cleveland OH). A 100  $\mu\text{g/mL}$  solution of fibrinogen in pH 8.0 PBS was allowed to adsorb onto the mica in the fluid AFM cell for 5 min. The protein solution was then exchanged for buffer. A moderate repulsive force of 30 nN was applied and seven adjacent 2000 nm by 2000 nm areas were scanned twice each in the form of a block U. The applied force was then minimized to 4 nN and the scan area was increased to 10  $\mu\text{m}$  by 10  $\mu\text{m}$  for observation.

## Results and Discussion

When IgM adsorption was imaged with the atomic force microscope using an initial force of approximately 4 nN, the first IgM molecules appeared as aggregates on the mica surface (Figure 1). It is not known if the IgM adsorbs in the form of aggregates existing in solution or if the cantilever tip pushes individual proteins already on the surface together to form these small aggregates. The former is possible since the protein solution was buffered to the isoelectric point of the IgM, the pH at which maximum aggregation is expected to occur. As time progressed, more aggregates appeared and they began to line up in strands oriented perpendicularly to the fast-scanning ( $x$ ) direction (Figure 2).<sup>20</sup> The implications are that the adhesion between the IgM and the mica under these conditions is weak and easily disrupted by the scanning cantilever tip.

Figure 3 shows the image of IgM adsorption after 12 min (a 9700 nm by 9700 nm area captured in constant-height mode). Two partially superimposed 3000 nm by 3000 nm areas that were previously scanned are indicated in the lower right portion (area 1). The lower third of the entire 9700 nm by 9700 nm area was scanned twice (indicated as area 2), and the upper two-thirds only once

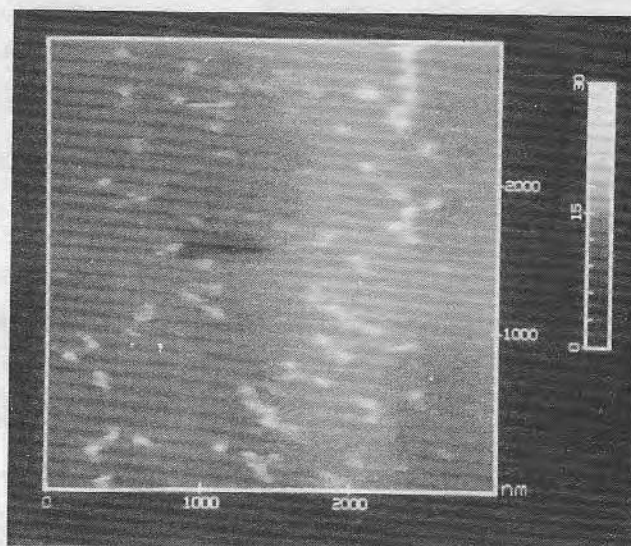


**Figure 1.** A 3000 nm by 3000 nm AFM constant-force image of IgM 18-2-3 deposited on mica from a 20  $\mu\text{g/mL}$  pH 8.0 PBS solution after a 1-min adsorption time using a 4-nN force. The vertical scale is height in nanometers. The dark wedge is a pit in the mica possibly formed from the force minimization process.

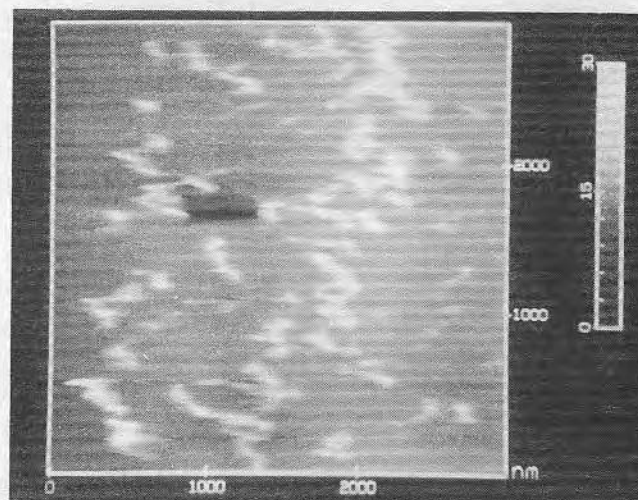


**Figure 2.** A 3000 nm by 3000 nm AFM constant-force image of IgM 18-2-3 deposited on mica from a 20  $\mu\text{g/mL}$  pH 8.0 PBS solution after a 2.5-min adsorption time using a 4-nN force (identical area is in Figure 1). The vertical scale is height in nanometers.

(indicated as area 3). It is evident that in the less scanned areas, the IgM is more uniformly distributed over the surface and is not forced by the cantilever tip to line up in strands. Figure 4 shows that further scanning of the whole 9700 nm by 9700 nm area causes the unperturbed IgM to align in strands and apparently increases the amount of IgM on the surface.

The phenomenon of molecular alignment by AFM was observed previously with fibrin monomers in PBS on mica,<sup>5</sup> with a monoclonal IgG in PBS on mica in solution,<sup>6</sup> and with von Willebrand's factor on mica in air,<sup>9</sup> where the applied force is much greater. Apparently, the cantilever tip behaves as a "molecular broom" that sweeps individual proteins or small protein aggregates into larger piles in the fast-scanning direction. As will be shown later, the exact orientation of the protein aggregates will depend on the orientation of the facets of the cantilever tip relative to the scanning axes. Figures 5 and 6 show that the tip-induced aggregation depends on which scanning mode is used. The individual proteins and protein aggregates exert a force, which can be broken down into horizontal and

(18) Alexander, S.; Hellemans, L.; Marti, O.; Schneir, J.; Elings, V.; Hansma, P. K.; Longmire, M.; Gurley, J. *J. Appl. Phys.* 1989, 65, 164.

(19) Since the force minimization was done while the IgM was adsorbing, it is not known if this reported force was between the cantilever tip and mica, the cantilever tip and IgM (if the tip was positioned above the protein), IgM and mica (if IgM had adsorbed onto the cantilever), or IgM molecules (if an IgM-coated cantilever was positioned above adsorbed IgM). These different situations would not necessarily yield the same forces.

(20) The microscope scans the surface in a raster pattern with a frequency of 18 Hz in the  $x$  direction and 0.05 Hz in the  $y$  direction. The  $x$  direction is therefore referred to as the fast-scanning direction.

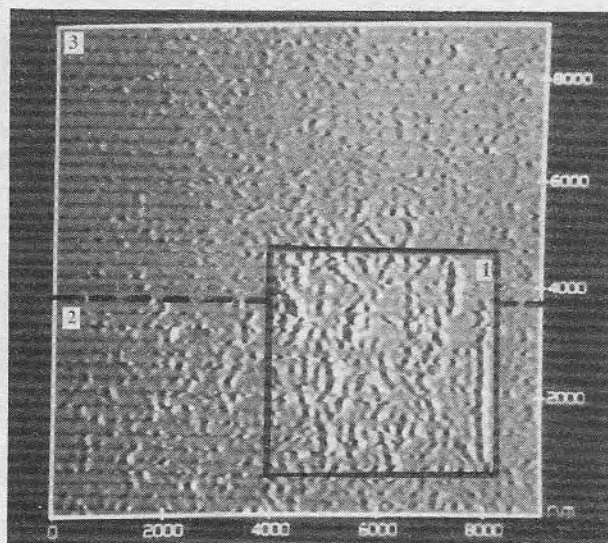


**Figure 3.** A 9000 nm by 9000 nm AFM constant-height image of IgM 18-2-3 deposited on mica from a 20  $\mu\text{g/mL}$  pH 8.0 PBS solution after a 12-min adsorption time using a 4-nN force. The vertical scale is force (uncalibrated). In the lower right are two superimposable 3000 nm by 3000 nm areas, previously scanned. The rest of the area was previous unscanned.

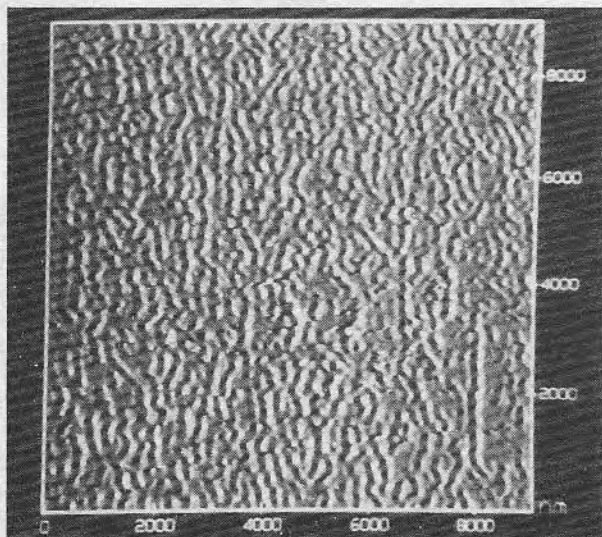


**Figure 4.** A 9000 nm by 9000 nm AFM constant-height image of IgM 18-2-3 deposited on mica from a 20  $\mu\text{g/mL}$  pH 8.0 PBS solution 1.5 min after the previous image using a 4-nN force. The vertical scale is force (uncalibrated). The protein in the previously unscanned area now resembles the previously scanned areas.

vertical components, on the sweeping cantilever tip. When the protein pile gets too large and its interaction with the surface increases above a critical value, the vertical force exerted on the cantilever tip increases to a detectable level. In the constant-force mode (Figure 5), the piezoelectric crystal will retract to maintain constant force allowing the cantilever tip to slide over the aggregate. At this point, the cantilever tip no longer pushes the aggregate. Once past the aggregate, however, it begins the sweeping process again. In the constant-height mode (Figure 6), the piezoelectric crystal does not respond to the cantilever deflection. Instead, the vertical force component will increase to the point where the cantilever is deflected up over the aggregate. Then, the vertical force decreases and the cantilever deflects back toward its initial position (Figure 6). These processes repeat themselves as the cantilever tip moves to the next position in the slow- ( $y$ ) scanning direction.

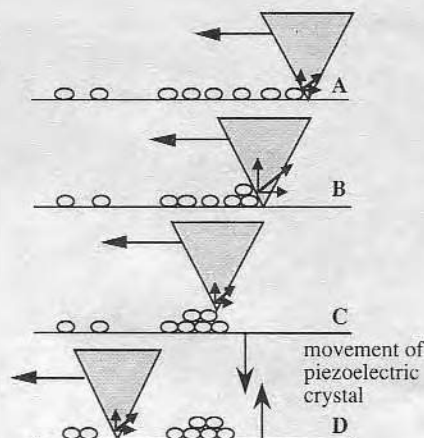


**Figure 5.** Schematic representation of protein manipulation on a surface by the cantilever tip in constant-force mode. (A) Tip moving in the fast-scanning direction begins sweeping the proteins across the surface, provided the vertical force exerted on the tip by the protein is small. (B) As the protein begins piling up, the interaction of the aggregate with the surface increases, producing a larger vertical force exerted on the cantilever. (C) When the vertical force becomes sufficiently large to cause cantilever deflection, the feedback system retracts the piezoelectric crystal, as indicated by the downward arrow, to maintain constant force. (D) The piezoelectric crystal advances, as indicated by the upward arrow, when the vertical force is diminished and the sweeping process begins again.

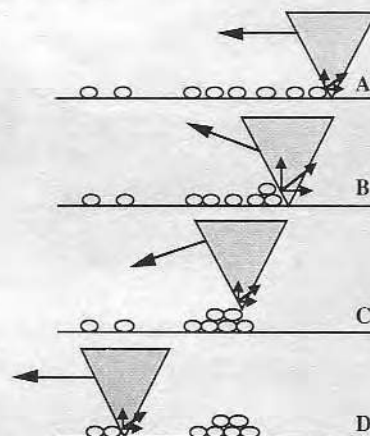


**Figure 6.** Schematic representation of protein manipulation on a surface by the cantilever tip in constant-height mode. (A) Tip moving in the fast-scanning direction begins sweeping the proteins across the surface, provided the vertical force exerted on the tip by the protein is small. (B) As the protein begins piling up, the overall interaction of the aggregate with the surface increases, producing a larger vertical force exerted on the cantilever. When the vertical force becomes sufficiently large, the cantilever deflects up over the aggregate. (C) Once the vertical force decreases, the cantilever deflects back toward its original position. (D) The sweeping process begins again.

When comparing these two scanning modes, one would expect that protein perturbation would be greater for constant-height scanning than for constant-force scanning. Assume the imaging by each mode is done at the same initial applied force. The difference in the force the protein experiences with the tip positioned above it,  $\Delta F$ , would be given by eq 1, where  $k$  is the spring constant of the

$$\Delta F = k(\Delta z - \delta) \quad (1)$$

cantilever,  $\Delta z$  is the distance the cantilever would deflect above the protein (tens of angstroms) in the constant-height mode, and  $\delta$  is the minimum cantilever deflection distance the split photodiode can detect ( $\sim 1$  Å).



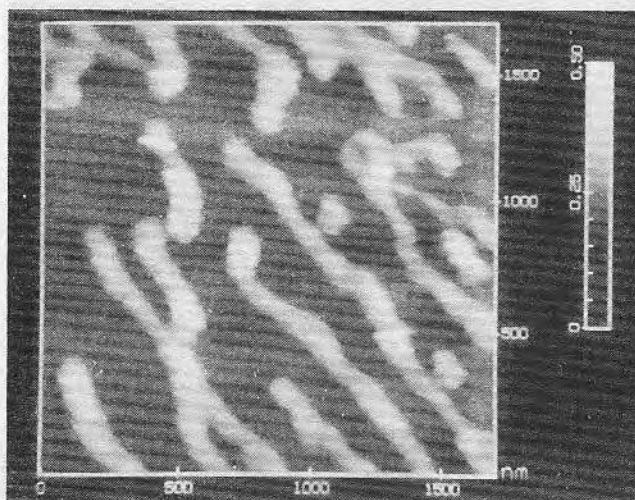


**Figure 7.** A 1700 nm by 1700 nm constant-height AFM image of IgM 18-2-3 on mica, using an 8-nN force. The IgM was allowed to adsorb for 13.5 min from a 20  $\mu\text{g}/\text{mL}$  solution in PBS at pH 8.0 and was then scanned three times before this image was taken.

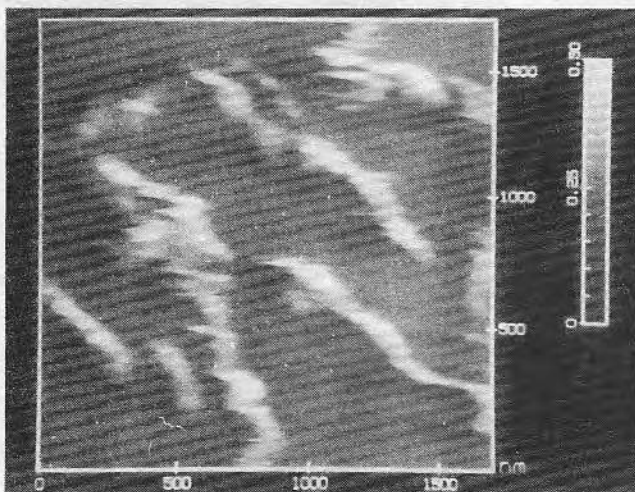


**Figure 8.** A 1700 nm by 1700 nm constant-height AFM image of IgM 18-2-3 on mica, using a 12-nN force. The IgM was allowed to adsorb for 18 min from a 20  $\mu\text{g}/\text{mL}$  solution in PBS at pH 8.0 and was then scanned three times before this image was taken.

The applied forces that are exerted on the cantilever are the overall forces, and they depend on the geometry and volume of the cantilever. The localized forces, however, can be very different. From the interaction potential calculations, one can conclude that the force between the apex of the cantilever tip and the substrate would have a greater repulsive contribution to the overall force than the rest of the tip would. At present, it is not known over what area this overall force is exerted. The influence of the tip at three different applied forces (i.e., at 8, 12, and 14 nN) on the protein adsorption process is shown in Figures 7–9. These three images were taken consecutively, beginning at low force and ending with high force, and each was taken after three successive scans of 1700 nm by 1700 nm areas. Two effects are evident in Figures 7–9: (a) with increasing force, the spacing between the adsorbed protein strands increases, and (b) protein strands are oriented diagonally with the respect to the scanned area.

The effect of the applied force to the spacing between the strands can be explained by eq 2. As the applied force,

$$F = F_{\text{applied}} + k\Delta z \quad (2)$$

$F_{\text{applied}}$ , increases, the force exerted on the cantilever,  $F$ ,

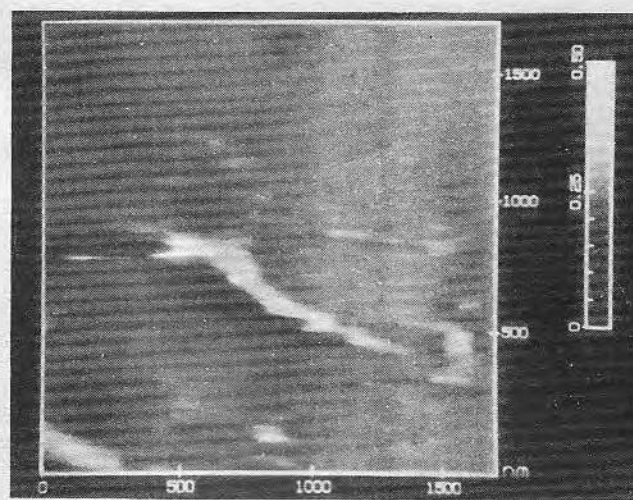


**Figure 9.** A 1700 nm by 1700 nm constant-height AFM image of IgM 18-2-3 on mica, using a 14-nN force. The IgM was allowed to adsorb for 19.5 min from a 20  $\mu\text{g}/\text{mL}$  solution in PBS at pH 8.0 and was then scanned three times before this image was taken.

**Table I.** Percent Surface Coverage of Mica by Adsorbed IgM

image, figure	surface coverage, %	applied force, nN	image, figure	surface coverage, %	applied force, nN
1	12	4	4	34	4
2	17	4	7	42	8
3, area 1	28	4	8	34	12
3, area 2	18	4	9	8	14
3, area 3	8	4			

for the same height deflection of the cantilever,  $\Delta z$ , also increases. The smaller aggregates that appear in Figure 7, where  $F_{\text{applied}}$  was 8 nN, were insufficient to deflect the cantilever when larger forces are applied (Figures 8 and 9), apparently due to the smaller overall adsorption interactions between the protein aggregates and the surface. The small aggregates are swept further along in the fast-scanning direction, picking up more protein, until the growing aggregate acquired an interaction with the surface sufficient to deflect the cantilever. Consequently, the spacing between the strands must increase when the applied force increases, according to the proposed model. The surface coverage data in Table I confirm this by indicating a smaller surface coverage at increased applied force.

One noticeable difference between Figures 7–9 and Figures 1–4 is the orientation of the strands. In Figures 1–4 the strands are generally oriented vertically, while in Figures 7–9 they run diagonally across the images. As it turned out, the difference was due to the angle between the fast-scanning direction and the orientation of the pyramidal cantilever tip. In the experiment presented by Figures 1–4, the scan orientation was  $0^\circ$  and the front facet of the pyramid first contacted the protein (Figure 10A). When the scan orientation was  $45^\circ$ , as was the case in the experiment presented by Figures 7–9, the edge between two facets contacted the proteins first (Figure 10B). The facet then pushed the protein at an angle  $45^\circ$  from the fast-scanning direction. In this manner, the protein strands can be seen to align parallel to the plane of the pyramid facets.

Scanning over adsorbed protein aggregates in the constant-height mode can produce other artifacts as well. While traversing over a very large protein aggregate, the cantilever tip can push part of the aggregate in front of itself, which produces "streaking" in the image. This effect appears as a white horizontal line like the one visible in the left side of Figure 9. Or, after crossing over an ad-

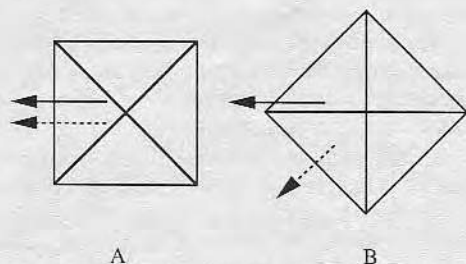


**Figure 10.** Schematic of orientation of the pyramidal tip to the fast-scanning direction. (A) With  $0^\circ$  rotation (Figures 1–4), the relative movement of one of the pyramidal facets is parallel to the fast-scanning direction (solid arrow). (B) With  $45^\circ$  rotation (Figures 7–9), the edge between two faces is parallel to the fast-scanning direction (solid arrow). The dashed arrows show the direction protein would be moved by the pyramidal facets.

sorbed aggregate, the cantilever tip can also adhere to it. This will cause a temporary deflection of the cantilever toward the surface which, in turn, appears in the image as a dark horizontal line (Figures 8 and 9). As a reminder, it has to be mentioned that the cantilever tip scans back and forth over the surface in the fast- ( $x$ ) scanning direction. However, the images captured by the instrument are composed from the signal derived from the forward scanning only. The forward scanning direction corresponds to the right-to-left direction in all images presented here. Thus, the protein adsorption images obtained by AFM present a dynamical picture composed from the spatially and temporally distinct interactions between the tip, protein, and surface.

The percentage of apparent protein surface coverage was calculated for each of the images as an area above background. The results are presented in Table I. As expected, Figure 2 shows a higher degree of surface coverage compared to Figure 1, which was obtained at a shorter adsorption time. In the case of Figures 3 and 4, it is not known whether the background is an image of mica or of a smooth layer of adsorbed IgM due to the lack of molecular specificity of the cantilever tip. In Figure 3, the most scanned area (area 1) had the highest apparent surface coverage, whereas the area scanned only once (area 3) had the lowest apparent surface coverage. There are two plausible explanations for this perceived increase in coverage as the number of scans over the same area is increased. One explanation is that the scanning process increases the adsorption rate. Normally, there is an unstirred layer of solution, referred to as the quiescent boundary layer, close to the surface. The rate of protein deposition is limited by the rate of diffusion of the protein through the quiescent boundary layer. During the scanning process, however, the relative motion of the cantilever tip with respect to the surface produces convective currents which can reduce the quiescent boundary layer thickness and thus increase the rate transport of IgM to the mica surface. Note that in Figure 4, the surface coverage over any reasonably sized area was 34%. Thus, within 1.5 min of scanning, the apparent surface coverage increased from 8% (area 3 in Figure 3 after 12 min of adsorption) to 34% (Figure 4 after 13.5 min of adsorption). The results suggest that, if the increase of the IgM transport rate is responsible for the sudden surface coverage increase, one can control the effect by varying the scan rate. A second explanation is that, if the smooth background is an adsorbed IgM monolayer, then the cantilever can push protein molecules within this layer, producing a greater corrugation. In this situation, only those molecules pushed into large mounds would be included in the coverage calculations. The coverage would reflect the extent of the molecular broom

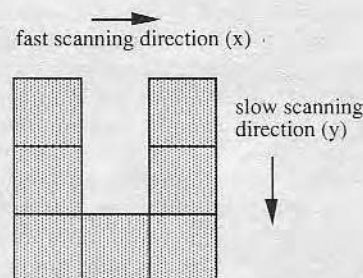


**Figure 11.** Schematic of the seven adjacent 2000 nm by 2000 nm scan areas used to produce the block letter U.

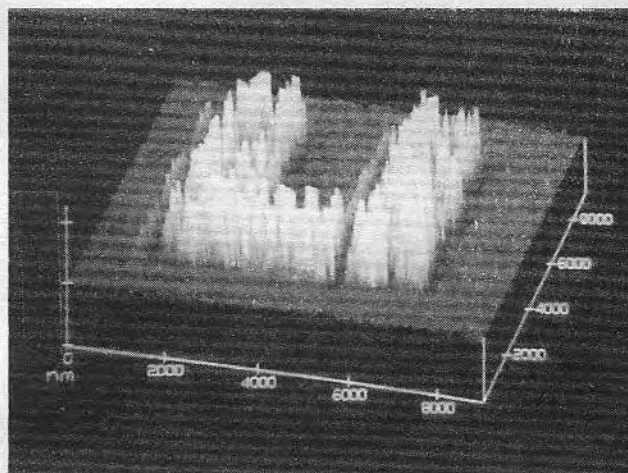


**Figure 12.** A  $10\ \mu\text{m}$  by  $10\ \mu\text{m}$  constant-height AFM image of the block letter U formed by scanning seven adjacent 2000 nm by 2000 nm areas of fibrinogen adsorbed on mica using an applied 30-nN repulsive force. The vertical scale is uncalibrated force.

effect. If the molecular broom effect is the dominant mechanism, one concludes that the perturbation occurs very rapidly (within a few scans).

The observation of unintentional manipulation of adsorbed proteins by the cantilever tip naturally led us to examine whether proteins could be manipulated into desired designs. An intriguing extension of this would be to use the AFM as an instrument to construct patterned protein surfaces to be used in biosensors or organized multienzyme arrays. We needed to start with a layer of protein on the surface under a protein-free supernatant since further protein deposition would complicate our design. We found that fibrinogen had the proper surface binding affinity to conduct the experiment and provided a sufficiently stable protein layer for this work. Drake et al.<sup>5</sup> showed that adsorbed fibrinogen could not be observed on mica with the AFM, probably because of the protein's weak interaction with the surface. However, when thrombin was added, causing the fibrinogen to cleave into fibrin monomers, the activated fibrinogen molecules adsorbed to the surface and the whole process was observed with the AFM. We found that we could observe the adsorbed fibrinogen without addition of thrombin. This was probably due to a somewhat higher level of impurity of our fibrinogen sample. After the fibrinogen solution was exchanged for buffer, a moderate repulsive force of 30 nN was applied and seven adjacent 2000 nm by 2000 nm areas were scanned twice each in the form of a letter U, as indicated by Figure 11. The applied force was then decreased to 4 nN while the scan area was increased to  $10\ \mu\text{m}$  by  $10\ \mu\text{m}$  for observation. Figure 12 shows the results: fibrinogen was uniformly distributed within the large unscanned area, but within the confines of the letter U, fibrinogen strands were oriented by the scanning procedure. The height of the strands was approximately 20–40



nm. With 4-nN applied force, the fibrinogen layer remained stable. We noticed a slight increase in protein surface roughness, but only after observing the fibrinogen for tens of minutes. When forces much larger than 30 nN were applied to the U-shaped fibrinogen layer, the entire scan area was swept clean of protein, indicating that even the largest of aggregates could not withstand the disruptive force of the cantilever tip. The swept aggregates would appear piled up just beyond the edges of the scan area in the  $+x$  and  $-x$  directions, demonstrating again that aggregates are pushed in the fast-scan direction.

### Conclusions

It has been shown that adsorbed proteins on mica are swept into strands of aggregates oriented parallel to the plane of the cantilever tip facet. This is a manifestation of the relatively weak interaction between individual molecules or small protein aggregates and the surface of mica. The area continuously scanned by the cantilever tip had higher apparent surface coverage than the regions that were scanned fewer times. It is proposed that the cantilever tip either increases the adsorbed amount by increasing the rate of transport of protein to the surface or produces corrugations within a fully adsorbed protein layer (a "molecular broom" effect). As the applied force is increased in the constant-height scanning mode, the size of the aggregates that can be swept by the cantilever increases, which causes the distance between the strands to increase. Researchers should therefore be wary that when studying weakly bound macromolecules at surfaces by AFM, the results will be strongly influenced by the cantilever tip and by the forces involved. Thus, AFM images of adsorbed proteins, fluid membranes, and other

"soft" biological specimens may represent a system perturbed by the probe (the cantilever tip). In addition, these images are composite pictures made from the spatially and temporally distinct interactions between the tip, sample, and underlying surface.

The cantilever tip can be used to manipulate protein molecules so that desired designs can be obtained. Although this manipulation is crude, it demonstrates the potential for manipulation on a finer scale such that placement of individual proteins or protein aggregates at desired positions can be achieved. Manipulation of a deposited fibrinogen layer with a 4-nN repulsive force was observed only after tens of minutes, but not to the extent that strands formed, indicating a greater adhesion between the fibrinogen and mica than between IgM and mica. The difference between fibrinogen and IgM suggest that it is possible to use the perturbation of the protein layer caused by the AFM tip to measure the strength of interactions of proteins with surfaces. If the perturbation of the observed process by AFM could be sufficiently minimized, it might be possible to extract quantitative information regarding these interactions using the unperturbed image as a reference state.

**Acknowledgment.** We are grateful to J. Brophy for suggesting the U experiment as a graphic way to show the manipulative capabilities of AFM. We also acknowledge C. C. Williams and T. P. Beebe for their helpful discussions in preparing this article and thank the Center for Biopolymers at Interfaces at the University of Utah, National Institute of Health Grant HL-44538-01, and University of Utah Graduate Research Committee for financial support.

## Chapter 20

## Measurement of Steric Exclusion Forces with the Atomic Force Microscope

A. S. Lea, J. D. Andrade, and V. Hlady

Department of Bioengineering, University of Utah, Salt Lake City, UT 84112

Atomic force microscope probes were modified by attaching polyethylene oxide to the silicon nitride cantilever tip. Two high molecular weight species, 200 and 900 kDa, were attached by physical adsorption from a dilute polymer solution. One low molecular weight species, 2 kDa, was chemically bound to the surface. Force-distance plots were obtained for modified tips and freshly cleaved mica and for plasma cleaned, unmodified tips and PEO adsorbed silicon nitride substrate in the presence of 0.1 M KNO<sub>3</sub>. Force-distance plots were also obtained in a 0.1 % w/v aqueous polyethylene oxide ( $M_w$  900 kDa) solution containing 0.1 M KNO<sub>3</sub> with tips that were plasma cleaned only. The force-distance plots show the existence of a steric exclusion force as the tip and sample are brought closer together, when the high molecular weight polyethylene oxide is adsorbed on either the substrate or the tip and when plasma cleaned, unmodified tips, incubated for at least 8 hr in the polyethylene oxide solution, are used.

The operation of the atomic force microscope (AFM) relies upon the intermolecular forces that are exerted on the probe tip by the surface of a closely placed sample (1-3). The majority of the AFM research has relied heavily upon hard core repulsion forces, otherwise known as 'contact forces', to produce the images that are widespread in the literature. Naturally, this is the intermolecular force of choice when obtaining atomic scale images, since it is the only one capable of providing such high resolution using the currently available probe tips (4). When operating in liquid environments, it is no longer the hard core repulsion, but the hydration forces that exist between the probe tip and sample that produce these images (5-6). These forces are short-range forces and are predominant at tip-sample separations less than a few angstroms.

Because of the macroscopic nature of the tip and the sample, long-range intermolecular forces also become important, especially at distances greater than a few angstroms. Long-range intermolecular forces that have been utilized to date with the AFM are attractive van der Waals forces (2,7), electrostatic forces (6,8,9), and magnetic forces (10-11). This paper describes the use of long-range steric exclusion repulsive forces in atomic force microscopy. This was accomplished by attaching water soluble polyethylene oxide (PEO) to the probe tip and by operating the instrument with the probe in an aqueous PEO solution.

In good solvents, surfaces covered with polymer chains repel each other when brought together due to the steric exclusion forces manifested by the extended polymer chains (12-14). The origin of these repulsive forces is attributed to two components: an elastic component and an osmotic component (15-16). The elastic component arises from the chain segments that have a tendency to extend themselves upon compression. The osmotic component arises from the local increase in chain segment concentration upon compression resulting in a loss of configurational entropy.

The onset of the steric exclusion force depends on the means of attaching the polymer chains to the substrates. For physically adsorbed polymer chains covering both surfaces, the steric exclusion force becomes detectable around  $6R_g$ , where  $R_g$  is the unperturbed radius of gyration of the random polymer coil in solution (12). For terminally attached polymer chains, the repulsion commences around  $12R_g$  (14). These values are approximate and depend on a number of factors including solvent quality, temperature, surface concentration and type of polymer chains attached to the surfaces.

If the steric exclusion force commences at a larger separation distance than the attractive van der Waals force, then the steric exclusion force dominates the attractive van der Waals force and a monotonically increasing repulsion is observed in the force-separation distance profiles. This occurs when attaching polymer chains containing a large number of segments, i.e. at large  $M_w$ , to the surface. Attaching low molecular weight polymer chains shifts the onset of the steric exclusion force closer to the surface and the attractive van der Waals component could dominate, resulting in an overall attractive interaction in a region of the force-distance profile.

We have modified conventional AFM tips by attaching PEO of different molecular weights to the tips with the intention of using steric exclusion forces as the predominate imaging force. PEO with molecular weight of 200 kDa or 900 kDa was physically adsorbed to the cantilever tips, whereas low molecular weight PEO (or PEG: polyethylene glycol) was covalently bound to the tip to prevent desorption of the polymer chains. It is possible that these cantilevers could greatly reduce the lateral translation of surface adsorbed entities in aqueous solutions (17-18). The AFM tips covered with polymeric PEO chains are expected to provide a more forgiving imaging force.

### Experimental

**Materials.** Gold-chromium coated silicon nitride cantilevers with integrated tips (spring constants of 0.064 N/m) were obtained from Park Scientific Inc. PEO with molecular weights of 200 kDa and 900 kDa, polyethylene glycol monomethyl ether (PEG) with a molecular weight of 2 kDa, and 3-aminopropyltriethoxysilane were obtained from Aldrich Chemical Co.. The water used in this study was microelectronics lab quality deionized water, which was subsequently passed through an organic removal cartridge and a particle filter. Muscovite mica was obtained from Asheville-Schoonmaker. Silicon wafers with a 250-300 Å CVD silicon nitride coating were obtained from Hedco lab at the University of Utah. The AFM is a NanoScope II from Digital Instruments.

**Methods. Physical adsorption.** PEO was adsorbed either onto the silicon nitride cantilever tip or onto a piece of silicon nitride coated silicon wafer. The substrates were cleaned by placing them in an oxygen plasma (200 mm Hg, 25 W) for 5 minutes. Adsorption of the PEO to the clean surface was accomplished by placing the cantilever or the wafer piece in a 0.1% w/v solution of PEO in water. Adsorption was allowed to take place for at least 18 hours (sometimes as much as a week). The substrate was then placed in water for 22-24 hours to allow desorption of the weakly bound polymer chains. The substrate was vacuum dried prior to use.



## Compression of polyethylene glycol chains grafted onto silicon nitride surface as measured by scanning force microscopy

A.S. Lea<sup>1</sup>, J.D. Andrade, V. Hlady<sup>\*</sup>

*Department of Bioengineering, University of Utah, Salt Lake City, UT84112, USA*

Received 3 November 1993; accepted 2 March 1994

### Abstract

Monomethoxypolyethylene glycol (PEG) with a molecular weight of 2000 Da has been grafted to a silicon nitride surface that has been silanized with 3-aminopropyltriethoxysilane (APS). A scanning force microscope (SFM) was used to measure a force–distance profile between the PEG-modified surface and the unmodified silicon nitride SFM tip. In 0.1 M KNO<sub>3</sub> solution the force increased monotonically with distance, showing no adhesion between the SFM probe and the PEG-modified surface. The monotonically increasing force is interpreted as a steric repulsion force. Increasing solution concentration of MgSO<sub>4</sub> caused the appearance of a weak attractive force between the SFM probe and the PEG-modified surface. The magnitude of the attractive force increased with increasing MgSO<sub>4</sub> solution concentration. The addition of MgSO<sub>4</sub> generated poor solvent conditions for grafted PEG chains and eliminated the steric repulsion force, probably through a collapse of the tethered chains. The interpretation of the MgSO<sub>4</sub> effect on the tethered PEG chains is hindered by the fact that surfaces treated with APS alone caused a cantilever instability at a separation distance of approximately 25 nm. An attractive force at this large separation distance suggested that APS treatment resulted in a surface coating thicker than a monolayer.

**Keywords:** Atomic force microscopy; Polyethylene glycol; Polyethylene oxide; Steric repulsion force

### 1. Introduction

The adsorption of soluble polymers onto colloids can cause stabilization of the colloidal particles in solution. The stabilization effect is attributed to a repulsive steric exclusion force that develops when the adsorbed polymer chains are encroached upon by nearby chains from other particles [1,2]. Compressed chains are sterically excluded from the volume occupied by neighboring chains which resist this encroachment and a steric repulsion

force develops [3]. Steric repulsion can also result from the grafting of polymer chains onto surfaces [4,5].

Grafted polymer chains are often described as being either in the “brush” regime or in the “mushroom” regime depending on the density of grafted chains on the surface. In the low surface density mushroom regime, the tethered chain can fold back upon itself and may even have multiple contacts with the surface. In the high surface density brush regime, the chain is stretched and projects itself normal to the surface. Grafted chains are useful in stabilization of colloidal suspensions, provided that the surface density of the grafted chains is moderately high. Most of the theories describing grafted

<sup>\*</sup>Corresponding author.

<sup>1</sup> Present address: Molecular Science Research Center, Battelle Pacific Northwest Laboratory, Richland, WA 99352, USA.

# NATURE OF WATER IN SYNTHETIC GELS. II. PROTON PULSE NMR OF POLYHYDROXYETHYL METHACRYLATE

by  
Hai Bang Lee, J. D. Andrade and M. S. Jhon\*  
Division of Materials Science and Engineering  
University of Utah  
Salt Lake City, Utah 84112

## INTRODUCTION

The apparent biocompatibility of many synthetic and natural aqueous gel materials has encouraged their study and testing for a wide variety of biomedical device application.<sup>1-3</sup> The presence of large quantities of water in biological tissues and their molecular organization give rise to critical biological functions.<sup>2-4</sup> The structure of water near biological and synthetic hydrogels has been discussed by Drost-Hansen,<sup>5</sup> Bruck,<sup>2</sup> and others.<sup>2-6</sup> Many of the physical, physiological and interfacial properties of such gels appear to be dependent on the organization of water within and on the surface of the hydrogels.

We have hypothesized that hydrogels may contain three classes of water:<sup>4</sup> X water (bulk water), Z water (bound water), and Y water (intermediate forms we call interfacial water). To check the validity of the hypothesis, dilatometric, specific conductivity, and differential scanning calorimetry studies<sup>8</sup> were conducted for polyhydroxyethyl methacrylate (PHEMA) gels of various non-equilibrium water contents. A series of proton spin-lattice relaxation time,  $T_1$ , experiments are reported here for a range of gel water contents. A relation is developed between the relaxation times of the three classes of water; the relaxation time of interfacial water is obtained. Also the  $\beta$ -viscosity coefficients of water in PHEMA gels and lecithin gels<sup>9</sup> were determined. Differences in the activation energy for interchange of the three types of water are obtained from the local relaxation time. Also the differences in the activation energy are compared with the activation energy for viscous flow of water from reference data.<sup>10</sup> The correlation times of bound water and interfacial water are estimated.

## EXPERIMENT

Commercial 2-hydroxyethyl methacrylate (HEMA) was obtained (Trans Chem Industries, Inc., New York, New York) and used as received. The monomer was polymerized as described elsewhere.<sup>8,11,12</sup> The gels were placed in 1 cm outer diameter NMR sample tubes (approx. 1 ml volume) and sealed. All the proton  $T_1$  measurements were made on a proton pulse NMR spectrometer (Bruker Magnetics, Inc., Mini Spec 20) at 20 MHz and 34°C. The  $T_1$  measurements were made using a 180-T-90° pulse sequence. The precision on the  $T_1$  values was estimated at  $\pm 2\%$ .

## THEORY

The measured value of the proton spin-lattice relaxation time,  $T_1$ , is considered as an average of the  $T_1$ 's of the three classes of water molecules in the gel<sup>4,8,13,14</sup>: Bound water near the polymer networks, interfacial water near the bound water, and bulk water.

$$\frac{1}{T_1} = \frac{f_w}{T_{1w}} + \frac{f_i}{T_{1i}} + \frac{f_b}{T_{1b}} \quad (1)$$

where  $f_w$  is the fraction of bulk water,  $f_i$  the fraction of interfacial water,

\*On leave from the Korea Advanced Institute of Science; Seoul, Korea

and  $f_b$  the fraction of bound water and  $T_{1w}$ ,  $T_{1i}$ , and  $T_{1b}$  are the corresponding local relaxation times of protons in these three classes of water. This expression is an extension of the two site treatment developed by Fabricand, et al.<sup>14</sup> The value of  $T_{1w}$  is taken to be that of pure water,  $f_w$ ,  $f_i$  and  $f_b$  are obtained from our previous experimental data.<sup>8</sup> Let us assume that  $T_{1b}$  corresponds to the measured  $T_1$  for a 20% (wt) water content gel, as our previous studies<sup>8</sup> indicate that PHEMA gels contain about 20% by wt. of bound water. As  $T_{1w}$  is known from bulk water data, 4.5 s. at 34°C, the  $T_1$  for interfacial water,  $T_{1i}$ , can be estimated by equation (1).

The average correlation time,  $\tau_c$ , which describes the random motion of water molecules in the gel, can be estimated from the ratio  $T_{1w}/T_1$ . Let us assume that  $1/T_1$  for the gel is proportional to the viscosity  $\eta$ .<sup>14</sup> A relationship between  $T_{1w}/T_1$ ,  $\tau_c/\tau_w$  and  $\eta/\eta_w$  is suggested in eq

$$\frac{T_{1w}}{T_1} = \frac{\eta}{\eta_w} = 1 + B C = \frac{\tau_c}{\tau_w} = \exp \frac{\Delta E}{RT} \quad (2)$$

where  $\eta$  is the water viscosity in the gels,  $\eta_w$  is the viscosity of pure water,  $B$  is the viscosity coefficient,  $C$  is the fraction of bound water in the gels,  $\tau_c$  is the correlation time of water in the gel,  $\tau_w$  is the correlation time for pure water,  $\Delta E$  is the activation energy difference for different classes of water,  $R$  is the gas constant and  $T$  is the absolute temperature.

## RESULT AND DISCUSSION

Table 1 presents our earlier data<sup>8</sup> for the proportion of the three classes of water in PHEMA gels of different water contents. Table 2 presents the  $T_1$  data and  $T_{1i}$  determined by equation (1). The spin-lattice relaxation time of interfacial water,  $T_{1i}$ , appears to reach a near constant value 0.17s for gels of 40% to 60% water. These results tend to agree with our dilatometric data.<sup>8</sup> The difference in the activation energy corresponding to interchange between three classes of water were evaluated from the relationship between relaxation time and viscosity (equation 2):

$$H_2O \text{ (interfacial)} \rightleftharpoons H_2O \text{ (bulk)}; (3) \quad \Delta E = 2.0 \text{ Kcal/mole}$$

$$H_2O \text{ (bound)} \rightleftharpoons H_2O \text{ (bulk)}; (4) \quad \Delta E = 2.5 \text{ Kcal/mole}$$

By comparison of (3) and (4) we obtain:

$$H_2O \text{ (bound)} \rightleftharpoons H_2O \text{ (interfacial)}; (5) \quad \Delta E = 0.5 \text{ Kcal/mole}$$

Those values which are obtained from viscosity equation are comparable to the energy of activation for viscous flow of water,  $E_{vis} = 4 \text{ Kcal}^{10}$  at 34°C. Fig. 1 presents the data of Table 1 relating the water content of gel,<sup>8</sup> assuming a bound water fraction of 20 wt %. It is reasonable that the fraction of bound water decreases with increasing total water content. Fig. 2 shows the ratio of the relaxation times of water molecules in the gel,  $T_1$ , to that in pure water,  $T_{1w}$ . It is interesting to compare Fig. 2 with Fig. 3, where the same relaxation time ratio is plotted for the lecithin system.<sup>19</sup> In Figs. 2 and 3,  $T_{1w}/T_1$  is linearly proportional to the fraction of bound water, confirming the linear relationship in equation (2). The  $B$  viscosity coefficients are calculated from the slopes of Figs. 2 and 3. The viscosity coefficient for PHEMA gels is about 82 and



for lecithin gels about 38. The assumption that the bulk water in the gels has the same proton relaxation time as pure water is supported by the fact that the curves in Figs. 2 and 3 are largely linear with Y-intercepts corresponding to the pure water value. A comparison between the  $T_1$  for purewater and/or bound water gives us a measure of the difference in structure between the two classes of water. The correlation time for PHEMA-bound and PHEMA-interfacial water are approximately 75 and 27 times, respectively, longer than that for pure water. These values may indicate a more ordered state of water in the polymer network. Using a value of  $3 \cdot 10^{-12}$ s for the correlation time of pure water,<sup>15</sup> we can estimate the correlation time for PHEMA-bound and PHEMA-interfacial water to be  $2 \cdot 10^{-10}$ s and  $8 \cdot 10^{-11}$ s, respectively. The value of  $\tau_c$  for PHEMA-bound water is greater than that corresponding to lecithin-bound water ( $9 \cdot 10^{-11}$ s)<sup>9</sup> or for water in the presence of tetra alkyl cations (approx.  $10^{-11}$ s),<sup>6</sup> but almost the same as that corresponding to water bound to a macromolecular species, such as hemoglobin in solution (approx.  $5 \cdot 10^{-10}$ s).<sup>17</sup> There has been a general impression that the biocompatibility of a gel interface should increase with its water content.<sup>2-3</sup> The role and organization of water in the gel and particularly on its surface has also been considered.<sup>2-4</sup> The interfaces of platelets, red cells and endothelium may have bound water and interfacial water on their surfaces. The equilibrium between bound, interfacial, and bulk water may be important in deducing the interfacial interactions between syntehtic gels, cell surface gels, and physiological solutions.

#### ACKNOWLEDGMENT

This work was supported by the U. S. Atomic Energy Comission, Contract At(11-1)-2147. We thank Dr. S. Ma and Dr. H. N. Yeng for many helpful discussions and assistance.

#### REFERENCES

1. O. Wichterle and D. Lim, Nature **185**, 117 (1960).
2. S. D. Bruck, J. Biomed. Materials Res. **7**, 387 (1973).
3. J. D. Andrade, H. B. Lee, M. S. Jhon, S. W. Kim, and J. B. Hibbs, Trans. Amer. Soc. Artif. Int. Organs **19**, 1 (1973).
4. M. S. Jhon and J. D. Andrade, J. Biomedical Material Res. (in press).
5. W. Drost-Hansen, in Chemistry of the Cell Interface, Part B, H. D. Brown, ed., Academic Press, New York (1971).
6. K. Green and T. Otori, J. Physiol., London **207**, 93 (1970).
7. A. Szent-Gyorgy, Bioenergetics, Academic Press, New York (1957).
8. H. B. Lee, M. S. Jhon and J. D. Andrade, submitted.
9. A. M. Gottlieb, P. T. Inglefield and Y. Lange, Biochim. Biophys. Acta, **307**, 444 (1973).
10. S. Glasstone, K. J. Laidler, and H. Eyring, The Theory of Rate Process McGraw-Hill, New York (1941).
11. M. F. Refojo, J. Poly. Sci. **5**, 3103 (1967).
12. M. F. Refojo, J. Appl. Poly. Sci. **9**, 3417 (1965).

13. M. J. Tait, S. Ablett and F. W. Wood, J. Colloid Interface Sci., **43**, 594 (1972).
14. B. P. Fabricand, S. S. Goldberg, R. Leifer and S. G. Unger, Molec. Phys. **7**, 425 (1964).
15. Z. Luz and S. Meiboom, J. Chem. Phys. **40**, 2686 (1964).
16. H. G. Hertz and M. D. Zeidler Ber. Bunsenges, Phys. Chem. **68**, 821 (1964).
17. T. R. Stengle and J. D. Baldeschwieler, Proc. Natl. Acad. Sci. U. S. **55**, 1020 (1966).

TABLE 1. The Fraction of Water in PHEMA Gels of Different Total Water Content (Wt%) (from reference 8)

Wt % of Total Water in the Gel	20	25	30	35	40	45	50	55	60
$f_w$ : Fraction of bulk water	0	0	0	0.09	0.21	0.30	0.37	0.42	0.47
$f_i$ : Fraction of interfacial water	0	0.2	0.33	0.34	0.29	0.26	0.33	0.22	0.20
$f_b$ : Fraction of bound water	1.0	0.8	0.67	0.57	0.50	0.44	0.40	0.36	0.33

TABLE 2. Proton NMR Spin-Lattice Relaxation Times for PHEMA Gels of Different Total Water Content (Wt %)

Wt % of Total Water in gel	20	30	40	50	60
Average $T_1$ , sec, of all water	0.065	0.0816	0.107	0.132	0.158
$T_{1b}$ , sec: $T_1$ for bound water	0.065	0.065	0.065	0.065	0.065
$T_{1i}$ , sec: $T_1$ for interfacial water	0	0.138	0.122	0.174	0.160

$T_{1w}$ : 4.5 s. at 34°C

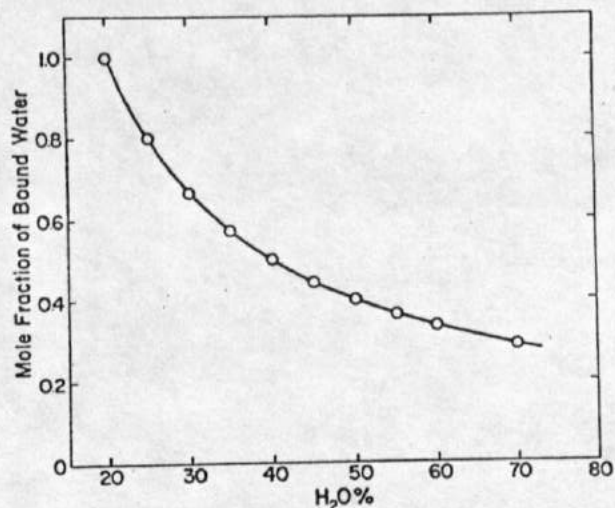


Figure 1. The Mole Fraction of Bound Water Versus The Total Water Content (Wt %) for PHEMA Gels (from Reference 8)

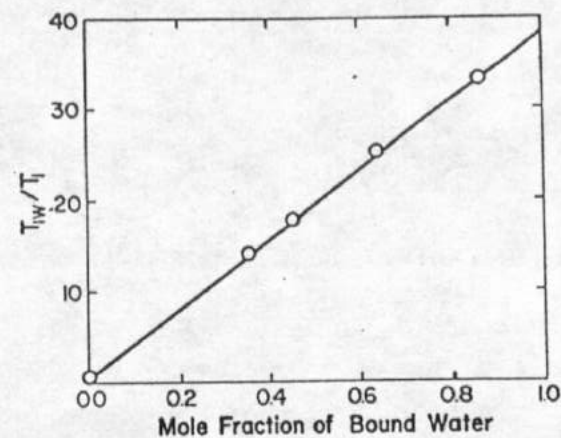


Figure 3. The Ratio of Proton Spin-Lattice Relaxation Times of Pure Water to the Gel,  $T_{1w}/T_1$ , Versus the Mole Fraction of Bound Water for Lecithin Gels (from Reference 9)

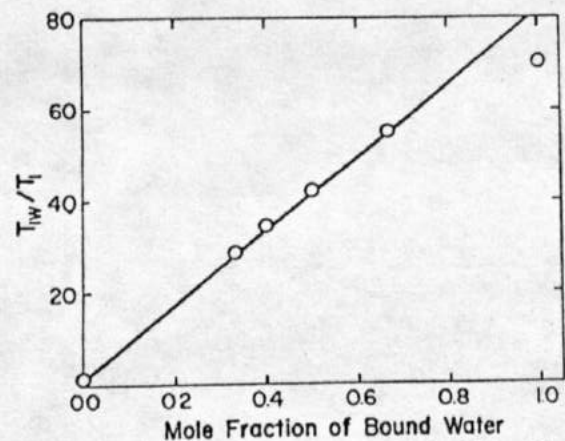


Figure 2. The Ratio of Proton Spin-Lattice Relaxation Times of Pure Water to the Gel,  $T_{1w}/T_1$ , Versus the Mole Fraction of Bound Water for PHEMA Gels



chains assume the grafted chains are brushes which simplifies the calculation of the polymer segment density distributions within the grafted layer.

Although primarily used as an imaging device, the scanning force microscope (SFM) [6] is increasingly being used to study intermolecular forces. While the surface force apparatus (SFA) [7] has been the standard technique for measuring surface and intermolecular forces, the SFM has two distinct advantages that make it useful in probing these forces: the relatively small interaction area (as compared to the SFA) allows one to probe forces on a submicroscopic scale, and one can also use the surfaces of opaque materials.

The SFM measurements, however, do not include an independent measure of absolute separation distances between the interacting surfaces and therefore can not be considered as a replacement for the SFA. Some of the intermolecular forces that have been probed with the SFM to date are van der Waals forces [8–10], electrostatic [11,12], hydrophobic, [13,14] and steric repulsion forces [15,16].

Unlike previous work on physisorbed polyethylene oxides [15,16], this work uses the SFM to measure the steric repulsion forces that are generated by the compression of *grafted* polyethylene glycol (PEG) chains. By tethering a polymer chain to a surface through a covalent bond, the conformation of the chain becomes markedly different from a physically adsorbed polymer chain. While physically adsorbed polymer chains are modeled with the trains, loops and tails model, grafted chains are not. If the physically adsorbed polymer chain is compressed, it can rearrange its conformation. One expects no permanent changes of the conformation of a tethered chain after its compression. One also expects that repeated compression–decompression cycles performed on an assembly of tethered chains will generate identical force–distance plots, unlike the case of physically adsorbed polymer chains [16].

A typical force response (an SFM force plot) obtained for a clean silicon nitride tip interacting with a clean, flat silicon nitride surface in 0.1 M  $\text{KNO}_3$  is schematically shown in Fig. 1. In the absence of electrostatic and hydration repulsive forces, when the SFM tip approaches the surface,

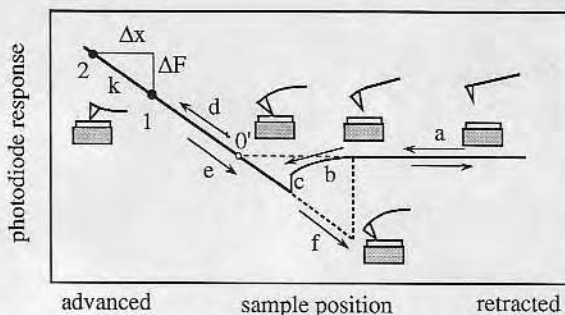


Fig. 1. A schematic of a typical SFM force plot for an untreated plasma cleaned tip and silicon nitride substrate in water. Depicted in the figure are the relative locations of the tip and substrate and extent of cantilever bending at a number of positions on the force plot.

van der Waals attraction between the tip and the surface results in the bending of the cantilever towards the flat surface which is counteracted by a cantilever restoring force. The bending of the cantilever is measured by the photodiode detector. When the force gradient exceeds the cantilever spring constant, the cantilever experiences an instability, the tip is pulled toward the surface and a “jump” into contact occurs. In the case of a non-deformable surface, the movement of the cantilever and the sample surface becomes linear and identical after the contact is established. The net force between the tip and the sample can be calculated by multiplying the spring constant by the distance the sample has moved,  $F=kx$ . Retraction of the sample often results in an adhesive force between the tip and the sample. Although no independent distance measurements are performed, a zero separation distance can be assigned to the intersection between the linear part of the force–distance plot where the SFM tip and the sample surface travel in contact and the zero force line determined by the resting position of the cantilever.

Fig. 2 shows schematically an expected SFM force plot in the case when the surface is grafted with PEG chains with a surface density sufficient for brush formation. No longer is there a jump into contact since the repulsive steric exclusion force dominates the attractive van der Waals force at all separation distances. Note that in the case of grafted chains only a relative separation distance can be assigned to each force–distance curve

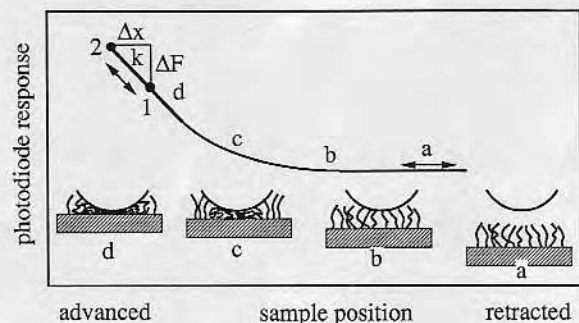


Fig. 2. A schematic of a typical SFM force plot for a polyethylene glycol grafted silicon nitride substrate and a plasma cleaned tip in water. Also shown in the figure are the relative extents of polyethylene glycol chain compression at a number of positions on the force plot.

because there is no way of knowing how thick is the compressed brush layer between the tip and the substrate.

We have used a self-consistent mean field lattice theory to predict the forces and force gradients that are generated upon compression of the grafted PEG chains. The theory, implemented as a numerical computation using program GOLIAD based upon the Scheutjens–Fleer theory [17,18], can be used to calculate the free energy change as chains grafted to flat plates are compressed. Derjaguin's approximation is used to calculate the force between the flat surface and the spherically approximated probe tip from the computed free energy. These computations were used in determining the magnitude of forces one expects to measure with cantilevers of different spring constants. A description of the GOLIAD program has been given by Barneveld [19].

## 2. Experimental section

### 2.1. Computation of the interaction energies

Grafted PEG was modeled as a polymer with the sequence  $N[CCO_x]B$ , where  $x$  denotes the number of ethylene oxide monomer units in the chain. The terminal groups are the end through which a covalent bond with the surface is formed (N) and the free methoxy end (B). The other

components in the system are water, W, and the surface, S. The Flory–Huggins interaction parameter,  $\chi$ , (in  $kT$ ) is specified for each pair of components in the system. The methyl end group, B, was treated as a methylene unit, C, and it is assumed to have the same interaction energies as the methylene unit does with the other components of the system. The value of the interaction parameters  $\chi_{co}$ ,  $\chi_{cw}$ , and  $\chi_{wo}$ , taken from Barneveld [20] are 2.0, 2.0, and  $-1.6$  respectively. The methyl and methylene units are assumed to have an interaction parameter of 0.5 with the surface. In order to simulate a covalent bond, all N units must have a strong irreversible interaction with the surface. During the course of computation, the N terminus–surface interaction energy was incrementally increased until all Ns in the system were in contact with the surface. It has been found that a value of  $-300kT$  is sufficient to covalently bond all N termini with the surface. All other interaction parameters are assumed to be zero. It was assumed that the surface coverage equaled one equivalent monolayer for PEG; this amount was in agreement with the coverage measured in a similar experimental system [21].

### 2.2. PEG grafting to the silicon nitride surface

The silicon nitride surfaces and cantilevers were cleaned for 5 min with an oxygen plasma at 25 W and a pressure of 200  $\mu\text{mHg}$ . The procedure for coupling PEG to the silicon nitride surfaces involved a surface treatment with 3-aminopropyltriethoxysilane (immersion of surface in 15-min old 5 vol.% aqueous APS solution for 15 min) followed by attachment of aldehyde terminated monomethoxy PEG to the surface amine through a Schiff base reaction [22,23]. The presence of PEG was verified by the appearance of an ether carbon peak in the X-ray photoelectron spectroscopy (XPS) spectra.

### 2.3. Force–distance plots

SFM force–distance plots were always obtained in 0.1 M  $\text{KNO}_3$  solutions initially. Force–distance plots in  $\text{MgSO}_4$  were taken by exchanging the 0.1 M  $\text{KNO}_3$  solution in the fluid cell with solutions



containing  $\text{MgSO}_4$ . The  $\text{MgSO}_4$  concentration was increased or decreased in 0.2 M steps. Since the refractive index of solutions depends on  $\text{MgSO}_4$  concentration, the laser light passing through the fluid became misaligned with respect to the photodiode detector after the  $\text{MgSO}_4$  concentration was changed. It was necessary to realign the photodiode detector before each set of measurements. Whenever possible, the setting-up of the SFM and the alignment of the laser beam were accomplished with the probe positioned in one location over the sample and then the force measurements were taken in a different location. This procedure enabled one to obtain force–distance plots on pristine areas of the PEG grafted sample.

Collection of the SFM force plots was accomplished using a Hewlett–Packard 54200AD digital storage oscilloscope and a Hewlett–Packard 9300 computer [16]. The high voltage signal that drives the piezoelectric crystal in the  $z$  direction and the  $(A - B)/(A + B)$  signal arising from the split photodiode detector were supplied to the digital storage oscilloscope. The frequency of SFM force measurements was 1 Hz, i.e. the sample approach and retraction speed was approximately  $74 \text{ nm s}^{-1}$  for PEG grafted surfaces and  $0.74 \mu\text{m s}^{-1}$  for the APS treated surface. A computer program was written to calculate force and distance traveled by the sample. Force was calibrated from the linear part of the force–distance plot where the SFM tip and the sample surface traveled in contact using the cantilever spring constant and the  $z$ -expansion factor of the piezoelectric crystal ( $10 \text{ \AA V}^{-1}$ ). The zero force was defined from the resting position of the cantilever.

### 3. Results

#### 3.1. Computer modeling

Figs. 3 and 4 summarize the results of the computer modeling using the self-consistent mean field lattice theory. The free energies computed by the GOLIAD program for a symmetrical flat plate geometry were used to calculate the force between a flat surface and a spherically approximated probe tip (20 nm in radius) using Derjaguin's approxima-

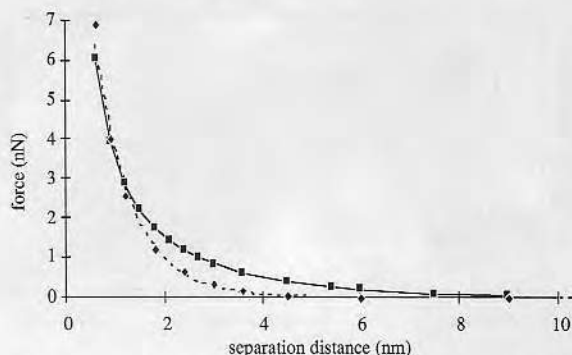


Fig. 3. Predicted steric repulsion force vs. separation distance data based on GOLIAD computations for 2000 Da PEG (diamonds) and 5000 Da PEG (squares) grafted onto silicon nitride surfaces, using water as a solvent and a grafting density of one equivalent monolayer of PEG segment on each surface. The free energy vs. distance GOLIAD computation results were converted into force vs. distance using Derjaguin's approximation assuming a 20 nm radius spherical tip. The curves represent the analytical equations determined from least squares difference.

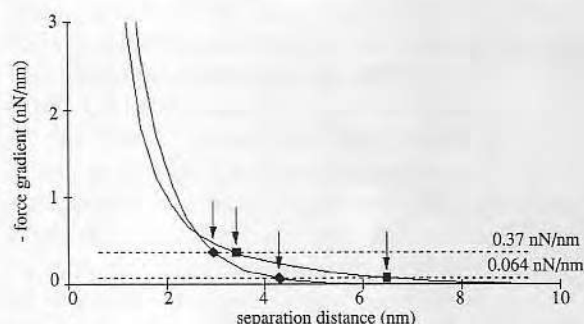


Fig. 4. Predicted force gradient vs. separation distance data for 2000 Da PEG (diamonds) and 5000 Da PEG (squares) grafted onto silicon nitride surfaces. These curves were calculated by taking the derivatives of the analytical expressions determined from least squares difference shown in Fig. 3. Shown by two horizontal dashed lines are the magnitude of the spring constants of the two cantilevers used in the SFM experiments. The steric exclusion force can be measured using each cantilever only up to the separation distances indicated by the arrows.

tion. Fig. 3 shows the predicted forces which would develop upon compression of two layers of grafted PEG chains. The assumed PEG surface density was one equivalent monolayer of PEG segments. As expected, the force produced is greater for the 5000 Da (squares) than the 2000 Da PEG (diamonds) at given separation distances. At separation

distances less than 1.5 nm, the force curves coincide. Fig. 4 shows the gradient of forces from Fig. 3. Shown by two horizontal dashed lines on this figure are the magnitude of the spring constants of the two cantilevers used in the experiments. At force gradients greater than the spring constant, the cantilever could not compress the chains further. Instead, the cantilever would deflect upwards together with the partially compressed chains leaving a region of separation distances and forces inaccessible for measurements. For the 5000 Da PEG, measurable forces would be obtained in the 4–7 nm range of separation distance; for the 2000 Da PEG, 3–4 nm. This variability would depend on cantilever spring constants and a minimum detectable force.

### 3.2. SFM force–distance plots

A typical SFM force–distance plot for an APS treated silicon nitride surface and an oxygen plasma cleaned tip in 0.1 M  $\text{KNO}_3$  is shown in Fig. 5. The tip, being negatively charged [24–26] at pH 5–6, was attracted to the positively charged substrate [27] upon approach, causing the instability of the cantilever and its jump into contact. The retraction curve showed a large adhesive force upon separation of the tip and substrate. The assignment of the zero separation distance indicates that the cantilever instability and the jump into contact occurred at a separation distance of 20–25 nm. The origin of the cantilever instability

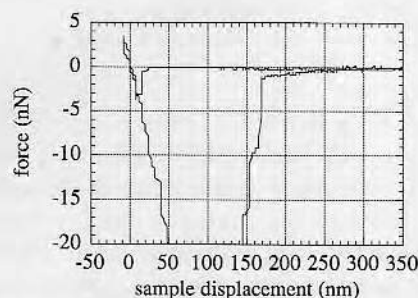


Fig. 5. SFM force plot of an APS treated silicon nitride surface and an oxygen plasma cleaned AFM probe tip in 0.1 M  $\text{KNO}_3$ . An attractive jump into contact upon approach is observed 20–25 nm from the assigned zero separation distance point. Upon retraction, a large adhesive force is observed.

at such a large separation distance is not known and could not be predicted either by the largely screened electrostatic force existing in 0.1 M  $\text{KNO}_3$  solution, or by the van der Waals forces.

When PEG was grafted to the APS treated silicon nitride surface, the SFM force–distance plots were different. Fig. 6(a) shows a force–distance plot for a 2000 Da PEG grafted onto silicon nitride substrate and an oxygen plasma cleaned tip in 0.1 M  $\text{KNO}_3$ . No longer is any attractive force observed; any attractive contribution is dwarfed by the repulsive steric contribution due to chain compression. Figs. 6(b)–6(e) show the effect of increasing the  $\text{MgSO}_4$  concentration from 0.2 to 1.0 M on force–distance plots. Up to concentrations of 0.4 M  $\text{MgSO}_4$  (not shown), there was no indication of change in the shape of the force plots. At a concentration of 0.6 M  $\text{MgSO}_4$ , however, an attractive force became discernible. The magnitude of the attractive force increased gradually as the  $\text{MgSO}_4$  concentration was increased. Upon reduction of  $\text{MgSO}_4$  concentration, the attractive force gradually diminished and the repulsive force began to dominate again. A repeated titration with the  $\text{MgSO}_4$  resulted in repeated behavior. In all cases, the retraction curve coincided with the approach curve and no excess adhesive force was noted.

## 4. Discussion

The presence of salts in aqueous solutions of polyethylene glycol reduces the water solvent quality. At a critical concentration of salt, the polymer segment–segment interaction becomes greater than segment–solvent interaction and phase separation (precipitation) occurs [28–30]. These changes are results of: (i) changes in the hydrophilic and hydrophobic interactions among polymer and solvent; (ii) changes in water structure brought about by structure making or breaking ions, and (iii) influences of salts on the hydration sheath of the polymer [28]. Trivalent ions are more effective than divalent ions, which in turn are more effective than univalent ions.

The behavior of the grafted PEG, as reflected by the SFM force–distance plots measured in the



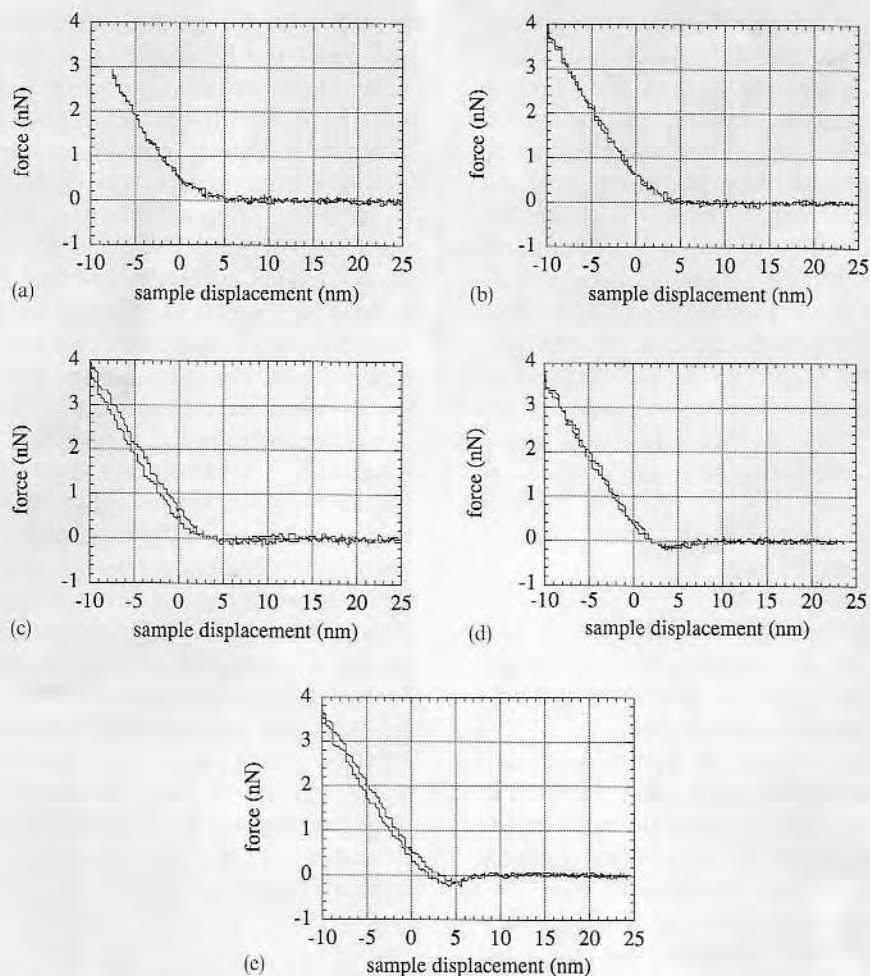


Fig. 6. SFM force-distance plot of a 2000 Da PEG grafted silicon nitride surface and an oxygen plasma cleaned tip in 0.1 M  $\text{KNO}_3$ . (a) The monotonically increasing curve is due to repulsive steric exclusion forces. (b) The addition of 0.2 M  $\text{MgSO}_4$  does not measurably change the repulsive steric exclusion force. (c) With the addition of 0.6 M  $\text{MgSO}_4$ , a weak 0.1 nN attractive force is observed. (d) At 0.8 M  $\text{MgSO}_4$ , a 0.2 nN attractive force is observed. (e) At 1.0 M  $\text{MgSO}_4$ , the attractive force is now 0.3 nN. The attractive force disappears and the repulsive steric exclusion force is restored by a decrease of  $\text{MgSO}_4$  concentration.

presence of varying concentrations of  $\text{MgSO}_4$  (Fig. 6), can be interpreted as the effect of solvent quality change. Collapsed PEG chains would not produce steric exclusion forces, whereas extended chains would [31].  $\text{MgSO}_4$  was used in these experiments since the theta temperature equals room temperature (299 K) at 0.50 M [30]. The use of univalent ions was not practical since the high concentration required for the collapse of PEG chains increased the refractive index of the solution in the SFM fluid cell and would misalign

the SFM optical lever. Of the trivalent anions, only phosphate ions were preliminarily studied since their concentration effect on PEG cloud point temperature is closely related to theta temperature [28]. Phosphates, however, are known to have specific interactions with silica [32] whose surface is closely related to the surface of silicon nitride in water.

The experimental behavior of the grafted 2000 Da PEG can not be directly compared with the results computed from the self-consistent mean

field lattice theory. The separation distance could not be measured by an independent means. This is probably the most serious disadvantage of SFM. The theoretical predictions refer to a symmetrical system, i.e. two grafted polymer layers interacting with each other. In addition, the application of Derjaguin's approximation requires that the radius of the sphere is much greater than the range of the force, an assumption that is hardly satisfied under the present experimental conditions. Therefore, the computed forces (Figs. 3 and 4) can serve only as an illustration for the limitation of SFM force-distance measurements. For example, one finds that the SFM can only measure a small portion of the steric repulsion force-distance curves (Fig. 4). Whereas the weaker cantilevers ( $0.064 \text{ N m}^{-1}$ ) are more sensitive and are able to measure small forces at greater separation distances, they are unable to compress the PEG chains as much as the stiffer cantilevers ( $0.37 \text{ N m}^{-1}$ ) do. The increased sensitivity may actually be disadvantageous. The thermal noise one measures with the SFM [33] may exceed the sensitivity of the cantilever to the point where the force gradient exceeds the cantilever spring constant. In some circumstances, the cantilever stops compressing the grafted chains before the deflection signal exceeds the noise level and no part of the force curve is measurable. Such would be the case for the  $0.064 \text{ N m}^{-1}$  cantilever compressing 2000 Da PEG chains with a surface coverage of 1 equivalent monolayer. Figs. 3 and 4 indicate that the stiffer  $0.37 \text{ N m}^{-1}$  cantilever could measure a larger portion of the force-distance curve. All steric repulsion experiments, therefore, were performed with the stiffer cantilever.

Up to a concentration of  $0.6 \text{ M MgSO}_4$ , the grafted PEG layer shows no visible change in the repulsive steric exclusion force. This behavior agrees with the stated value of  $0.5 \text{ M MgSO}_4$  for the concentration at which the theta temperature equals room temperature. At greater  $\text{MgSO}_4$  concentrations, the collapse of the grafted PEG chains diminishes the repulsive steric exclusion force and an attractive force begins to appear. In solution, the collapse of free PEG chains would be a discrete first-order transition. The gradual increase of the attractive force indicates that the collapse of the grafted PEG chains is not a discrete first-order

transition. This behavior is in agreement with the theoretical predictions of Shim and Cates [34] and Zhulina et al. [35]. The effect of  $\text{MgSO}_4$  on the force-distance plots for surfaces grafted with 5000 Da PEG (not shown) did not differ appreciably from those of 2000 Da PEG. All force measurements were performed in a dynamic fashion using the slowest available frequency ( $1 \text{ Hz}$ ) and the results (Fig. 6) show that the approach and retraction forces coincided. Although the compression speed was rather slow (approximately  $75 \text{ nm s}^{-1}$ ), more measurements in a wider range of frequency are needed to determine whether the measured forces were indeed the equilibrium forces or not.

The occurrence of cantilever instability and the jump into contact of the plasma cleaned tip onto the APS treated surface at a separation distance of 20–25 nm was not expected. This phenomenon could not be explained by the largely screened electrostatic force in  $0.1 \text{ M KNO}_3$  solution, nor by the van der Waals forces. Our hypothesis is that the effect is due to the presence of more than a monolayer of APS on the silicon nitride surface. It is possible that APS, being a trifunctional silane, polymerizes to form a three-dimensional polymer network on the surface of silicon nitride. Vandenberg et al. [36] indicated that polymerization occurs continually in liquid APS and distillation should be performed prior to reaction with the surface. This precaution, however, does not prevent the possibility of an aqueous APS cross-reaction prior to and during the immersion of the silicon nitride surface which could adsorb and/or react with these polymer networks. Boerio et al. [37] have indicated that even after washing with water, a 6 nm layer remains bound to the surface. We have recorded the SFM force plots for surfaces treated with other trifunctional silanes and found similar effects. To eliminate the possibility of silane polymerization, a monofunctional silane should be used. For example, the SFM force plots on hydrolyzed isocyanatopropyltrimethylchlorosilane (IPS) treated silicon nitride surfaces [16] showed the attractive forces that can be predicted by the DLVO theory. Although the PEG coupling to IPS derivatized substrates has been achieved [21], the SFM force-distance plots in these systems, however, have not been measured.



## 5. Conclusions

This research investigated the forces generated from compression of grafted PEG chains in solution experimentally by SFM. The computer modeling indicated that steric exclusion forces generated from compression of two layers of 2000 and 5000 Da PEG are indeed measurable by SFM, provided cantilevers of the appropriate stiffness are used. The spring constant of the weaker cantilevers is quickly exceeded by the force gradients making them ineffective for measuring forces at short separation distances. The SFM compression experiments on 2000 Da PEG chains grafted onto silicon nitride did demonstrate a repulsive steric exclusion force. The addition of  $\text{MgSO}_4$  to the solution reduced the solvent quality and collapsed the PEG chains. This collapse was a continuous one, unlike the first-order phase transitions observed for free unbound PEG in solution. The collapse of the chains was first observed at a  $\text{MgSO}_4$  concentration of 0.6 M, which agrees with solution theta solvent conditions.

## Acknowledgments

The authors would like to thank A. Pungor and Y.-S. Lin for technical assistance. GOLIAD was provided gratis by the late J.M.H.M. Scheutjens. Financial support for this work was provided by NIH (Grant HL-44538) and by the Whitaker Foundation. Financial support was also provided by the University of Utah Graduate Research Committee (A.S.L.).

## References

- [1] D.H. Napper, *J. Colloid Interface Sci.*, 58 (1977) 390–407.
- [2] D.H. Napper, *Polymeric Stabilization of Colloidal Dispersions*, Academic Press, New York, 1983.
- [3] A.K. Dolan and S.F. Edwards, *Proc. R. Soc. London Ser. A*, 343 (1975) 427–442.
- [4] H.J. Taunton, C. Toprakcioglu, L.J. Fetters and J. Klein, *Nature*, 332 (1988) 712–740.
- [5] P. Auroy, L. Auvray and L. Léger, *J. Colloid Interface Sci.*, 150 (1992) 187–194.
- [6] G. Binnig, C.F. Quate and C. Gerber, *Phys. Rev. Lett.*, 56 (1986) 930–933.
- [7] J.N. Israelachvili and G.E. Adams, *J. Chem. Soc., Faraday Trans. I*, 74 (1978) 975–983.
- [8] N.A. Burnham and R.J. Colton, *J. Vac. Sci. Technol. A*, 7 (1989) 2906–2913.
- [9] C.M. Mate, M.R. Lorenz and V.J. Novotny, *J. Chem. Phys.*, 90 (1989) 7550–7559.
- [10] N.A. Burnham, D.D. Dominguez, R.L. Mowery and R.J. Colton, *Phys. Rev. Lett.*, 64 (1990) 1931–1934.
- [11] H.-J. Bütt, *Biophys. J.*, 60 (1992) 777–785.
- [12] W.A. Ducker, T.J. Senden and R.M. Pashley, *Nature*, 353 (1991) 239–241.
- [13] L. Olsson, P. Tengvall, R. Wigren and R. Erlandsson, *Ultramicroscopy*, 42–44 (1992) 73–79.
- [14] Y.-H. Tsao, D. Fennell Evans and H. Wennerström, *Science*, 262 (1993) 547–550.
- [15] M.W. Rutland and T.J. Senden, *Langmuir*, 9 (1993) 412–418.
- [16] A.S. Lea, Ph.D. Dissertation, University of Utah, 1993.
- [17] J.M.H.M. Scheutjens and G.J. Fleer, *J. Phys. Chem.*, 83 (1979) 1619–1635.
- [18] J.M.H.M. Scheutjens and G.J. Fleer, *J. Phys. Chem.*, 84 (1980) 178–189.
- [19] P. Barneveld, Ph.D. Dissertation, Wageningen Agricultural University, 1992.
- [20] P.A. Barneveld, J.M.H.M. Scheutjens and J. Lyklema, *Colloids Surfaces*, 52 (1991) 107–121.
- [21] Y.-L. Lin, C.-G. Gölander and V. Hlady, *Colloids Surfaces B: Biointerfaces*, 3 (1994) 49–62.
- [22] J.M. Harris, E.C. Struck, M.G. Case, M.S. Paley, J.M.V. Alstine and D.E. Brooks, *J. Polym. Sci.*, 22 (1984) 341–352.
- [23] J.M. Harris, *JMS-Rev. Macromol. Chem. Phys.*, C25 (1985) 325–373.
- [24] L. Bousse and S. Mostarshed, *J. Electroanal. Chem.*, 302 (1991) 269–274.
- [25] D.L. Harame, L.J. Bousse, J.D. Shott and J.D. Meindl, *IEEE Trans. Electron Devices*, 34 (1987) 1700–1706.
- [26] N. Jaffrezic-Renault, A. De, P. Clechet and A. Maaref, *Colloids Surfaces*, 36 (1989) 59–68.
- [27] Y.-S. Lin and V. Hlady, *Colloids Surfaces B: Biointerfaces*, in press.
- [28] M. Ataman, *Colloid Polym. Sci.*, 265 (1987) 16–25.
- [29] T.C. Amu, *Polymer*, 23 (1982) 1775–1779.
- [30] E.A. Boucher and P.M. Hines, *J. Polym. Sci.*, 16 (1978) 501–511.
- [31] V.V. Lent, R. Israels, J.M.H.M. Scheutjens and G.J. Fleer, *J. Colloid Interface Sci.*, 137 (1990) 380–394.
- [32] P. Claesson, Ph.D. Dissertation, The Royal Institute of Technology, Stockholm, 1986.
- [33] G.M. McClelland, R. Erlandsson and S. Chiang, in D.O. Thompson and D.E. Chimenti (Eds.), *Review of Progress in Quantitative Nondestructive Evaluation*, Vol. 6B, Plenum Press, New York, 1987, pp. 1307–1314.
- [34] D.F.K. Shim and M.E. Cates, *J. Phys. (Paris)*, 50 (1989) 3535–3551.

- [35] E.B. Zhulina, O.V. Borisov, V.A. Pryamitsyn and T.M. Birshtein, *Macromolecules*, 24 (1991) 140–149.
- [36] E.T. Vandenberg, L. Bertilsson, B. Liedberg, K. Uvdal, R. Erlandsson, H. Elwing and I. L ndstrom, *J. Colloid Interface Sci.*, 147 (1991) 103–118.
- [37] F.J. Boerio, L. Armogan and S.Y. Cheng, *J. Colloid Interface Sci.*, 73 (1980) 416–423.



Adsorption of PEO was also accomplished *in situ* by mounting a plasma cleaned cantilever to the AFM fluid cell. The fluid cell was mounted on a freshly cleaved mica surface. A 0.1% w/v solution of PEO in 0.1M KNO<sub>3</sub> was injected into the fluid cell.

**Chemical binding.** Synthesis of the aldehyde-terminated PEG (PEG-CHO) was accomplished by a modification of the acetic anhydride method of Harris et al. (19). All solvents, excluding acetic anhydride, were dried over molecular sieves. The formation of aldehydes was monitored at 560 nm using the Schiff reagent (19).

The silicon nitride cantilevers with tip were treated with an oxygen plasma to remove carbon contamination from the surface. Amine groups were incorporated onto the surface by placing the cantilever in a 5% v/v 3-aminopropyltriethoxysilane (APS) in water solution for 10 minutes and then rinsing thoroughly with water (20).

Chemical binding of the PEG 2 kDa to the APS derivatized cantilevers was achieved by placing the cantilevers into a 50 mg/ml solution of PEG-CHO in a pH 5.2 acetate buffered 11% w/v K<sub>2</sub>SO<sub>4</sub> solution at 60°C for 40 hours (20). The cantilevers were rinsed with water and placed in a 8.45 mg/ml solution of NaCNBH<sub>4</sub> in water at room temperature for 4 hr to reduce the Schiff base. The cantilevers were rinsed with water and vacuum dried before use.

**Force plots.** The cantilever tips were positioned near a freshly cleaved mica surface in the AFM fluid cell. 0.1 M KNO<sub>3</sub> was injected into the fluid cell and AFM force-distance plots were obtained by oscillating the piezoelectric crystal with the sample in the z-direction. This commercial instrument requires that the tip 'engages' with the surface before any imaging or force plots are obtained. Except for a few cases, all force plots were obtained from the commercial AFM software. The other method for obtaining force-distance plots uses an external data collection system. The photodiode signal, [A-B]/[A+B], and the voltage signal that drives the piezoelectric crystal in the z direction were collected by a HP 24000A digital oscilloscope (7-bit resolution), which could average the waveforms and store them in memory. A computer program was written to collect and plot the data from the oscilloscope using an HP 9300 computer.

**Ellipsometry.** Measurements of the index of refraction and film thickness were performed on a Rudolph Research model 43603-200E ellipsometer with a 642.8 nm He-Ne laser.

**Computer Modelling.** The computer program POLAD (21) was employed to model the distribution of trains, loops, and tails of the PEO physically adsorbed to the silicon nitride surface. This program is based on interaction parameters of the polymer segments with the surface and the solvent ( $c_s$  and  $c$ ) and considers the chains as connected sequences of segments. For the physically adsorbed PEO, the interaction parameters were 1.00 for the surface and 0.45 for the solvent. The bulk volume fraction,  $f_b$ , was  $10^{-3}$ . Milner has made a quantitative comparison of the experimental forces generated by compression of terminally attached polystyrene brushes with those calculated from self-consistent field equations (22). The theoretical forces are in good agreement with those obtained experimentally, provided the chains are not compressed too much. The program GOLIAD (23) was used here to model the distribution of terminally attached PEG segments and to model the free energy change upon chain compression. A covalent bond was simulated by increasing the interaction energy of one terminal segment until a stable attachment occurred.

## Results and Discussion

ESCA studies of the 'as received' cantilever tips (24) show a considerable amount of carbon on the surface (27%) (Table 1). A high resolution scan of the C(1s) peak shows 82% of the carbon is aliphatic. Oxygen plasma treatment of the cantilever tips shows a decrease in the carbon signal from 27% to 5% indicating that plasma treatment removes this contamination layer. Oxygen plasma treatment also enriches the surface concentration of oxygen from 19% to 33%. We opted for this treatment as chromic acid etching would remove the gold-chromium backing on the cantilever necessary for reflection of the laser beam. The outer 6 - 9 Å of the silicon nitride surface has been reported to be a silicon oxynitride of variable stoichiometry (25-27). The outermost layer of the surface is essentially silicon oxide and behaves just like a silica surface electrophoretically (28). Oxygen plasma treatment then would introduce enough silanol groups to the surface for silane chemistry to occur.

The covalent binding of PEG-CHO 2 kDa on silicon nitride coated silicon wafer pieces was monitored by ESCA. The surface of these wafer pieces were shown by ESCA to be very similar to that of the cantilever tips, especially following oxygen plasma treatment (ESCA results of the oxygen plasma treated wafer piece are also shown in Table 1). The APS derivatized cantilevers show an increase in the carbon signal (from 2 to 19%), a slight reduction in silicon signal, and a reduction of the oxygen signal. In addition, there is a slight increase in the binding energy bandwidth of the N(1s) peak. These results are consistent with the binding of APS to the surface of the silicon nitride coated wafer (20). The PEG bound surfaces show a decrease in both carbon and oxygen content, which is not expected. Yet, the FWHM bandwidth of the O(1s) peak has increased from 1.71 and 1.75 eV for the oxygen plasma treated and APS bound surfaces to 2.30 eV for the PEG bound surface, indicating the presence of an additional chemical species of oxygen. A peak-fitting routine of a high resolution oxygen spectrum reveals an additional peak shifted to lower binding energy by 1.2 eV that comprises 10% of the total oxygen signal. Furthermore, a high resolution spectrum of the C(1s) peak shows that 72% of the carbon signal is in the ether form. These last two results indicate the presence of PEG on the surface of the wafer piece.

Sample	Silicon	Oxygen	Nitrogen	Carbon
As received cantilever	31 %	19 %	22 %	27 %
Plasma treated cantilever	39 %	33 %	22 %	5 %
Plasma treated silicon nitride coated wafer	36 %	20 %	39 %	2 %
APS bound wafer	33 %	27 %	20 %	19 %
PEG 2 kDa bound wafer	36 %	12 %	36 %	16 % (72 %)
PEO 900 kDa adsorbed wafer	34 %	30 %	23 %	12 % (51 %)

Table 1. Summary of ESCA data for silicon nitride cantilevers 'as received' and oxygen plasma modified and for a silicon nitride coated silicon wafer 'as received', oxygen plasma modified, APS modified, PEG bound and PEO adsorbed. The values are in atomic percent. The numbers in the parentheses in the carbon column indicate what percentage of carbon is in the ether form

For the physically adsorbed PEO, high molecular weight polymer was used to prevent spontaneous desorption of the polymer. Although each segment of the PEO adsorbed to the surface may have an interaction energy of a few tenths of a kT, there are so many contacts that adsorption is essentially irreversible (29). Any loosely bound polymer was allowed to desorb by placing the cantilever or silicon nitride coated silicon wafer in polymer-free solution. The ESCA results indicate that of the 12 % of the carbon detected on the surface, 51 % of it is in the ether form. This demonstrates that PEO is present on the surface.

Ellipsometric measurements of the PEO 900 kDa physically adsorbed layer on the plasma cleaned silicon nitride coated wafer indicate that the PEO layer thickness in air is  $1.94 \pm 0.10$  nm using a measured refractive index of 1.94 for silicon nitride and an assumed refractive index of 1.45 for PEO in air.

The results of the computer modelling are shown in Table 2. The POLAD program produces the total adsorbed amount in equivalent monolayers, the ellipsometric thickness in number of segments, and hydrodynamic thickness in number of segments. Thicknesses in nm are calculated using 0.29 nm as the PEO segment length (30). The ellipsometric thickness of the physisorbed PEO 900 kDa layer was calculated to be 1.98 nm. This agrees with the experimental measurement of  $1.94 \pm 0.10$  nm. Also shown in the table is the total amount adsorbed and hydrodynamic thickness. Although, the surface has similar adsorbed amounts, 2.13 vs. 1.98 equivalent monolayers, the hydrodynamic thickness is substantially different. The PEO 900 kDa layer has a hydrodynamic thickness 6 times larger than the PEO 200 kDa layer, at identical hydrodynamic permeabilities. This large difference is attributed to the extension of the tails into the solvent (31). Although the hydrodynamic permeability is not known, it varies over a range of 0.5 to 2.0. Using these values, the hydrodynamic thickness varies between 64 and 102 nm for the physisorbed PEO 900 kDa chains and between 9.9 and 16 nm for the physisorbed PEO 200 kDa chains.

Table 2. Summary of POLAD modelling results for physically adsorbed PEO (900 kDa and 200 kDa) on silicon nitride using a hexagonal lattice,  $c=0.45$ ,  $c_s=1.0$ , and a volume fraction of  $10^{-3}$

System	Adsorbed amount (equivalent monolayers)	Ellipsometric thickness (nm)	Hydrodynamic thickness (nm), ( $c$ = hydrodynamic permeability (21))
adsorbed PEO 900 kDa	2.13	1.98	102 ( $c=0.5$ ) 84 ( $c=1$ ) 64 ( $c=2$ )
adsorbed PEO 200 kDa	1.98	1.73	16 ( $c=0.5$ ) 13 ( $c=1$ ) 9.9 ( $c=2$ )

Y. S. Lin et al. have measured ellipsometrically the maximum amount of PEG 2 kDa bound to a silica surface using the same chemistry described in this manuscript (20). The amount corresponded to 1.8 equivalent monolayers or one PEG 2 kDa chain per  $5 \text{ nm}^2$ . Using GOLIAD we calculated the free energy change for compression of two flat surfaces of PEG 2 kDa chains terminally attached carrying one equivalent monolayer (Figure 1). For one surface, this free energy change is approximately 1 kT per site ( $0.3 \text{ nm}^2$ ) when the separation distance reaches 0.6 nm (2

layers) corresponding to a free energy change of  $4.6 \times 10^{-18} \text{ J nm}^{-2}$  for one surface. Using the Derjaguin approximation relating the force between a sphere and a flat surface to the energy between two flat surfaces,  $F(D) = 2\pi RW(D)$ , and a radius of curvature of 20 nm for the silicon nitride tip (32), a force of 5.7 nN should be observed at a tip surface separation distance of 0.6 nm. At this separation we have calculated a non-retarded van der Waals attractive force of 0.5 nN using a Hamaker constant of  $0.5 \times 10^{-19} \text{ J}$ . The AFM is capable of measuring such forces and it is expected that steric exclusion forces would appear in the force-distance curves.

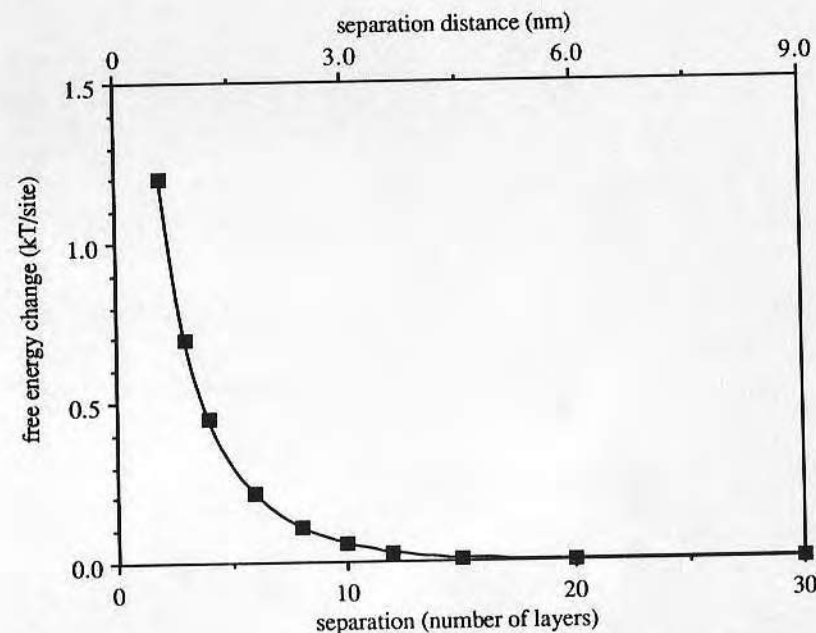


Figure 1. Free energy change due to compression of terminally bound PEG 2 kDa in kT per site as a function of number of layers and separation distance calculated by GOLIAD for 2 flat surfaces.

The AFM force-distance plots were obtained by oscillating the sample up and down and monitoring the response of the AFM cantilever. The sample had to come into contact with the AFM tip and retract from the tip with each oscillation. Under conditions of small cantilever bending, the force exerted on the cantilever is directly related to the extent of bending by  $F = k\Delta x$ , where  $\Delta x$  is the distance the tip of the cantilever has moved and  $k$  is the spring constant of the cantilever.

The AFM force-distance plots are similar, but not identical to the force-distance profiles obtained by the surface force apparatus. The bending of the cantilever can follow the force exerted on it by the sample as long as the spring constant of the cantilever exceeds the force gradient of the exerted force. Otherwise, the cantilever jumps into contact with the surface in an attractive regime and in the repulsive regime, is merely pushed a distance equal to the distance the sample is moved, thus



maintaining a constant separation distance between the two. The same is true in the steric repulsion case; once the force gradient exceeds the cantilever spring constant, the polymer layer can not be compressed by the restoring force of the cantilever. This is depicted as a linear portion in the AFM force-distance plot. With the surface force apparatus, the spring is significantly stiffer so that the spring constant exceeds the force gradients of the force-distance profiles. Only at very small separation distances does the force gradient exceed the spring constant of the cantilever. In addition, there is no independent means of determining the absolute separation distance between the tip and the sample with the AFM. The location of the 'zero' separation distance is arbitrarily defined by the position of the sample where the linear portion of the force-distance plot commences. Retraction of the sample from this location leads to larger separation distances.

Figure 2a depicts a typical force-distance plot in the absence of PEO derivatization. The abscissa is the response of the photodiode and is directly related to cantilever bending. The ordinate is the distance the sample has moved when oscillating up and down (larger separations are to the right). At large separation

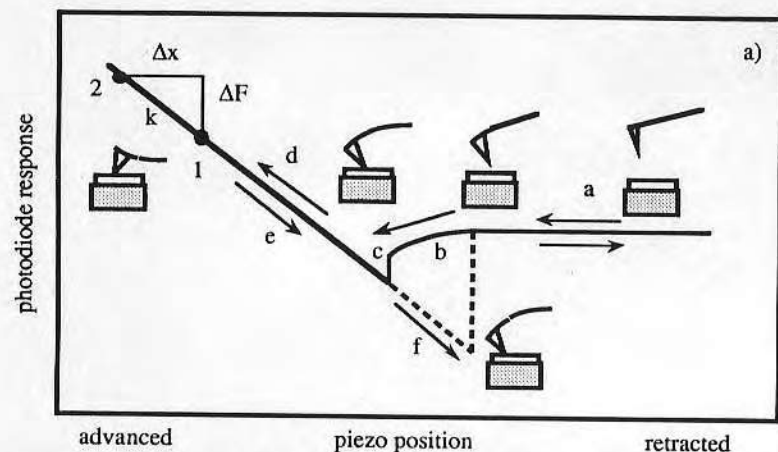


Figure 2a. A schematic of a typical AFM force-distance plot using unmodified tips. The arrows show how the force plot is generated as the sample is advanced and retracted. At (a) the tip and sample are far apart. When the tip gets close enough to experience the attractive van der Waals force, the cantilever starts to bend (b). When the force gradient exceeds the cantilever spring constant, the tip jumps into contact with the surface (c). Once in contact, the tip and sample move the same amount as shown by the linear portion (d). Upon the retraction (e), the cantilever relaxes a distance equal to the amount the sample has been retracted. If there is an adhesive force, then there is hysteresis in the loop (f). The inset depicts the state of cantilever bending. Positions 1 and 2 show how to calibrate the force scale. The distance the cantilever has moved,  $\Delta x$ , multiplied by the spring constant,  $k$ , yields the force difference,  $\Delta F$ , between the two positions.

distances (a), there is negligible force exerted on the cantilever by the sample and there is no cantilever bending as indicated by the flatness of this portion of the plot. As the sample is raised up (b), an attractive van der Waals force is exerted on the tip and the cantilever begins to bend downward. At point (c), the force gradient exceeds

the spring constant of the cantilever and the cantilever 'jumps' into contact with the surface. Further raising of the sample causes the cantilever to deflect an equal amount (d). The beginning of this linear portion is defined as 'zero' separation distance. In reality, the cantilever tip can not get closer to the surface than a few Ångströms. Upon retraction (e), the cantilever relaxes an amount equal to the sample retraction. If there is any adhesion that exists between the tip and sample, the sample must be retracted further for the two surfaces to separate (f). With PEO modified tips (Figure 2b), the steric exclusion force dominates the attractive van der Waals force and a monotonically increasing repulsive force is observed. Only at small separations, where the repulsive force gradient exceeds the cantilever spring constant does the curve become linear, as in the case of an untreated tip. Upon retraction, there is no adhesion and the retraction curve follows the advancing curve.

The abscissa of the plots is already calibrated by the instrument, only the 'zero' separation distance needs to be determined. The ordinate can be easily calibrated to show force units because in the linear region of the force-distance plot, the slope equals  $k$ , the spring constant of the cantilever:  $\Delta F = k\Delta x$  (see Figure 2a). Zero force is defined by the flat part of the plot.

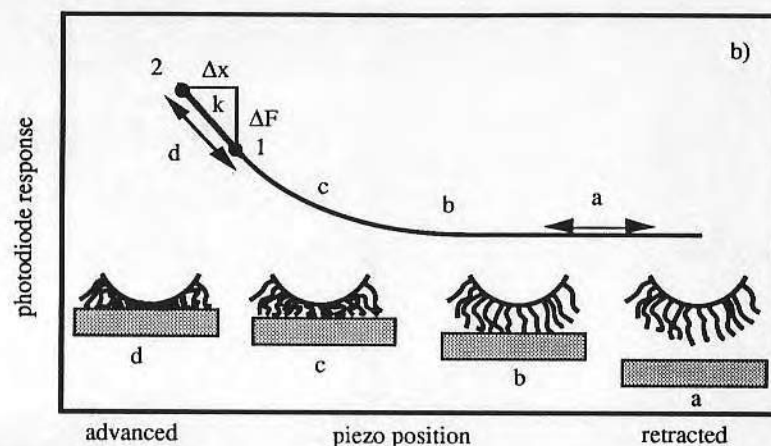


Figure 2b. A schematic of a typical AFM force-distance plot using a PEO modified tip. At (a), there is no interaction between tip and surface. As the chains begin to compress (b) a repulsive steric exclusion force is observed. At (c), the chains are compressed even more producing an even larger repulsive force that dominates the attractive van der Waals force. At (d), the chains are so much compressed that the cantilever spring constant is much weaker than the 'spring constant' of the PEO chains and the cantilever continues to bend upward the same amount as the sample has been moved due to the large repulsive force gradient. Upon retraction, no adhesion is observed (provided there is no bridging) and the curve coincides with the approach curve.

A typical AFM force-distance plot using a plasma cleaned silicon nitride tip and a freshly cleaved mica surface in the presence of 0.1 M  $\text{KNO}_3$  is shown in Figure 3 (plot A). The advancing curve and the receding curve should be coincident along the linear and flat portions, but the instrumentation does not always depict this superposition. In this plot, as is the case in all other plots, the advancing curve is

shown displaced vertically above the receding curve for clarity. This plot shows the jump into contact upon approach of the sample due to the gradient of the attractive van der Waals force exceeding the cantilever spring constant. There is an adhesive force between the tip and sample upon retraction. This adhesion is presumably due to some contamination that exists on the surfaces (33). The magnitude of this adhesive force is on the order of  $0.3 \text{ nN}$  ( $1.0 \text{ div} \cdot 4.03 \text{ nm/div} \cdot 0.064 \text{ nN/nm}$ ). This plot is similar to those obtained by Weisenhorn et al. (3).

Plot B in Figure 3 shows the AFM force-distance curves obtained when a PEG 2 kDa covalently bound to the tip compresses against a freshly cleaved mica sample in the presence of  $0.1 \text{ M KNO}_3$ . A small attractive force just prior to the linear portion of the force-distance plot is observed. This implies that the steric exclusion force at this position is weaker than the van der Waals attractive force. This is not unexpected, since such a small molecular weight PEG is bound to the surface. With a 2 kDa PEG polymer attached, the  $R_g$  is  $1.7 \text{ nm}$  and the steric exclusion force should commence at about  $4 \text{ nm}$  ( $2.5 R_g$ ). Computer modelling by GOLIAD indicated that a force of  $5.2 \text{ nN}$  ( $5.7 \text{ minus } 0.5 \text{ nN}$ ) can be expected at a  $0.6 \text{ nm}$  separation distance when one equivalent monolayer of PEG segments was present on the surface of the probe. Such a force is detectable by the AFM. One possibility why a repulsive force does not appear in this experiment is that a lesser amount of PEG 2 kDa than one equivalent monolayer is bound to the surface.

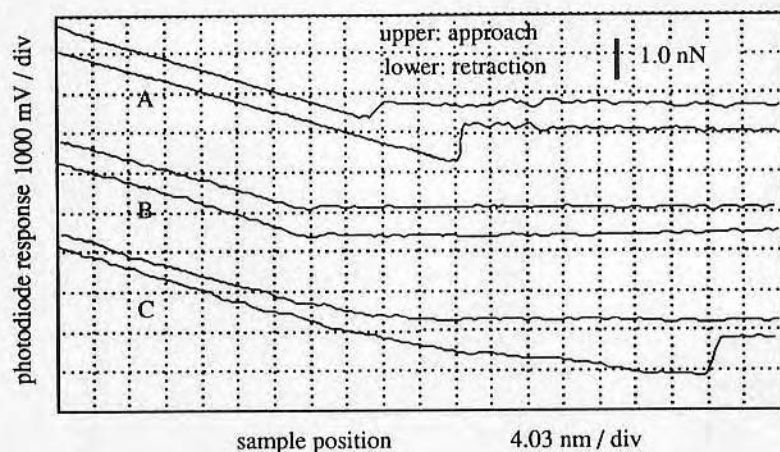


Figure 3. Plot A depicts force-distance curves recorded using a plasma cleaned tip and freshly cleaved mica in the presence of  $0.1 \text{ N KNO}_3$ . These curves display a jump into contact upon approach and an adhesive force upon retraction of the tip. Plot B shows force-distance curves recorded using a PEG 2 kDa treated tip and freshly cleaved mica in the presence of  $0.1 \text{ N KNO}_3$ . This plot does not show a monotonically increasing repulsive force upon approach, but does show an adhesive force upon retraction and is similar to the force-distance plot of a tip plasma cleaned only. Plot C shows force-distance curves recorded using a PEO 900 kDa treated tip and freshly cleaved mica in the presence of  $0.1 \text{ N KNO}_3$ . This plot shows no jump into contact upon approach and an adhesive force upon retraction. The cantilever spring constant was  $0.064 \text{ nN/nm}$  and the frequency of oscillation was  $25 \text{ Hz}$  in all cases.

Plot C in Figure 3 shows AFM force-distance curves recorded using a tip coated with physically adsorbed  $900 \text{ kDa}$  PEO and freshly cleaved mica in  $0.1 \text{ M KNO}_3$ . Upon approach of the sample to the tip, there is a monotonically increasing repulsive force that commences at about  $25 \text{ nm}$  from the linear portion of the force curve which signals the onset of the steric exclusion force. This distance is considerably less than the  $2.5 - 3.5 R_g$  observed in surface force apparatus experiments (12-13). Since in the AFM experiment the sample and the PEO coated tip have to engage with a moderate force prior to obtaining the force curves, it is likely that some of the PEO has been extruded from the contact area. This would result in a steric exclusion force commencing at smaller separation distances. Also shown in Figure 3, plot C is a  $1 \text{ nN}$  adhesive force upon retraction. The presence of this adhesive force can be explained by the bridging that occurs between the PEO and the uncovered mica surface (34). This is a reasonable explanation since the surfaces were compressed together with a force of  $50 - 100 \text{ nN}$ . When one considers that the contact area is small, perhaps on the order of  $100 \text{ nm}^2$ , the pressure between the silicon nitride tip and the mica is in the MPa to GPa range. This pressure can force the PEO to make contacts with the surface even though the duration of contact is short ( $25 \text{ Hz}$  oscillation of the piezoelectric crystal). One notes that the adhesive force is also non-linear which indicates that there has been a transfer of chains from the tip to the surface which become entangled upon compression and become untangled upon retraction.

Force-distance curves have also been obtained with a plasma cleaned probe and mica in a  $0.1\%$  PEO  $900 \text{ kDa}$  solution containing  $0.1 \text{ M KNO}_3$  so that PEO adsorbs on both surface and AFM tip. The first force-distance curve was taken within a few minutes of injection of the PEO solution (Figure 4, plot A). After  $8 \text{ hr}$  of incubation (Figure 4, plot B), a repulsive force develops for both approaching and receding curves. This phenomenon has also been observed by Klein and Luckham with the surface force apparatus (34). The repulsive force commences at a distance of  $100 \text{ nm}$  from the contact point. This distance is about  $6 R_g$  and agrees well with the observations of Klein and Luckham. Continued compression cycles strip the PEO from the contact area as evidenced by the appearance of an adhesive force upon retraction (Figure 4, plot C). The repulsive force commencing at only  $50 \text{ nm}$  is another indicator of this PEO expulsion.

To verify the existence of the effect of tip curvature, we have performed identical experiments, but now with the PEO adsorbed only to the silicon nitride substrate. PEO  $200 \text{ kDa}$  and  $900 \text{ kDa}$  were physisorbed on a silicon nitride surface and obtained force-distance curves with a plasma cleaned probe. Figure 5 (plot A) shows the initial force-distance curves with PEO  $900 \text{ kDa}$ . The repulsive steric exclusion force commences at around  $50 \text{ nm}$ , which is agrees with a  $3 R_g$  distance of  $51 \text{ nm}$  expected for one modified surface. Again, continued compression cycles results in the development of an adhesive force due to polymer expulsion. Occasionally, force-distance curves similar to that shown in Figure 5 (plot B) will appear. The sawtooth appearances upon retraction are a result of either PEO bridging that occurs between the probe and the surface or chain entanglement of the PEO on both surfaces. If there is bridging, then as the sample is retracted there is resistance to separation due to the bridging. The adhesion, however, terminates sharply when the retraction force 'snaps-off' the PEO chains from the surface. This particular curve shows a series of three successive releases of the PEO from the neighboring surface, each one having longer chain lengths between the bridging points. If there is chain entanglement, however, then the resistance to separation is due to interlocking of the chains from the two surfaces. The three abrupt jumps to zero force would then be a result of the chains becoming untangled or the chains being pulled off the surface by the retracting entanglement.

Figure 6 shows two force-distance plots for a PEO  $200 \text{ kDa}$  adsorbed silicon nitride surface. The initial curve recorded at the pristine site (Figure 6, plot A) shows



the repulsive steric exclusion force upon approach, but an adhesion due to PEO expulsion upon withdrawal. The repulsive steric repulsion force commences at about 25 nm which is in agreement with the 25 nm expected for a  $3 R_g$  distance with only one surface modified. Subsequent compressions at the same site (Figure 6, plot B) show the development of a jump into contact and a large retractive adhesive force, both indications of further PEO expulsion.

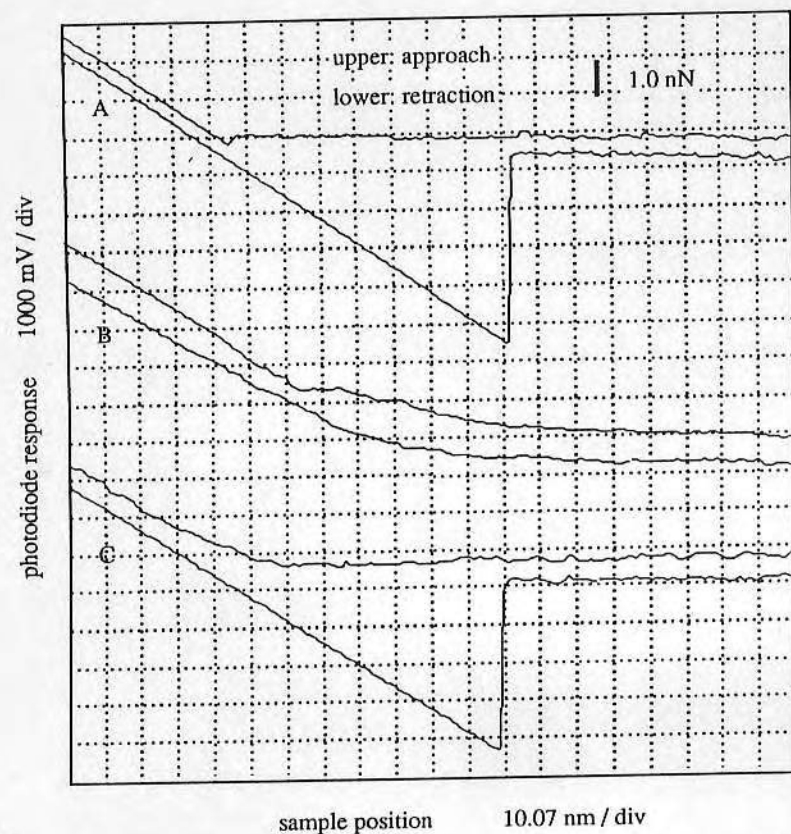


Figure 4. This series of force-distance plots shows the measured forces when a plasma cleaned tip and mica are used to obtain force-distance plots in the presence of a 0.1 % w/v PEO 900 kDa solution containing 0.1N  $\text{KNO}_3$  as a function of incubation time. Immediately after injection (plot A), following an 8 hour incubation (plot B), and after 2 minutes of oscillations following an 8 hour incubation (plot C). The cantilever spring constant was 0.064 nN/nm and the frequency of oscillation was 1 Hz.

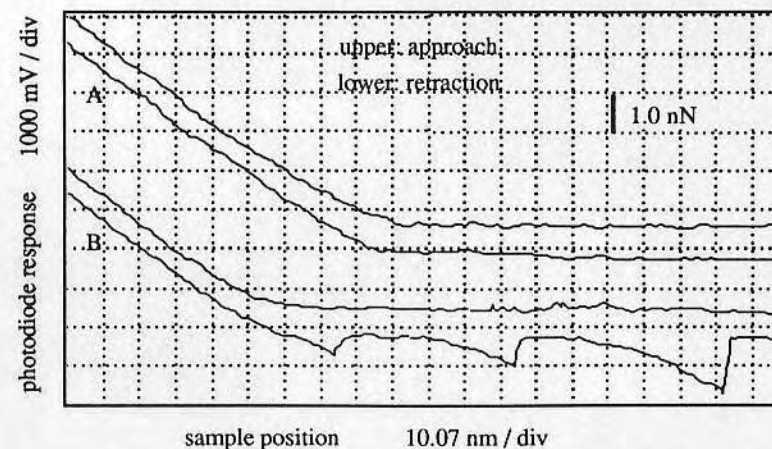


Figure 5. Two force-distance plots obtained when the PEO 900 kDa has been physically adsorbed to the silicon nitride surface in the presence of 0.1 N  $\text{KNO}_3$ . A pristine site compression cycle is shown by the curves A. Occasionally, a compression cycle would yield a force-plot similar to the curves B. Here, a series of adhesive "snap-offs" upon retraction is most likely due to the ripping of PEO chains off from one of two surfaces after they have bridged the two surfaces. The cantilever spring constant was 0.064 nN/nm and the frequency of oscillation was 1 Hz.

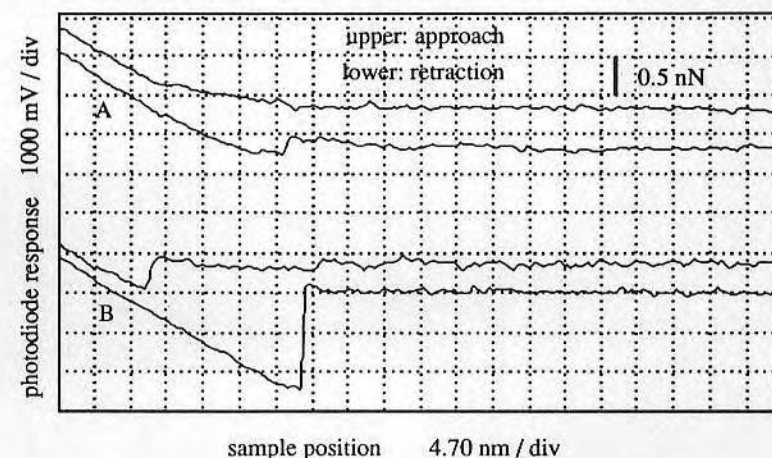


Figure 6. Two force-distance plots obtained when the PEO 200 kDa has been physically adsorbed to the silicon nitride surface in the presence of 0.1 N  $\text{KNO}_3$ . As in figure 5, an pristine site is used to obtain a force plot (plot A). After several compressions (plot B) a jump into contact and an adhesive component developed indicating that the PEO has been expelled from the contact area. The cantilever spring constant was 0.064 nN/nm and the frequency of oscillation was 1 Hz.

### Conclusions

PEO of high molecular weight was physically adsorbed to AFM cantilever probes. These probes initially produced steric exclusion forces in 0.1 M KNO<sub>3</sub> upon compression of the adsorbed PEO chains by the sample. The observation of a steric exclusion force commencing at a distance less than 2.5 - 3.5 R<sub>g</sub> was an indication of expulsion of the PEO from the contact area. Also, observed was the presence of a long range attractive force upon retraction of the sample. The origin of this force is likely due to bridging that occurs between the uncoated surface and the physically adsorbed PEO. PEO physically adsorbed to the sample also demonstrated steric exclusion forces, expulsion of PEO from the contact area and bridging of the PEO to the uncoated probe.

Force-distance curves obtained in 0.1 M KNO<sub>3</sub> containing 0.1 % PEO showed no repulsive steric exclusion force initially. After 8 hr of incubation, a steric expulsion force was observed which commenced at a distance near 6 R<sub>g</sub>. Often curves which demonstrated bridging or entanglement were visible.

PEG with a molecular weight of 2 kDa was chemically bound to the surface of the silicon nitride tip, as shown by ESCA. Magnitude calculations from GOLIAD indicate that a steric repulsive force of 6 nN would be present at a separation distance of 0.6 nm. The force-distance plots do not show a monotonically increasing repulsive force, indicating that there is much less than one equivalent monolayer of PEG on the surface or the force gradient is larger than the cantilever spring constant at a measurable force.

### Acknowledgements

The authors wish to thank Y.-S. Lin for assistance in the PEG surface binding chemistry, A. Pungor and E. W. Stroup for technical assistance and helpful discussions, and P. Barnevald and late J. M. H. M. Scheutjens for providing us with the computer modelling programs POLAD and GOLIAD. We also are grateful for financial support provided by the NIH (Grant HL-44538-02) and the University of Utah Graduate Research Committee.

### Literature Cited

- Binnig, G.; Quate, C. F.; Gerber, C. *Phys. Rev. Lett.* **1986** *56*, 930-933.
- Martin, Y.; Williams, C. C.; Wickramasinghe, H. K. *J. Appl. Phys.* **1987** *61*, 4723-4729.
- Weisenhorn, A. L.; Hansma, P. K.; Albrecht, T. R.; Quate, C. F. *Appl. Phys. Lett.* **1989** *54*, 2651-2653.
- Albrecht, T. R. *Ph.D. Dissertation*, Stanford University 1989.
- Pashley, R. M. *J. Colloid Interface Sci.* **1981** *80*, 153-162.
- Hartmann, U. *Ultramicroscopy* **1992** *42-44*, 59-65.
- McClelland, G. M.; Erlandsson, R.; Chiang, S. In *Review of Progress in Quantitative Nondestructive Evaluation*, **1987** *6B*, 1307-1314.
- Stern, J. E.; Terris, B. D.; Mamin, H. J.; Rugar, D. *Appl. Phys. Lett.* **1988** *53*, 2717-2719.
- Ducker, W. A.; Senden, T. J.; Pashley, R. M. *Nature* **1991** *353*, 239-241.
- Martin, Y.; Wickramasinghe, H. K. *Appl. Phys. Lett.* **1987** *50*, 1455-1457.
- Grütter, P.; Meyer, E.; Heinzelmann, H.; Rosenthaler, L.; Hidber, H.-R.; Güntherodt, H.-J. *J. Vac. Sci. Technol.* **1988** *A6*, 279-282.
- Klein, J.; Luckham, P. *Nature* **1982** *300*, 429-431.
- Claesson, P. M.; Gölander, C.-G. *J. Colloid Interface Sci.* **1987** *117*, 366-374.
- Taunton, H. J.; Toprakcioglu, C.; Fetters, L. J.; Klein, J. *Nature* **1988** *332*, 712-714.

- de Gennes, P. G. *Macromolecules* **1981** *14*, 1637-1644.
- Milner, S. T. *Science* **1991** *251*, 905-914.
- Lea, A. S.; Pungor, A.; Hlady, V.; Andrade, J. D.; Herron, J. N.; Voss Jr., E. W. *Langmuir* **1992** *8*, 68-73.
- Marchant, R. E.; Lea, A. S.; Andrade, J. D.; Bockenstedt, P. J. *Colloid Interface Sci.* **1992** *148*, 261-272.
- Harris, M. J.; Struck, E. C.; Case, M. G.; Paley, M. S.; Van Alstine, J. M.; Brooks, D. E. *J. Polymer Sci., Polym. Chem. Ed.* **1984** *22*, 341-352.
- Lin, Y.-S. and Hlady, V. *Book of Abstracts, Part I*, 203rd ACS National Meeting, ACS, San Francisco, 1992, abstr. # COLL361.
- Scheutjens, J. M. H. M.; Fleer, G. J.; Cohen Stuart, M. A. *Colloids Surfaces* **1986** *21*, 285-306.
- Milner, S. T. *Europhys. Lett.* **1988** *7*, 695-699.
- Barnevald, P. A.; *Doctoral Thesis*, Agricultural University, Wageningen, The Netherlands, 1991.
- The ESCA data were actually obtained from the chip holding the cantilever. Being of the same surface chemistry, the tip and the chip are expected to produce similar results.
- Sobolewski, M. A.; Helms, C. R. *J. Vac. Sci. Technol.* **1988** *A6*, 1358-1362.
- Bergström, L.; Bostedt, E. *Colloids Surfaces* **1990** *49*, 183-197.
- Bergström, L.; Pugh, R. J. *J. Am. Ceram. Soc.* **1989** *72*, 103-109.
- Jaffrezic-Renault, N.; De, A.; Clechet, P.; Maaref, A. *Colloids Surfaces* **1989** *36*, 59-68.
- Fleer, G. J.; Lyklema, J. In *Adsorption from Solution at the Solid/Liquid Interface*; Parfitt, G. D. and Rochester, C. H., Eds., Academic Press: London, UK, 1983, pp 153-220.
- Ben Ouada, H.; Hommel, H.; Legrand, A. P.; Balard, H.; Papirer, E. *J. Colloid Interface Sci.* **1988** *122*, 441-449.
- Cohen Stuart, M. A.; Waajen, F. H. W. H.; Cosgrove, T.; Vincent, B.; Crowley, T. L. *Macromolecules* **1984** *17*, 1825-1830.
- Albrecht, T. R. *Ph.D. Thesis*, Stanford University, 1991.
- Drake, B.; Prater, C. B.; Weisenhorn, A. L.; Gould, S. A. C.; Albrecht, T. R.; Quate, C. F.; Cannell, D. S.; Hansma, H. G.; Hansma, P. K. *Science* **1989** *243*, 586-589.
- Klein, J.; Luckham, P. F. *Nature* **1984** *308*, 836-837.

RECEIVED February 23, 1993

Reprinted from ACS Symposium Series No. 532  
*Colloid-Polymer Interactions: Particulate, Amphiphilic, and Biological Surfaces*  
 Paul L. Dubin and Penger Tong, Editors  
 Copyright © 1993 by the American Chemical Society  
 Reprinted by permission of the copyright owner



# Colloid-Polymer Interactions

## Particulate, Amphiphilic, and Biological Surfaces

**Paul L. Dubin, EDITOR**

*Indiana University-Purdue University*

**Penger Tong, EDITOR**

*Oklahoma State University*

Developed from a symposium sponsored  
by the Divisions of Polymer Chemistry, Inc.,  
and of Colloid and Surface Chemistry  
at the 203rd National Meeting  
of the American Chemical Society,  
San Francisco, California,  
April 5-10, 1992



American Chemical Society, Washington, DC 1993



Ab-Lee, H. 1

UTEC 72-072  
April 1972

RADIATION GRAFTING OF SYNTHETIC HYDROGELS TO INERT POLYMER SURFACES  
1. HYDROXYETHYL METHACRYLATE

by

H. B. Lee, H. S. Shim, and J. D. Andrade  
Division of Materials Science and Engineering  
University of Utah  
Salt Lake City, Utah 84112

Background and Rationale

There is great interest in the development of materials which can be used for biomedical applications, such as implants, tissue culture substrates, extracorporeal devices, sensors, etc. Most of the materials used for implant applications are the relatively inert, hydrophobic polymers, such as polydimethyl siloxane, polyethylene terephthalate, and polytetrafluoroethylene. The fact that these materials have such low surface free energies (25, 43, 17 ergs/cm<sup>2</sup>, respectively) means that their interfacial free energies in an aqueous medium must be quite high. The air/water interfacial energy is 73 ergs/cm<sup>2</sup>; this is sufficient to denature proteins and produce cellular damage - one might expect interfacial energies of the order of 50 ergs/cm<sup>2</sup> to do likewise.

We have previously hypothesized that an interface with aqueous solutions of minimum interfacial energy is desirable for biological tolerability. Such an interface is approached with highly water swollen, non-ionic, synthetic gels, such as the hydroxy alkyl methacrylates(3). Wichterle and Lim have proposed many medical applications for such gels(3). These materials are quite stable in aqueous solutions and do not suffer from hydrolysis, as do many other gel systems.

The problem of poor mechanical strength of gels may be circumvented by utilizing the unique biological compatibility of a gel only at the surface of the device, perhaps as a simple coating. Theoretical evidence(4) indicates that a neutral interface of the order of a hundred Angstroms thick and having a high water content will not adsorb compounds from an aqueous solution. The interfacial tension of a gel interface approaches zero and thus there is little free energy advantage in adsorption.

One may obtain the biocompatibility characteristics of a gel with the desired physical and mechanical properties of a substrate material by surface grafting or coating(5). The interface between the gel surface and the solution is not a true interface at all. Lightly crosslinked gel systems are not "inert, passive" barriers or discontinuities in a physiological environment. Ionic transport, molecular migration and water transport can occur.

Our group(5) and Hoffmann, et al.(6) have demonstrated that hydroxyethyl methacrylate (HEMA) can be radiation grafted onto inert polymeric substrates.

Experimental Methods

Hydroxyethyl methacrylate (HEMA), (Hydron Labs., New Brunswick, New Jersey) was used without further purification. The composition was 0.012% ethylene glycol dimethacrylate and 0.15% methacrylic acid.

Polydimethyl siloxane elastomer (Silastic, Medical Grade, Dow Corning Company, Midland, Michigan) and a commercial polypropylene film (Utah Plastics Company, Salt Lake City, Utah) were of 0.005 inch thickness. Ethanol (95%) was used as the solvent; reagent grade C Cl<sub>4</sub> was used as a chain transfer agent(7).

*polymer preprints*

*Vol. 13, No. 2, 1972*



The samples were cut, washed with soap, acetone, and ethanol, and dried at 60°C under vacuum (1 mm Hg) for eight hours; the initial weight,  $W_0$ , was then measured. The HEMA concentration in ethanol was 0, 5, 10, 15, or 20 wt %. The radiation dose ranged from 0 to 1.5 Mrads with a 350 rad/minute  $Co^{60}$  source. Grafting was by the mutual irradiation method at room temperature. Inert gas was not passed through the solution.

The grafted samples were extracted in ethanol at 60°C for 24 hours. The extracted samples were then placed in distilled water for 24 hours at room temperature for swelling, blotted dry of surface water with absorbent paper and weighed to determine the total weight of the swollen samples,  $W_s$ . The sample is then dried at 60°C under vacuum (1 mm Hg) for eight hours, and the dry grafted weight,  $W_g$ , was determined. The net weight increase due to grafted HEMA,  $\Delta W_{HEMA}$ , and the fraction of water in the graft,  $W_f$ , were obtained:

$$\Delta W_{HEMA} = (W_g - W_0)/\text{area}$$

$$W_f = \frac{\Delta W_s}{\Delta W_s + \Delta W_{HEMA}}, \text{ where}$$

$$\Delta W_s = (W_s - W_0)/\text{area}$$

Each of the grafted surfaces on polypropylene and polydimethyl siloxane substrates were examined in the dry state, by scanning electron microscopy. A Cambridge Stereoscan Mark II scanning electron microscope was operated at 20 kv. All samples were gold coated.

Tensile specimens (Type D ASTM D-11 die) were prepared in the manner described and tested in an Instron Corporation Model 1130 Testing Machine using a crosshead speed of 2 inches/minute for polypropylene and 10 inches/minute for Silastic. The samples were tested fully wet.

## Results and Discussion

Figure 1 presents the dry graft weight per unit sample area as a function of total dose for various monomer solutions and a polypropylene substrate. Analogous data for polydimethyl siloxane (Silastic) substrates is given in Figure 5. Figures 2 and 6 present the distilled water swelling data for polypropylene and Silastic substrates. Elongation and yield stress results are given in Figures 3, 4, 7, and 8.

The dry weight increase is roughly linear at low doses, reaches a maximum, and then decreases. A plateau is reached with polypropylene, though the Silastic substrate graft appears to further degrade with increasing dose. The highest monomer concentrations (20%) gives the smallest maximum and apparently the most rapid initial degradation. Maximum graft in polypropylene for the 5, 10, and 15% solutions is about 0, 3.6, and 5.0 mg/cm<sup>2</sup>, respectively, for a 0.5 Mrad dose.

The Silastic results are quite different. Maximum graft occurs with maximum monomer concentrations, but degradation occurs at lower doses with increasing monomer levels. As expected, the amount of material grafted is higher than in the polypropylene; much of the Silastic graft is internal, as the sample swells greatly during the grafting process.

The fraction of water in the gel graft is of major interest to us (Figures 2 and 6). It is clear from Figure 2 that the water fraction increases almost linearly with dose, up to 0.5 Mrad. Comparison with Figure 1 indicates that the water fraction is increasing with graft thickness. Figures 9a to 9e are a series of scanning electron micrographs of these

surfaces. Figure 9a is the control substrate. Figure 9b represents a sample grafted in 5% monomer solution. There is no apparent morphological change - in agreement with Figures 1 and 2 which indicate negligible grafting. Figures 9c and 9d represent a 15% monomer solution and total doses of 1/4 and 1 Mrad, respectively. We interpret this as follows: The grafting at low doses may begin somewhat uniformly. As the dose increases, the surface graft becomes heterogeneous, reaching a plateau heterogeneity at a dose of about 0.5 Mrad for these samples. As the heterogeneities develop, water can condense between the asperities, leading to a higher apparent graft water content. This apparently occurs in a roughly linear manner with dose. The effect plateaus off at 0.5 Mrad, when the grafted weight no longer increases with dose.

The silicone rubber material does not show this effect. Figure 10 represents the Silastic surface. No surface morphological changes are evident over the ranges studied (Figure 5). The water fraction for the Silastic substrate is 20 to 30%, independent of dose and graft thickness. This may be a little lower than expected(5) as some of the graft is internal and unavailable for water interaction.

The mechanical properties data indicate significant changes in the polypropylene substrate at doses of the order of 0.1 Mrad and higher. This could be due to surface oxidation during grafting. Mechanical changes in the Silastic material are also evident at doses greater than 0.1 Mrad. Though the grafted material is stronger, its lower elongation might be a problem in implant applications where flexibility and fatigue resistance is desired.

Detailed surface characterization of these systems is presently being completed, including wetting kinetics, equilibrium contact angles, protein adsorption, and analysis of surface heterogeneity.

The micrographs presented, Figure 10a to 10e, represent a true surface heterogeneity. They are not dehydration artifacts. The heterogeneous nature of these polypropylene grafts are clearly evident optically, even with a totally wet sample which has never been dried.

## Conclusions

Dry graft weight and water swelling data have been presented for grafts of HEMA onto polypropylene and polydimethyl siloxane substrates. The results have been interpreted in terms of surface morphology, as detected by scanning electron microscopy and optical examination. Mechanical property data was also presented.

The heterogeneous nature of HEMA grafts onto some substrates must be considered in analyzing any interfacial phenomenon associated with these systems.

## Acknowledgements

This work is supported by the U. S. Atomic Energy Commission, Division of Applied Technology, Contract AT(11-1)-2147. Stimulating discussions with Professor Allan Hoffman (University of Washington, Seattle, Washington) and Professor W. O. Statton (University of Utah, Salt Lake City, Utah) have aided us in this work. Mr. Richard Van Wagenen produced the scanning electron micrographs.

# References

1. J. D. Andrade and S. W. Kim, Prog. Chem. and Chemical Industry (Korea), 12, (1972) in press.
2. J. D. Andrade, K. Kunitomo, R. Van Wageningen, B. Kastigir, D. Gough, and W. J. Kolff, Trans. Amer. Soc. Artificial Internal Organs, 17, 222 (1971).
3. O. Wichterle and D. Lim, Nature, 185, 117 (1960).
4. J. D. Andrade, Dissertation Abstracts, 30, 3614-B (1970).
5. J. D. Andrade, D. Gough, R. Van Wageningen, D. Hill, Macromolecular Preprints, 1, 23rd Int. Cong. Pure Appl. Chem., (1971) p. 620.
6. A. S. Hoffman, G. Schuer, C. Harris, and W. Kraft, Trans. Amer. Society Artificial Internal Organs, 18, (1972) in press.
7. H. F. Hamil, M. Adams, W. Harlowe, Jr., and E. C. Martin, J. Polymer Sci., A-1, 363 (1971).

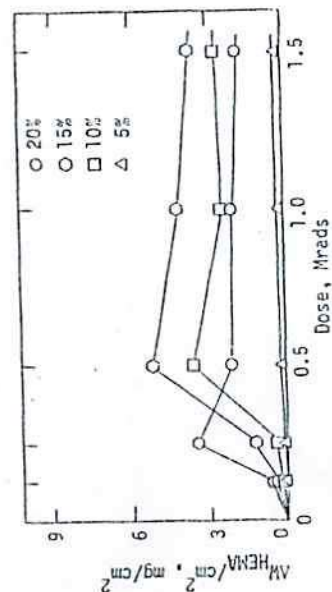


Figure 1. Dry Graft vs Dose for HEMA on Polypropylene

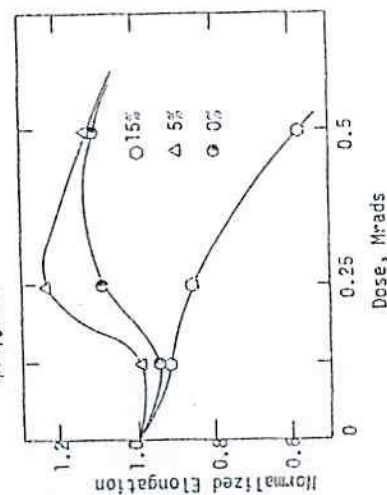


Figure 3. Normalized Elongation vs Dose for HEMA on Polypropylene

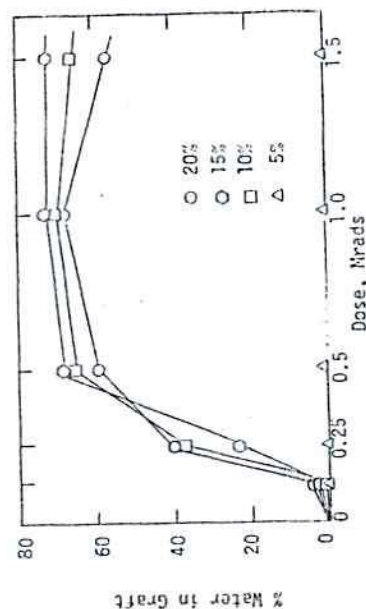


Figure 2. Graft Water Concentration vs Dose for HEMA on Polypropylene

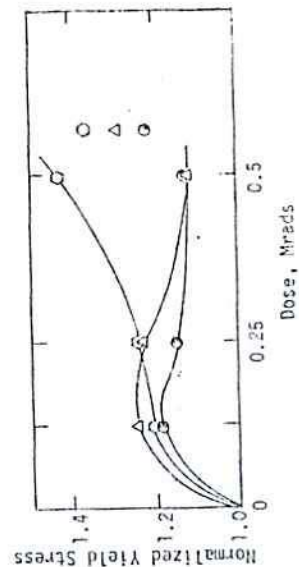


Figure 4. Normalized Yield Stress vs Dose for HEMA on Polypropylene



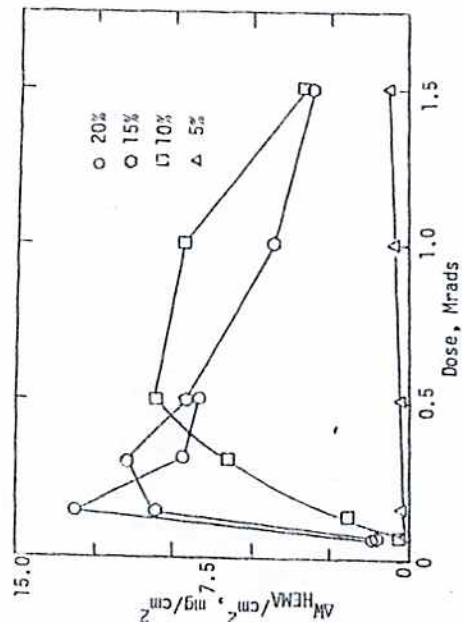


Figure 5. Dry Graft vs Dose for HEMA onto Polydimethyl Siloxane (Silastic)

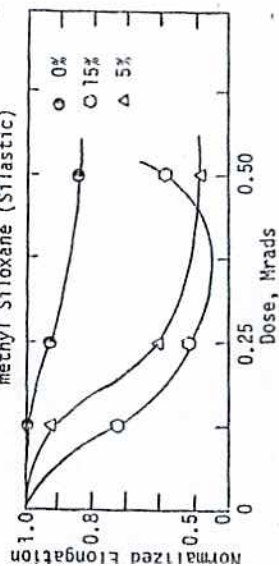


Figure 7. Normalized Elongation vs Dose for HEMA on Silastic

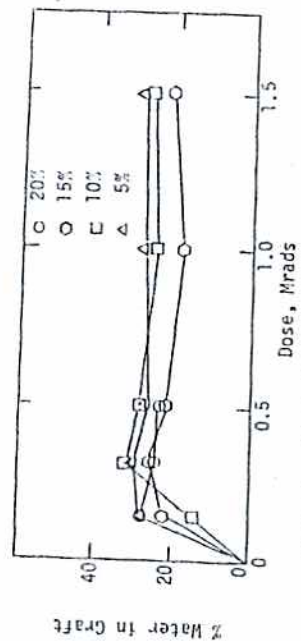


Figure 6. Graft Water Concentration vs Dose for HEMA onto Silastic

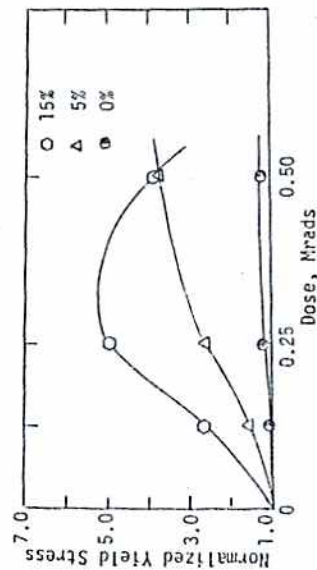


Figure 8. Normalized Yield Stress vs Dose for HEMA on Silastic

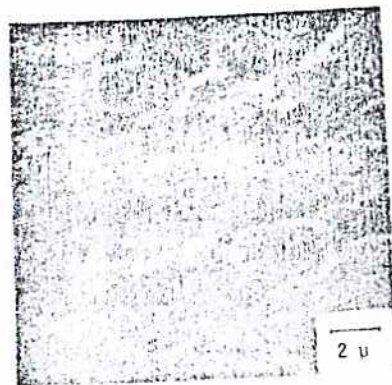


Figure 9a

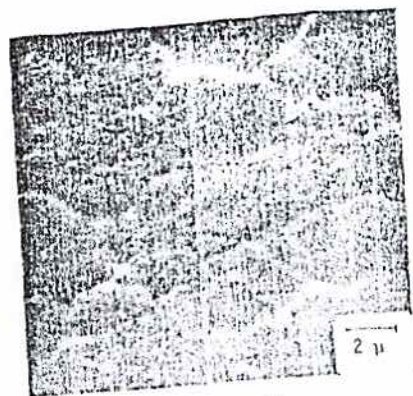


Figure 9b

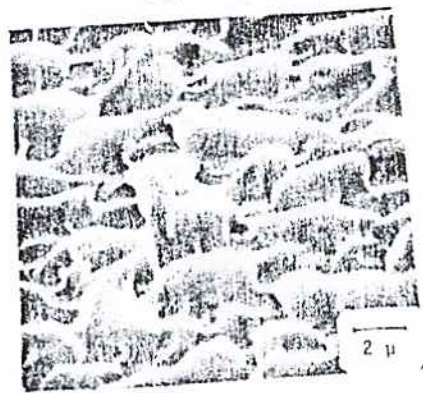


Figure 9c

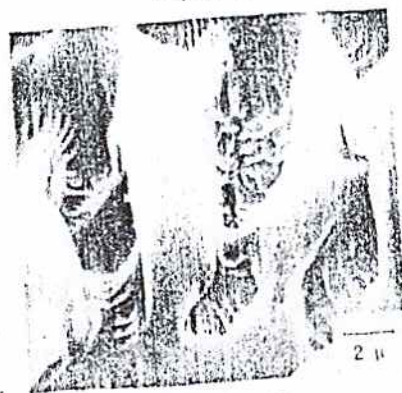


Figure 9d

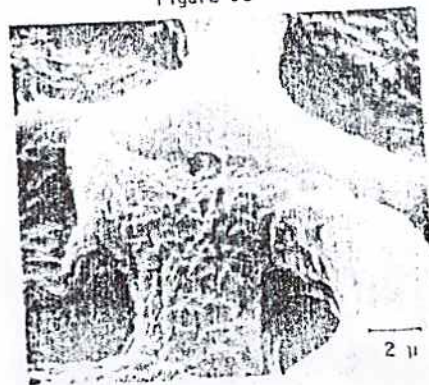


Figure 9e

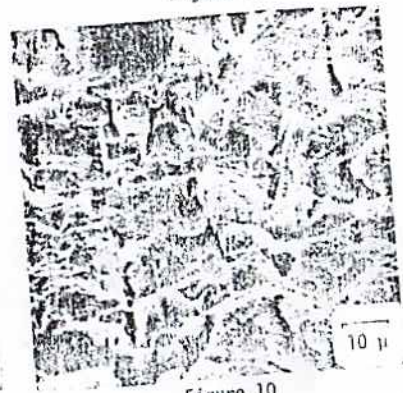


Figure 10

Figure 9. SEM photos of HEMA grafts on polypropylene; original magnifications, 5000 X. (a) control, (b) 5% HEMA, 1 Mrad, (c) 15% HEMA, 0.25 Mrad, (d) 15% HEMA, 1 Mrad, (e) 20% HEMA, 0.5 Mrad.

Figure 10. SEM of HEMA on Silastic, control, 1 Mrad, 1000 X; There is no apparent change in surface morphology with increasing dose.

## Nature of Water in Synthetic Hydrogels

### I. Dilatometry, Specific Conductivity, and Differential Scanning Calorimetry of Polyhydroxyethyl Methacrylate

HAI BANG LEE, MU<sup>-</sup>SHIK JHON,\* JOSEPH D. ANDRADE†

*Department of Materials Science and Engineering, University of Utah, Salt Lake City, Utah 84112*

Received June 11, 1974; accepted December 30, 1974

Three classes of water may exist in certain hydrogels. We have previously labeled these as *X* water (bulk water), *Z* water (bound water) and *Y* water (intermediate forms we call interfacial water). Bulk gel conductivity data for poly (2-hydroxyethyl methacrylate) (PHEMA) were obtained. The activation energy for specific conduction was calculated. A plot of the activation energy versus wt percent of water in the gel clearly indicated three different zones, showing three possible classes of water in the gels. These results were confirmed by thermal expansion measurements. The high water content gels (50%) demonstrated an extremely sharp volume change at 0°C, indicating the presence of normal bulk water. Lower water content gels (20%) showed no anomalous change in thermal expansion, indicating that the water is bound. The medium water content gels exhibited intermediate behavior. A semiquantitative analysis of the three classes of water is presented. A further verification of these results was obtained by differential scanning calorimetry (DSC) studies. The low water content gel (20%) consists mainly of bound water, which exhibited no phase transitions over the range -15 to 24°C. The high water content gels showed phase transitions near 0°C. The medium water content gels show gradual shifts of the phase transition temperatures near 0°C.

#### INTRODUCTION

There is substantial interest in the development of synthetic hydrogels for biomedical applications (1-3). There has been some interest in the possible correlation between the nature of water in hydrogels and their biomedical properties (2, 3). As the blood compatibility of hydrogels is not necessarily a simple function of gel water content (2, 3), it is reasonable to suspect that the nature of water in the gels and at the gel interface may be important (3).

Drost-Hansen (4) has discussed a three layer model for the structure of water near certain water/solid interfaces. Aizawa *et al.* (5-7) have proposed that water in natural macromolecular gels be classified into three

groups according to their experimental data from specific conductivity, dilatometry and NMR measurements. Krishnamurthy *et al.* (8) have indicated the existence of three states of water in membranes of cellulose acetate by NMR studies.

We have also suggested that hydrogels may contain three classes of water: *X* water (bulk water-like), *Z* water (bound water-like) and *Y* water (intermediate forms which we have chosen to call interfacial water) (9). To check the validity of the hypothesis, dilatometric, specific conductivity, and differential scanning calorimetry (DSC) studies have been carried out from -15°C to room temperature for poly(hydroxyethyl methacrylate) (PHEMA) gels of various water contents.

#### MATERIALS AND METHOD

Commercial 2-hydroxyethyl methacrylate (HEMA) was obtained (Trans Chemic Indus-

\* On leave from the Korea Advanced Institute of Science, Seoul, Korea.

† To whom correspondence should be addressed.



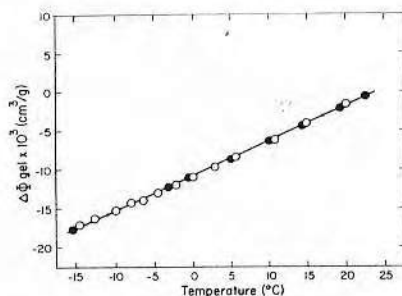


FIG. 1. The specific volume change  $\Delta\Phi_g \times 10^3$  ( $\text{cm}^3/\text{g}$ ) versus temperature ( $^{\circ}\text{C}$ ) for a 20% water PHEMA gel.

tries, Inc., New York, N. Y.) and used as received. The impurity content was 0.5% free acid and 0.3% diester. One percent by weight of ethylene dimethacrylate (EDMA) cross linker was added unless otherwise noted. The redox initiator used was  $10^{-3}$  mole of  $\text{Na}_2\text{S}_2\text{O}_8$  and of  $(\text{NH}_4)_2\text{S}_2\text{O}_8$  (10–12). The monomer was dissolved in the desired amount of distilled water, and the solution was polymerized in a  $60^{\circ}\text{C}$  water bath for one hour. The impurity levels present did not significantly affect the physical properties discussed here. The gels thus contained the amount of water present in the original monomer solution. They were not equilibrated with water. A constant temperature circulator with  $\pm 0.02^{\circ}\text{C}$  control accuracy was used as a temperature bath for both specific conductivity and dilatometric studies. Equilibrium temperatures were obtained after equilibrating the gels for three hours for each measurement.

#### A. Dilatometric Measurements

The dilatometer (5) was filled with the sample and mercury. Thermal expansion measurements were determined at temperatures ranging from  $-15^{\circ}\text{C}$  to  $24^{\circ}\text{C}$ . The total volume change,  $\Delta\Phi_{\text{tot}}$ , is given by the following equations (5):

$$\begin{aligned}\Delta\Phi_{\text{tot}} &= \Delta\Phi_{\text{gel}} + \Delta\Phi_{\text{Hg}}, \\ \Delta\Phi_{\text{gel}} &= \Delta\Phi_{\text{tot}} - \Delta\Phi_{\text{Hg}}, \\ &= \{(h - h^{\circ})\end{aligned}\quad [1]$$

$$- (1/S)Q_{\text{Hg}}V_{\text{Hg}}^{24}(t - 24)\}(S/M_s), \quad [2]$$

where  $\Delta\Phi_{\text{Hg}}$  is the specific volume change of the mercury and  $\Delta\Phi_{\text{gel}}$  is the specific volume change of the gel;  $h$  and  $h^{\circ}$  are the height of the mercury column at the temperature  $t^{\circ}$  and  $24^{\circ}\text{C}$  (the reference temperature), respectively;  $S$  is the capillary cross sectional area ( $\text{cm}^2$ );  $Q_{\text{Hg}}$  is the thermal expansion coefficient of mercury (13);  $V_{\text{Hg}}^{24}$  is the volume of the mercury in the dilatometer at  $24^{\circ}\text{C}$ ; and  $M_s$  is the mass of the sample. The data are reproducible within  $\pm 2\%$ .

#### B. The Specific Conductivity

The specific conductivity was measured with an impedance bridge (Electro Scientific Industry, Inc. Model 291B), using a 1000 Hertz AC signal. The use of alternating current avoids polarization of the electrode in the conduction cell (14, 15). The design of the cell and other experimental details are available (15). Platinum foil (A. D. McKay Co., New York) was used for electrodes; the electrodes were not platinized.

#### C. Differential Scanning Calorimetry

The transition points of water in the gels were determined with a Perkin-Elmer DSC-1B differential scanning calorimeter. The sample (20 to 30 mg) was cooled from room temperature to  $-20^{\circ}\text{C}$  at cooling rates of  $1.25^{\circ}\text{C}/\text{min}$ ,

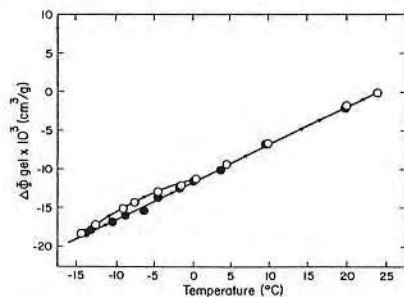


FIG. 2. The specific volume change  $\Delta\Phi_g \times 10^3$  ( $\text{cm}^3/\text{g}$ ) versus temperature ( $^{\circ}\text{C}$ ) for a 25% water PHEMA gel.

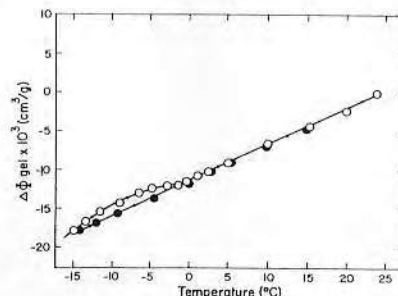


FIG. 3. The specific volume change  $\Delta\Phi_g \times 10^3$  ( $\text{cm}^3/\text{g}$ ) versus temperature ( $^{\circ}\text{C}$ ) for a 30% water PHEMA gel.

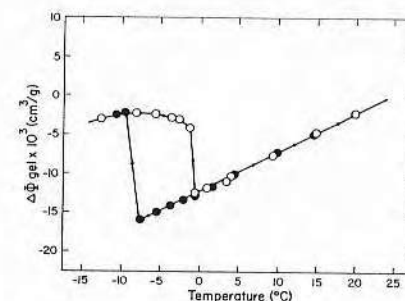


FIG. 4. The specific volume change  $\Delta\Phi_g \times 10^3$  ( $\text{cm}^3/\text{g}$ ) versus temperature ( $^{\circ}\text{C}$ ) for a 40% water PHEMA gel.

$2.5^{\circ}\text{C}/\text{min}$  and  $5^{\circ}\text{C}/\text{min}$  for the various PHEMA gels. Scanning speed had no significant effect on the temperature of transition. Heating curves were also obtained and some hysteresis was noted (15).

### RESULTS

#### A. Dilatometric Measurements

The specific volume change of the gel,  $\Delta\Phi_g$ , was obtained from the dilatometry measurements by Eq. [2]. Hysteresis in thermal expansion of the PHEMA gels from  $-15^{\circ}$  to  $24^{\circ}\text{C}$  is shown in Figs. 1 to 5. The specific volume for each gel decreases upon cooling. The gels containing 25% or more water (Figs. 2 to 5) showed a hysteresis in thermal expansion over the temperature range of  $-15^{\circ}$  to  $24^{\circ}\text{C}$ . One sees that the 20% water gel shows no transition (Fig. 1), probably indicating that most of the water is "bound" (Z water).

The 25% water gel shows a slight hysteresis, the heating path discontinuously joining the cooling path in the vicinity of  $0^{\circ}\text{C}$  (Fig. 2). The hysteresis increases as the water content of the hydrogel increases (Figs. 3 and 4). The hysteresis is most pronounced in the high water content hydrogel (50% water). The extremely sharp specific volume change near  $0^{\circ}\text{C}$  for the higher water content gels (40% and 50% water) is probably due to "normal" water (X water). The transition of ice to water

involves a volume change of  $-8.27\%$  (16) or  $-91.1 \times 10^{-3} \text{ cm}^3 \text{ g}^{-1}$  at  $0^{\circ}\text{C}$ .

These dilatometric studies suggest that three general states of water may exist in hydrogels and that the transition temperature of X water is  $0^{\circ}\text{C}$  (Figs. 4 and 5), that of Y water may range from  $-15^{\circ}$  to  $0^{\circ}\text{C}$  and Z water shows no transition over the range from  $-15^{\circ}$  to  $24^{\circ}\text{C}$  (Fig. 1). The data indicate the PHEMA network contains about 20% of bound or Z water. If we make the assumption that the transition near  $0^{\circ}\text{C}$  is due mainly to nonbound or X water, then the amount of normal or X water and interfacial or Y water in the gels can be determined from Eqs. [3] and [4]:

$$X \simeq (\Delta\Phi_{\text{gel}}/\Delta\Phi_w) \cdot 100 \quad [3]$$

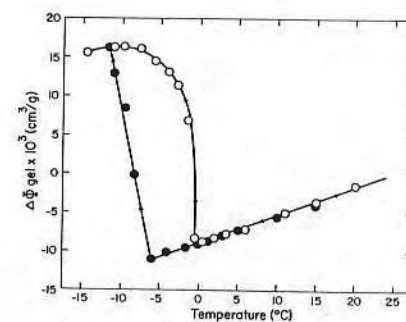


FIG. 5. The specific volume change  $\Delta\Phi_g \times 10^3$  ( $\text{cm}^3/\text{g}$ ) versus temperature ( $^{\circ}\text{C}$ ) for a 50% water PHEMA gel.

TABLE I  
APPROXIMATE CONTRIBUTION OF "X, Y, AND Z" WATER  
TO THE TOTAL WATER CONTENT (W)  
OF PHEMA GELS  
(ALL VALUES ARE Wt. %)

W	20	25	30	40	50
X	0	0	0	8.3	18.4
Y	0	5	10	11.7	11.6
Z	20	20	20	20	20

and

$$Y \approx W - X - Z, \quad [4]$$

where  $X$  is the percentage of normal water in the gel;  $\Delta\Phi_w$  is the volume change of ice to water at  $0^\circ\text{C}$ ;  $Y$  is the percentage of interfacial water in the gel;  $W$  is the total percentage of water in the gel; and  $Z$  is the percentage of bound water in the gel. The amount of "normal" water in the gel was obtained using Eq. [3] with  $\Delta\Phi_{\text{gel}}$  values taken from Figs. 4 and 5 and  $\Delta\Phi_w$  value from Ref. (11). Also the amount of interfacial water was obtained using Eq. [4], assuming that 20% of the gel was bound water. The results are shown in Table I, where the amount of interfacial water appears to reach a near constant value for gels of 40 to 50% water content.

There is apparently no bulk or normal water in the gel until the maximum interfacial ( $Y$ ) water content is reached; after that point all additional water in the gel behaves as bulk or  $X$  water.

### B. Specific Conductivity

According to absolute reaction rate theory, the specific conductivity,  $K$ , can be written as follows (6, 17).

$$K = \text{const} \{z(Ne)^2/Nh\} \exp(-\Delta E_a/RT), \quad [5]$$

where  $z$ ,  $N$ ,  $e$ ,  $R$ ,  $\Delta E_a$ , and  $h$  are ionic valence, Avogadro's number, electronic charge, gas constant, activation energy, and Planck's constant, respectively. Equation [5] can be rewritten as (6, 17),

$$\log K = \text{const} - (\Delta E_a/2.303RT). \quad [6]$$

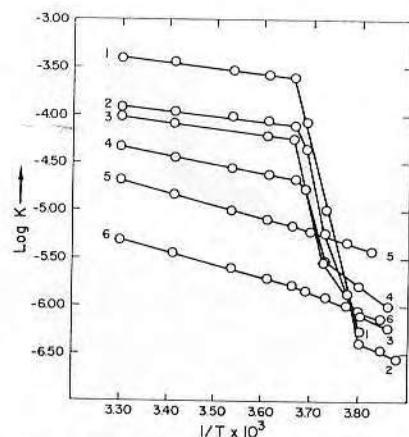


FIG. 6. Specific conductivity versus reciprocal temperature for PHEMA hydrogels as a function of water content. 1 = 70, 2 = 60, 3 = 50, 4 = 40, 5 = 30, 6 = 20%  $\text{H}_2\text{O}$ .

Plots of specific conductivity versus temperature for PHEMA gels of different water contents are presented in Fig. 6.  $\log K$  is linearly proportional to  $1/T$  for temperatures higher than the transition temperatures. One can obtain the apparent activation energy for specific conduction for each different gel (Fig. 7) from the slope of the straight lines in Fig. 6. One can analyze Fig. 7 in terms of three classes of activation energies (5-7) which may correspond to the activation energies of "normal"

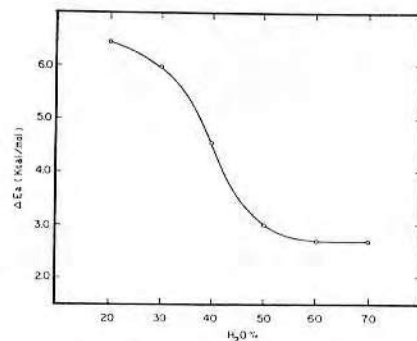


FIG. 7. Activation energy for conductivity versus water content for PHEMA hydrogels.

water ( $X$  water), that of "bound" water ( $Z$  water), and that of  $Y$  water. A sharp discontinuous change in the  $\log K$  vs  $1/T$  curve near  $0^\circ\text{C}$  indicates that the high water content gels (1-4 in Fig. 6) have significant amounts of "normal" or  $X$  water.

Even though  $10^{-3}$  mole of initiator salts were used for polymerization of monomer, the activation energy value, 2.7 Kcal/mole for gels of 60 to 70% water content in Fig. 7 is of the same order of magnitude as the activation energy for proton transport in aqueous solutions, 2.5 to 2.8 Kcal/mole (18).

The general expression for the ionic conductivity (19) in water and ice is

$$\sigma_i = nzeU_i = C_i e^{-\Delta E_a/RT}, \quad [7]$$

where  $\sigma_i$  is the ionic conductivity;  $i$  is 1 or 2 referring to water and ice, respectively;  $n$  is the number of charge carriers;  $U_i$  is the ion mobility, and  $C_i$  is the constant. Therefore,

$$\frac{\sigma_1}{\sigma_2} = \frac{U_1}{U_2} = \frac{C_1}{C_2} e^{(\Delta E_a)_2 - 1/RT}, \quad [8]$$

where  $(\Delta E_a)_{2-1} = \Delta E_{a2} - \Delta E_{a1}$ . The frequency factors,  $C_1$  and  $C_2$  are approximately equal because the fundamental vibration frequencies of ice and water (16, 20, 21) are almost the same; the volume change from ice to water should not significantly affect  $C_i$ . Equation [8] can be written as:

$$U_1/U_2 = 10^3 \approx e^{(\Delta E_a)_{2-1}/RT},$$

because the proton mobility in water,  $U_1$ , is of the order of  $10^3$  times higher than in ice,  $U_2$  (18). The ion mobility ratio is probably greater than  $10^4$  (18). The activation energy difference between gels with 20% water and 60% water, as given in Fig. 7, is 4 Kcal/mole which is near the value of 4.1 Kcal/mole for the activation energy difference for proton transport between ice and water. This fact suggests that in the low water content gels the conductivity is largely determined by

bound water, perhaps with ice-like behavior, while in the high water content gels it is largely determined by nonbound water with normal water behavior. Because the ion mobility in ice (18) is small in comparison to that in water, the contribution of bound water to the conductivity in the latter case may be very small.

We are aware of the controversy in the literature on proton and ion mobility in ice (22). The arguments presented above are largely qualitative in nature and are given merely to show that the concepts of bulk, bound, and intermediate water in gels are reasonable with respect to conductivity data. Even though the exact nature of the charge carriers in the gels are not known (protons, sodium ions, and ammonium ions are probably predominant), the qualitative argument given above is valid whether we consider protons ( $U_1/U_2 \approx 10^3$ ) or small univalent ions ( $U_1/U_2 \geq 10^4$ ). More direct methods are available to quantitatively determine the classes of water in hydrogels (15, 23).

### C. Differential Scanning Calorimetry (DSC)

The thermal behavior of hydrogels due to physical or chemical changes during heating or cooling can be studied by DSC. DSC curves directly give the heat evolved or absorbed during a phase transition, thus permitting a direct thermal analysis (24). The endothermic energy (cal/sec) as a function of temperature is presented in Fig. 8 for 5 gels of different water content, pure water, and a sample of 60% water gel in contact with pure water. One sees that no change is detected in the 20% water gel, confirming that most of the water must be "bound" or  $Z$  water. The other gels (above 20% water) show a definite phase change below  $0^\circ\text{C}$  on cooling, and it is interesting to see that the transition temperatures shift upwards toward  $0^\circ\text{C}$  as the water content of the gel increases. Pure water shows the expected sharp transition at  $0^\circ\text{C}$ . To determine the effect of cross-linker in PHEMA gels, the monomer solution was also polymer-



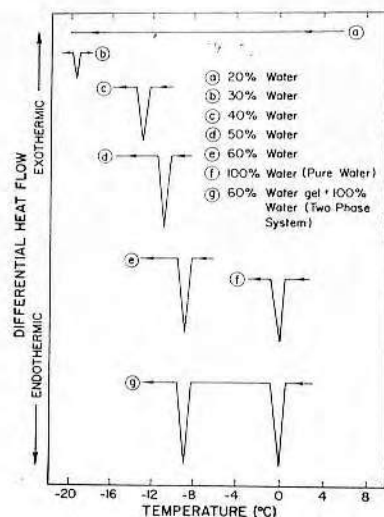


FIG. 8. DSC thermograms for PHEMA (1% cross linker added) hydrogels of different water contents, for pure water, and for a 60% water gel/pure water system.

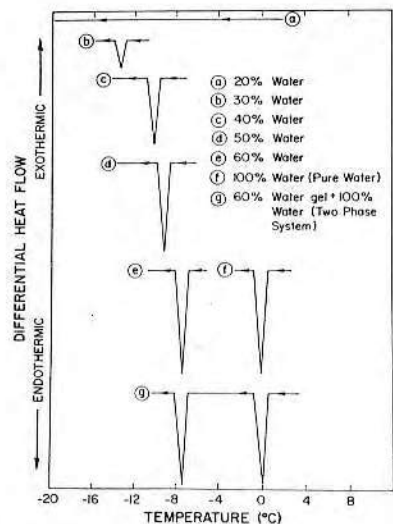


FIG. 9. DSC thermograms for PHEMA (no cross linker added) hydrogels of different water contents, for pure water, and for a 60% water gel/pure water system.

ized without adding cross-linker. The other conditions were the same as described in experimental procedures. The DSC data are shown in Fig. 9.

The transition points of gels with cross-linker were at lower temperatures than those of the gels without cross-linker. This shift may be due to the differences in the amounts of the three classes of water in these gels.

#### DISCUSSION

Our results are in qualitative agreement with those of Aizawa *et al.* on agar gels (5, 6), and of Baresova (25) on polyhydroxyethyl methacrylate gels. Our data provide evidence that various forms of water exist in PHEMA hydrogels. The water probably consists of a fraction which is significantly affected by the polymer network (Z water), a fraction relatively unaffected by the network (X or normal water), and an intermediate fraction (Y water). The Y fraction appears to reach a limiting value of about 12% of the total gel. The X fraction increases with increasing water content above 35 to 40% water.

PHEMA gels are observed to be complex systems with regard to the role of water, as well as with respect to their network structure (10, 11, 26–28). The homogeneity of the gels depends on the concentration of water in the starting mixture. The polymerization process yields either a homogeneous and optically clear gel (up to about 40 wt. % water in the starting mixture), or a heterogeneous, turbid gel if the initial water content exceeds about 40 wt. %.

It is generally believed that PHEMA gels of 40% water or less are homogeneous systems (10, 11, 26–28), while such gels containing over 40% water are heterogeneous, possibly two-phase systems exhibiting “microsyneresis” (27, 28) and thought to have a “micro-mesomorphic” structure (29). At water contents of about 40% or less, the polymer network does not exhibit a microphase separation and thus appears optically homogeneous on visual inspection. As this phenomena is somewhat independent of covalent cross-link

concentration (11, 26), it has been attributed to noncovalent cross-links due to polymer/water interactions (11, 26). It is thus reasonable to suspect that it may be related to the nature of water (or types of water) in the gels.

#### SUMMARY

The nature of water in a synthetic hydrogel has been studied by applying three different techniques: dilatometry, specific conductivity, and differential scanning calorimetry. The results obtained by the three techniques agree with each other and support the hypothesis that there exists three classes of water in hydrogels. The data suggested that approximately up to 20 wt. % of the hydrated gel is water bound to the polymer network. A semiquantitative analysis of three classes of water in the gels was obtained from the dilatometric results.

#### ACKNOWLEDGMENTS

This work was supported by the U. S. Atomic Energy Commission, Contract AT(11-1)-2147. We thank Dr. R. H. Boyd and Dr. K. Biliyar for the use of the differential scanning calorimeter, and Dr. S. W. Kim, Dr. S. Ma, Dr. S. Paek, and Dr. D. Lentz for many helpful discussions and assistance. We also thank Dr. Edward Eyring and his group, University of Utah, for the loan of the AC Bridge.

#### REFERENCES

1. WICHTERLE, O., AND LIM, D., *Nature* **185**, 117 (1960).
2. BRUCK, S. D., *J. Biomed. Mater. Res.* **7**, 387 (1973).
3. ANDRADE, J. D., LEE, H. B., JHON, M. S., KIM, S. W., AND HIBBS, J. B., *Trans. Amer. Soc. Artif. Int. Organs* **19**, 1 (1973).
4. DROST-HANSEN, W., *Indust. Eng. Chem.* **61**, 10 (1969).
5. AIZAWA, M., AND SUZUKI, S., *Bull. Chem. Soc. Japan* **44**, 2967 (1971).
6. MIZUGUCHI, J., TAKAHASHI, M., AND AIZAWA, M., *Nippon Kagaku Zasshi* **91**, 723 (1970).
7. AIZAWA, M., MIZUGUCHI, J., SUZUKI, S., HAYASHI, S., SUZUKI, T., MITOMO, N., AND TOYAMA, H., *Bull. Chem. Soc. Japan* **45**, 3031 (1972).
8. KRISHNAMURTHY, S., MCINTYRE, D., AND SANTEE, E. R., JR., *J. Polym. Sci.* **11**, 427 (1973).
9. JHON, M. S., AND ANDRADE, J. D., *J. Biomed. Mater. Res.* **7**, 509 (1973).
10. REFOJO, M. F., *J. Polym. Sci. A-1* **5**, 3103 (1967).
11. REFOJO, M. F., *J. Appl. Polym. Sci.*, **9**, 3417 (1965).
12. YASUDA, H., GOCHIN, M., AND STONE, W., JR., *J. Polym. Sci. A-1* **4**, 2913 (1966).
13. WEAST, R. C., Ed., “Handbook of Chemistry and Physics,” 51st ed., The Chemical Rubber Co., 1971.
14. BETTELHEIM, F. A., “Experimental Physical Chemistry,” p. 323. W. B. Saunders, Company, Philadelphia, PA, 1971.
15. LEE, H. B., The nature of water in a synthetic hydrogel: poly (2-hydroxyethyl methacrylate), Ph.D. Dissertation, University of Utah, June, 1974.
16. MOELWYN-HUGHES, E. A., “Physical Chemistry,” pp. 464 and 748. Pergamon Press, London, 1961.
17. GLASSTONE, S., LAIDLER, K. J., AND EYRING, H., “The Theory of Rate Processes,” Chap. 10, McGraw-Hill, New York, 1941.
18. BOCKRIS, J. O., AND REDDY, A. K., “Modern Electrochemistry,” Vol. 1, p. 471, Plenum Press, New York, 1970.
19. VAN VLACK, L. H., “Materials Science for Engineers,” p. 277, Addison Wesley, New York, 1970.
20. FRANKS, F., “Water,” Vol. 1, p. 135, Plenum Press, New York, 1972.
21. AMDUR, I., AND HAMMES, G. G., “Chemical Kinetics: Principles and Selected Topics,” p. 63, McGraw-Hill Book Co., New York, 1966.
22. MAIDIQUE, M. A., VON HIPPEL, A. L., AND WESTPHAL, W. B., *J. Chem. Phys.* **54**, 150 (1971).
23. LEE, H. B., ANDRADE, J. D., AND JHON, M. S., *Polymer Preprints* **15**, 706 (1974).
24. KARMAS, E., AND DIMARCO, G. R., in “Analytical Calorimetry” (R. S. Porter and J. F. Johnson, Eds.) Vol. II, Plenum Press, New York, 1970.
25. BARESOVA, V., *Coll. Czech. Chem. Comm.* **34**, 545, 707 (1969).
26. ILAVSKY, M., AND PRINS, W., *Macromolecules* **3**, 415 (1970).
27. DUSEK, K., AND SEDLACEK, B., *European Polym. J.* **7**, 1275 (1971).
28. DUSEK, K., “Polymer Networks: Structure and Mechanical Properties,” (A. J. Chomppf and S. Newman, Eds.), p. 245, Plenum Press, New York, 1971.
29. GOUDA, J. H., PROVODATOR, K., WARREN, T. C., AND PRINS, W., *Polymer Letters* **8**, 225 (1970).

# POLYMER SURFACE DYNAMICS

Edited by  
J. D. Andrade  
The University of Utah  
Salt Lake City, Utah

1988

PLENUM PRESS • NEW YORK AND LONDON

Polymer Surface Dynamics

J. D. Andrade, ed.,  
Plenum Press, 1988.

SURFACE PROPERTIES OF  
AQUEOUS PEO/PPO BLOCK COPOLYMER SURFACTANTS

J.H. Lee and J.D. Andrade

Department of Materials Science and Engineering  
University of Utah  
Salt Lake City, Utah 84112

## ABSTRACT

Surface tension and adsorption properties of various PEO-PPO-PEO triblock and related surfactants were investigated using the Wilhelmy plate technique and X-ray photoelectron spectroscopy (XPS). The effects of PEO (poly ethylene oxide) chain length, PPO (poly propylene oxide) chain length, and polymer structure were evaluated by surface tension measurements of the aqueous surfactant solutions and by adsorption studies of the surfactants on dimethyl dichloro silane (DDS)-coated surfaces, which are strongly hydrophobic. The conformations of the surfactant adsorbed at air/water interface and at hydrophobic solid/water interface were also considered. It was observed that as the hydrophobic character of the surfactant increases, surface tension rapidly decreases with increasing solution concentration. The adsorbed amount of polymer at the DDS surface/water interface increased with decrease in PEO chain length. PPO blocks did not show strong adsorption onto the hydrophobic surface. The possibility of producing PEO-rich surfaces by adsorption of unique PEO copolymers from aqueous solution was discussed.

## INTRODUCTION

Polyethylene oxide (PEO) surfaces are becoming recognized as exhibiting low protein adsorption and low cell adhesion characteristics. The hydrophilicity and unique solubility properties of PEO produces surfaces that are in a liquid-like state with the polymer chains exhibiting considerable flexibility or mobility<sup>1-12</sup>. A number of groups<sup>13-16</sup>, including our own<sup>4,12</sup>, have demonstrated greatly decreased adsorption of plasma and other proteins on PEO surfaces.

The immunology community has been recently modifying proteins by the attachment of PEO chains to produce a molecule



with minimal antigenicity. Antigens coated with PEO chains are apparently shielded from immune recognition<sup>7,8</sup>, providing a general method for reducing immunogenicity. PEO is also used as a means to passivate silica and glass columns to minimize adsorption of other species, including proteins, viruses and cells<sup>10,11</sup>.

A possible explanation of such passivity relates to PEO's relatively unique solution properties<sup>17,18</sup> and its molecular conformation in aqueous solution<sup>17-19</sup>. In addition, a more general volume restriction effect has been hypothesized<sup>20,21</sup>. It is thought that a repulsive force exists due to a loss of configurational entropy of the surface bound PEO when a protein or other particle approaches the PEO surface<sup>2,13,22,23</sup>. There is also an osmotic repulsion component due to polymer chain interpenetration<sup>2,22</sup>.

To date, PEO surfaces which have been used for biomaterials and/or medical device applications generally consist of PEO block copolymers<sup>1,2,3,15</sup> or cross-linked PEO networks<sup>1,24</sup>. Surface treatments have included direct adsorption of high molecular weight PEO<sup>10,11</sup> or the covalent grafting of PEO to silica and other surfaces<sup>4,12</sup>.

Nagaoka, et al.<sup>13</sup> have shown by NMR methods that the surface mobility of PEO chains is maximal when the number of repeat units approaches 100. They further showed that a PEO graft copolymer (many methoxy free ends) is more effective than a network or block system where most PEO is present as loops. Merrill, et al.<sup>15</sup> recently showed that end linked PEO-monomethyl ether and PEO networks both greatly reduce protein adsorption and platelet retention. Our own data on PEO end bonded to reactive silica surfaces<sup>12</sup> tend to support the results of Nagaoka, et al.<sup>13</sup> and Merrill, et al.<sup>15</sup>.

In view of the apparent success of PEO surfaces in reducing protein adsorption and platelet adhesion, we began considering a simple means of producing such surfaces, ideally by a simple coating process, so that catheters and even more complex medical devices could be treated.

We have chosen PEO-PPO-PEO triblock and related copolymers with which to initiate this work as they are readily available, non-toxic, and have many of the properties desired. PEO is water soluble<sup>17</sup> and polypropylene oxide (PPO) is water insoluble<sup>17,18</sup>. PEO-PPO-PEO triblock copolymers are widely used nonionic polymeric surfactants<sup>18</sup> which have been employed in cardiovascular surgery as defoaming agents. They are also widely used in pharmaceuticals and cosmetics<sup>18</sup>. At water/air or water/hydrophobic surface interfaces, it is probable that these surfactants are adsorbed via the PPO block with the PEO chains at least partially extended onto the aqueous solution.

In this work, we studied the surface properties of the surfactants at air/water interface by measuring surface tension. The adsorption of the surfactants at hydrophobic solid/water interface was also studied by XPS analysis. We

considered the effects of the PEO chains, the PPO chains and the structures of the surfactants used. We also considered surface conformations for the PEO-PPO-PEO triblock surfactants adsorbed on the air/water interface and adsorbed on the hydrophobic solid/water interface.

## EXPERIMENTAL

### Materials

Commercially available PEO-PPO-PEO triblock and related copolymers were used as received (Table 1). All of those copolymers are nonionic surfactants, and their molecular weights and the wt % of PEO are mean values. Pure PPO with various molecular weights were also used (Table 1).

As a substrate, we used glass slides (Corning cover glass 2940, No.1 1/2, 24X50mm, 0.16-0.19mm). The glass slides were treated with dimethyl dichloro silane (DDS, Petrarch Systems, Inc.) to produce the hydrophobic surfaces used in the adsorption studies.

### Methods

Surface tension measurement. The surface tensions of water and aqueous surfactant solutions were measured by the Wilhelmy plate method<sup>25</sup> using clean, hydrophilic glass slides.

The apparatus consists of an electrobalance (Cahn model RM-2) to which the sample is attached, and a movable shelf driven by a motor generator (Motomatic, Electro-craft Co.), which can be raised or lowered at controlled speeds to advance or recede a beaker of water over the sample. The tester is contained in an insulated enclosure maintained at constant temperature (20°C). Electrical signals from the balance are fed to an X-Y plotter (Gould, Series 60,000) to obtain wetting curves.

Glass slides were cleaned with chromic acid at 80°C for 30min, followed by careful rinsing with purified water (Milli-Q reagent water system, Millipore Corp.) and then dried overnight in an oven at 120°C in air. All glassware used was also carefully cleaned by the same process. Cleanliness of the glass slides was examined by measuring the surface tension of purified water (72.6±0.5dyne/cm) and by verifying that the slides were perfectly wetting as shown by the lack of any contact angle hysteresis<sup>26</sup>.

The surfactants used were soluble in water at room temperature for the concentration range used (10<sup>-5</sup> mg/ml to 1.0mg/ml). Each stock aqueous surfactant solution (1.0mg/ml) was freshly prepared 1 hr before use in order to minimize any effects due to oxidation and to allow sufficient time for equilibrium. Measurement was made 10 min after each dilution and checked several times to insure reproducibility of measurement.

Table 1. Structure and Properties of PEO/PPO Block Copolymers and PPO Used<sup>a</sup>

Commercial name	Source <sup>b</sup>	Structure	Appearance Ave. at R.T.	Mol. wt.	Wt% PEO	Specific gravity	Solubility(w/v) in water at 25°C	Cloud point (°C)
GENAPOL PF-10	Hoechst	(PEO) <sub>2</sub> -(PPO) <sub>30</sub> -(PEO) <sub>2</sub>	Liquid	1950 <sup>c</sup>	10	1.02(20°C)	Turbid at 10%	35-36(25% aq.)
PF-20		(PEO) <sub>5</sub> -(PPO) <sub>30</sub> -(PEO) <sub>5</sub>	Liquid	2190 <sup>c</sup>	20	1.04( " )	>10%	56-57( " )
PF-40		(PEO) <sub>13</sub> -(PPO) <sub>30</sub> -(PEO) <sub>13</sub>	Liquid	2920 <sup>c</sup>	40	1.05( " )	>10%	67-68( " )
PF-80		(PEO) <sub>80</sub> -(PPO) <sub>30</sub> -(PEO) <sub>80</sub>	Powder	8750 <sup>c</sup>	80	1.08( " )	>10%	70-71(10% aq.)
SYNPERONIC PE-L64	ICI	(PEO) <sub>13</sub> -(PPO) <sub>30</sub> -(PEO) <sub>13</sub>	Liquid	2900	40	-	>10%	58(1% aq.)
PE-L64C	BASF	Condensation product of PE-L64	Liquid	5900	40	1.02(20°C)	>10%	30(1% aq.)
TETRONIC 1504	Wyandotte	(PEO) <sub>26</sub> -(PPO) <sub>29</sub>	Paste	12000	40	1.02(60°C)	>10%	90(1% aq.)
		(PEO) <sub>26</sub> -(PPO) <sub>29</sub> NCH <sub>2</sub> CH <sub>2</sub> N						
PPO	Aldrich	(PPO) <sub>7</sub>	Liquid	425	-	1.004(20°C)	Solubled	-
		(PPO) <sub>17</sub>	Liquid	1000	-	1.005( " )	>2% <sup>d</sup>	-
		(PPO) <sub>34</sub>	Liquid	2000	-	1.005( " )	<0.1% <sup>d</sup>	-
		(PPO) <sub>69</sub>	Liquid	4000	-	1.004( " )	Insoluble	-

a. Data are supplied by the manufacturer.

b. Address of the manufacturer : Hoechst Aktiengesellschaft, Verauf TH, D-6230, Frankfurt am Main 80, West Germany  
ICI, Petrochemicals Div., P.O.Box 90, Wilton, Middlesbrough, Cleveland, TS6 8JE, England  
BASF-Wyandotte Co., Performance Chemicals, 100 Cherry Hill Road, Parsippany, NJ 07054, U.S.A.  
Aldrich Chemical Co., 940 West Saint Paul Ave., Milwaukee, Wisconsin 53233, U.S.A.

c. From ref. (14).  
d. From ref. (27).

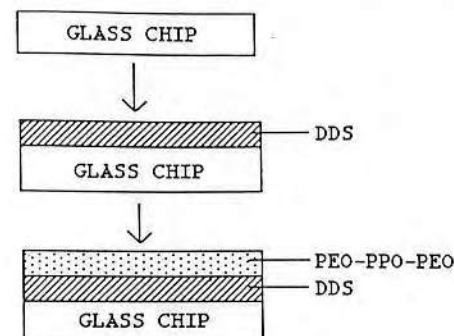


Fig. 1. Sample preparation for adsorption studies

PPO above  $M=2,000$  dalton was not soluble in water at room temperature as expected. As PPO exhibits an inverse solubility-temperature relationship in water<sup>27</sup>, the  $M=2,000$  dalton PPO at a concentration of 1.0mg/ml was cooled to 4°C and well mixed. Although most of the PPO dissolved, the solution showed some cloudiness at room temperature. This solution was diluted in the cooled state to 0.1mg/ml and did not show any cloudiness at room temperature.  $M=4,000$  dalton solution could be prepared for concentration  $\leq 0.001$ mg/ml without any cloudiness at room temperature.

In each case, clean glass slides were immersed into or drawn out of the prepared solution at the speed of 40mm/min<sup>26</sup> to measure surface tension. The values of surface tensions were obtained at the moment that the glass slide just touched the surfactant solution when it was wetted and immersed into the solution. The surface tension of each sample was measured three times and it was observed the values of the surface tensions are well matched within  $\pm 2.0\%$ .

**Adsorption studies.** To prepare the hydrophobic surfaces, the clean glass slides were immersed in a solution of 10% DDS in toluene (EM Science) dried with molecular sieve particles (MCB Manufacturing Chemicals, Inc.) for 30 min and then rinsed three times in pure ethanol followed by one rinse in purified water and one rinse again in ethanol. The DDS treated glass slides were cured by placing them in an oven at 70°C for 3 hr in a nitrogen atmosphere. The DDS coated glass slides were immersed in surfactant solutions of different concentrations for various times at room temperature (Figure 1). Desorption studies consisted simply of immersing the adsorbed slides in purified water for the given time.

The surfactant-coated surfaces were analyzed by electron spectroscopy for chemical analysis (ESCA) using a Hewlett-Packard 5950B electron spectrometer equipped with a



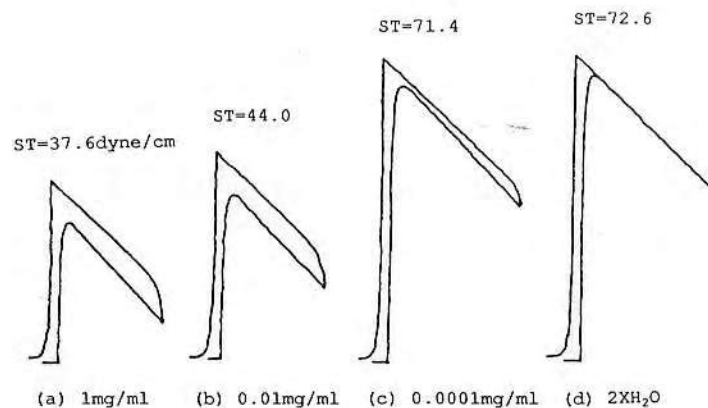


Fig. 2. Wetting curves for (PEO)<sub>13</sub>-(PPO)<sub>30</sub>-(PEO)<sub>13</sub> solution and purified water

monochromatic Al Ka 1,2 radiation source at 1487 eV and 400 watt power at the anode. An electron flood gun operated at 6.0 eV was used for charge compensation. Wide scan and narrow scans for carbon 1S and silicon 2S were taken and normalized using the Scofield cross-sections<sup>28</sup>.

## RESULTS AND DISCUSSION

### Surface Properties of PEO/PPO Block Surfactants at Air/Water Interface

Figure 2 shows wetting curves of a PEO-PPO-PEO triblock surfactant sample obtained by the Wilhelmy plate method. In the case of purified water, the wetting curve did not show hysteresis (Fig. 2(d)). As a glass slide was immersed into and drawn out of the surfactant solution, some hysteresis developed (Fig. 2(a)-(c)), most likely due to the adsorption of surfactant molecules on the surface. That is why the surface tension measurement was taken at the moment that the glass slide just touched the solution surface<sup>29</sup>. As shown in Figure 2, surface tension decreased as the surfactant concentration increased, as expected.

Figure 3 shows the effect of surfactant concentration and type on the surface tension. Surfactants with PEO/PPO blocks showed good surface tension reduction in aqueous solution as the concentration increases. Figure 3 (a) is the result for PEO-PPO-PEO triblock surfactants with the same PPO chain length ( $n=30$ ). There is a sharp reduction in surface tension with the increasing solution concentration. Reduction of surface

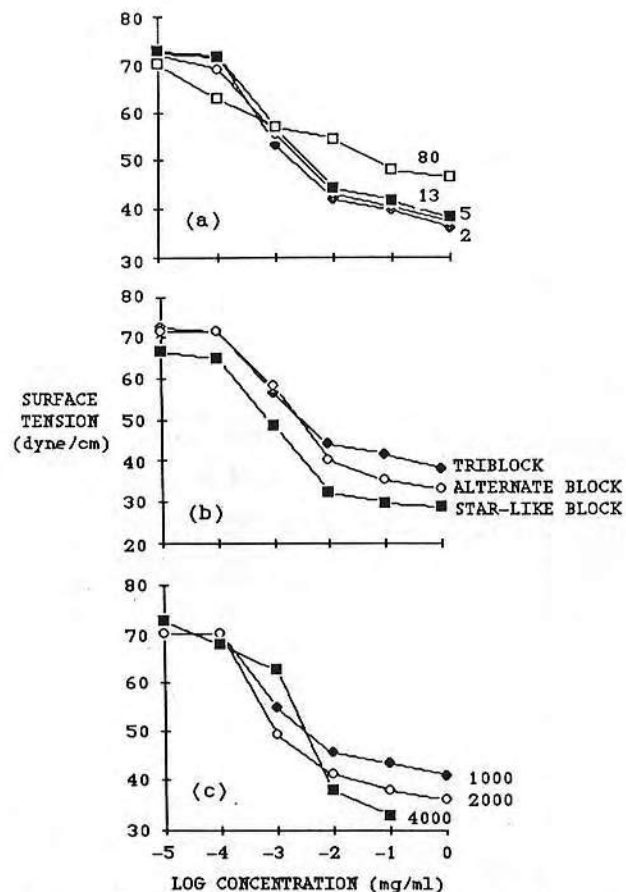


Fig. 3. Surface tension-log concentration plots of the surfactant and PPO solutions.  
(a) PEO-PPO-PEO triblock surfactants with different chain length (PPO chain length : 30)  
(b) Different PEO/PPO block surfactants (PPO chain length : 29-30, PEO wt% : 40)  
(c) Pure PPO with different molecular weight

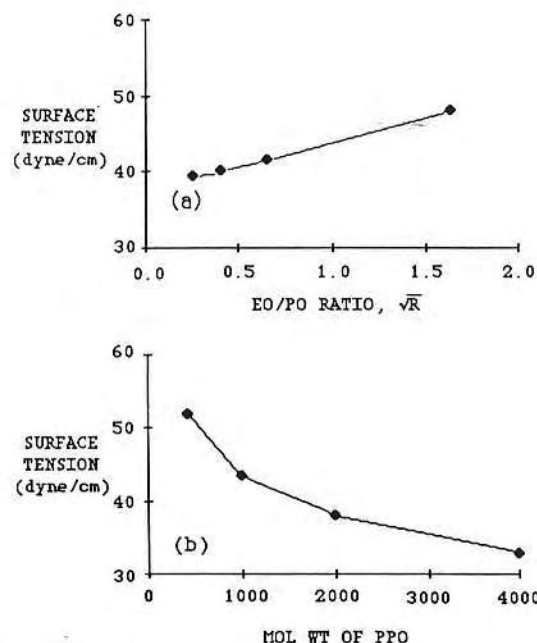


Fig. 4. (a) Surface tension of PEO-PPO-PEO triblock surfactants as a function of EO/PO ratio (surfactant concentration : 0.1mg/ml, PPO chain length : 30) (b) Surface tension of PPO as a function of molecular weight (PPO homopolymer concentration : 0.1mg/ml)

tension is one of the most commonly measured properties of surfactants in aqueous solution. It depends directly on the replacement of molecules of water at the interface by molecules of surfactant<sup>30</sup>. It is also a rather direct measure of adsorption of the surfactant at the air/water interface. We expect the hydrophobic PPO segment predominates at the air/water interface while the hydrophilic PEO segments tend to extend into the aqueous phase. The increase in surface tension reduction with concentration is indicative of the amount of the surfactant adsorbed at the air/water interface. Figure 3 (b) shows the surface tension change of the surfactants having different structures, PEO-PPO-PEO triblock, alternate PEO/PPO block, and star-like 4 PPO and 4 PEO blocks. They showed different values of surface tension even though they have similar PPO chain length ( $n=29$  or  $30$ ) and the same PEO content (40 wt%). The star-like block structure exhibits more adsorption to the surface than the triblock or the alternate block structure, and gives more hydrophobic character on the surface. Figure 3 (c) shows the effect of pure PPO chain length on the surface tension. PPO of molecular weight,  $M=1,000$  showed good solubility in water for our concentration

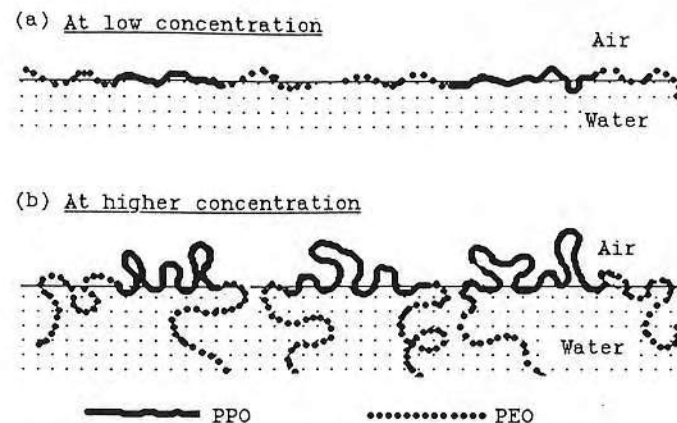


Fig. 5. Possible conformations of PEO-PPO-PEO triblock surfactants at air/water interface.

range at room temperature, but  $M=2,000$  showed a little cloudiness in water at 1.0mg/ml.  $M=4,000$  clouded above 0.01mg/ml and showed no solubility at 1.0mg/ml. Figure 3 (c) shows that surface tension drops more rapidly as the molecular weight of the PPO increases. Surface tension reduction in aqueous solution increases with increase in hydrophobic character. Surface tension decreases with decrease in EO/PO ratio and with increase in the molecular weight of PPO due to the increased hydrophobic character as seen in Figure 4.

These results and evidence from the literature<sup>31-36</sup> suggests possible conformations of PEO-PPO-PEO triblock surfactants at the air/water interface (Fig. 5). At low concentration, the surfactant molecules probably have a nearly flat conformation at the air/water interface by replacing water molecules with surfactant molecules (Fig. 5(a)). As concentration increases, the hydrophobic PPO segments will be squeezed and folded out of the air/water interface due to the increased number of surfactant molecules on the surface, and the hydrophilic PEO segments will be extended into water phase (Fig. 5(b)). Thus, as the concentration increases, the hydrophobicity of the surface increases. As the PPO chain length increases, the chain will be folded more extensively out of the air/water interface, producing a more hydrophobic surface as suggested by Figures 3(c) and 4(b).

As mentioned before, surface tensions sharply decrease and inflection points develop with increase in concentration (Fig. 3). It has been reported that these inflection points reflect "CMC" (critical micelle concentrations)<sup>37-40</sup>. Although our surfactants do show a sharp decrease in surface tension with solution concentration, there is some controversy<sup>41-43</sup> as to whether or not the concentration



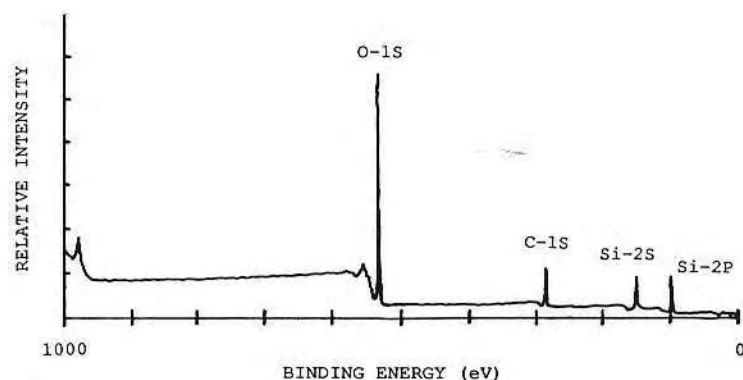


Fig. 6. XPS wide scan of PEO-PPO-PEO triblock surfactant-coated surface. (Glass + DDS + Genapol PF-40 (0.1mg/ml, 30min adsorption), power=400W)

involved is indeed a CMC. These surfactants may form intermolecular micelles only partially or not form micelles at all.

#### Adsorption of PEO-PPO-PEO Triblock Surfactants at Hydrophobic Solid/Water Interface

The adsorbed amount of surfactant molecules on the DDS surface was measured using XPS (or ESCA). Although XPS analysis does not provide absolute quantification, it is very sensitive to very low adsorbed amounts. It gives useful comparative information for the adsorption of surfactants. Figure 6 shows a wide scan for one of the surfactant-coated surfaces. It shows, as expected, the silicon 2S and 2P peaks (149 and 99 eV, respectively), the carbon 1S peak (284 eV) and the oxygen 2S peak (532 eV). This surface has two different types of carbon, alkyl and ether, each with a different binding energy (Fig. 7). The DDS coated surface has only alkyl carbons. As the surfactant concentration increases, adsorbed amount of the surfactant increases, and the ether carbon peak raises. The ether carbon peak thus provides information of the amount of surfactant adsorbed on the DDS surface.

The ether carbon to silicon atomic ratio, as determined by XPS analysis, of the surfactants and PPO adsorbed on the DDS surfaces are presented in Table 2. This table shows the effect of PEO chain length (from Genapols) and the effect of PPO chain length alone on adsorption. In this table, the numbers are only meaningful as compared vertically in the table because different samples have different numbers of ether carbons.

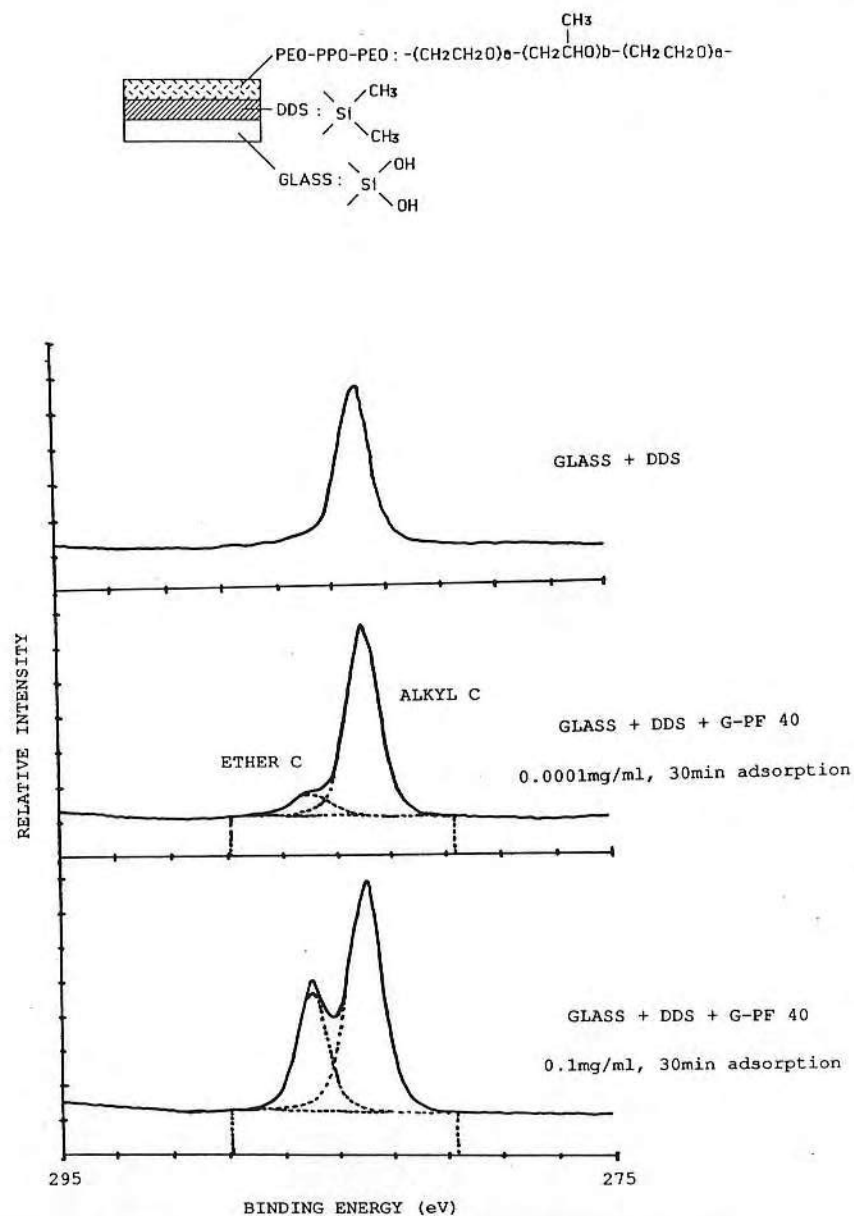


Fig. 7. XPS narrow scan of carbon for PEO-PPO-PEO triblock surfactant-coated surface. (Power=400W)

Table 2. Atomic ratio of ether carbon/silicon (ether C-1S/Si-2S) for the surfactants adsorbed on DDS surface<sup>a</sup>. (Compare only vertically)

Concentration (mg/ml)	Condition	GENAPOLS			PPO			
		PF-10	PF-40	PF-80	425	1000	2000	4000
0.1	1min	0.24	0.32	0.16	0.23	0.24	0.38	-
	adsorption							
	30min	0.29	0.33	0.22	0.29	0.29	0.65	-
	adsorption							
	30min	0.21	0.31	0.15	0.24	0.25	0.61	-
	desorption <sup>b</sup>							
0.0001	1min	0.08	0.09	0.08	0.06	0.07	0.14	0.15
	adsorption							
	30min	0.09	0.09	0.08	0.10	0.10	0.19	0.16
	adsorption							
	30min	0.07	0.09	0.07	0.06	0.08	0.19	0.14
	desorption <sup>b</sup>							

a. Ether carbon/silicon ratio for DDS surface  $\leq 0.04$

b. After 30min adsorption.

Table 3. Relative amount of the surfactants adsorbed on DDS surface. (Normalized from Table 2)

Concentration (mg/ml)	Condition	GENAPOLS			PPO			
		PF-10	PF-40	PF-80	425	1000	2000	4000
0.1	1min	3.53	2.86	0.42	16.43	7.06	5.59	-
	adsorption							
	30min	4.26	2.95	0.58	20.71	8.53	9.59	-
	adsorption							
	30min	3.09	2.77	0.39	17.14	7.35	8.97	-
	desorption							
0.0001	1min	1.18	0.80	0.21	4.29	2.06	2.06	1.09
	adsorption							
	30min	1.32	0.80	0.21	7.14	2.94	2.79	1.16
	adsorption							
	30min	1.03	0.80	0.18	4.29	2.35	2.79	1.01
	desorption							

\* Numbers are multiplied by  $10^3$ .

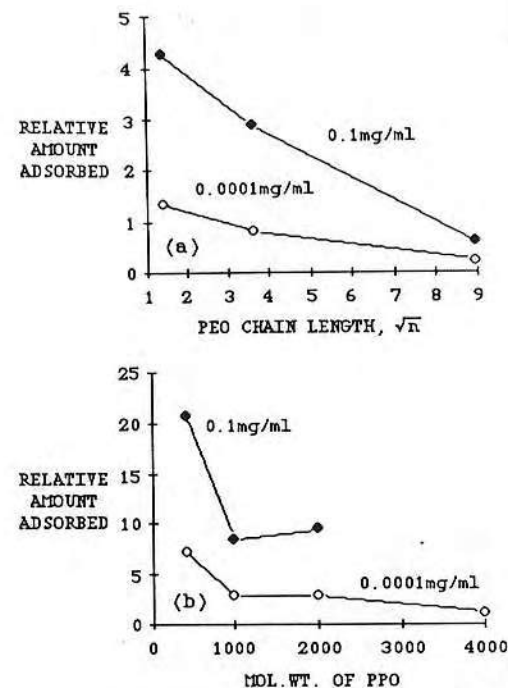


Fig. 8. (a) Relative amount of PEO-PPO-PEO triblock surfactant adsorbed on DDS surface (PPO chain length: 30) (b) Relative amount of PPO adsorbed on DDS surface.

The ether carbon/silicon ratio is a good qualitative indicator of the amount of the surfactant adsorbed, however, it is not directly related to the adsorbed amount. Each ethylene oxide and propylene oxide unit has two ether carbons. So total ether carbons per chain change with the PPO chain length and PEO chain length. We can determine the relative amount of adsorbed surfactant by comparing the surfactant:Si ratio which can be estimated by dividing the total ether C:Si atomic ratio by the number of ether carbons in the surfactant. For example, Genapol PF-40 has 112 ether carbons. So the total ether carbon/Si ratio in Table 2 is divided by 112 to estimate the relative adsorbed amount. Table 3 shows the normalized values from Table 2. Figure 8 (a) shows that the adsorbed amount increases as the surfactant concentration increases and as the PEO chain length decreases. Figure 8 (b) shows the effect of PPO chain length.

We assume that the surfactant molecules are physically adsorbed on the hydrophobic surface, probably via hydrophobic interactions of the PPO block with the surface. The function of the hydrophilic PEO blocks is to interact with water<sup>30</sup>. We



suggest that adsorption occurs between the PPO blocks of the surfactant and the strongly hydrophobic DDS coated surface. The PEO chains of the surfactant are extended into aqueous solution, where they are expected to be highly mobile.

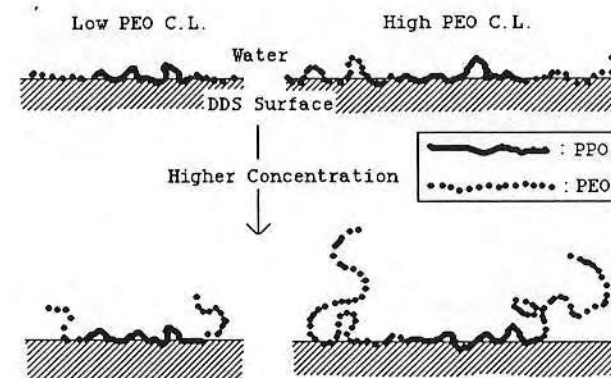
During the adsorption of the surfactants onto the hydrophobic surface from aqueous solution, orientation changes probably occur<sup>31</sup>. At low surfactant concentration, the surfactants will be adsorbed on a surface where there are very few other adsorbate molecules. At this stage, the surfactants may lie flat on the surface. After most of the free water molecules are replaced with surfactant, the monolayer is saturated with molecules lying flat. Increasing the size of the surfactant molecule by lengthening the PPO or PEO chains can cause a decrease in adsorption as seen in the case of the 0.0001mg/ml concentration in Figure 8. The subsequent stages of adsorption will be increasingly dominated by the hydrophobic interactions between the hydrophobic portions of the surfactant and the hydrophobic surface.

As the concentration increases, there will be a tendency for the hydrophobic chains of the adsorbed molecules to aggregate. This will cause the hydrophilic chains to become vertically oriented because the lateral forces due to hydrophobic chain interactions in the adsorbed layer will compress the molecule, and the PEO chains may have a less coiled, more extended conformation. We assume that longer PPO chain leads to a dense coil structure at higher solution concentrations due to the increased cohesion force. Thus, the surfactant molecule has a smaller cross sectional area on the surface. Therefore, at high concentration, the adsorbed amount increases with increase of PPO chain length, if the PPO chain length is sufficiently long (above  $M=1,000$ ), and with decrease in PEO chain length, as seen in the case of the 0.1mg/ml concentration in Figure 8.

The results of our XPS studies and evidence from the literature<sup>14,31,44</sup>, suggest the possible conformations shown in Figure 9. At low surfactant concentration, shorter PEO chains may lie nearly flat on the hydrophobic surface and longer PEO chains will prefer to form small loops because it is entropically more favorable than when they are attached tightly on the surface. The center hydrophobic PPO block is probably adsorbed on the surface through a hydrophobic interaction. As the concentration increases, PEO chains lying flat will be displaced from the surface by the PPO chains of adjacent molecules. Thus, PEO chains will tend to be oriented vertically at the water phase. The PEO chain is water soluble but it seems not to be fully extended in the aqueous phase (Fig. 9(a)). Therefore, as the PEO chain length increases, the occupied area of the surfactant molecules will be increased, and the adsorbed amount per unit area decreases as evidenced in Figure 8 (a).

For the low molecular weight PPO, the PPO chains of the surfactant will be adsorbed with small loops on the hydrophobic surface. As the molecular weight of PPO increases, the occupied area of the molecule on the surface will be increased. However, as the molecular weight of PPO is much higher ( $M.W. \leq 1000$  from Fig. 8(b)), we assume that it is tightly coiled on

(a) Effect of PEO Chain Length (C.L.)



(b) Effect of PPO Chain Length (at higher concentration)

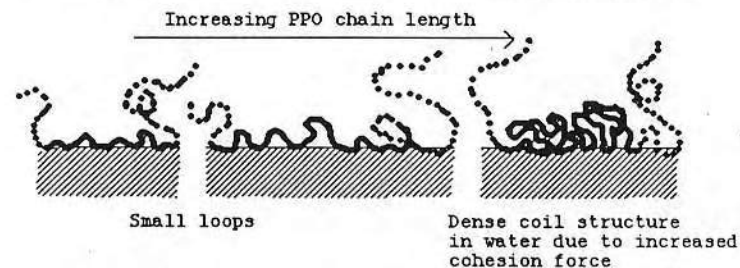


Fig. 9. Possible conformations of PEO-PPO-PEO triblock surfactant molecules at hydrophobic solid/water interface.

the surface because longer PPO chain will form a dense coil structure in water phase at higher concentration due to increased cohesion force, that is, increased hydrophobic interaction between side methyl groups of the PPO segment (Fig. 9(b)). Thus, occupied area of the molecule increases and then decreases with increasing PPO chain length. Figure 8(b) does not match this situation (Fig. 9(b)) exactly because it is for PPO homopolymers, not for PEO-PPO-PEO block copolymers. However, we expect that Fig. 8(b) will be able to explain the effect of PPO chain length for adsorption of the block copolymers.

XPS analysis of adsorption at the solid/water interface may be a problem because the analysis is done at the dried state. However, we do not expect that the adsorbed amount measured in the dried state will be much different from that for the wet state because DDS coated glass is a rigid surface and it will not have any penetration effect of the surfactant molecules into the surface.

## CONCLUSIONS

### A) Adsorption of PEO/PPO Block Surfactants at Air/Water Interface

1. Surface tension decreases as the hydrophobic character of the surfactant increases (increase in concentration and decrease in EO/PO ratio).
2. At low concentration, both PEO and PPO chains may have nearly flat conformation.
3. At higher concentration, surfactant molecules will be oriented in the surface with the PPO chains partly out of water phase and the PEO chains partly extended into the water phase.

### B) Adsorption of PEO/PPO Block Surfactants at Hydrophobic Solid/Water Interface

1. Adsorbed amount of the surfactant increases with increasing concentration and decreasing PEO chain length.
2. At low concentration, PEO chains may lie nearly flat (for shorter chains) on the surface or form small loops (for longer chains).
3. At higher concentration, PEO chains will extend into the water phase.
4. PPO chains prefer to form small loops (for shorter chains) or be tightly coiled (M.W.  $\leq 1000$ ) on the surface.

- C) Adsorption of PEO/PPO block surfactants directly on the hydrophobic surface provides a simple and rapid means of producing PEO-rich surfaces. The desorption studies (Table 2 and 3) suggest that the PPO segment does not have sufficient hydrophobic character for strong adsorption. We are beginning to study block copolymers with PEO chains and sufficient hydrophobic character to

be able to show strong adsorption on hydrophobic surfaces.

## ACKNOWLEDGEMENT

WE wish to thank Mr. Paul Dryden for help with the XPS work and the companies of ICI, BASF-Wyandotte and Hoechst for gifts of the surfactant samples.

## REFERENCES

1. E. W. Merrill and E. W. Salzman, ASAIO J., 6:60 (1983).
2. Y. Mori, S. Nagaoka, H. Takiuchi, T. Kikuchi, N. Noguchi, H. Tanzawa, and Y. Noishiki, Trans. Am. Soc. Artif. Intern. Organs, 28:459 (1982).
3. S. Nagaoka, Y. Mori, H. Takiuchi, K. Tanzawa and S. Nishiumi, Polymer Preprints, 24:67 (1983).
4. D. E. Gregonis, D. E. Buerger, R. A. Van Wagenen, S. K. Hunter and J. D. Andrade, Second World Congress on Biomaterials, abstracts, 266 (1984).
5. T. Matsuda and T. Akutsu, Organic Coatings Preprints, ACS abstracts (March, 1983).
6. F. Hasko, R. Yaszileva and L. Halasz, Biotech. and Bioeng., 24:1931 (1982).
7. F. F. Davis, A. Abuchowski, T. Van Es, N. C. Palczuk, K. Savoca, R. H-L Chen and P. Pyatak, "Biomedical Polymeric Materials and Pharmaceuticals for Biomedical Use," E. P. Goldberg and A. Nakajima, ed., P.441-452, Academic Press (1980).
8. A. Abuchowski, T. Van Es, N. C. Palczuk and F. F. Davis, J. Biol. Chem., 252:3578 (1977).
9. D. A. Knoll and J. Hermans, Biopolymers, 20:1745 (1981).
10. C. W. Hiatt, A. Shelokov, E. J. Rosenthal and J. M. Galimore, J. Chromatography, 56:362 (1971).
11. G. L. Hawk, J. A. Cameron and L. D. Dufault, Preparative Biochem., 2:193 (1972).
12. S. Winters, Ph.D. Thesis, University of Utah (1986).
13. S. Nagaoka, Y. Mori, H. Takiuchi, K. Yokota, H. Tanzawa and S. Nishu "Polymers as Biomaterials," S. W. Shalaby, A.S. Hoffman, B. D. Ratner and T. A. Horbett, ed., P.361-374, Plenum Press (1984).
14. H. Thurow and K. Geisen, Diabetologia, 27:212 (1984).
15. E. W. Merrill, R. W. Pekala, E. W. Salzman, J. N. Lindon and L. Kuchner, 11th Ann. Meet. Soc. for Biomaterials, abstracts, 106 (1985).
16. T. Suzuki, N. Kanbara, T. Tomomo, N. Hayashi and I. Shinohara Biochim. Biophys. Acta, 788:248 (1984).
17. F. E. Bailey Jr. and J. Y. Koleske, "Poly (Ethylene Oxide)," Academic Press (1976).
18. M. J. Schick, ed., "Nonionic Surfactants," Dekker (1966).
19. J. L. Koenig and A. C. Angood, J. Poly. Sci., Part A-2, 8:1787 (1970).
20. J. Hermans, J. Chem. Phys., 77:2193 (1982).



21. D. A. Knoll and J. Hermans, J. Biol. Chem., 258:5710 (1983).
22. Th. F. Tadros, ed., "The Effect of Polymers on Dispersion Properties," P.1-38, Academic Press (1982).
23. E. W. Merrill, Ann. N. Y. Acad. Sci., 283:6 (1977).
24. N. B. Graham, "Hydrogels," N. A. Peppas, ed., CRC Press, in press.
25. J. D. Andrade, L. M. Smith and D. E. Gregonis, "Surface and Interfacial Aspects of Biomedical Polymers," J. D. Andrade, ed., Vol. 1, Chap. 7, P.262, Plenum Press (1985).
26. L. M. Smith, C. Doyle, D. E. Gregonis and J. D. Andrade, J. Appl. Poly. Sci., 26:1269 (1982).
27. P. Molyneux, "Water Soluble Synthetic Polymers : Properties and Behavior," Vol. 1, Chap. 2, CRC Press (1983).
28. J. D. Andrade, ed., "Surface and Interfacial Aspects of Biomedical Polymers," Vol. 1, Chap. 5, P.127, Plenum Press (1985).
29. T. C. Kendrick and M. J. Owen, Chim. Phys. Appl. Prat. Ag. Surface Congr. Int. Deterg., 5th, 2:571 (1969).
30. M. J. Rosen, "Surfactants and Interfacial Phenomena," Chap. 1 and 5, Wiley-Interscience (1978).
31. J. S. Clunie and B. T. Ingram, "Adsorption from Solution at the Solid/Liquid Interface," G. D. Parfitt and C. H. Rochester, ed., Chap. 3, Academic Press (1983).
32. H. H. Teo, S. G. Yeates, C. Price and C. Booth, J. Chem. Soc., Faraday Trans. 1, 80:1787 (1984).
33. K. N. Prasad, T. T. Luong, A. T. Florence, J. Paris, C. Vaution and M. Seiller, J. Colloid Interface Sci., 69:225 (1979).
34. G. J. Howard and P. McConnel, J. Phys. Chem., 71:2974 (1967).
35. M. J. Schick, J. Colloid Sci., 17:801 (1962).
36. D. Guveli, S. S. Davis and J. B. Kayes, J. Colloid Interface Sci., 91:1 (1983).
37. W. Saski and S. G. Shah, J. Pharmaceutical Sci., 54:71 (1965).
38. M. Y. Pletnev and N. B. Tereshchenko, Colloid J.-USSR, 46:820 (1984).
39. S. Kucharski and J. Chlebicki, J. Colloid Interface Sci., 46:518 (1974).
40. D. Attwood and A. T. Florence, "Surfactant Systems : Their Chemistry, Pharmacy and Biology," P.13, Chapman & Hall (1983).
41. W. E. Bell, J. Phys. Chem., 63:299 (1959).
42. A. M. Mankowich, J. Phys. Chem., 58:1027 (1954).
43. J. M. G. Cowie and A. F. Sirriani, J. Amer. Oil Chem. Soc., 43:572 (1966).
44. J. B. Kayes and D. A. Rawlins, Colloid and Polymer Sci., 257:622 (1979).

# POLYMER SURFACE DYNAMICS

Edited by  
**J. D. Andrade**  
*The University of Utah*  
*Salt Lake City, Utah*

1988

PLENUM PRESS • NEW YORK AND LONDON

II

co  
st  
sy:  
so:  
co:  
mar  
sur  
pol

poly  
qual  
Spec  
XPS  
angu  
fluor  
anal  
local  
subpe  
permi  
more

that  
polyme  
more  
tetraf  
length  
surfac  
(morph  
polyur  
of mul  
diol),  
extende  
to affe  
nonfluor

## Protein-resistant surfaces prepared by PEO-containing block copolymer surfactants

Jin Ho Lee, Jindrich Kopecek,\* and Joseph D. Andrade†

Department of Materials Science and Engineering, University of Utah, Salt Lake City, Utah 84112

Polyethylene oxide(PEO)-containing non-ionic polymeric surfactants were studied as a possible means to produce PEO-rich surfaces by a simple coating treatment of a common hydrophobic medical material—polyethylene. Surface tension and adsorption properties of PEO/polypropylene oxide(PPO) and PEO/polybutylene oxide(PBO) block copolymer surfactants on a hydrophobic surface (low density polyethylene, LDPE) were investigated, using the Wilhelmy plate surface tension technique and x-ray photoelectron spectro-

scopy(XPS). The protein resistance of the surfactant-treated surfaces was evaluated by XPS and <sup>125</sup>I-labeled proteins. The data presented indicate that adsorption of the surfactants on LDPE is dependent on the molecular geometry of the surfactants. Adsorption of human albumin was significantly decreased on the surfactant-treated LDPE surfaces, as compared with the untreated surface. Surfactants suitable for the preparation of PEO-rich surfaces and possible mechanisms for their protein resistance are discussed.

### INTRODUCTION

Proteins adsorb to almost all surfaces during the first few minutes of blood exposure.<sup>1</sup> There has been much effort in minimizing or eliminating protein adsorption, because surfaces which show minimal protein adsorption are important in many applications, including blood-contacting devices, membranes for separation processes, sensors, chromatographic supports, contact lenses, immunoassays, blood and protein storage applications, etc.

An effective polymer for protein-resistant surfaces appears to be PEO probably due to its low interfacial free energy with water, unique solution properties and molecular conformation in aqueous solution, hydrophilicity, high surface mobility and steric stabilization effects.<sup>2-19</sup> We will discuss in more detail possible factors involved in PEO's passivity.

One possible component of PEO's passivity may be its minimum interfacial free energy.<sup>2-4</sup> PEO-water interfaces have very low interfacial free energies, and thus low driving forces for protein adsorption. Proteins at or near a low interfacial energy interface will not feel any greater effects from the

oxyethylene oxypropylene polymers," *J. Pharmaceutical Sci.*, **54**, 71-74 (1965).

48. M. J. Schick, "Surface films of nonionic detergents—I. Surface tension study," *J. Colloid Sci.*, **17**, 801-813 (1962).
49. Th. van der Boomgaard, Sh. M. Zourab, and J. Lyklema, "On the influence of concentrated electrolytes on the association behavior of a non-ionic surfactant," *Prog. Colloid & Polym. Sci.*, **68**, 25-32 (1983).
50. A. M. Mankowich, "Micellar molecular weights of selected surface active agents," *J. Phys. Chem.*, **58**, 1027-1030 (1954).
51. C. W. Diggings, R. J. Bolen, and H. N. Dunning, "Ultracentrifugal determination of the micellar character of non-ionic detergent solutions," *J. Phys. Chem.*, **64**, 1175-1178 (1960).
52. S. Ross and J. P. Olivier, "A new method for the determination of critical micelle concentrations of un-ionized association colloids in aqueous or in non-aqueous solution," *J. Phys. Chem.*, **63**, 1671-1674 (1959).

Received January 4, 1988

Accepted July 19, 1988

\*Institute of Macromolecular Chemistry, Czechoslovak Academy of Sciences, 16206 Prague 6, Czechoslovakia.

†To whom correspondence should be addressed.



surface than they do from the bulk solution. However, other neutral, hydrophilic polymers (such as agarose, dextran, methylcellulose, polyacrylamide, etc.) also have very low interfacial free energies. Although their protein adsorption tendencies are small, these materials appear to be more interactive than PEO surfaces.<sup>2-4</sup> This means that other factors are involved in PEO's passivity.

Another component of PEO's passivity may be explained by its unique solution properties<sup>5,6</sup> and its molecular conformation in aqueous solution.<sup>7</sup> At room temperature, PEO is completely miscible with water in all proportions.<sup>6</sup> In contrast to the complete water solubility of PEO, closely related polymers such as polymethylene oxide, polytrimethylene oxide, polyacetaldehyde, and polypropylene oxide are water insoluble under ordinary conditions.<sup>6</sup> The reason why PEO shows water solubility (at least up to temperatures slightly below 100°C), in contrast to the other polyethers, was well explained by PEO-water interactions.<sup>7</sup> In pure liquid water the hydrogen bonding results in a highly connected network of tetrahedrally coordinated water molecules; it was suggested that PEO segments nicely fill out voids in the water structure and minimally perturb the structure of water itself, thereby minimizing the tendency for hydrophobic interactions. The hydrophilicity and unique solubility properties of PEO produces surfaces that are in a liquid-like state with the polymer chains exhibiting considerable flexibility or mobility.<sup>5-7</sup> The rapid movement of hydrated PEO chains attached on a surface probably influences the micro-thermodynamics at the protein solution/surface interface and prevents adsorption or adhesion of proteins.<sup>8</sup>

PEO's passivity may be also explained by the steric stabilization effect. Steric stabilization has basically two contributions; first, a volume restriction<sup>8-10</sup> (or elastic<sup>11</sup> or configurational entropy loss<sup>12</sup>) term, associated with the reduction in the total number of conformations available to the adsorbed polymer on the approach of a protein or other particle, since the free space is reduced. It is thought that a repulsive force develops, due to a loss of configurational entropy of the surface-bound PEO, when a protein or other particle approaches the PEO surface. Second, an excluded volume<sup>12-15</sup> or osmotic pressure<sup>8,16</sup> or free energy of mixing<sup>11</sup>) term, associated with changes in the mixing of polymer segments-solvent molecules as the particles approach. In this case, the number of available conformations is decreased due to polymer chain interpenetration and an osmotic repulsion component develops. The excluded volume theory has been developed in detail for the PEO case.<sup>17-19</sup> It appears that PEO surfaces in water have rapid motions<sup>8</sup> and a large excluded volume compared to the less water-soluble or insoluble polyethers, thereby actively minimizing the adsorption of proteins. The long range repulsion between two PEO surfaces has been directly measured by Klein and Luckham<sup>20,21</sup> and Claesson and Golander<sup>22</sup> using the curved mica surface forces apparatus, developed and described by Israelachvili and co-workers.<sup>23,24</sup> Measurements of interactions between two protein-coated surfaces and between PEO-coated and protein-coated surfaces are in progress by several groups.

PEO surfaces have been prepared by block copolymerization,<sup>5,25,26</sup> cross-linking to produce a PEO network,<sup>5</sup> or surface treatments, such as direct adsorption of high molecular weight PEO<sup>27,28</sup> or the covalent grafting of PEO<sup>29,30</sup> to silica and other surfaces.

We consider a simple means of producing PEO surfaces, ideally by a simple coating process, so that catheters and even more complex medical devices could be treated. The basic approach to obtaining a PEO surface is to select a polymer with a sufficient water-insoluble component and hydrophilic PEO blocks or side chains. The polymer will adsorb on a hydrophobic surface from aqueous solution via hydrophobic interactions between the surface and the hydrophobic segments. The PEO chains are at least partially extended into the aqueous solution.<sup>31-33</sup> This provides a simple and rapid means of producing a PEO-rich surface.

We first treat a hydrophobic polymer surface (LDPE) with PEO-containing block copolymer surfactants in aqueous solution. We used PEO/PPO and PEO/PBO block copolymer surfactants for this purpose. The PPO or PBO components are water-insoluble, while the PEO is water-soluble.<sup>6,34</sup> We have used commercially available nonionic surfactants of a range of molecular weights. They are nontoxic and have well characterized properties, and are thus widely used as emulsifying and demulsifying agents, detergents, colloid dispersants or stabilizers, wetting agents, rinse aids, etc. At air/water or water/hydrophobic surface interfaces, these surfactants adsorb via PPO or PBO blocks with their PEO chains extended into the aqueous solution. We studied the surface properties of the surfactants at the air/water interface by measuring surface tension. The adsorption properties of the surfactants on LDPE substrates were investigated using XPS. The protein-resistant character of the polymer surfaces coated with surfactant by a simple solution treatment were also evaluated by XPS and <sup>125</sup>I-labeled albumin.

## MATERIALS AND METHODS

### Materials

Commercially available PEO/PPO and PEO/PBO block copolymers were supplied by BASF-Wyandotte and ICI (Table I) and used without any further treatment. Their molecular weights, numbers of chain length and the weight% of PEO in the table are consequently mean values.<sup>34</sup> For the studies of protein resistance, human albumin (crystallized, purity 99%, Miles Diagnostics) was used as received. Iodine-125 (<sup>125</sup>I, 100 mCi/mL, Amersham) was supplied as sodium iodide in dilute sodium hydroxide solution, pH 7-11, free from reducing agents.

The solid substrate was LDPE film (NHLBI DTB Polyethylene Primary Reference Material); the cleanliness of its surface was verified by XPS.

TABLE I  
Structure and Properties of PEO-Containing Block Copolymer Surfactants Used<sup>a</sup>

Commercial name	Source <sup>b</sup>	Structure	Ave. mol. wt.	Wt % PEO	Solubility (w/v) in water at 25°C	Description
Pluronic L64	BASF-Wyandotte	(EO) <sub>13</sub> —(PO) <sub>30</sub> —(EO) <sub>13</sub>	2900	40	>10%	PEO/PPO/PEO triblock (P)
Synperonic PE-L64C	ICI	Condensation product of (EO) <sub>13</sub> —(PO) <sub>30</sub> —(EO) <sub>13</sub>	5900	40 40	>10%	PEO/PPO alternate block (S)
Tetronic 1504	BASF-Wyandotte	(EO) <sub>25</sub> —(PO) <sub>25</sub> —N(CH <sub>2</sub> CH <sub>2</sub> ) <sub>2</sub> N—(PO) <sub>25</sub> —(EO) <sub>25</sub>	12000	40	>10%	PEO/PPO star-like block (T)
Butronic 184	BASF-Wyandotte	(EO) <sub>13</sub> —(BO) <sub>25</sub> —(EO) <sub>13</sub>	3000	40	>1%	PEO/PBO/PEO triblock (B)

<sup>a</sup>Data are supplied by the manufacturer.

<sup>b</sup>Address of the manufacturers: BASF-Wyandotte Co., Performance Chemicals, 100 Cherry Hill Road, Parsippany, NJ 07054, USA; ICI, Petrochemicals Div., P.O. Box 90, Wilton, Middlesbrough, Cleveland, TS6 8JE, England.

## Methods

### Surface tension measurement at air/water interface

Surface tensions at air/water interfaces were measured by the Wilhelmy plate method using clean, hydrophilic glass slides (Corning cover glass 2940, No. 1, 1½, 24 × 50 mm, 0.16–0.19 mm thick). The apparatus and procedure of the Wilhelmy plate method, the cleaning procedure of the glass slides, and examination of cleanliness of the glass slides were described in detail in a previous paper.<sup>35</sup> The surfactants used were soluble in water at room temperature (20°C) for the concentration range used (10<sup>-5</sup> mg/mL to 1.0 mg/mL). Time-dependent surface tension was measured for selected surfactant solutions. For this, a cleaned glass slide was allowed to just touch and stay on the surface of the surfactant solution prepared freshly from stock solution, while the force changes are recorded continuously as a function of time.

Surface tension for each surfactant solution was measured 10 min after each dilution of the solution (discussed later). The degree of reproducibility was within ±1.0 dyne/cm.

### Adsorption of surfactants at hydrophobic solid (LDPE)/water interfaces

LDPE films were immersed in surfactant solutions of different concentrations for 30 min at room temperature (Step 1 in Fig. 1). We used paper clips to hang the LDPE films in water because LDPE is lighter than water. The surfactant-adsorbed films were rinsed in purified water<sup>35</sup> (Step 2) and then vacuum dried overnight in an air atmosphere. Desorption studies consisted simply of immersing the surfactant-treated films in purified water for 30 min and rinsing (Step 3 and 4). An earlier study of the kinetics of desorption showed that a 30-min exposure was sufficient to achieve equilibrium.<sup>36</sup> The surfactant-treated surfaces were analyzed in a Hewlett-Packard 5950B x-ray photoelectron spectrometer (XPS) equipped with a monochromatic Al Kα<sub>1,2</sub> radiation source at 1487 eV and 400 W power at the anode. An electron flood gun operated at 6.0 eV was used for charge compensation. Wide scan and narrow scans for carbon 1s and oxygen 1s were taken and normalized using the Scofield cross sections.<sup>37</sup>

### Adsorption of human albumin on surfactant-treated LDPE surfaces

The surfactant-treated surfaces were immersed in protein solutions (phosphate buffer solution (PBS) at pH = 7.4) for 30 min (Step 5 in Fig. 1) and rinsed in PBS, following by rinsing in purified water (Step 6 and 7) and vacuum drying, then analyzed by XPS. The nitrogen 1s peak was used for the analysis of adsorbed protein.



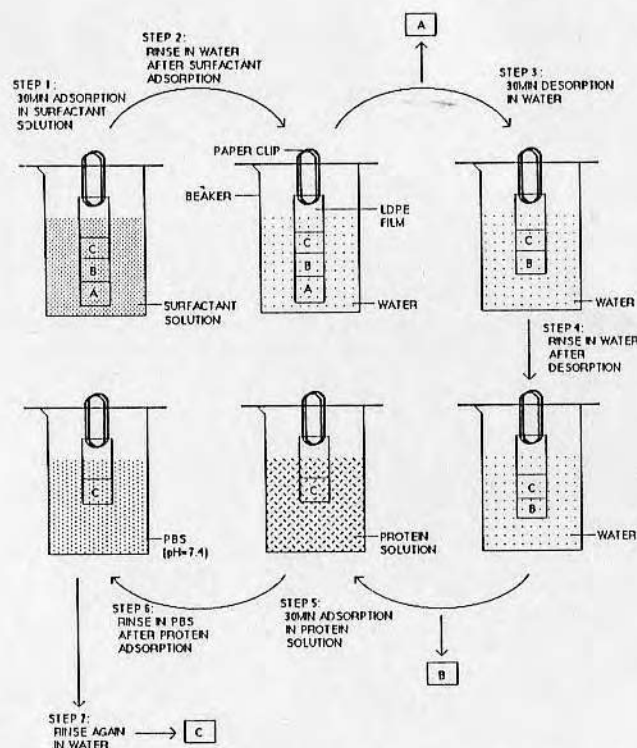


Figure 1. Consecutive steps of sample treatment for the studies of surfactants or protein adsorption. (A, sampling for the study of surfactant adsorption on LDPE surface; B, sampling for the study of surfactant desorption on LDPE surface; C, sampling for the study of protein adsorption of surfactant-treated surface.)

For the quantitation of protein adsorption,  $^{125}\text{I}$ -labeled human albumin was prepared by a modified Chloramine-T method.<sup>38</sup> This method is suitable to incorporate carrier-free radioactivity in small quantities of protein rapidly and with good efficiency.

Iodination was performed at room temperature (20°C) using 200  $\mu\text{g}$  human albumin dissolved in 0.5 mL PBS at pH = 7.4 (i.e., concentration of human albumin, 0.4 mg/mL). A volume corresponding to 0.3 mCi of  $\text{Na}^{125}\text{I}$  was added to the albumin solution. After 50  $\mu\text{L}$  freshly made chloramine-T solution (4 mg/mL in  $\text{H}_2\text{O}$ , Kodak) was added, the protein solution was gently mixed for 1 min. Immediately, 50  $\mu\text{L}$  sodium metabisulfite ( $\text{Na}_2\text{S}_2\text{O}_5$ , 4.8 mg/mL in  $\text{H}_2\text{O}$ , Fisher Scientific) was added to the mixture to stop the oxidation reaction. Free  $^{125}\text{I}$  was removed by centrifugation of Sephadex G-25 coarse grade resin (Sigma) mini-columns (6.0–6.5 cm long, about 1 cm

wide) having about 0.3 mL of iodinated protein solution.<sup>39</sup> The final concentration of  $^{125}\text{I}$ -labeled protein solution was determined by a UV-Visible spectrophotometer (Beckman, Model 35) at 280 nm. Typically, 60–70% protein recovery was obtained after passing through the column.

Labeling efficiency after removing free  $^{125}\text{I}$  was determined by precipitating the human albumin molecules with 20% trichloroacetic acid (TCA, Sigma) in the presence of bovine serum albumin (BSA, 20 mg/mL in PBS, Miles Diagnostics). The BSA functions as a carrier for the small amount of human albumin while TCA acts as a precipitating agent. To one of the two microcentrifuge vials (polypropylene, Fisher Scientific), 5  $\mu\text{L}$   $^{125}\text{I}$ -labeled albumin sample, 45  $\mu\text{L}$  BSA, and 50  $\mu\text{L}$  TCA were taken (A). The other vial contained  $^{125}\text{I}$ -labeled albumin sample and 95  $\mu\text{L}$  PBS (B). Both vials were centrifuged for 20 min at high speed (18,000 rpm, Fisher Scientific Model 235). From each vial, 5  $\mu\text{L}$  supernatant was taken into counting vial (polyethylene, Kimble) and the retained radioactivity was counted in gamma counter (Beckman, Model 170). The labeling efficiency was determined as follows:

$$\% \text{Eff.} = 1 - (\text{Counting from vial A} / \text{Counting from vial B})$$

Normally, more than 95% of labeling efficiency was obtained by this method.

For the adsorption of protein, the surfactant-treated surfaces were immersed in a solution of known ratio of labeled and unlabeled albumin (the concentration of unlabeled albumin was adjusted so that the final mixed solution concentration is 1 mg/mL) and adsorption was done with the same procedure as in the case for the samples for XPS analysis. After protein adsorption and following rinsing, the polymer film, whose surface area was predetermined, was directly placed in counting vials and the retained radioactivity was measured in the gamma counter. Corrections for background, radioactive decay of  $^{125}\text{I}$ , ratio of labeled protein with unlabeled one, and the surface area of the LDPE sample were made to determine the adsorbed amount of protein on the surface.

## RESULTS AND DISCUSSION

### Surface properties of the surfactants at air/water interfaces

Figure 2 shows the time-dependent surface tension of Tetronic 150 and Synperonic PE-L64C as a function of concentration. At high concentration (1 mg/mL), equilibrium was reached rapidly. At very low concentration (0.0001 mg/mL), surface tension decreased with time, however, after 5 or 10 min, the change of surface tension was very small and slow. We measured the surface tension of the different surfactant solutions 10 min after each dilution. Ten minutes was sufficient to achieve equilibrium except possibly for the very low surfactant concentrations. It is the higher concentrations which are of major interest in this paper.

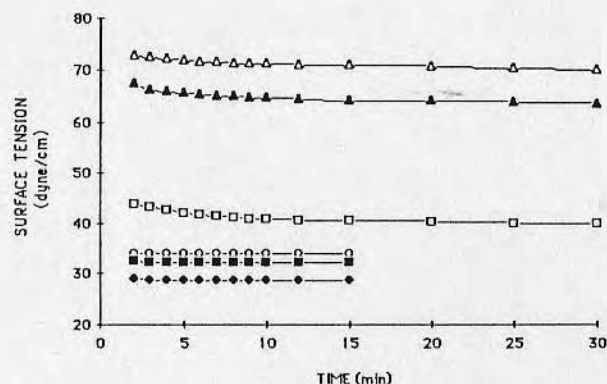


Figure 2. Time dependence of surface tension of the surfactant solutions as a function of concentration. (Solid points, Tetronic 1504; open points, Synperonic PE-L64C; triangle, 0.0001 mg/mL; square, 0.01 mg/mL; diamond, 1 mg/mL.)

Figure 3 shows the effect of surfactant concentration and type on the surface tension. The surfactants showed a sharp surface tension reduction in aqueous solution as the concentration increased. Reduction of surface tension is one of the most commonly measured properties of surfactants in aqueous solution. It depends directly on the replacement of molecules of water at the interface by molecules of surfactant.<sup>40</sup> The hydrophobic PPO or PBO segments will predominate at the air/water interface while the more hydrophilic PEO segments tend to extend into the aqueous phase.<sup>31,35,41-44</sup> The decrease in surface tension with concentration is related to the amount of surfactant adsorbed at the air/water interface. Surfactants having different structures, PEO/PPO/PEO triblock (Pluronic L64, P) PEO/PPO/PEO triblock (Butronic 184, B), condensed polymer of PEO/PPO/PEO triblock (or alternate PEO/PPO block, Synperonic PE-L64C, S) and a starlike polymer containing 4 PPO and 4 PEO blocks (Tetronic 1504, T), showed different surface tensions, even though the polymers have similar PPO or PBO chain lengths ( $n = 29(T)$  or  $30(P \text{ and } B)$  for PPO, and  $25(B)$  for PBO) and the same PEO content (40 wt %), probably due to different conformations and hydrophobicity at the air/water interface. As seen in Figure 3, surface tensions sharply decrease and inflection points develop with increase in solution concentration. It has been reported that these inflection points reflect a critical micelle concentration (CMC).<sup>34,41,45-49</sup> Although the surfactants used in this study do show a sharp decrease in surface tension with solution concentration, there is some controversy<sup>50-52</sup> as to whether or not the concentration involved is indeed a CMC.

These surface tension results and evidence from the literature<sup>31,41-44</sup> suggest possible conformations of PEO-PPO-PEO or PEO-PBO-PEO triblock

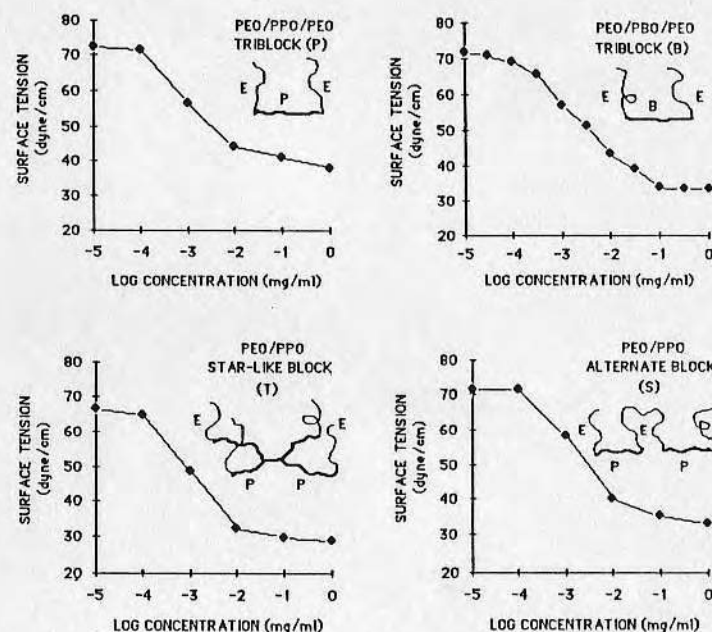


Figure 3. Surface tensions of the surfactants with different structure as a function of surfactant solution concentration. Data points represent average values of 3 samples, with deviations  $\leq 1.0$  dyne/cm. (PPO chain length, 29(T) to 30(others); PBO chain length, 25; PEO wt%, 40; E = PEO, P = PPO, B = PBO.)

surfactants at air/water interfaces (Fig. 4). At low solution concentration, the surfactant molecules probably have a nearly flat conformation at the air/water interface (A in Fig. 4). After the surface is saturated with the surfactant molecules lying flat (B in Fig. 4), as the solution concentration of surfactant increases, the hydrophobic segments on the surface will be squeezed and folded out of the air/water interface due to the increased number of surfactant molecules on the surface, and the hydrophilic PEO segments will be extended into water phase (C in Fig. 4). As the concentration of the surfactant solution further increases, the surface will be saturated with the folded surfactant molecules, or form molecular aggregates or micelles of the surfactant (D in Fig. 4). Thus, as the solution concentration increases, the hydrophobicity of the surface increases due to the folded or aggregated hydrophobic segments, and thus the surface tension decreases until it approaches the surface saturation.

The conformations of the surfactants at air/water interfaces will be related to those at the LDPE solid/water interface (we can consider air as a free hydrophobic surface while LDPE is a rigid hydrophobic surface).



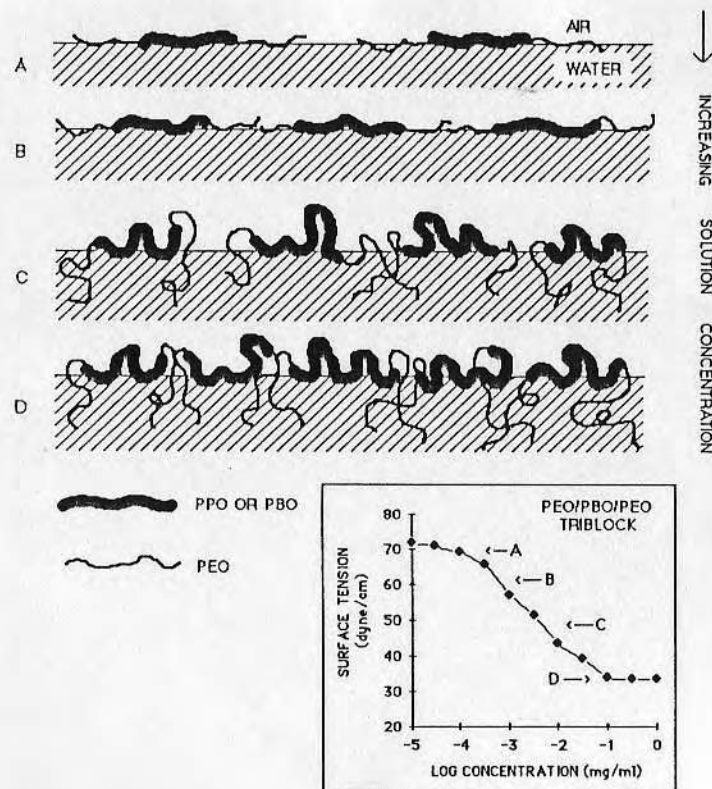


Figure 4. Suggested ideal conformations of PEO-PPO-PEO or PEO-PBO-PEO triblock surfactants at air/water interface. (Points A-D shown in the inserted surface tension plot do not represent exact positions.)

#### Adsorption of the surfactants at hydrophobic solid/water interfaces

The surfactants were adsorbed onto LDPE from aqueous solution, and the relative amount of adsorption was evaluated by XPS (or ESCA). Although XPS analysis does not provide absolute quantitation, it is very sensitive to very low adsorbed amounts. It gives useful and rapid comparative information for the adsorption of surfactants. The oxygen atomic% on the LDPE surface, as determined by XPS analysis, was used as an indicator of the amount of the surfactant adsorbed, as LDPE does not show any oxygen peaks (Fig. 5). We assume that the surfactant molecules are physically adsorbed on the LDPE surface via hydrophobic interactions of the PPO or PBO blocks with the surface.<sup>31-33</sup> The hydrophilic PEO chains of the surfactant will be extended into aqueous solution, where they are expected to be

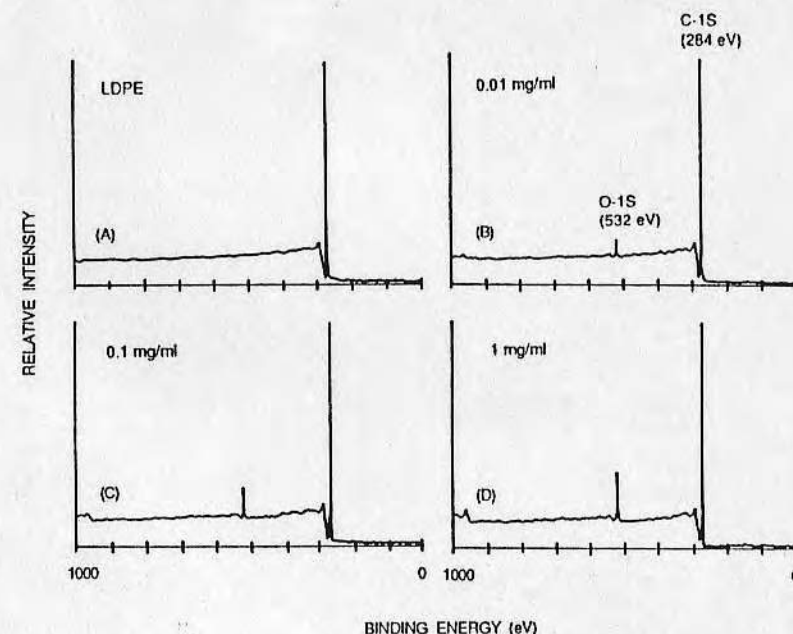


Figure 5. XPS wide scan of pure and PEO-PBO-PEO triblock surfactant-treated LDPE surface after 30 min adsorption. (Power, 400 W; flood gun, 6.0 eV.) (A) Pure LDPE surface, (B), (C), and (D) LDPE surfaces treated with the surfactant at different solution concentrations.

highly mobile.<sup>8</sup> We used surfactants having a PPO chain length of 29-30. It has been reported that a PPO chain length of about 30 is the maximum which can exist in a linear form in aqueous solution and will bind strongly onto a hydrophobic surface.<sup>33</sup> It was suggested that PPO chains shorter than about 30 will bind weakly on the surface due to the smaller number of binding sites for hydrophobic interactions, and that longer PPO chains will easily form intra-aggregates (micelle-like structures) in aqueous solution, resulting in weak binding onto the surface. For strong adsorption of surfactants, the PEO content and chain length are also important. In our previous work on dimethyl dichlorosilane (DDS)-coated glass slides,<sup>35</sup> which are strongly hydrophobic, we observed that the surfactants with high PEO content or long PEO chain lengths are not desirable for stable adsorption, because the PEO-water interactions are stronger than the PPO-hydrophobic surface interactions; also, surfactants with shorter PEO chain length will probably have lower protein resistance properties due to lower chain mobility and lower steric effects.<sup>8</sup>

Figure 6 shows that the adsorption of the surfactants on the LDPE surface is highly structure dependent. The starlike block copolymer, and especially

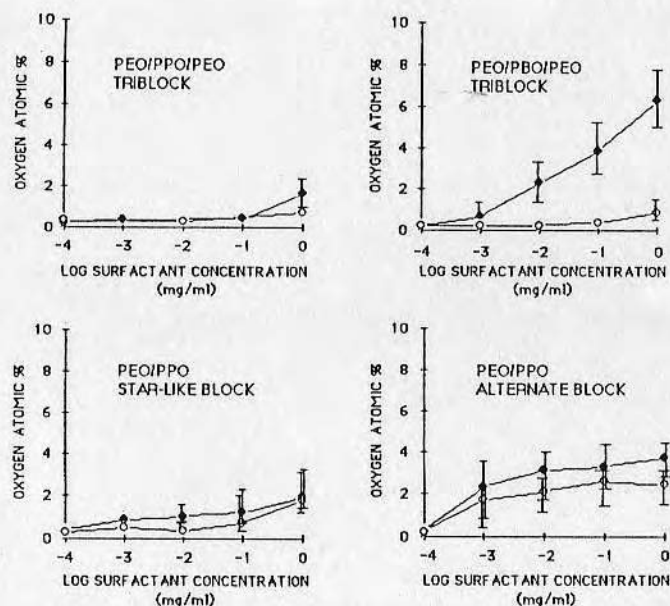


Figure 6. Adsorption and desorption properties of the surfactants with different structure on LDPE surface. Oxygen atomic % represents adsorbed amount of surfactant (see text for detail). Data points represent average values of 3–5 samples. (Solid points, 30 min adsorption of surfactants; open points, 30 min desorption in water after 30 min adsorption.)

the alternate block copolymer, surfactants appear much more effective for strong adsorption onto the LDPE surface than the triblocks, probably due to the greater number of hydrophobic binding sites of the blocks. PEO–PBO–PEO triblock surfactants show unstable adsorption. This phenomenon can possibly be explained by aggregation of the molecule in aqueous solution, i.e., PBO blocks have a more hydrophobic character than PPO blocks, as evidenced by their lower solubility in water (Table I) and lower surface tension values (Fig. 3), suggesting a higher possibility to self-aggregate in aqueous solution. If this type of aggregate, with PEO segments on the outside, contacts the hydrophobic surface, it will be readily desorbed.

The oxygen atomic% on the surface is a good qualitative indicator of the amount of the surfactant adsorbed, however, it is not directly proportional to the adsorbed amount because the surfactants have different oxygen contents. We can determine the relative amount of adsorbed surfactant by comparing the oxygen atomic% divided by the total number of oxygens in the surfactant. We compared the results of the starlike PEO/PPO block and the alternate PEO/PPO block (A and B in Fig. 7). The alternate block surfactant shows much better adsorption than the starlike block surfactant. Less adsorption of the starlike block copolymer may be due to the high mobility of tail-type PEO chains.

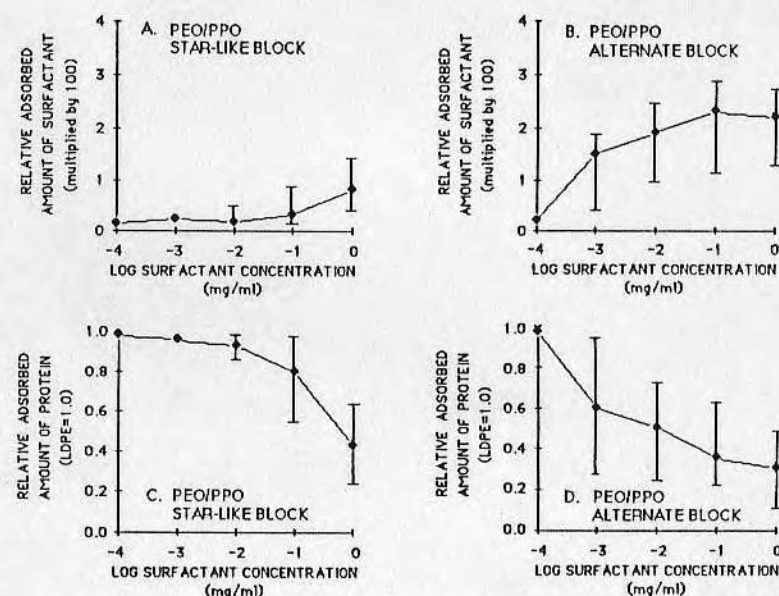


Figure 7. (A, B) Relative adsorbed amount of the surfactants on LDPE surface (30 min desorption in water after 30 min adsorption of surfactants). (C, D) Relative adsorbed amount of human albumin on the surfactant-treated LDPE surfaces (1 mg/mL, 30 min adsorption of protein; nitrogen atomic % of albumin adsorbed on untreated LDPE,  $10.4 \pm 3.3\%$ ).

#### Protein-resistant properties of the surfactant-treated surfaces

The protein resistant character of LDPE surfaces preadsorbed with starlike block and alternate block surfactants was also evaluated by XPS. We compared the protein nitrogen signal of the surfactant-treated surface with that of untreated LDPE (C and D in Fig. 7). Relative adsorbed amount of protein (human albumin) was determined as follows:

$$\text{Relative adsorbed amount of protein} = (\text{N\% of surfactant-treated surface}) / (\text{N\% of untreated surface})$$

We also evaluated the adsorbed amount of human albumin on LDPE surfaces by  $^{125}\text{I}$ -labeling of the protein and compared the results with those of XPS analysis (Table II). The results show that the amount of adsorbed protein on the surfactant-treated surfaces significantly decreased, compared with the untreated surface. Possible explanations include PEO's low interfacial free energy with water, unique solution properties and molecular conformation in aqueous solution, hydrophilicity, high surface mobility, and steric stabilization effects as discussed earlier.



TABLE II  
Adsorbed Amount of Human Albumin on LDPE Surface  
(Adsorption Condition: 1 mg/mL in PBS pH = 7.4, 30 min Adsorption)

Surfaces	$\mu\text{g}/\text{cm}^2$ ( $^{125}\text{I}$ -labeling)	N % (XPS)
Intreated LDPE	$0.45 \pm 0.08$	$10.4 \pm 3.3$
EO/PPO starlike block surfactant-treated LDPE (surfactant treatment at 1 mg/mL conc.)	$0.26 \pm 0.09$	$4.3 \pm 1.5$
EO/PPO alternate block surfactant-treated LDPE (surfactant treatment at 1 mg/mL conc.)	$0.20 \pm 0.02$	$3.9 \pm 1.1$

Sample numbers: 3-5.

By comparing C and D with A and B in Figure 7, we can see that the protein resistance of the surfactant-treated surface is highly dependent on the adsorbed amount of the surfactants and on PEO chain mobility. The starlike block surfactant at high concentration (1 mg/mL) shows a protein repulsion effect similar to that of the alternate block surfactant, even though its adsorbed amount on the LDPE surface was very small. This result suggests that the mobility of chains is an important factor for protein repulsion, because the starlike block has four tail-type PEO chains in its structure which are more mobile than the PEO loop present in the alternate block copolymer.

## CONCLUSIONS

Adsorption of PEO-containing block copolymer surfactants on a hydrophobic solid (LDPE) was highly dependent on the detailed structure (tri-, starlike, or alternate block) of the surfactants, even though they have the same PEO content and similar solubility, and on the nature of the hydrophobic segment (PPO or PBO). Protein resistance was also highly dependent on the adsorbed amount of the surfactants and on PEO chain mobility.

From this study, we showed a possible means to produce PEO-rich surfaces by a simple solution treatment of hydrophobic polyethylene; however, PPO or PBO are not strongly hydrophobic due to the presence of their ether oxygens; thus the molecule will be adsorbed on hydrophobic surfaces as small loops. Also PPO or PBO blocks should have limited chain lengths ( $n < 30$ ) to prevent self-aggregation in aqueous solution. Such small hydrophobic blocks result in weak bonding of the surfactant molecules on the surface. That is the reason why starlike or alternate block structures have better surface adsorption properties. Also the surfactants with longer PEO chains will be better for protein resistance,<sup>8</sup> if they can be adsorbed strongly on the surface.

We have some questions about the stability of surfactants adsorbed on LDPE surfaces. As water-soluble surfactants are adsorbed on a hydrophobic surface, will the surfactant molecules adsorbed on the surface be not desorbed or exchanged with the proteins during exposure to a protein solu-

tion? What will happen to the surfactant molecules adsorbed on the surface if flowing water or blood is used instead of a static system? PPO or PBO segments are not strongly hydrophobic for stable adsorption. Are there other structures to produce stable PEO surfaces for this approach? To overcome the limitations of commercial block copolymer surfactants, we are synthesizing new polymeric surfactants, copolymers of alkyl methacrylates with methoxy (polyethylene oxide) methacrylates<sup>36</sup> as the next step of this study. From the preliminary results, we observed that the synthesized copolymers are strongly adsorbed on LDPE surface, probably due to insoluble, hydrophobic, long polymethacrylate backbone and side alkyl chains of the copolymers.<sup>36</sup> From the time-dependent protein adsorption on the LDPE surfaces pre-treated with the  $^{125}\text{I}$ -labeled copolymers,<sup>36</sup> we also observed that there is little evidence of exchange of the polymer molecules with albumin for up to 100 min exposure, even though the copolymers are water soluble. These copolymer-treated surfaces also show excellent protein-resistant character. We are doing experiments to evaluate the long-term stability of this approach in a flowing environment.

This study was supported in part by a fellowship from Baxter and by NIH grant (HL 37046). We thank BASF-Wyandotte (Wyandotte, Michigan) and ICI (Cleveland, England) for gifts of the surfactant samples and for technical information, and the National Institutes of Health for the LDPE samples.

We further thank Dr. Ron Camp (BASF-Wyandotte); Drs. Ed Spaeth, Roger Drake, and Ken Mayhen (Baxter); and Dr. Irwin Schmolka (Grosse Ile, Michigan) for helpful advice and discussions.

## References

1. L. Vroman, *Blood*, Natural History Press, Doubleday and Co., Inc., New York, 1967.
2. J. D. Andrade, "Interfacial phenomena and biomaterials," *Med. Instrum.*, **7**, 110-120 (1973).
3. D. L. Coleman, D. E. Gregonis, and J. D. Andrade, "The minimum interfacial free energy and the optimum polar/apolar ratio hypothesis," *J. Biomed. Mater. Res.*, **16**, 381-398 (1982).
4. D. L. Coleman, "In vitro blood-materials interactions: A multi-test approach," Ph.D. Thesis, University of Utah (1980).
5. E. W. Merrill and E. W. Salzman, "Polyethylene oxide as a biomaterial," *ASAIO J.*, **6**, 60-64 (1983).
6. F. E. Bailey Jr. and J. Y. Koleske, *Poly (Ethylene Oxide)*, Academic Press, New York, 1976.
7. R. Kjellander and E. Florin, "Water structure and changes in thermal stability of the system poly(ethylene oxide)-water," *J. Chem. Soc., Faraday Trans.*, **1**, **77**, 2053-2077 (1981).
8. S. Nagaoka, Y. Mori, H. Tanzawa, and S. Nishiumi, "Interaction between blood components and hydrogels with poly(oxyethylene) chains," in *Polymers as Biomaterials*, S. W. Shalaby, A. S. Hoffman, B. D. Ratner, and T. A. Horbett (Eds.), Plenum Press, New York, 1984, pp. 361-374.
9. P. Bongrand and G. I. Bell, "Cell-cell adhesion: Parameters and possible mechanisms," in *Cell Surface Dynamics: Concepts and Models*, A. S. Perelson, C. DeLisi, and F. W. Wiegel (Eds.), Marcel Dekker, New York, 1984, pp. 459-493.

10. D. W. J. Osmond, B. Vincent, and F. A. Waite, "Steric stabilization: A reappraisal of current theory," *Colloid Polymer Sci.*, **253**, 676-682 (1983).
11. D. H. Napper, "Steric stabilization," *J. Colloid Interface Sci.*, **58**, 390-407 (1977).
12. A. K. Dolan and S. F. Edwards, "The effect of excluded volume on polymer dispersant action," *Proc. Royal Soc. London, A*, **343**, 427-442 (1975).
13. Th. F. Tadros, "Polymer adsorption and dispersion stability," in *The Effect of Polymers on Dispersion Properties*, Th. F. Tadros (Ed.), Academic Press, New York, 1982, pp. 1-38.
14. G. I. Bell, M. Dembo, and P. Bongrand, "Cell adhesion: Nonspecific repulsion and specific binding," *Biophys. J.*, **45**, 1051-1064 (1984).
15. N. G. Maroudas, "Polymer exclusion, cell adhesion and membrane fusion," *Nature*, **254**, 695-696 (1975).
16. F. Th. Hesselink, A. Vrij, and J. Th. Overbeek, "On the theory of the stabilization of dispersions by adsorbed macromolecules: II. Interaction between two flat particles," *J. Phys. Chem.*, **75**, 2094-2103 (1971).
17. D. H. Atha and K. C. Ingham, "Mechanism of precipitation of proteins by polyethylene glycols: Analysis in terms of excluded volume," *J. Biol. Chem.*, **256**, 12108-12117 (1981).
18. J. Hermans, "Excluded volume theory of polymer-protein interactions based on polymer chain statistics," *J. Chem. Phys.*, **77**, 2193-2203 (1982).
19. D. Knoll and J. Hermans, "Polymer-protein interactions comparison experiment and excluded volume theory," *J. Biol. Chem.*, **258**, 5710-5715 (1983).
20. J. Klein and P. Luckham, "Forces between two adsorbed polyethylene oxide layers immersed in a good aqueous solvent," *Nature*, **300**, 429-431 (1982).
21. J. Klein and P. Luckham, "Forces between two adsorbed poly(ethylene oxide) layers in a good aqueous solvent in the range 0-150 nm," *Macromolecules*, **17**, 1041-1048 (1984).
22. P. M. Claesson and C. G. Golander, "Direct measurements of steric interactions between mica surfaces covered with electrostatically bound low-molecular-weight polyethylene oxide," *J. Colloid Interface Sci.*, **117**, 366-374 (1987).
23. J. N. Israelachvili and G. E. Adams, "Measurement of forces between two mica surfaces in aqueous electrolyte solutions in the range 0-100 nm," *J. Chem. Soc., Faraday 1*, **74**, 975-1001 (1978).
24. J. N. Israelachvili, R. K. Tandon, and L. R. White, "Measurement of forces between two mica surfaces in aqueous polyethylene oxide solution," *J. Colloid Interface Sci.*, **78**, 430-443 (1980).
25. Y. Mori, S. Nagaoka, H. Takiuchi, T. Kikuchi, N. Noguchi, H. Tanazawa, and Y. Noishiki, "A new antithrombogenic material with long polyethylene oxide chains," *Trans. Am. Soc. Artif. Intern. Organs*, **28**, 459-463 (1982).
26. E. W. Merrill, E. W. Salzman, S. Wan, N. Mahmud, L. Kushner, J. N. Lindon, and J. Curme, "Platelet-compatible hydrophilic segmented polyurethanes from polyethylene glycols and cyclohexane diisocyanate," *Trans. Am. Soc. Artif. Intern. Organs*, **28**, 482-486 (1982).
27. C. W. Hiatt, A. Shelokov, E. J. Rosenthal, and J. M. Galimore, "Treatment of controlled pore glass with poly(ethylene oxide) to prevent adsorption of rabies virus," *J. Chromatography*, **56**, 362-364 (1971).
28. G. L. Hawk, J. A. Cameron, and L. B. Dufault, "Chromatography of biological materials on polyethylene glycol treated controlled-pore glass," *Preparative Biochem.*, **2**, 193-203 (1972).
29. D. E. Gregonis, D. E. Buerger, R. A. Van Wagenen, S. K. Hunter, and J. D. Andrade, "Poly(ethylene glycol) surfaces to minimize protein adsorption," *Transactions of the Second World Congress on Biomaterials*, 1984, pp. 266.
30. S. Winters, "Immobilized heparin via a long chain poly(ethylene oxide) spacer for protein and platelet compatibility," Ph.D. Thesis, University of Utah (1986).
31. J. S. Clunie and B. T. Ingram, "Adsorption of nonionic surfactants," in *Adsorption from Solution at the Solid/Liquid Interface*, G. D. Parfitt and C. H. Rochester (Eds.), Academic Press, New York, 1983, pp. 105-152.
32. J. B. Kayes and D. A. Rawlins, "Adsorption characteristics of certain polyoxyethylene-polyoxypropylene block co-polymers on polystyrene latex," *Colloid & Polymer Sci.*, **257**, 622-629 (1979).
33. H. Thurow and K. Geisen, "Stabilisation of dissolved proteins against denaturation at hydrophobic interfaces," *Diabetologia*, **27**, 212-218 (1984).
34. M. J. Schick (Ed.), *Nonionic Surfactants*, Marcel Dekker, New York, 1967, Chap. 10.
35. J. H. Lee and J. D. Andrade, "Surface properties of aqueous PEO/PPO block copolymer surfactants," in *Polymer Surface Dynamics*, J. D. Andrade (Ed.), Plenum Press, New York, 1988, pp. 119-136.
36. J. H. Lee, "Interactions of PEO-containing polymeric surfactants with hydrophobic surfaces," Ph.D. Thesis, University of Utah (1988).
37. J. D. Andrade, "X-ray photoelectron spectroscopy," in *Surface and Interfacial Aspects of Biomedical Polymers: Vol. 1. Surface Chemistry and Physics*, J. D. Andrade (Ed.), Plenum Press, New York, 1985, pp. 105-195.
38. H. Y. K. Chuang, W. F. King, and R. G. Mason, "Interaction of plasma proteins with artificial surfaces: Protein adsorption isotherms," *J. Lab. Clin. Med.*, **92**, 483-496 (1978).
39. G. P. Tuszyński, L. Knight, J. R. Piperno, and P. N. Walsh, "A rapid method for removal of [<sup>125</sup>I] iodine following iodination of protein solutions," *Anal. Biochem.*, **106**, 118-122 (1980).
40. M. J. Rosen, "Reduction of surface and interfacial tension by surfactants," in *Surfactants and Interfacial Phenomena*, Wiley-Interscience, New York, 1978, pp. 149-173.
41. H. H. Teo, S. G. Yeates, C. Price, and C. Booth, "Micellisation and surface properties of poly(oxyethylene) alkyl ethers," *J. Chem. Soc., Faraday Trans. 1*, **80**, 1787-1794 (1984).
42. K. N. Prasad, T. T. Luong, A. T. Florence, J. Paris, C. Vaution, and M. Seiller, "Surface activity and association of ABA polyoxyethylene-polyoxypropylene block copolymers in aqueous solution," *J. Colloid Interface Sci.*, **69**, 225-232 (1979).
43. G. J. Howard and P. McConnell, "Adsorption of polymers at the solution-solid interface. I. Polyethers on silica," *J. Phys. Chem.*, **71**, 2974-2980 (1967).
44. D. E. Guveli, S. S. Davis, and J. B. Kayes, "Critical micelle concentration, surface, volumetric, and hydrodynamic properties of polyoxyethylene monohexadecyl ethers," *J. Colloid Interface Sci.*, **91**, 1-11 (1983).
45. S. Kucharski and J. Chlebicki, "The effect of polyoxypropylene chain length on the critical micelle concentration of propylene oxide-ethylene oxide block copolymers," *J. Colloid Interface Sci.*, **46**, 518-521 (1974).
46. D. Attwood and A. T. Florence, *Surfactant Systems: Their Chemistry, Pharmacology and Biology*, Chapman & Hall, London, 1983.
47. W. Sasaki and S. H. Shah, "Availability of drugs in the presence of surface-active agents. I. Critical micelle concentrations of some



Lee J - 74  
Korea / cells

세포적합성 고분자 표면에 관한 연구

I. 고분자 표면 개질과 ESCA 분석

이진호 · 강길선 · 박경희 · 이해방 · Joseph D. Andrade

**Polymer Surfaces for Cell Adhesion**  
**I. Surface Modification of Polymers and ESCA Analysis**

Jin Ho Lee, Gil Son Khang, Kyung Hee Park,  
Hai Bang Lee, Joseph D. Andrade

醫工學會誌別冊

J. of the Korea Society of Medical & Biological Engineering

Vol. 10, No. 1, 1989

pp. 43-51

## 세포적합성 고분자 표면에 관한 연구 I. 고분자 표면 개질과 ESCA 분석

이진호 · 강길선 · 박경희 · 이해방 · \*Joseph D. Andrade

### Polymer Surfaces for Cell Adhesion I. Surface Modification of Polymers and ESCA Analysis

Jin Ho Lee, Gil Son Khang, Kyung Hee Park,  
Hai Bang Lee, Joseph D. Andrade\*

#### — Abstract —

We modified polymer surfaces, polyethylene, polystyrene and polyester, to improve cell-compatibility. For surface modification of the polymers, we used various surface treatment methods: physicochemical oxidation methods such as plasma discharge, corona discharge, sulfuric acid and chloric acid treatments, and biological methods such as adsorption of plasma protein and fibronectin onto the polymer surfaces. The treated polymer surfaces were characterized by electron spectroscopy for chemical analysis (ESCA). The physicochemically treated polymers showed different surface chemical structures depending on the treated methods. The sulfuric acid-treated surfaces showed greater carboxyl groups than those of plasma- or corona-treated surfaces, while the chloric acid-treated one showed high density of hydroxyl group on the surface. By the biological treatments, the surfaces were uniformly coated with proteins. The fibronectin adsorbed on the surface seems to have unique properties for cell binding.

#### 1. 서 론

의학 및 과학, 문명의 발달에 따라 수술이나 약리적 치료로 치유 불가능한 인체장기를 인공장기로 대체 이식하고자 하는 연구들이 세계적으로 널리 행해지고 있다. 특히 고분자 재료는 인공장기

를 만드는데 가장 중요한 소재로서, 인공심장, 인공신장, 인공혈관, 인공관절 등의 개발에 널리 이용되고 있다.

고분자를 이용한 인공장기 개발에 가장 큰 문제가 되는 것은 인공장기를 인체내에 이식시켰을 때 혈액 및 생체적합성 문제이다. 즉 이물질이 인체내에 삽입되었을 때, 이에 대한 생체내 거부반응으로 인해 주변의 조직세포에 변질이 생기고 이로 인해 인체내에 부작용이 생기거나, 인공장기 표면에 인체내의 여러가지 단백질이나 혈액 구성분들이 흡착됨으로서 인공장기의 기능이 시간이 경과함에 따라 저하하게 된다. 특히 인공혈관의 경우, 인체내 이식시 생체 거부현상이 없어야 함은 물론

<접수: 1989년 6월19일>

한국 화학 연구소, 고분자 제3연구실

Polymer Research Lab. 3, Korea Research Institute  
of Chemical Technology

\*Utah 대학교, 생체공학과

\*Dept. of Bioengineering, University of Utah, U.S.A.



이러니와 끊임없는 수축 팽창을 통해 혈관내를 상당한 압력을 받으며 흐르는 혈류에 견딜 수 있는 유연성과 기계적, 물리적 특성을 지녀야 하며, 혈관내 혈액 응고 현상등을 유발시키지 않아야 한다. 혈액은 매우 복잡한 화학적 조성을 지니고 있는데, 구성분의 반 정도가 적혈구(red blood cells or erythrocytes), 백혈구(white blood cells or leukocytes), 혈소판(platelets) 등의 세포로 구성되어 있고 나머지 반 정도가 액체 성분인 혈장(blood plasma)으로 되어 있다.<sup>1)</sup> 혈장은 약 90%가 물이고 약 10%의 고체 성분이 물속에 용해되어 있는데, 고체 성분중 약 70% 정도가 단백질(plasma proteins)이고 20% 정도가 유기물, 나머지 10% 정도가 무기염으로 구성되어 있다.<sup>2)</sup> 이와같이 복잡한 구조를 하고 있는 혈액이 인체내 삽입된 이물질과 접촉하게 되면 수분내에 단백질이 이물질 표면에 흡착하게 되고, 그로인해 여러가지 혈액내 구성분들과의 상호작용이 촉진되어 “내인계 응혈현상(intrinsic blood coagulation system)”, “외인계 응혈현상(extrinsic blood coagulation system)”, “혈소판계 응집현상” 등과 같은 복잡한 과정을 통해 혈액이 이물질 표면에서 응고하게 된다.<sup>3, 4)</sup>

고분자 표면의 “항응혈성(anticoagulation)” 또는 “항혈전성(thromboresistance)”을 향상시켜 주기 위한 여러가지 시도가 지난 30 여년간 계속되어져 왔는데,<sup>5-12)</sup> 아직 인체내 혈관 “내피표면(endothelium or endothelial surface)”과 같은 완벽한 항혈전성을 지닌 재료가 개발되지 못하고 있는 실정이다. 내피표면은 “내피세포(endothelial cell)”라 불리는 얇은 다각형 세포들이 단일층 (약 1 micron 두께)으로 밀집되어 이루어진 표면이다. 고분자 표면의 항혈전성을 향상시켜주기 위한 하나의 방법으로 이와같은 내피세포를 고분자 표면에 균일하게 이식시켜 주면 인체내 혈관 내피표면과 유사한 항혈전성을 지닐수가 있게 되지만, 일반적으로 고분자 표면은 세포와의 적합성이 좋지 않아 쉽사리 세포가 고분자 표면에서 부착 성장할 수가 없다.

따라서 본 연구에서는 polyethylene, polystyrene

Table 1. Polymer surface modification methods used.

- |                                    |
|------------------------------------|
| I. Physicochemical                 |
| A. O <sub>2</sub> plasma discharge |
| B. Corona discharge                |
| C. Sulfuric acid treatment         |
| D. Chloric acid treatment          |
| II. Biological                     |
| A. Plasma protein adsorption       |
| B. Fibronectin adsorption          |

과 같은 단순한 화학적 구조를 가지는 고분자와 인공혈관 재료로 널리 쓰이는 polyester의 표면을 세포적합성이 좋도록 여러가지 방법으로 개질하였다(표 1). 본 연구실에서 행한 연구 결과에 의하면,<sup>13)</sup> 세포는 소수성 표면보다는 어느정도 친수성을 가진 표면에서 더 잘 부착 성장하므로 고분자 시료의 친수성을 향상시키기 위해 플라즈마 방전, 코로나방전, sulfuric acid, chloric acid 처리등과 같은 물리화학적 방법으로 표면을 산화시켰다. 산화처리후 표면에서 나타나는 화학적 구조 변화를 electron spectroscopy for chemical analysis(ESCA)에 의해 분석하였다. 또한 생물학적인 표면처리 방법으로서 세포부착 및 성장촉진 단백질로 알려진 fibronectin이나<sup>14, 15)</sup> fibronectin이 함유된 plasma protein을 고분자 표면에 흡착시킨 후 역시 ESCA로 분석하였다. 이들 서로 다른 화학적 구조를 가진 고분자 표면이 세포적합성에 어떻게 영향을 미치는지는 본 논문의 후편(part II)에서 논의 될 것이다.

## 2. 실험

### 2-1 고분자 시료 및 시료의 전처리

사용한 고분자 시료는 첨가제가 전혀 함유되어 있지 않은 저밀도 polyethylene(LDPE, 한양화학) film, polystyrene(PS) plate(녹십자 의료공업(주)), polyethylene terephthalate (PET) film ((주) 신경) 등이다. 이들 고분자 시료들을 적당한 크기로 잘라 ethanol에서 2회 30분간씩 ultrasonication 시킨후 ethanol로 여러번 세척하여 진공 건조후 진공 데시케이터에 사용시까지 보관하였다.

이들 시료 표면은 ESCA에 의한 관찰 결과 위와 같은 처리후 아무 오염이 되지 않은 깨끗한 상태임이 확인되었다.

## 2-2 표면개질 방법

### 1) 산소 플라즈마 방전 처리

본 연구실에서 자체 제작한 Bell-jar형 플라즈마 방전 장치를 사용하였다. 고분자 시료의 처리 과정 및 조건은 그림. 1과 같다.

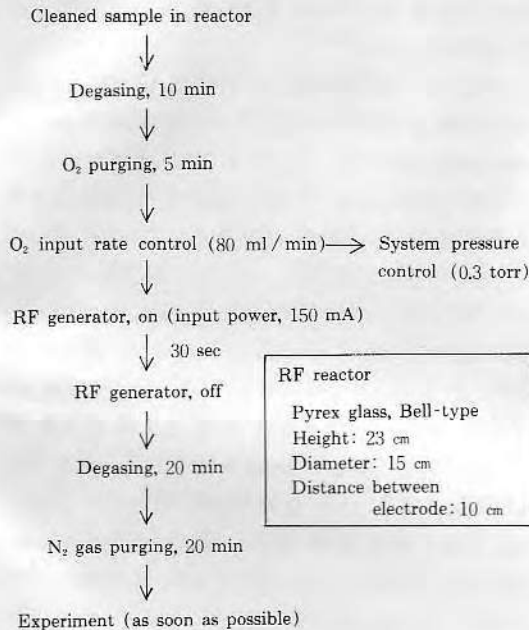


Fig 1. Plasma discharging process and operation condition

### 2) 코로나 방전 처리

역시 본 연구실에서 자체 제작한 코로나 방전 장치를 이용하여 대기중에서 고분자 시료를 60초 동안 처리하였다.

### 3) Sulfuric acid 처리

상온에서 고분자 시료를 진한 황산(98%)내에 10분동안 담갔다가 꺼낸후 초순수(MPI ultrapure water system)로 철저히 세척한 후 진공 건조시켰다.

### 4) Chloric acid 처리

상온에서 70% perchloric acid( $\text{HClO}_4$ )와 수용액내에서 포화된 potassium chlorate( $\text{KClO}_3$ )를 3:2로 혼합한 chloric acid mixture 용액에 고분자 시료를 10분간 담가 표면을 산화시킨후 꺼내어 초순수로 철저히 세척하고 진공 건조시켰다.

### 5) Plasma protein 흡착

백명 이상의 건강한 20-40대 남자들로부터 혈액을 채취하여 추출한 standard human plasma (lyophilized powder, Sigma)를 phosphate buffer saline(PBS, pH 7.2-7.3) 용액에 용해시킨 다음 1% 농도로 희석한후 상온에서 고분자 시료를 30분간 담갔다가 꺼내 PBS로 철저히 세척한후 다시 고분자 시료를 PBS에 30분간 담가 표면에 약하게 결합된 단백질을 탈착시키고 다시 PBS로 여러번 세척하고 초순수로 세척하여 진공 건조시켰다.

### 6) fibronectin 흡착

Bovine plasma로부터 추출된 fibronectin (lyophilized powder, Sigma)을 PBS(pH 7.2-7.3)에 용해시켜 50  $\mu\text{g}/\text{ml}$ 의 농도로 만들었다. 상온에서 고분자 시료를 fibronectin 용액에 1시간동안 담그어 fibronectin을 고분자 표면에 흡착시켰다. 고분자 시료를 PBS로 여러번 세척한 다음 다시 PBS에 30분동안 담갔다가 꺼내 PBS로 여러번 세척하고 초순수로 다시 세척하여 진공 건조시켰다.

## 2-3 사용한 기기

표면처리후 고분자 시료 표면에서 나타나는 화학적 구조 변화를 ESCA로 분석하였다. ESCA는 일명 X-ray photoelectron spectroscopy(XPS)라고도 불리며 V.G. Scientific사의 ESCALAB MK II model을 사용하였다(Radiation source, Mg  $K\alpha$  at 1253.6 eV; power at anode, 300 W).

## 3. 결과 및 고찰

고분자 시료를 여러가지 물리화학적 방법으로 산화처리하였을때 시료 표면의 화학적 구조 변화를 확인하기 위해, 우선 고분자들 중에서는 가장 단순한 화학적 구조를 가진 polyethylene (LDPE)

film에 여러가지로 표면처리를 하여 ESCA로 분석하였다. ESCA(또는 XPS)는 고체 표면에 존재하는 수소와 헬륨을 제외한 모든 원소의 분석을 가능하게 해주며, 표면에 존재하는 원소들의 화학적 결합방식에 대한 정보도 제공해 준다. ESCA는 시료 분석시 표면에 아무 손상을 주지 않으며, 시료에 방사되는 photons (electromagnetic radiations)이 표면으로부터 수십 Å까지만 투과하므로 표면에 아주 민감하게 작용하는 분석기기이다<sup>16)</sup> (ATR-IR의 경우 표면으로부터 수백 Å까지 투과하므로 ESCA에 비해 표면에 덜 민감하게 작용한다). ESCA의 기본원리는 "photon electron effect" 즉 시료 표면에 photons가 방사될때 저에너지 전자들이 표면으로부터 방출되는 현상인데, ESCA는 표면으로부터 방출되는 이들 전자의 수를 측정하는 기기이다. 시료 표면에 방사된 photon energy( $h\nu$ )가 표면에 존재하는 원소내 전자들의 결합에너지( $E_b$ )보다 크면, 원소로부터 일정한 운

동에너지( $E_k$ )를 가진 전자가 방출하기 된다. ESCA에 적용되는 기본 방정식은,

$$E_b \approx h\nu - E_k$$

로서 모든 에너지는 electron volts(eV)로 표시된다. 방출되는 전자의 운동에너지를 측정하므로써 위 식에 의해 원소내에서 전자들의 결합에너지를 산출할수가 있다. 각 원소들은 그 종류에 따라서 또는 원소들의 결합 방식에 따라서 고유의 결합에너지를 가지므로, 산출된 결합에너지로부터 존재하는 원소들의 종류와 원소들의 화학적 결합구조를 알수있게 된다.<sup>16-18)</sup>

그림. 2는 표면처리를 하지않은 LDPE와 산소 플라즈마 방전처리한 LDPE 표면의 ESCA survey scan spectrum들을 보여주고 있다. 표면처리를 하지않은 경우(그림. 2(A)), LDPE이 탄소들로만 구성되어 있기 때문에 결합에너지 285 eV 부근에서 커다란 탄소 피크가 나타난다. 결합에너지 532 eV 부근에서 보이는 조그만 피크는 산소 피크인데, 고분자 시료의 공기중 산화에 의한 것으로 추정할 수 있다. 결합에너지 770 eV 부근과 990 eV 부근에 나타나는 피크들은 각각 산소와 탄소로부터 수반되는 Auger peak들이다.<sup>16, 19)</sup> 이와같은 LDPE 표면을 산소 플라즈마로 방전처리 하게되면, 표면산화에 의해 산소 피크가 크게 나타나는 데(그림. 2(B)), 이들 두 피크의 면적비로부터 구해진 표면의 조성은 산소와 탄소가 22.4:77.6 atomic %로 나타났다.

표면처리에 의해 산화된 고분자 시료의 화학적 구조변화, 즉 표면에 부착된 산소의 관능기(functional group) 분포도는 탄소 피크 부분만을 따로 scanning한 C-1S core level spectrum을 분석함으로써 알수있다(그림. 3). 즉 표면처리를 하지않은 LDPE의 경우(그림. 3(A)), C-1S core level 피크가 결합에너지 285 eV(C-C bond)근처에서 나타나지만 표면의 탄소가 산화처리에 의해 산소와 결합하게 될때 결합된 화학적 구조에 따라 탄소의 결합에너지가 달라지게 된다. 즉 한개의 산소와 단일결합된 탄소(C-O)의 결합에너지는 286.6 eV 정도이며, 두개의 산소와 단일결합된 탄소

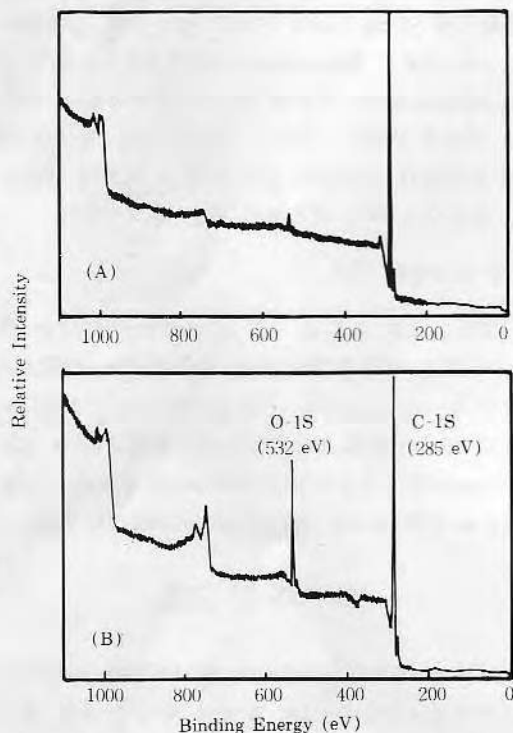


Fig 2. Survey scan spectra of LDPE  
(A) Untreated, (B) O<sub>2</sub> plasma-discharged



(O-C-O) 또는 한개의 산소와 이중결합된 탄소(C=O)의 결합에너지는 287.9 eV 정도이며, carboxylate  $C\begin{smallmatrix} \diagup O \\ \diagdown \end{smallmatrix}$ 와 carbonate  $O-C\begin{smallmatrix} \diagup O \\ \diagdown \end{smallmatrix}$  탄소의 결합에너지는 각각 289.1 eV와 290.4 eV 정도로 나타난다.<sup>20)</sup> 즉 고분자 시료의 산화처리에 의해

C-1S spectrum 상에 나타날수 있는 결합에너지들은 다음과 같은 순서로 되어있다.

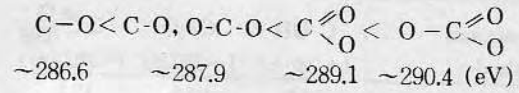


그림. 3((B)-(E))은 여러가지 방법으로 표면 처리된 LDPE의 C-1S core level spectrum들을 보여주고 있다. 그림. 3(A)에서 보듯이 미처리된 LDPE은 alkyl carbon들만으로 구성되어 있기 때문에 하나의 탄소 피크를 나타내는 반면, LDPE이 산소 플라즈마에 노출하게되면 표면산화 반응에 의해 탄소 피크가 복잡한 양상을 띠게 된다(그림. 3(B)). 각 피크들의 결합에너지들로부터 예측되는 표면의 탄소들은 alkyl carbon(C-C bond, ~285 eV), hydroxyl group이 결합된 carbon (C-OH bond, ~286.6 eV), carbonyl carbon(C=O bond,

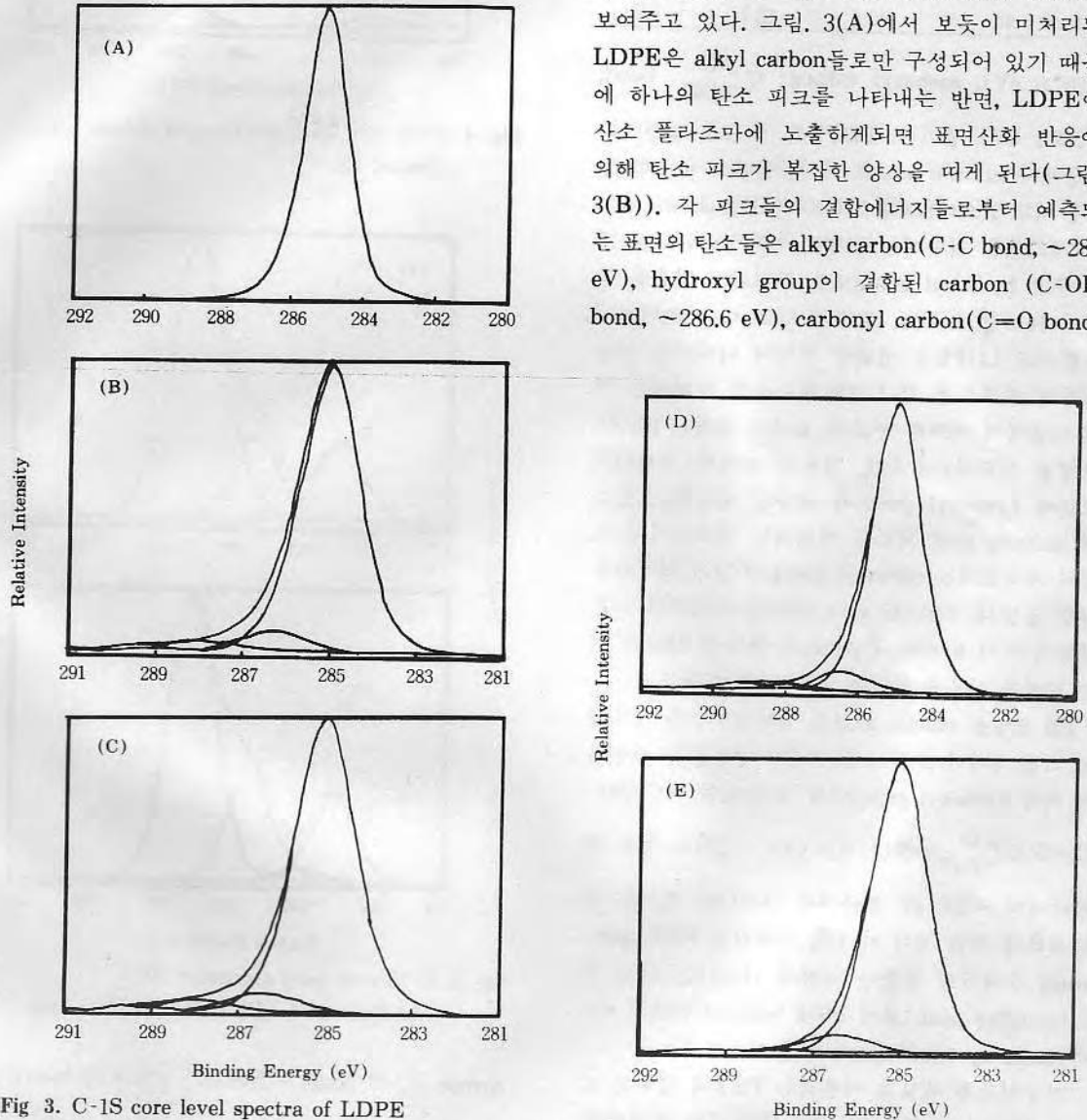


Fig 3. C-1S core level spectra of LDPE  
(A) Untreated, (B) O<sub>2</sub> plasma-discharged, (C) Corona-discharged, (D) Sulfuric acid-treated, (E) Chloric acid-treated

**Table 2.** Composition (%) of oxidized functional groups on the LDPE surfaces

Treatment method	C-OH (~286.6)	C=O (~287.9)	C $\begin{smallmatrix} \text{O} \\ \parallel \\ \text{OH} \end{smallmatrix}$ (~289.1)(eV)
O <sub>2</sub> plasma	59.5	27.9	12.1
Corona	58.2	30.9	10.9
Sulfuric acid	60.0	20.0	20.0
Chloric acid	86.4	12.1	1.5

~287.9 eV), carboxyl carbon( C  $\begin{smallmatrix} \text{O} \\ \parallel \\ \text{OH} \end{smallmatrix}$  bond,

~289.1 eV) 등이다. LDPE를 코로나 방전처리했을때나 sulfuric acid로 처리했을때도 비슷한 양상을 띠고 있으나(그림. 3(C)와 (D)), chloric acid로 처리했을 경우에는 표면에서 형성되는 관능기가 주로 hydroxyl group으로 구성되어 있음을 알 수 있다(그림. 3(E)). 표 2에 서로 다른 표면처리 방법으로 LDPE를 산화한 표면에 나타나는 관능기들의 분포도를 각 C-1S 피크들의 면적비로부터 산출하여 비교해 놓았다. 표에서 보듯이 LDPE 표면을 산화처리했을때, 사용한 방법에 상관없이 표면에 hydroxyl group이 상당량 형성되고 있으며, sulfuric acid 처리를 하게되면 플라스마나 코로나 처리보다는 carboxyl group이 많이 형성됨을 알 수 있었다. Chloric acid 처리를 하게되면 다른 방법에 비해 hydroxyl group의 분포가 상당히 많은 표면을 얻을 수 있다는 것도 알게 되었다.

PS 표면을 chloric acid로 산화처리했을 경우에도 그림. 4에서 보듯이 표면에서 형성되는 관능기가 거의 hydroxyl group임을 알 수 있었다(C-OH: C=O: C  $\begin{smallmatrix} \text{O} \\ \parallel \\ \text{OH} \end{smallmatrix}$  = 88.7: 9.9: 1.4). PS의 경우 결합에너지 ~292 eV 부근에서 나타나는 피크는 표면산화에 의한 것이 아니고, 미처리된 PS의 spectrum 상에서도 동일한 지점에 나타나는 위성 피크(satellite peak)로서 PS내 benzene ring의  $\pi-\pi^*$  shake-up transition에 의한 것이다.<sup>20)</sup>

인공혈관용 재료로 사용되는 PET의 경우는 고분자 자체의 구조가 PE이나 PS보다는 복잡하여, 미처리된 PET의 C-1S spectrum을 보면(그림. 5(A)), PET 자체의 화학적 구조로부터 alkyl

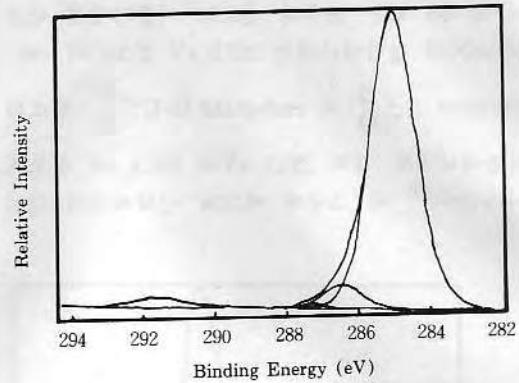


**Fig 4.** C-1S core level spectrum of chloric acid-treated PS.

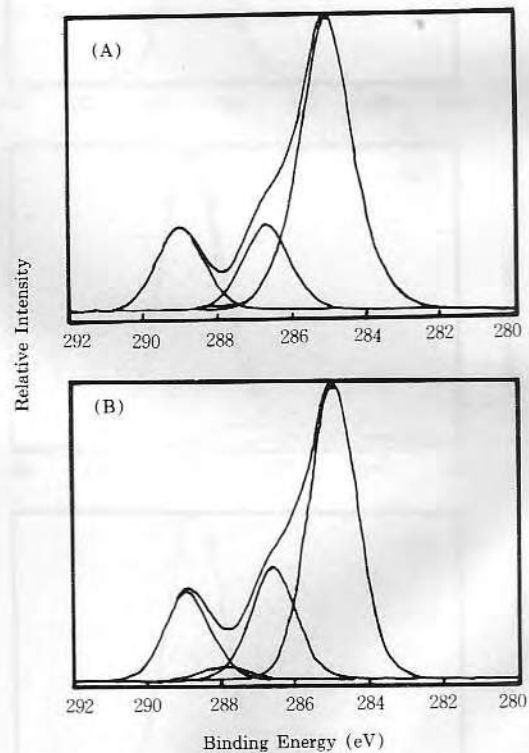


**Fig 5.** C-1S core level spectra of PET  
(A) Untreated, (B) Chloric acid-treated

carbon (C-C bond, ~285 eV), ether carbon(C-O-C bond, ~286.6 eV), ester carbon(C  $\begin{smallmatrix} \text{O} \\ \parallel \\ \text{O}-\text{C} \end{smallmatrix}$  bond, ~289.1 eV) 등 세개의 피크가 대략 3:

1:1의 면적비로 나타난다. PET를 chloric acid로 산화처리 하게되면 PE이나 PS의 경우와 마찬가지로 표면에서 형성되는 hydroxyl group의 증가로 인해 미처리 시료보다 결합에너지  $\sim 286.6$  eV 부근의 피크가 증가하게 된다(그림. 5(B)). 그림. 5(B)에서 볼때, PET자체의 구조로부터의 ether carbon 피크와 산화처리에 의해 새로 형성된 hydroxyl group에 의한 피크의 결합에너지가 거의 동일해( $\sim 286.6$  eV) 하나의 피크로 나타나고, PET 자체의 ester carbon 피크와 산화에 의한 carboxyl group 피크 역시 동일한 지점에서 하나의 피크로 나타난다(결합에너지,  $\sim 289.1$  eV).

생물학적으로 표면을 개질하는 방법으로 LDPE 표면에 blood plasma protein과 fibronectin을 흡착시켰을때의 ESCA 분석 결과를 그림. 6과 7에 나타내었다. LDPE표면이 탄소 피크와 공기중 산화

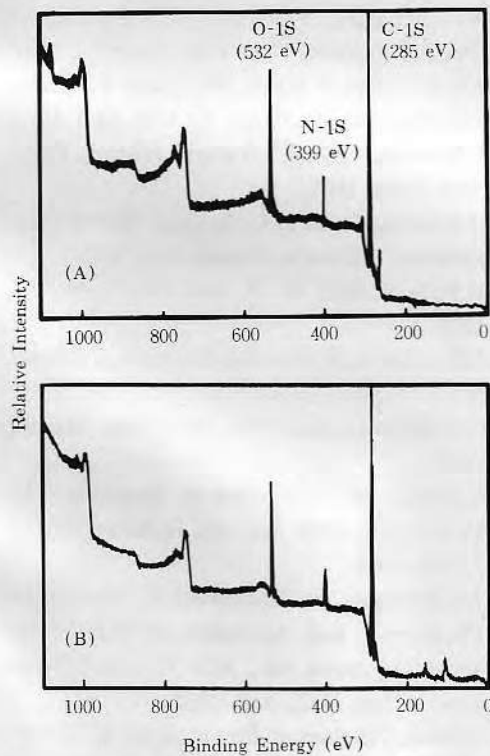


Fig 6. Survey scan spectra of protein-adsorbed LDPE (A) Plasma protein-adsorbed, (B) Fibronectin-adsorbed

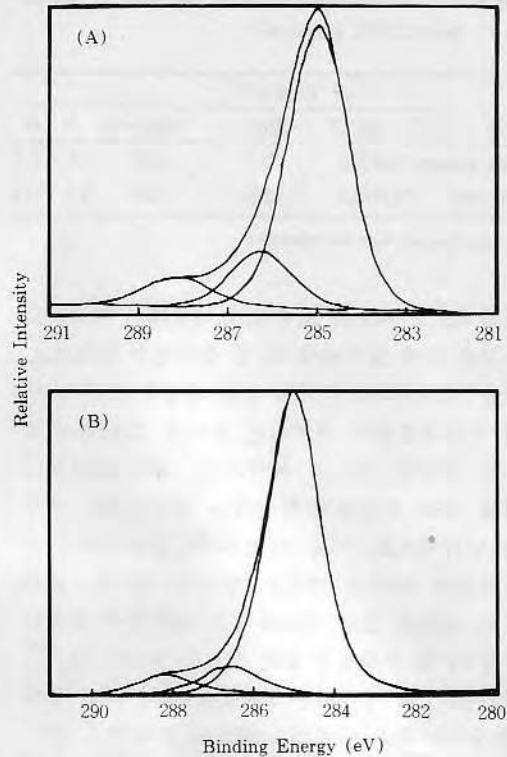


Fig 7. C-1S core level spectra of protein-adsorbed LDPE (A) Plasma protein-adsorbed, (B) Fibronectin-adsorbed

에 의한 아주 작은 산소 피크를 가진 단순한 survey scan spectrum을 보이는데 비해(그림. 1(A) 참조), 단백질들이 흡착된 LDPE 표면은 탄소, 질소, 산소를 포함하는 비교적 복잡한 양상의 spectrum을 보여주고 있다(그림. 6). Spectrum상에 나타나는 질소와 산소 피크들은 단백질이 peptide bond (CO-NH)로 이루어졌기 때문에 단백질이 고분자 표면에 흡착되었을때 나타나는 전형적인 피크들로서, 특히 질소 피크는 흡착된 단백질의 양을 결정해주는 척도로서 이용되고 있다.<sup>21)</sup> Peptide bond에 의한 탄소 피크는 그림. 7의 C-1S spectrum에서 보듯이 결합에너지  $\sim 288.1$  eV 부근에서 나타나고 있다. 그림. 6과 7의 spectrum 상에 나타난 피크들의 면적비로부터 산출된 원소분석 결과를 표-3에 나타내었다.



**Table 3.** Elemental composition of the protein-adsorbed LDPE surfaces

Protein	Atomic % <sup>a</sup>			N	O
	C (~285 eV)	~286.6 eV	~288.1 eV		
Plasma protein	75.4(76.5)	15.3	8.2)	6.9	17.7
Fibronectin	78.9(88.0)	7.0	5.0)	5.7	15.4

<sup>a</sup> S or other elements were not measured.

일반적으로 세포는 소수성 표면보다는 어느정도 친수성을 가진 표면에서 더 잘 증식될수 있으므로, 표면을 산화처리해서 친수성이 향상된 고분자 시료의 세포적합성이 미처리된 소수성 고분자 시료보다는 향상될 것으로 예측된다. 특히 표면처리 방법에 따라 표면에서 형성되는 관능기들의 분포도가 달라지므로, 이들 서로 다른 관능기들이 세포적합성에 미치는 영향도 달라질 것이다. 또한 세포는 고분자 표면 자체보다는 단백질이 흡착된 표면에 더 잘 부착할수 있는 것으로 알려져 있고<sup>22)</sup> 특히 단백질들 중에서는 fibronectin이 세포 부착을 촉진시켜 주는 단백질로 알려져 있다.<sup>14, 15)</sup> Fibronectin 은 blood plasma 내에 0.3 g/l 의 농도로 존재하는 단백질로서 세포와 결합할 수 있는 domain 구조를 가지고 있다.<sup>23)</sup> 따라서 fibronectin 이 고분자 표면에 흡착되면, 고분자 표면의 세포적합성이 향상될 것으로 기대할 수 있다.

#### 4. 결 론

본 연구를 통하여, 고분자 표면에 세포를 이식하여 항응혈성이 향상되도록 하기 위한 시도로서 다양한 방법으로 표면을 개질하였다. 개질된 고분자 시료는 처리방법에 따라 표면에서 형성되는 화학적 구조가 달라지는 것을 ESCA 분석을 통해 확인하였다.

고분자 시료의 세포적합성을 향상시키기 위해서 사용한 물리화학적 표면개질 방법들은 플라스마 방전처리, 코로나 방전처리, sulfuric acid처리, chloric acid처리등과 같은 산화 처리 방법들인데, 사용한 방법에 관계없이 표면에 hydroxyl group이 상당량 형성되었다. 특히 sulfuric acid처리를 하게

되면 플라스마나 코로나 방전처리를 했을때보다 표면에 carboxyl group의 형성이 증가하였고, chloric acid 처리를 하게되면 다른 방법에 비해 hydroxyl group의 분포가 상당히 많이 형성되었다. 생물학적인 표면개질 방법으로서 plasma protein 이나 fibronectin을 고분자 표면에 흡착시켰는데, 두 단백질의 흡착 양상이 ESCA의 spectrum 상에서는 비슷하게 나타나지만 이들 단백질의 특성에 따라 세포적합성은 달리 나타날 것으로 판단된다. 각 표면개질 방법에 따른 세포적합성 향상 여부는 후편(part II)에서 논의될 것이다.

**감사문:** 이 논문은 1988년도 과학 기술처 특정 연구 개발사업(N88-0124)의 연구비 지원으로 연구되었다.

#### 참 고 문 헌

- 1) A.L.Lehninger "Principles of Biochemistry," Worth Publishers, New York, Chap. 12, 1982.
- 2) J.D.Andrade, H.B.Lee, M.S.Jhon, S.W.Kim, and J.B.Hibbs, Jr., Trans. ASAIO, 19, 1, 1973.
- 3) L.Vroman, "Blood," Natural History Press, New York, 1967.
- 4) R.F.A.Zwaal and H.C.Hemker, "Blood Coagulation," Elsevier, Amsterdam, 1986.
- 5) R.E.Baier, Bull. N. Y. Acad. Med., 48, 257, 1972.
- 6) J.D.Andrade, S.Nagaoka, S.Cooper, T.Okano, and S.W.Kim, ASAIO J., 10, 75, 1987.
- 7) A.S.Hoffman, Ann N.Y. Acad. Sci., 516, 96, 1987.
- 8) Y.Ikada, in "Polymers in Medicine," K. Dusek, ed., APS Ser. 57, Springer-Verlag, p. 103, 1984.
- 9) A.S.Hoffman, in "Biomaterials: Interfacial Phenomena and Applications," S.L.Cooper and N.A.Peppas, eds., ACS 199, ACS Press, Washington, D.C., p. 3, 1982.
- 10) J.Block, "Biological Performance of Materials," Marcel Dekker, New York, 1981.
- 11) L.L.Hench and E.C.Ethridge, "Biomaterials: An Interfacial Approach," Academic

- Press, New York, 1981.
- 12) S.W.Kim and J.Fejin, in "CRC Critical Reviews in Biocompatibility," Vol. 1, CRC Press, Boca Raton, p. 215, 1985.
  - 13) H.B.Lee and J.D.Andrade, Trans. 3rd World Biomaterials Congress, Kyoto, Japan, p. 43, 1988.
  - 14) K.M.Yamada, Ann. Rev. Biochem., 52, 761, 1983.
  - 15) K.M.Yamada and K. Olden, Nature, 275, 179, 1978.
  - 16) J.D.Andrade, in "Surface and Interfacial Aspects of Biomedical Polymers, Vol. 1. Surface Chemistry and Physics," J.D.Andrade, ed., Plenum Press, New York, Chap. 5, 1985.
  - 17) B.D.Ratner, Ann. Biomed. Eng., 11, 313, 1983.
  - 18) M.P.Seah, Surface Int. Anal., 2, 222, 1980.
  - 19) T.A.Carlson, "Photoelectron and Auger Spectroscopy," Plenum Press, New York, Chap. 6, 1975.
  - 20) D.T.Clark and A.Dilks, J. Polymer Sci., Polymer Chem. Ed., 17, 957, 1979.
  - 21) J.H.Lee, "Interactions of PEO-containing Polymeric Surfactants with Hydrophobic Surfaces," Ph.D. Thesis, University of Utah, U.S.A., 1988.
  - 22) A.S.G.Curtis and J.Pitts, "Cell Adhesion and Mobility," Cambridge University Press, p. 357, 1980.
  - 23) R.O.Hynes, Sci. Amer., 254(6), 32, 1986.

세포적합성 고분자 표면에 관한 연구  
II. 표면 개질된 고분자에의 세포 배양

이진호 · 강길선 · 박경희 · 이해방 · Joseph D. Andrade

Polymer Surfaces for Cell Adhesion  
II. Cell Culture on Surface-modified Polymers

Jin Ho Lee, Gil Son Khang, Kyung Hee Park, Hai Bang Lee, Joseph D. Andrade

醫工學會誌別冊

J. of the Korea Society of Medical & Biological Engineering

~~Vol.~~ 10, No. 2, 1989

PP-195-200



## 세포적합성 고분자 표면에 관한 연구 II. 표면 개질된 고분자에의 세포 배양

이진호 · 강길선 · 박경희 · 이해방 · \*Joseph D. Andrade

### Polymer Surfaces for Cell Adhesion II. Cell Culture on Surface-modified Polymers

Jin Ho Lee, Gil Son Khang, Kyung Hee Park, Hai Bang Lee, \*Joseph D. Andrade

#### — Abstract —

Chinese Hamster Ovary(CHO) cells were cultured on the surface-modified polymers described in the previous study("Polymer Surfaces for Cell Adhesion, I. Surface Modification of Polymers and ESCA Analysis," J. of KOSOMBE, Vol. 10, No. 1, 43-51, 1989). Among the physicochemical treatment methods, the chloric acid treatment was found to be the best method of rendering the polymer surfaces adhesive for CHO cells probably due to the high density of hydroxyl groups on the surface. Among the biological methods, the fibronectin treatment was best for CHO cell-compatibility probably due to specific active sites existed on the cell-binding domains of the fibronectin structure. When we compare the cell-compatibility of the chloric acid—and the fibronectin—treated PET surfaces, the number of cells attached on the surfaces were increased by 460.5 % and 559.0 %, respectively, after 32 hr CHO cell culture, compared to that of untreated PET.

#### 1. 서 론

고분자를 이용한 인공장기 개발에 가장 큰 문제가 되는 것은 인공장기를 인체내에 이식시켰을때 혈액

<접수: 1989년 6월19일>

한국 화학 연구소, 고분자 제3연구실

Polymer Research Lab. 3, Korea Research Institute of Chemical Technology

\*Utah 대학교, 생체공학과

\*Dept. of Bioengineering, University of Utah, U. S.A.

및 생체적합성 문제이다. 즉 이물질이 인체내에 삽입되었을때, 이에 대한 생체내 거부반응으로 인해 주변의 조직세포에 변질이 생기고 이로 인해 인체내에 부작용이 생기거나, 인공장기 표면에 인체내의 여러가지 단백질이나 혈액 구성분들이 흡착됨으로서 인공장기의 기능이 시간이 경과함에 따라 저하하게 된다. 특히 인공혈관의 경우 "혈액적합성(blood compatibility)"이 가장 중요한 요인이 되고 있는데, 혈액적합성을 가지려면 재료표면이 "항혈전성(thromboresistance)" 또는 "항응혈성(anticoagulation)"을 가져야 함은 물론이러니와 혈액과 접촉시 혈액내 단백질, 효소, 혈소판, 혈구등과 같은 구성분들을 변

질시키거나 손상해서도 안된다.

고분자 재료의 혈액적합성을 향상시켜 주기 위한 연구가 세계 곳곳에서 수십년동안 진행되어 왔지만 아직 완벽한 혈액적합성을 나타내는 재료는 개발되지 않고 있는 실정이다.<sup>1-8)</sup> 완벽한 혈액적합성을 나타내는 model case로서 혈관 내벽을 예로 들 수가 있는데, 혈관 내벽이 혈액적합성을 가지는 것은 혈관 내벽에 단일층으로 도포되어 있는 "내피세포(endothelial cell)"라 불리는 얇은 다각형 세포들에 의한 것이다.<sup>9, 10)</sup> 따라서 우리가 인위적으로 고분자 시료에 내피세포를 이식 배양시켜 준다면 혈관 내벽과 유사한 혈액적합성을 가진 표면을 만들 수가 있을 것이지만, 일반적으로 내피세포나 이와 유사한 세포들이 고분자 표면에 쉽게 부착 성장하지 않는다는 것이 문제되고 있다.

따라서 본 연구의 전편<sup>11)</sup>에서는 polyethylene, polystyrene과 같은 단순한 화학적 구조를 가진 고분자와 인공혈관 재료로 널리 쓰이는 polyester의 표면을 세포적합성이 향상되도록 여러가지 방법으로 개질하였다.

본 연구에서는 여러가지 물리화학적 및 생물학적으로 표면개질된 고분자 시료에 내피세포와 유사한 성질을 가진, 포유동물의 난황세포인 Chinese Hamster Ovary(CHO) cell을 부착 배양시키고, 각 표면개질 방법에 따른 세포적합성을 비교 검토하였다.

## 2. 실험

### 2-1 표면개질 방법

사용한 고분자 시료는 첨가제가 전혀 함유되어 있지 않은 저밀도 polyethylene(LDPE, 한양화학) film, polystyrene(PS) plate(녹십자 의료공업(주)), polyethylene terephthalate(PET) film ((주) 선경) 등이다. 이들 고분자 시료들을 적당한 크기로 잘라 ethanol에서 2회 30분간 ultrasonication 시킨후 ethanol로 여러번 세척하여 진공 건조후 사용하였다.

이들 고분자 시료의 세포적합성을 향상시키기 위해 사용한 표면개질 방법은 크게 두가지로 나눌 수 있는데, 하나는 O<sub>2</sub> 플라즈마 방전, 코로나 방전, sul-

Table 1. Surface modification methods and treatment condition.

Method	Treatment condition
I. physicochemical	
O <sub>2</sub> plasma discharge	0.3 torr vacuum, 30 sec
Corona discharge	Air atmosphere, 60 sec
Sulfuric acid treatment	H <sub>2</sub> SO <sub>4</sub> (98 %), 10 min
Chloric acid treatment	70 % HClO <sub>4</sub> / saturated aqueous KClO <sub>3</sub> (3 / 2 ratio), 10 min
II. Biological	
Plasma protein adsorption	1 % human plasma, 30 min
Serum protein adsorption	20 % fetal bovine serum, 37 °C, 24 hr
Fibronectin adsorption	50 µg / ml bovine fibronectin, 1 hr

furic acid 처리, chloric acid 처리 등과 같은 물리 화학적 표면산화 처리 방법이고 다른 하나는 plasma, serum, fibronectin 등과 같은 혈액내 단백질을 고분자 표면에 흡착시키는 생물학적인 방법이다. 이들 각각의 방법에 의한 고분자 시료의 처리조건을 간단히 요약하여 표 1에 나타내었다. 구체적인 처리방법에 대해서는 본 논문의 전편<sup>11)</sup>에 기술되어 있다.

### 2-2 세포 배양

#### 1) 시료 준비

표면처리된 고분자 시료를 무진실에서 15 W Germicidal U.V. lamp로 45 cm 거리에서 1시간동안 멸균하고 배양액내에서 1시간동안 평형시킨후 세포를 배양하였다.

#### 2) 사용세포 및 배양용액

인체내 혈관 내벽과 유사한 혈액적합성을 지닌 재료를 만들기 위해서는 고분자 시료 표면에 혈관 내피세포를 부착 증식시켜야 하는데, 내피세포는 세포의 채집 분리 뿐만 아니라 그 배양조건이 까다롭고, 구입이 쉽지 않아서 본 연구에서는 이와 유사한 특성을 가지며 세포의 구입, 채집 분리, 배양조건등이 비교적 쉬운 영구분열 세포인 Chinese Hamster

Ovary (CHO) cell(Oak Ridge National Laboratory)을 표면개질된 고분자 시료의 세포적합성을 조사하기 위해 사용하였다.

계대 배양을 위해 사용한 완충용액은  $Ca^{++}$ ,  $Mg^{++}$ 가 제거된 Dulbecco's phosphate buffered saline (PBS)<sup>12)</sup>을 pH 7.2-7.3으로 조절하여 121 °C, 1기압에서 15분간 autoclave 멸균처리하여 사용하였다.

Trysin 용액은  $Ca^{++}$ ,  $Mg^{++}$ 을 제거시킨 Hank's balanced salt solution<sup>12)</sup>을 pH 7.2-7.3으로 조절하여, 0.05 % 용액으로 제조하고 멸균후 사용하였다.

배양액은 Ham's F-12 nutrient mixture<sup>12)</sup>에 박테리아의 증식을 억제하기 위해서 penicilin G sodium (NF grade, GIBCO Laboratories) 100 unit/ml와 streptomycin sulfate(GIBCO Laboratories) 100 unit/ml를 첨가하고 세포의 부착과 성장을 촉진하며 trypsin inhibitor 역할을 하는 fatal bovine serum(FBS, GIBCO Laboratories)을 5 %로 혼합하여 membrane filter(Millipore Co., GS-0.2  $\mu$ m)로 여과 멸균하여 사용하였다.

### 3) CHO cell 배양 방법

(A) PBS 용액, 0.05 % trypsin 용액, 배양액을 미리 37 °C로 유지시켰다.

(B) 세포 배양용 polystyrene flask(녹십자 의료공업 (주))에서 계대 배양되고 있는 세포의 배양액을 pasteur pipette을 사용하여 제거하고, flask 표면에 남아있는 serum을 제거하기 위해 PBS로 두번 정도 행구어 주었다.

(C) 0.05 % trypsin 용액 1 ml을 flask 내에 넣고 바닥에 골고루 퍼지도록 흔들어 준후, 1-2분동안 37 °C로 유지해 준 다음 손바닥으로 flask 바닥을 부드럽게 쳐서 바닥에 부착되어 있던 세포를 suspension 상태로 떼어내었다.

(D) 떼어낸 세포를 배양액으로 희석하여, 자체 제작한 표면개질된 고분자 시료용 배양용기(배양면적, 9.06 cm<sup>2</sup>)에 분주하였다.

(E) 37 °C 포화 수증기와 5 % CO<sub>2</sub>가 유지되고 있는 incubator(Forma Science, Model 3326)에서 적정 시간동안 세포를 배양하였다.

(F) 배양하는 동안 세포의 성장을 억제하거나 형

태변화를 야기시킬수 있는 박테리아, 곰팡이의 오염을 수시로 점검하였다.

(G) 배양이 끝난후 PBS로 2회에 걸쳐 세척하여 미부착 세포를 시료 표면으로부터 제거한 다음, 0.05 % trypsin 용액으로 시료 표면에 부착된 세포를 suspension 상태로 떼어낸 후, 세포가 함유된 suspension 용액을 Haemocytometer의 counting chamber에 채워 3회에 걸쳐 세포수를 계산하고 평균을 내었다.

(H) 시료 표면에 부착되어 있는 세포를 10 % formalin 액으로 10분간 고정시킨 후 5 % Giemsa (BDH, England)액으로 30분간 염색하여 건조시킨뒤, 위상차 현미경(Nikon Inverted Microscope Diaphot-TMD)으로 세포의 부착 및 성장상태를 관찰하였다.

## 3. 결과 및 고찰

여러가지 방법으로 표면처리한 고분자 시료의 세포적합성을 평가하기 위해, CHO 세포를 이용해 각 시료의 세포 부착 및 증식 경향을 조사하였다. 일반적으로 혈관 내피세포나 CHO 세포와 같은 포유동물의 단층세포가 증식하려면 우선 세포가 재료표면에 강력히 부착되어야 한다. 세포가 재료표면에 부착되지 않으면 성장을 할수가 없기 때문에 재료표면의 세포 부착성을 높여주기 위해 여러가지 방법으로 표면처리를 하게 된다. 처리된 표면의 세포적합성을 평가하기 위해서는 in vitro 세포부착 실험을 통하여 일정시간 세포배양후 표면에 부착 성장된 세포수를 계산하여 평가하는 것이 일반적인 방법이 되고 있다.

표 2는 여러가지 물리화학적 및 생물학적으로 표면개질한 고분자 시료들에 일정량의 CHO 세포를 seeding 하고 일정시간동안 배양하여, 시료 표면에서 부착 증식된 세포수를 산출해 놓은 것이다. 일반적으로 세포는 재료 표면이 친수성을 어느정도 띠게 되면 부착이 잘 되어 증식성이 양호해지는데,<sup>13)</sup> LDPE, PS, PET와 같은 고분자들은 소수성 재료로서, 본 연구에서 사용한 물리화학적 또는 생물학적 표면처리에 의해 친수성이 증가된다. 표 2에서 보듯이 미



**Table 2.** Comparison of CHO cell-compatibility of surface-modified polymers (No. of seeded cells,  $4 \times 10^4 / \text{cm}^2$ ; Culture time, 32 hr)

Treatment method	polymer sample	No. of cells attached / $\text{cm}^2 (\times 10^4)$
Untreated	PET	1.9
Corona*	LDPE	3.1
Sulfuric acid(10 min)	PS	9.7
Chloric acid(10 min)	PS	16.6
	PET	9.0
Plasma protein*	LDPE	3.1
	PS	3.1
	PET	2.8
Serum protein	LDPE	3.2
	PET	3.3
Fibronectin	LDPE	7.9
	PS	12.7
	PET	10.9

\*No. of seeded cells,  $9 \times 10^4 / \text{cm}^2$ ; Culture time, 19 hr.

처리된 PET에 부착 증식된 세포수가  $1.95 \times 10^4 / \text{cm}^2$ 인데 비해 표면처리된 모든 시료에 부착 증식된 세포수가 증가하였다.

물리화학적 처리방법들 중에서는 chloric acid 처리한 표면의 세포적합성이 가장 좋게 나타났는데, 이는 전편 논문의 ESCA 분석 결과에서 고찰되었듯이<sup>11)</sup> chloric acid 처리를 하게 되면 다른 처리 방법에 비해 표면에 hydroxyl group의 분포가 많이 형성되기 때문인 것으로 판단된다. 아직 hydroxyl group의 분포가 많은 고분자 표면의 세포 친화력에 대한 구체적인 mechanism은 규명되어 있지 않지만, 고분자 표면의 hydroxyl group과 세포 표면의 polar group 사이의 hydrogen bonding에 의해 세포가 표면에 많이 부착하는 것이 아닌가하고 추정하고 있다.<sup>14)</sup>

생물화학적 처리방법들 중에서는 fibronectin을 흡착시킨 고분자 표면의 세포적합성이 가장 좋게 나타났는데, 그 원인을 규명하기 위해서는 fibronectin 분자의 구조와 성질, 세포와의 상관관계를 이해하여야 한다. Fibronectin은 blood plasma내에 0.3 g/l의 농도로 존재하는 단백질로서 분자량이 220,000

-250,000 dalton 정도의 단량체(subunit)들이 disulfide bond(-S-S-)로 연결되어진 dimer로 구성되어 있다.<sup>15, 16)</sup> 각 단량체들은 길이 60-70 nanometer, 두께 2-3 nanometer 정도의 길쭉한 모양을 하고 있으며, 일련의 domain 구조를 형성하고 있다. 단량체내의 각 domain들은 fibronectin이 fibrin, collagen, cell, heparin 등과 결합할수 있는 능력을 부여해 준다. 특히 세포와 결합할수 있는 domain은 arginine-glycine-aspartate-serine의 amino acid sequence로 구성된 active site를 가지고 있어, 세포 표면에 돌출되어 있는 glycoprotein들이 이 active site에 강하게 결합하게 된다.<sup>15)</sup> Fibronectin은 고분자 표면에 흡착되어, 고분자 표면과 세포를 결합시켜 주는 역할을 하는 이외에도, 각 domain 결합 특성에 따라 collagen, fibrin, heparin 등을 세포와 연결시켜 주는 매개체 역할을 하기도 한다.

표면처리 방법에 따른 세포적합성을 인공혈관 재료로 사용되는 PET경우만 따로 비교해 보면, 표 3에서 보듯이 chloric acid로 10분 처리했을때와 fibronectin 으로 처리했을때 미처리한 시료보다 각각 약 460 %와 560 % 정도로 세포적합성이 향상되었음을 알 수 있다. Chloric acid로 산화 처리한 경우에, 처리시간에 따라 표면에 부착된 세포의 수가 달라졌는데 10분간 처리했을때가 거의 최적 조건인 것으로

**Table 3.** Comparison of CHO cell-compatibility of untreated and surface-modified PET.

Treatment method	Cell culture time (hr)	No. of cells / $\text{cm}^2 (\times 10^4)$	Untreated PET base (%)
Control (untreated)	32	1.95	100.0
Chloric acid			
1 min	32	4.5	231.6
10 min	32	9.0	460.5
30 min	32	6.3	320.9
Plasma protein	19	2.8	143.1
Serum protein	32	3.3	170.0
Fibronectin	32	10.9	559.0

\*No. of seeded cells,  $9.0 \times 10^4 / \text{cm}^2$  for plasma protein-treated surfaces and  $4.0 \times 10^4 / \text{cm}^2$  for other surfaces.

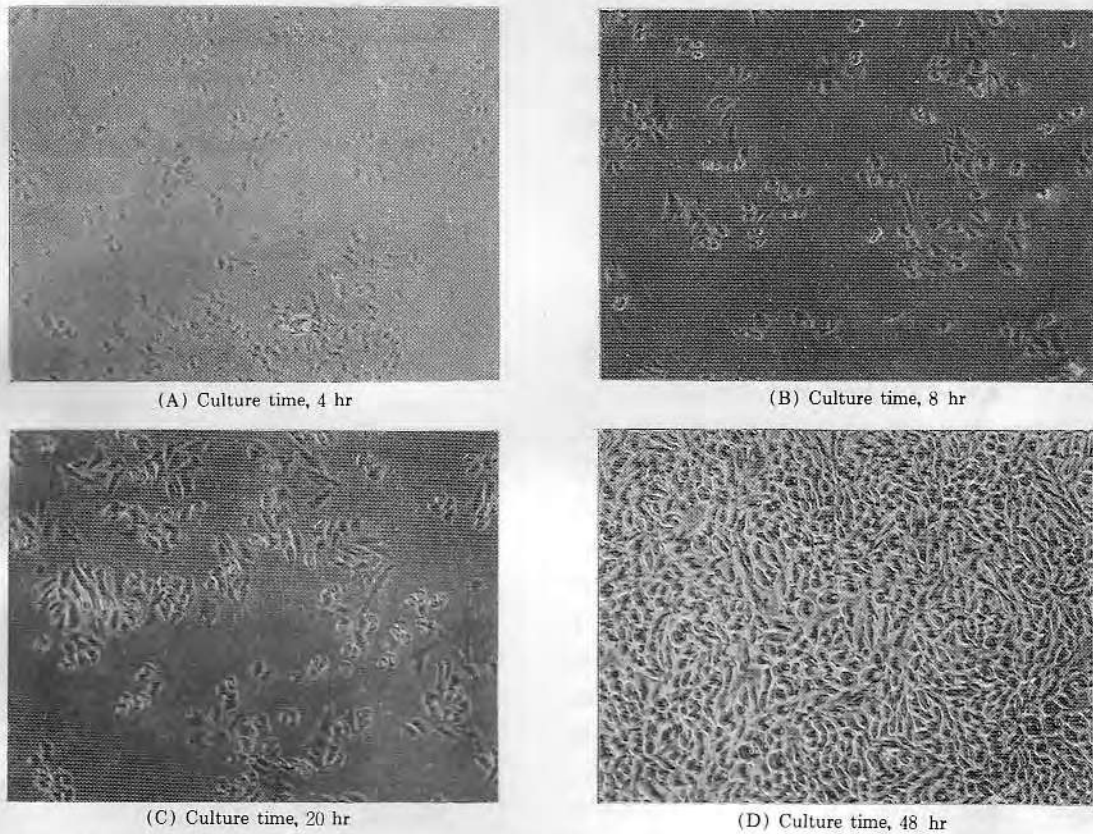


Fig 1. CHO cell growth on chloric acid(10 min)-treated PET surfaces (Inverted microscope,  $\times 100$ ).

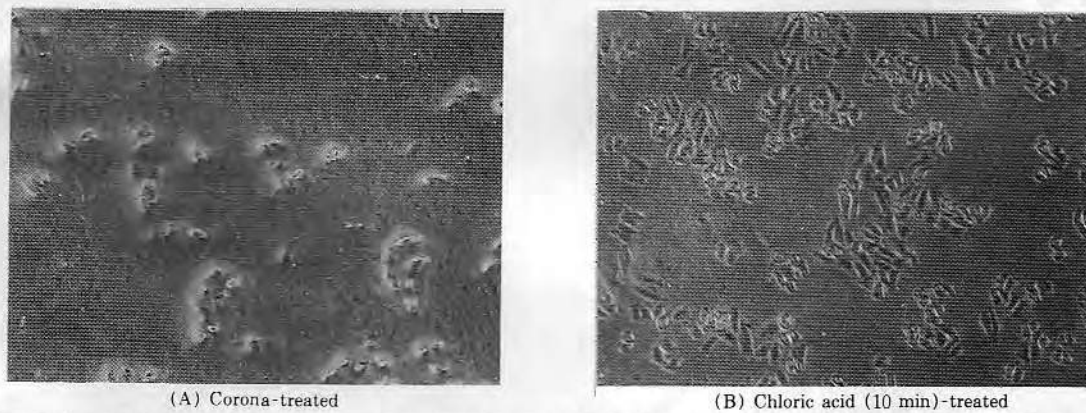


Fig 2. Comparison of CHO cell growth on corona-treated and chloric acid(10 min)-treated PET surfaces (Cell culture, 20 hr; Inverted microscope,  $\times 100$ )

나타났다.

Chloric acid로 10분간 처리한 PET 표면에 부착된 CHO 세포의 성장과정을 위상차 현미경으로 관

찰해 보면(그림. 1), 배양시간이 길어짐에 따라 표면에서의 세포수가 증가해 약 48시간 정도가 되면 시료 표면에서 세포가 완전히 밀집되어 있는 것을 볼

수가 있다.

그림. 2는 참고로 코로나 방전처리한 PET와 chloric acid 처리한 PET 표면에서 증식하고 있는 CHO 세포의 상태를 비교해 본 것이다. 그림에서 보듯이 chloric acid 처리한 시료 표면에서 훨씬 많은 세포들이 균일하게 퍼져 자라고 있는 것을 볼수 있었다.

#### 4. 결 론

본 연구를 통하여, 다양한 방법으로 표면개질된 고분자 시료의 세포적합성이 비교 검토되었다.

플라즈마 방전처리, 코로나 방전처리, sulfuric acid 처리, chloric acid 처리 등과 같은 물리화학적 산화 처리 방법들 중에서는, chloric acid 처리된 고분자 시료에 세포 부착 및 증식성이 가장 양호하게 나타났는데, 이는 chloric acid 처리시 표면에서 hydroxyl group의 분포가 상당히 많게 되어 이들 관능기가 hydrogen bonding을 통하여 세포표면과 결합력을 가지는 것으로 추정된다. Plasma protein, serum protein, fibronectin 등을 고분자 시료 표면에 흡착시키는 생물학적인 처리 방법들 중에서는, fibronectin을 고분자 시료에 흡착시킨 표면의 세포적합성이 가장 좋게 나타났는데, fibronectin 분자 구조내에 cell-binding domain이 있어 세포표면과 특수하게 결합할 수 있는 active site를 가지기 때문인 것으로 추정된다.

Chloric acid와 fibronectin 처리한 PET 표면의 세포적합성은, 미처리된 PET 표면과 비교할때 32시간 CHO 세포를 배양한 후 부착된 세포의 수가 각각 460.5 %와 559.0 % 정도로 증가하였다. Chloric acid 처리한 PET 표면에서의 세포 증식은 배양시간이 지남에 따라 증가하나 약 48시간 배양을 하게 되면 표면에서 세포가 완전히 밀집되어 있는 것을 볼수가 있었다.

본 연구 결과를 토대로, 인공혈관 내부 표면을 개질하고 내피세포를 이식하여 동물실험을 통해 성능을 평가하는 연구를 추진중에 있다.

감사의 글: 이 논문은 1988년도 과학 기술처 특정 연구 개발사업(N88-0124)의 연구비 지원으로 연구

되었다.

#### 참 고 문 헌

- 1) R.E.Baier, Bull. N. Y. Acad. Med., 48, 257, 1972.
- 2) J.D.Andrade, S.Nagaoka, S.Cooper, T.Okano, and S.W.Kim, ASAIO J., 10, 75, 1987.
- 3) A.S.Hoffman, Ann. N. Y. Acad. Sci., 516, 96, 1987.
- 4) Y.IKada, in "Polymers in Medicine," K. Dusek, ed., APS Ser. 57, Springer-Verlag, p. 103, 1984.
- 5) A.S.Hoffman, in "Biomaterials: Interfacial Phenomena and Applications," S.L.Cooper and N.A.Peppas, eds., ACS 199, ACS Press, Washington, D.C., p. 3, 1982.
- 6) J.Black, "Biological Performance of Materials," Marcel Dekker, New York, 1981.
- 7) L.L.Hench and E.C.Ethridge, "Biomaterials: An Interfacial Approach," Academic Press, New York, 1981.
- 8) S.W.Kim and J.Fejin, in "CRC Critical Reviews in Biocompatibility," Vol. 1, CRC Press, Boca Raton, p. 215, 1985.
- 9) W.Bloom and D.W.Fawcett, "A Textbook of Histology," 9th ed, Saunders, Philadelphia, 1968.
- 10) J.D.Andrade, H.B.Lee, and M.S.Jhon, Trans. ASAIO, 19, 1, 1973.
- 11) J.H.Lee, G.S.Khang, K.H.Park, H.B.Lee, and J.D.Andrade, J. KOSOME, 10, 43, 1989.
- 12) "GIBCO Laboratories Catalogue and Reference Guide," GIBCO Laboratories, Life Technologies, Inc., 1987.
- 13) H.B.Lee and J.D.Andrade, Trans. 3rd World Biomaterials Congress, Kyoto, Japan, p. 43, 1988.
- 14) A.S.G.Curtis, J.V.Forrester, C.McInnes, and F.Lawrie, J. Cell Biol., 97, 1500, 1983.
- 15) R.O.Hynes, Sci. Amer., 254(6), 32, 1986.
- 16) K.M.Yamada, Ann. Rew. Biochem., 52, 761, 1983.



# Surface properties of copolymers of alkyl methacrylates with methoxy (polyethylene oxide) methacrylates and their application as protein-resistant coatings

Jin Ho Lee\*, Pavla Kopeckova, Jindrich Kopecek and Joseph D. Andrade

*Departments of Materials Science and Engineering, and Bioengineering, University of Utah, Salt Lake City, UT 84112, USA  
(Received 8 October 1989; revised 28 March 1990; accepted 3 April 1990)*

**New polymeric surfactants, copolymers of alkyl methacrylates with methoxy (polyethylene oxide) methacrylates, were synthesized and characterized by gel permeation chromatography. They were studied as possible means to produce polyethylene oxide-rich surfaces by a simple coating treatment on common hydrophobic medical materials. They were further studied as cleaners for the removal of proteins pre-adsorbed on hydrophobic surfaces. The surface properties of the copolymers such as the adsorption properties of the copolymer on a hydrophobic surface, low density polyethylene, the protein-resistant character of the prepared polyethylene oxide surfaces and the effectiveness of the copolymers for removal of proteins pre-adsorbed on the surface, were investigated by X-ray photoelectron spectroscopy and by using  $^{125}\text{I}$ -labelled copolymers and  $^{125}\text{I}$ -labelled proteins. The surface properties of the synthesized copolymers were compared with those of commercially available polyethylene oxide containing block copolymer surfactants.**

*Keywords: Polyethylene oxide, alkyl methacrylates, protein resistance, protein removal*

Polyethylene oxide (PEO) has unique solution properties in aqueous systems<sup>1-3</sup>. At room temperature, PEO is completely miscible with water in all proportions. In contrast to the complete water solubility of PEO, closely related polymers such as polymethylene oxide, polytrimethylene oxide, polyacetaldehyde and polypropylene oxide (PPO) are water-insoluble under ordinary conditions<sup>4</sup>. To understand why PEO shows unlimited water solubility at least up to temperatures slightly below 100°C in contrast to the other polyethers, PEO-water interactions and their structural models were studied<sup>3</sup>. In pure liquid water, the hydrogen bonding results in a highly connected network of tetrahedrally coordinated water molecules<sup>5</sup> and it was suggested that PEO segments nicely fill out voids in the water structure and minimally perturb the structure of water itself, thereby minimizing the tendency for hydrophobic interaction<sup>3</sup>.

PEO is becoming recognized as an effective polymer for low protein adsorption and low cell adhesion, because the hydrophilicity and unique solubility properties of PEO

produce surfaces which are in a liquid-like state, with the polymer chains exhibiting considerable flexibility or mobility<sup>1-3,6</sup>. The rapid movement of hydrated PEO chains attached on a surface probably influences the microthermodynamics at the protein solution/surface interface and prevents adsorption or adhesion of proteins<sup>6</sup>. PEO has a steric stabilization effect in aqueous solution<sup>6-9</sup>. It is thought that a repulsive force develops, due to a loss of configurational entropy of the surface-bound PEO, when a protein or other particle approaches the PEO surface. It appears that a PEO surface in water has rapid motions<sup>6</sup> and a large excluded volume<sup>7-9</sup> compared to the less water soluble polyethers, thereby actively minimizing the adsorption of proteins. The PEO-water interface also has a very low interfacial free energy and thus a low driving force for protein adsorption<sup>10,11</sup>. Proteins at or near a low interfacial energy interface will not feel any greater effects from the surface than they do from the bulk solution.

There has been much effort in preparing PEO surfaces, for example, by block copolymerization<sup>2,6,12</sup>, cross-linking to produce a PEO network<sup>2</sup>, or surface treatments such as direct adsorption of high molecular weight PEO<sup>13,14</sup> or the

Correspondence to Dr J. Andrade.

\*Present address: Korea Institute of Chemical Technology, PO Box 9, Deaedeog-Danji, Daejeon, Korea.

covalent grafting of PEO<sup>15,16</sup> to silica and other surfaces. Surfaces which show minimal protein adsorption are important in many applications, including blood-contacting devices, membranes for separation processes, sensors, chromatographic supports, contact lenses, immunoassays and blood and protein storage applications, etc.

In previous papers<sup>17-19</sup>, hydrophobic surfaces were treated with commercially available PEO/PPO and PEO/polybutylene oxide (PBO) block copolymer surfactants in aqueous solution, by physically adsorbing those surfactants on to the surfaces. These surfactants have two components in their structure: a hydrophobic segment and a hydrophilic PEO segment. Hydrophobic segments are water-insoluble components to provide spontaneous adsorption on to hydrophobic surfaces via hydrophobic interaction. Hydrophilic PEO segments will interact with water via hydrogen bonding and serve to dissolve the surfactants in aqueous solution and to confer to the surfactant their unique protein-resistant character. We showed that strong physical adsorption of surfactants on hydrophobic materials provides a simple and rapid means of producing PEO surfaces as protein-resistant surfaces.

From previous work<sup>19</sup>, however, it was found that commercially available block surfactants have two limitations in producing stable PEO surfaces. First, a long hydrophobic block was needed to produce strong adsorption of the surfactant on a hydrophobic surface. However, it led easily to intermolecular aggregation in aqueous solution<sup>20</sup>, resulting in weak adsorption on to the surface. Second, a long PEO chain was needed to be highly mobile in aqueous solution and thus confer effective protein resistance<sup>6</sup>. It is, however, less strongly adsorbed on the surface than a shorter one, because the PEO-water interactions are stronger than the hydrophobic segment-hydrophobic surface interactions. That is the reason why new polymeric surfactants, copolymers of alkyl methacrylates with methoxy (polyethylene oxide) methacrylates, discussed in this paper, were synthesized. It is expected that the long hydrophobic polymethacrylate backbone and alkyl side chains will give effective protein resistance.

## MATERIALS AND METHODS

In this study, random copolymers of alkyl methacrylates (methyl and hexyl or lauryl) and methoxy (polyethylene oxide) methacrylates (mol wt of PEO, 1900 and 4000) were synthesized and characterized by gel permeation chromatography (GPC). The adsorption properties of the copolymers on low density polyethylene (LDPE) substrates were investigated using X-ray photoelectron spectroscopy (XPS) and <sup>125</sup>I-labelled polymers. Conformations of the polymers at the hydrophobic solid-water interface were considered. The protein-resistant character of the LDPE surfaces coated with the polymers by a simple solution treatment were also evaluated by XPS and <sup>125</sup>I-labelled proteins. The results were compared with those of commercial block copolymer surfactants.

The effectiveness of the polymeric surfactants for removal of proteins pre-adsorbed on hydrophobic surfaces were also studied. The purpose was to develop PEO-containing polymeric surfactants that can displace or desorb proteins adsorbed on hydrophobic surfaces. Efficient removal of adsorbed proteins is needed for many surfaces which have direct contact with biological systems; such proteins often cannot be easily removed. It is expected that PEO's

hydrophilicity, unique solubility and high mobility in aqueous solution, combined with the hydrophobic character of the surfactants, will permit removal of pre-adsorbed proteins. The removal properties of pre-adsorbed proteins by the synthesized or commercial polymeric surfactant solutions were evaluated by XPS and by radioisotopic measurement using <sup>125</sup>I-labelled proteins.

## EXPERIMENTAL

### Monomers and chemicals

The monomers and chemicals used for the synthesis of copolymers of alkyl methacrylates with methoxy (polyethylene oxide) methacrylates are as follows.

*Monomethoxy poly(ethylene oxide)<sub>1900</sub> methacrylate (MPEO<sub>1900</sub>MA)*. To a well-stirred solution of 15.2 g (8 mmol) monomethoxy poly(ethylene glycol) (Polyscience) in 20 ml dry methylene chloride (CH<sub>2</sub>Cl<sub>2</sub>) and 1.62 g (16 mmol) triethylamine cooled to 5°C, 1.67 g (16 mmol) methacryloyl chloride in 2 ml methylene chloride was slowly added dropwise. After that, the reactants were stirred at room temperature overnight in the presence of small amount of inhibitor, tertiary octylpyrocatechine. Precipitated triethyl amine hydrochloride was filtered off, macromonomer was isolated by precipitating the solution into cooled diethyl ether and powdered polymer was washed thoroughly with diethyl ether and dried.

*Monomethoxy poly(ethylene oxide)<sub>4000</sub> methacrylate (MPEO<sub>4000</sub>MA)*. This was kindly provided by S. Nagaoka (Toray Industries, Inc., Kanagawa, Japan).

*N-methacryloyl tyrosinamide (MA-Tyr-NH<sub>2</sub>)*. To a cooled solution of 3.6 g (20 mmol) tyrosinamide in 100 ml water, 1.04 g (10 mmol) methacryloyl chloride was slowly added dropwise. After 4 h of stirring at room temperature, the precipitated product was filtered off, washed thoroughly with water and recrystallized from ethanol. The product has an m.p. of 194–196°C, good elemental analysis and a molar extinction coefficient,  $\epsilon_{280} = 1.6 \times 10^3 \text{ l mol}^{-1} \text{ cm}^{-1}$  in ethanol. A small amount of MA-Tyr-NH<sub>2</sub> was incorporated in the copolymers to permit <sup>125</sup>I-labelling.

*2,2'-azobisisobutyronitrile (AIBN, Aldrich)*. This was purified by recrystallization from methanol and used as an initiator for polymerization.

*Methyl methacrylate (MMA), hexyl methacrylate (HMA) and lauryl methacrylate (LMA) (Polyscience)*. These were freshly distilled under reduced pressure before use.

### Preparation of copolymers

The copolymers were prepared by radical polymerization of monomers in toluene for 45 h at 50°C (Table 1).

A polymerization mixture, containing 14.0 wt% of monomer, 0.6 wt% of AIBN and 85.4 wt% toluene, was bubbled with nitrogen for 15 min then sealed in an ampoule. After the polymerization was finished, the volume of polymer solution was reduced by approximately 50% using a rotary vapour evaporator under reduced pressure. Polymers were precipitated into cooled diethyl ether, washed and dried. To remove non-copolymerized macromonomer (about 10–20%, as determined by GPC) the polymers containing



Table 1 Monomer composition and molecular weights of copolymers synthesized<sup>a</sup>

Polymer no.	MPEO <sub>1900</sub> MA	MPEO <sub>4000</sub> MA	MMA	HMA	LMA	MA-Tyr-NH <sub>2</sub>	Mol wt by GPC <sup>b</sup>	
							Mw	Mw/Mn
1	100	-	-	-	-	-	18 000	2.7
2	80	-	20	-	-	-	19 000	2.5
3	80	-	-	20	-	-	20 000	2.4
4	40	-	20	40	-	-	71 000	3.5
5	40	-	40	20	-	-	29 000	2.4
6	90	-	5	5	-	-	27 000	2.6
9	20	-	20	60	-	-	105 000 <sup>c</sup>	-
10	25	-	20	55	-	-	125 000 <sup>c</sup>	-
11	25	-	40	35	-	-	100 000 <sup>c</sup>	-
12	25	-	20	-	55	-	130 000 <sup>c</sup>	-
13	-	20	20	60	-	-	198 000	2.0
14	-	20	20	-	60	-	244 000	2.0
15	-	15	35	-	50	-	138 000	1.6
16	20	-	19	60	-	1	115 000 <sup>c</sup>	-
17	25	-	19	55	-	1	115 000 <sup>c</sup>	-
18	25	-	39	35	-	1	120 000 <sup>c</sup>	-
19	25	-	19	-	55	1	125 000 <sup>c</sup>	-
20	-	20	19	60	-	1	237 000	2.0
21	-	20	19	-	60	1	294 000	2.2
22	-	15	34	-	50	1	326 000	2.2
23	-	10	19	-	70	1	420 000	2.1

<sup>a</sup>Composition, mol%.<sup>b</sup>Using PEG calibration samples (rough estimation).<sup>c</sup>Polymer contains aggregates (see GPC profile, hatched area in Figure 1c).

Mw estimated without taking into account the hatched area.

PEG<sub>1900</sub> were dialysed for 3 d in Visking dialysis tubing (mol wt cut-off, 6000–8000). The polymers containing PEG<sub>4000</sub> were purified by using ultrafiltration (Amicon, membrane PM-30). The polymers were then isolated using lyophilization. The yields of polymers were 60–70%. As most of the polymers were not directly soluble in water or aqueous buffers, a special procedure was used for preparation of aqueous solutions for adsorption studies, GPC measurement or purification using dialysis or ultrafiltration.

### Preparation of aqueous solutions of polymers

Polymer (100 mg) was dissolved in 5 ml warm ethanol (about 50°C), then diluted with 20 ml of water and subsequently dialysed against water (for adsorption study) or against Tris buffer (for GPC measurement). Then the solutions were diluted to the concentrations needed.

### Characterization of copolymers by GPC

Polymers were applied on 1.6 × 80 cm column packed with Sepharose 4B and 6B (1:1) and eluted with 0.05 M Tris buffer pH 8.0, containing 0.5 M NaCl. The GPC showed typical profiles depending on the composition of the polymerization mixture (Figure 1).

Averages of molecular mass were estimated using PEG standards (mol wt 2000–22 000). As most of samples showed higher molecular mass than the highest standard, an extrapolation was necessary (Table 1). We used PEG standards, as the total mass of PEG fraction in the copolymers was never < 70 wt%. We are aware that calculated averages of molecular masses are very rough estimates only and can be only used for comparison within a group of polymers having a similar structure. A more complete characterization of these polymers is in progress.

### Radio-labelling of human albumin and copolymers

<sup>125</sup>I (100 mCi/ml, Amersham) as sodium iodide in dilute sodium hydroxide solution, pH 7–11, free from reducing agents, was used for labelling of human albumin and the synthesized copolymers.

<sup>125</sup>I-labelled human albumin was prepared by a modified chloramine-T method<sup>21</sup>. This method is suitable to incorporate carrier-free radioactivity in small quantities of protein rapidly and with good efficiency. Iodination was performed at r.t. (20°C) using 200 µg human albumin (crystallized, Miles Diagnostics) dissolved in 0.5 ml phosphate buffer solution (PBS) at pH 7.4. A volume corresponding to 0.3 mCi of Na-<sup>125</sup>I was added to the albumin solution. After 50 µl freshly made chloramine-T solution (4 mg/ml in H<sub>2</sub>O, oxidizing agent, Kodak) was added, the protein solution was gently mixed for 1 min. Immediately, 50 µl sodium metabisulphite (Na<sub>2</sub>S<sub>2</sub>O<sub>5</sub>, 4.8 mg/ml in H<sub>2</sub>O, reducing agent, Fisher Scientific) was added in the mixture to stop the oxidation reaction by mixing the solution for 1 min. Free <sup>125</sup>I was removed by centrifugation of Sephadex G-25 coarse grade resin (Sigma) minicolumn (6.0–6.5 cm long, about 1 cm wide) having about 0.3 ml of iodinated protein solution<sup>22</sup>. The final concentration of <sup>125</sup>I-labelled protein solution was determined by a UV-visible spectrophotometer (Beckman, Model 35) at the wavelength of 280 nm.

Labelling efficiency after removing free <sup>125</sup>I was determined by precipitating the human albumin molecules with 20% trichloroacetic acid (TCA in H<sub>2</sub>O, Sigma) in the presence of bovine serum albumin (BSA, crystallized, Miles Diagnostics), 20 mg/ml in PBS. The BSA functions as a carrier for the small amount of human albumin and TCA acts as a precipitating agent. The detailed procedure was described in a previous paper<sup>19</sup>. Normally, more than 95% of labelling efficiency was obtained by this method.



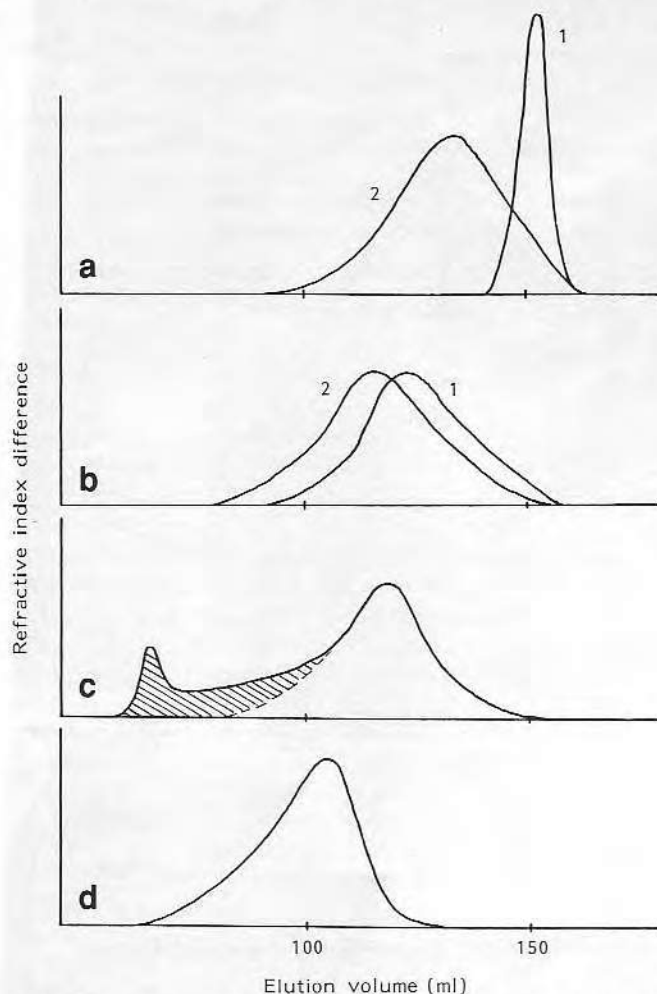


Figure 1 GPC chromatograms (column,  $80 \times 1.6$  cm; packing, Sepharose 4B and 6B, 1:1; flow rate, 12 ml/h; elution solution, Tris buffer pH 8.0 + 0.5 M NaCl). (a) Curve 1: MPEO<sub>1900</sub>MA macromonomer; Curve 2: Polymer No. 1 (homopolymer of MPEO<sub>1900</sub>MA). This is a typical curve obtained for polymers containing high amount of MPEO<sub>1900</sub> unit. Similar curves were obtained for polymers 2, 3 and 6 (results not shown). (b) Curve 1: Polymer No. 5; Curve 2: Polymer No. 4. (c) Polymer No. 9. This is a typical curve for polymers containing a low amount of MPEO<sub>1900</sub> unit. Similar curves were obtained for polymer Nos. 10, 11, 12, 16, 17, 18 and 19 (results not shown). (d) Polymer No. 13. This is a typical curve obtained for polymers containing MPEO<sub>4000</sub> unit. Similar curves were obtained for polymer Nos. 14, 15, 20, 21, 22 and 23 (results not shown).

For <sup>125</sup>I-labelling of copolymers, a small amount of methacryloyl tyrosinamide (Figure 2) was introduced in the structures of copolymers (polymer No. 16–23 in Table 1) during synthesis. The tyrosinamide content in all polymers was  $16 \pm 3$  nmol/mg which corresponds to approximately 1.0 mol%. It is expected that <sup>125</sup>I will be linked with the benzene ring in the structure of tyrosin. The chloramine-T method was also used for the labelling of these polymers. The labelling efficiency of the polymers (concentration, 1.0 mg/ml) determined by GPC profile using DP-10, Sephadex G-25M column (Pharmacia) was not good as shown in Figure 3a. Thus, the iodination reaction time was increased to 4 h and the reaction mixture was continuously shaken during reaction. After iodination, the <sup>125</sup>I-labelled polymer solution was passed twice through the Sephadex G-25 minicolumns prepared separately to remove free <sup>125</sup>I. Figure 3b shows that almost all free <sup>125</sup>I is removed by this treatment.

**Adsorption of copolymers on LDPE.** For adsorption of the copolymers (polymer No. 1–15 in Table 1) on to a hydro-

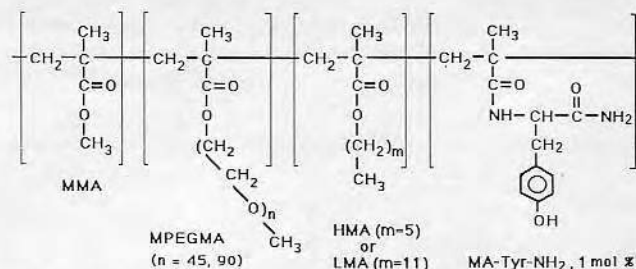


Figure 2 Structure of copolymers synthesized (polymer Nos. 16–23).

phobic surface, LDPE films (NHLBI DTB polyethylene primary reference material), whose surface cleanliness was verified by XPS, were immersed in aqueous polymer solutions for 30 min at room temperature. The polymer-adsorbed films were rinsed in purified water and then immersed in purified water for 30 min. After rinsing them again in purified water, the polymer-treated films were vacuum dried overnight in an air atmosphere (Figure 1)<sup>19</sup>. The polymer-treated surfaces were analysed in a Hewlett-Packard 5950B XPS equipped with a monochromatic Al K $\alpha_{1,2}$  radiation source at 1487 eV and 400 W power at the anode. An electron flood gun operated at 6.0 eV was used for charge compensation. Wide scan and narrow scans for carbon 1S and oxygen 1S were taken and normalized using Scofield cross-sections<sup>23</sup>.

For the quantitation of the polymer adsorption (polymer No. 16–23), LDPE films, whose surface area was pre-determined, were immersed in a solution of known ratio of <sup>125</sup>I-labelled and unlabelled polymer and adsorption was performed with the same procedure as for the samples for XPS analysis. After polymer adsorption and following

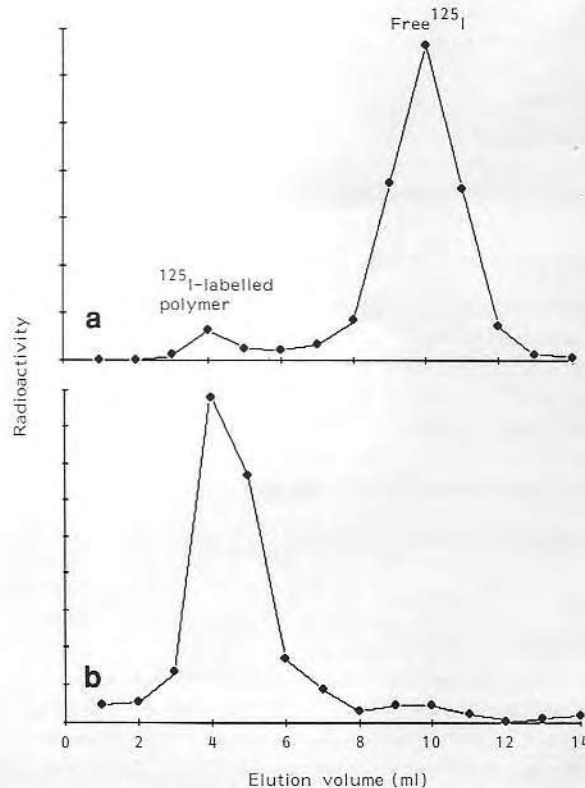


Figure 3 Typical GPC profile of <sup>125</sup>I-labelled polymers (column, PD-10, Sephadex G-25M; elution solution, purified water). (a) Same iodination reaction conditions as protein-labelling (gently mixing for 1 min and once passing through Sephadex G-25 minicolumn); (b) modified conditions for polymer iodination (mild shaking continuously for 4 h and twice passing through Sephadex G-25 minicolumn).

rinsing, the polymer-treated LDPE films were directly placed in counting vials (polyethylene, Kimble) and the retained radioactivity was measured in a gamma counter (Beckman, Model 170M). Corrections for background radioactive decay of  $^{125}\text{I}$ -iodine, ratio of labelled polymer with unlabelled one and surface area of the LDPE sample were made to determine the adsorbed amount of polymer on the surface.

**Protein resistance of polymer-treated surfaces.** For the studies of protein resistance, human albumin, the major constituent of plasma, as a model protein and human plasma were used. Blood plasma was prepared from freshly collected blood. The blood was drawn into a plastic syringe (Becton Dickinson Vacutainer systems) containing a buffered sodium citrate (10% of the final volume) as an anticoagulant. The blood was centrifuged at about  $10^\circ\text{C}$  for 20 min at 2000 rev min $^{-1}$ . The supernatant was carefully drawn off and freshly used for the studies of protein resistance.

The polymer-treated LDPE films were immersed in protein solutions prepared with PBS at pH 7.4 for a given time and rinsed in PBS, following by rinsing in purified water and vacuum drying (Figure 1)<sup>19</sup>, then analysed by XPS. The nitrogen 1S peak was used for the analysis of adsorbed protein. The  $^{125}\text{I}$ -labelled polymer-treated surfaces were also used and radioactivity was counted both before and after protein adsorption on those surfaces to see whether protein adsorption affected the amount of the polymer adsorbed on the surface, i.e. to see the effect of exchange of the protein with the polymer pre-adsorbed on the surface.

For the quantitation of protein adsorption, the polymer-treated surfaces were immersed in a solution of known ratio of labelled and unlabelled albumin (concentration of mixed solution, 1.0 mg/ml) and adsorption was performed with the same procedure as in the case for the samples for XPS analysis. After  $^{125}\text{I}$ -labelled albumin adsorption on to the polymer-treated surface, the radioactivity was also counted and converted to the adsorbed amount of protein on the surface.

**Removal of pre-adsorbed proteins by polymer solution treatment.** To study the removal of proteins pre-adsorbed on a hydrophobic surface, LDPE films were immersed in protein solutions prepared with PBS at pH 7.4 for 30 min and rinsed in PBS, following by rinsing in purified water. These protein pre-adsorbed LDPE films were immersed in the polymer solution for 30 min and also rinsed in PBS and purified water, vacuum dried, then analysed by XPS.  $^{125}\text{I}$ -labelled human albumin and  $^{125}\text{I}$ -labelled polymers were also used separately for quantitation and examination of the mechanism for removal of pre-adsorbed protein.

## RESULTS AND DISCUSSION

### Structure of copolymers

Graft copolymers used in this study were prepared by radical copolymerization of hydrophobic monomers (MMA and HMA or LMA) with a hydrophilic macromonomer (methacryloylated methoxy poly(ethylene oxides)). Since the aim of this study was to determine semiquantitatively the influence of copolymer structure on their surface properties, the monomer mixtures were copolymerized to high conversion (60–70%). Consequently, the copolymers studies have a distribution in chemical composition. The non-uniformity is generally higher, the higher the difference in copolymerization parameters.

The most questionable reactivity of all monomers used is that of the macromonomers. There are two main effects<sup>24</sup> which influence the ability of macromonomers to copolymerize: (1) the effect of side groups associated with the terminal double bond and (2) the length of the macromonomer chain. It appears<sup>25,26</sup> that the first parameter plays the major role. Both the conventional monomers and the macromonomers used in this study are methacrylates with different ester units. As polar effects of ester (alcoholic) parts do not differ substantially and the lengths of macromonomer side-chains used in this study should not have a pronounced effect on the macromonomer's reactivity<sup>24</sup>, the copolymerization parameters should be similar for all combinations used.

The discussion of the structure-properties relationship in this paper is based on the composition of the monomeric mixture. We are aware that the real copolymer composition is slightly different. As can be seen from Figure 7, copolymers 9, 10 and 11, which effectively repulse proteins, have quite different structures. Their main characteristic is that they are on the border of solubility in water. Thus the proper hydrophilic/hydrophobic balance in these copolymers is the decisive factor in determining their surface properties.

Copolymers with a higher content of hydrophobic conventional comonomers were not easily soluble in water. A special procedure (described in the experimental section) had to be used to dissolve them.

It had been observed previously<sup>27</sup> that hydrophilic copolymers containing hydrophobic side-chains associated in solution forming submicellar structures with the hydrophobic side-chains inside the core and the hydrophilic side-chains outside. The profiles of molecular weight distribution of copolymers studied obtained by GPC (Figure 1) were consistent with the formation of aggregates in water solutions. Bimodal distribution curves were obtained with copolymers containing a higher amount of hydrophobic side-chains. The amount of the high molecular weight fraction (aggregates) could be reduced when copolymers were eluted on an FPLC system with ethanol/water (1:1) instead of water (results not shown). The molecular weight averages shown in Table 1 are only rough estimations, but can be used as a comparative value for the group of copolymers studied.

Some of the copolymers prepared contained about 1 mol% of methacryloyl tyrosinamide to permit radio-labelling<sup>28</sup> with  $^{125}\text{I}$ -iodine to improve the analytical procedures described below.

### Adsorption on LDPE

The copolymers synthesized were adsorbed on to LDPE from aqueous solution. The copolymers have two functional units on their polymethyl methacrylate backbone: hexyl or lauryl side-chains as the hydrophobic unit and long PEO side-chains as the hydrophilic unit (Figure 4a). The hydrophobic, long polymethacrylate backbone and alkyl side-chains will interact strongly with the LDPE surface via hydrophobic interactions. The polymethacrylate backbone will be adsorbed with small loops on the surface, to provide a more entropically stable state<sup>29,30</sup>. The long, hydrophilic PEO chains will interact with water and be extended relatively freely into the water phase (Figure 4a)<sup>20,29-34</sup>.

After the polymers were adsorbed on to the LDPE surface, the relative amount of adsorption was evaluated by XPS. Although XPS analysis does not provide absolute quantitation, it is very sensitive to very low adsorbed amounts. It gives useful and rapid comparative information

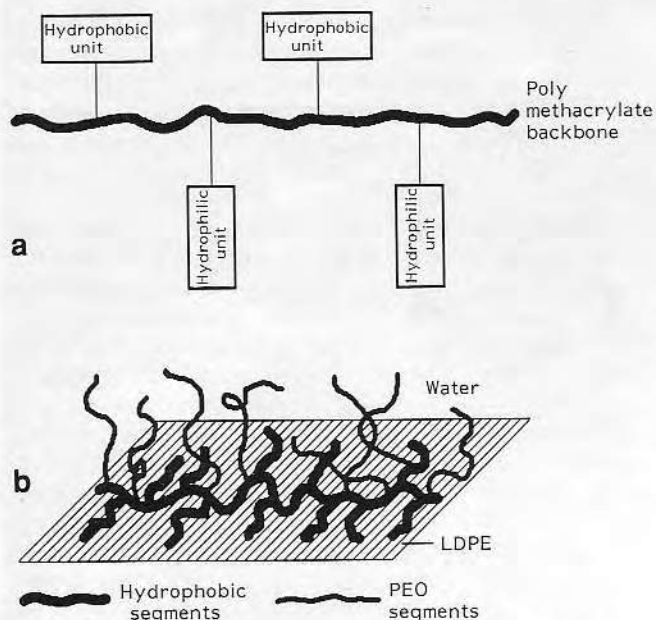


Figure 4 Methacrylate copolymers with side PEO and alkyl chains. (a) Simplified structure with functional units; (b) expected ideal conformation at hydrophobic solid (LDPE)-water interface.

for the adsorption of polymers. The oxygen atomic % on the LDPE surface, as determined by XPS analysis, was used as an indicator of the amount of the polymer adsorbed, as LDPE does not show any oxygen peaks (Figure 5). Figure 6 shows that the adsorption of the polymers (PEO mol wt 1900, polymer Nos. 1-11) is highly composition-dependent. The very hydrophobic polymers with MMA and HMA composition just below the solubility limit appear effective for stable adsorption on to the LDPE surface.

Adsorbed amounts of the polymers containing PEO of two different molecular weights, 1900 and 4000, were compared in Table 2. From the monomer composition of the copolymers in Table 1, it can be seen that polymer Nos. 9-12 and 16-19 and also polymer Nos. 13-15 and 20-22 have the same monomer composition, respectively, except for 1 mol% of MMA. Table 2 shows that addition of

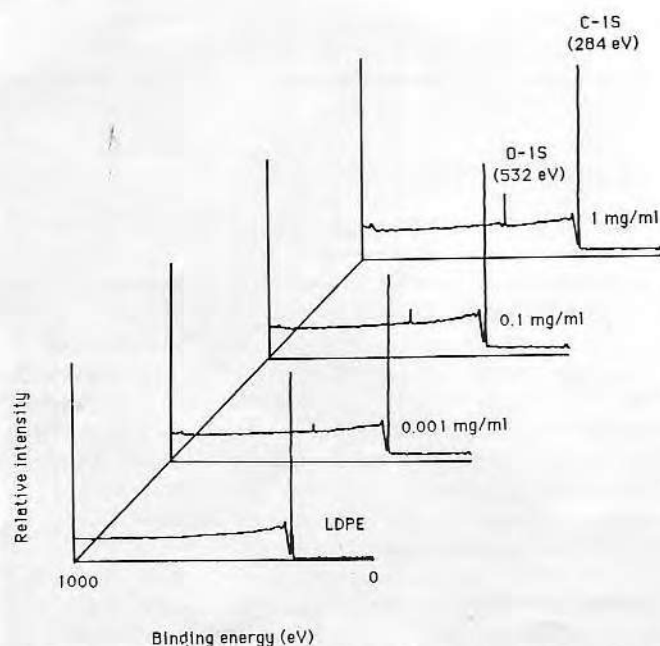


Figure 5 XPS wide-scan of pure and copolymer-treated LDPE surfaces (polymer No. 9, 30 min adsorption with different polymer concentration).

Table 2 Adsorbed amount of the copolymers on LDPE surface<sup>a</sup>

Polymer no.	MW <sub>PEO</sub>	Oxygen atomic % (XPS)	$\mu\text{g}/\text{cm}^2$ ( $^{125}\text{I}$ -labelling)
9	1900	$4.0 \pm 0.4$	-
10	1900	$4.0 \pm 0.4$	-
11	1900	$3.6 \pm 0.1$	-
12	1900	$5.4 \pm 2.0$	-
16	1900	$4.0 \pm 0.1$	0.25
17	1900	4.0	0.24
18	1900	$3.9 \pm 1.1$	$0.21 \pm 0.02$
19	1900	$4.5 \pm 2.1$	$0.33 \pm 0.09$
13	4000	$3.2 \pm 0.7$	-
14	4000	$4.5 \pm 0.9$	-
15	4000	$3.9 \pm 1.0$	-
20	4000	$2.4 \pm 0.4$	$0.20 \pm 0.01$
21	4000	4.1	0.24
22	4000	4.5	0.35
23	4000	9.0	0.80

<sup>a</sup>30 min desorption in water after 30 min adsorption of LDPE film in 1 mg/ml polymer solution.

1 mol% of MA-Tyr-NH<sub>2</sub> to the copolymers does not affect the adsorbed amount of the polymers on the LDPE surface. Polymer No. 23 shows an interesting feature; this polymer contains 90 mol% hydrophobic comonomers and shows excellent adsorption properties. This means that the adsorbed amount increases with increased hydrophobicity of the polymers. All polymers in Table 2 were not directly soluble in water, and a special treatment was used to dissolve them in water as discussed before.

### Protein resistance of pre-treated LDPE surfaces

The protein resistant character of the copolymer-treated LDPE surfaces was also evaluated by XPS. The protein nitrogen signal of the polymer-treated surface was compared with that of untreated LDPE for this purpose. Figure 7 shows the protein resistance of the polymer (PEO mol wt 1900,

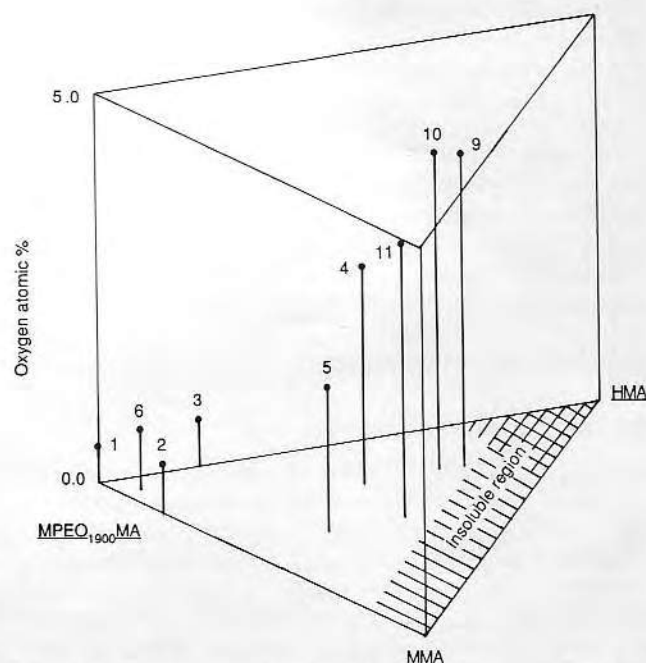


Figure 6 Relative adsorbed amount of the copolymers with different composition on LDPE surface (PEO mol wt 1900, polymer Nos. 1-11, 30 min desorption in water after 30 min adsorption in 1 mg/ml polymer solution). Data points represent average values of three samples,  $n = 3$ .



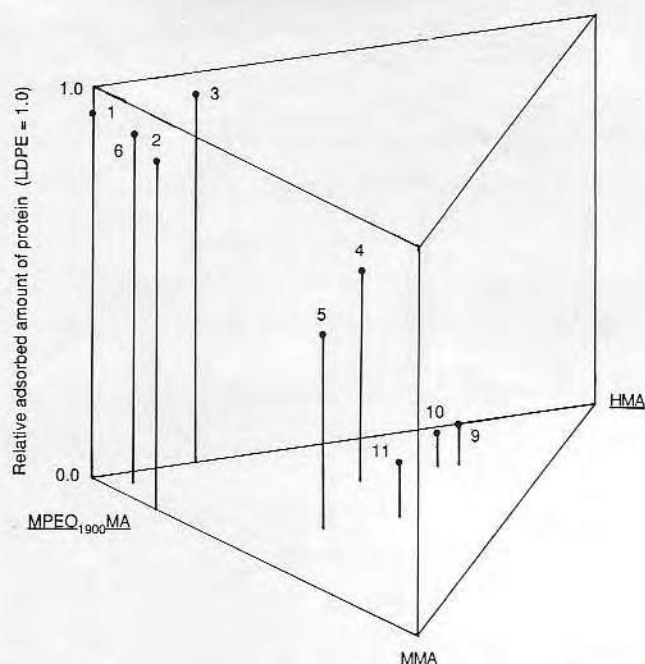


Figure 7 Relative adsorbed amount of human albumin on the copolymer-treated LDPE surfaces (PEO mol wt 1900, polymer Nos. 1–11; polymer treatment, 30 min desorption in water after 30 min adsorption in 1 mg/ml polymer solution; protein adsorption, human albumin 1 mg/ml, 30 min)  $n = 3$ .

polymer Nos. 1–11) treated LDPE surfaces. Relative adsorbed amount of protein was determined as follows:

$$\text{Relative adsorbed amount of protein} = (n\% \text{ of polymer-treated surface}) / n\% \text{ of untreated surface}$$

By comparing Figure 7 with Figure 6, we can see that the protein resistance of the polymer-treated surface is highly dependent on the adsorbed amount of the polymers on the LDPE surface. In the case of the surfaces treated with polymer Nos. 9 and 10, the amount of adsorbed human albumin decreased more than 90%, as compared with the untreated LDPE surface. The adsorbed amount of human albumin on the surfaces treated with different PEO mol wt, 1900 and 4000, was compared in Table 3 for both XPS and  $^{125}\text{I}$ -labelled protein analysis. The polymer No. 23-treated surface showed excellent protein-resistant properties, probably due to large amount of adsorption on LDPE surface,

Table 3 Adsorbed amount of human albumin<sup>a</sup> on untreated and copolymer-treated LDPE surfaces<sup>b</sup>

Polymer no.	MW <sub>PEO</sub>	Nitrogen atomic % (XPS)	$\mu\text{g}/\text{cm}^2$ ( $^{125}\text{I}$ -labelling)
Pure LDPE	1900	$10.4 \pm 3.3^c$	$0.45 \pm 0.08$
9	1900	$1.1 \pm 0.4$	–
10	1900	$0.8 \pm 0.1$	0.10
11	1900	$1.5 \pm 0.2$	0.13
12	1900	$1.2 \pm 0.7$	0.12
13	4000	$1.5 \pm 0.4$	0.15
14	4000	$1.3 \pm 0.2$	0.11
15	4000	$1.4 \pm 0.6$	0.11
23	4000	$0.4 \pm 0.1$	–

<sup>a</sup>Protein adsorption; human albumin 1 mg/ml in PBS pH 7.4, 30 min adsorption.

<sup>b</sup>Polymer treatment; 30 min desorption in water after 30 min adsorption of LDPE film in 1 mg/ml polymer solution.

<sup>c</sup>Nitrogen content of human albumin, 15.1% as determined by XPS analysis.

even though its PEO portion is only 10 mol%. Possible explanations for protein resistance of the polymer-treated surfaces include PEO's high mobility, its unique solution properties, its low interfacial free energy with water and steric effects, as discussed earlier.

Proteins are macromolecules. Will the copolymer molecules adsorbed on LDPE surface be exchanged with the proteins during exposure to a protein solution? To answer this question, time-dependent protein adsorption was done on the LDPE surfaces pre-treated with the  $^{125}\text{I}$ -labelled copolymers. After protein exposure for different time periods, the polymer radioactivity on the surface was counted, converted to values of adsorbed amount of the polymer on the surface and compared to the values present before protein adsorption (Figure 8). As seen in the figure, there is little evidence of exchange of the polymer molecules with human albumin for up to 100 min exposure time. Figure 9 also compares the adsorbed amount of the polymers on the LDPE surfaces both before and after albumin adsorption for 30 min. The large decrease of adsorbed amount of polymer No. 23 after protein exposure suggested a possibility of intramolecular aggregation of the polymer in aqueous solution.

### Removal of pre-adsorbed proteins

The effectiveness of the copolymers for removal of proteins pre-adsorbed on a hydrophobic surface was also studied by

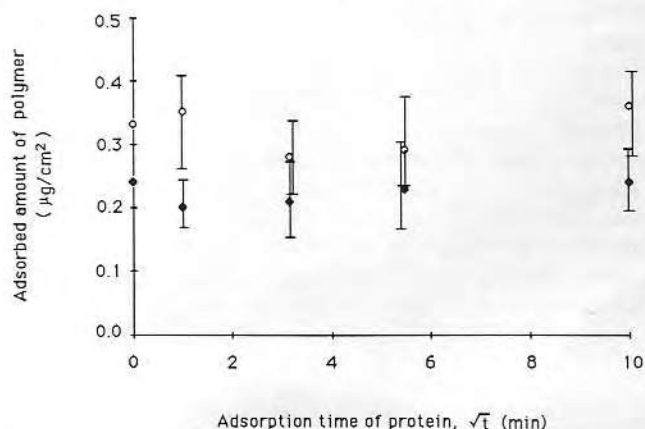


Figure 8 Amount of polymers remaining on LDPE surface after protein exposure (protein adsorption, human albumin 1 mg/ml solution; polymer treatment, 30 min desorption in water after 30 min adsorption in 1 mg/ml polymer solution). ( $\diamond$ ), polymer No. 19; ( $\blacklozenge$ ), polymer No. 21,  $n = 3$ .

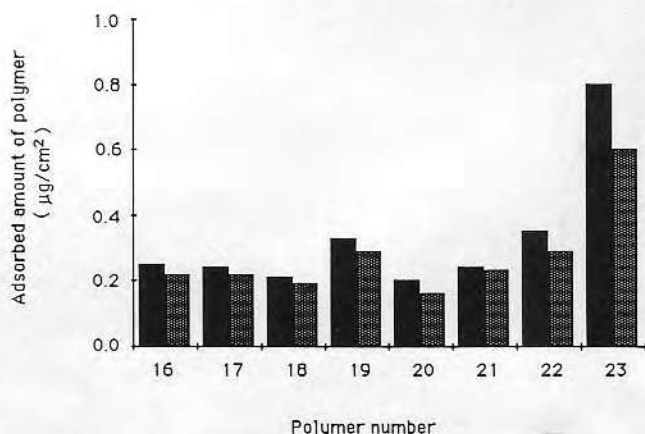


Figure 9 Adsorbed amount of polymers on LDPE surface before and after protein adsorption (protein adsorption, human albumin 1 mg/ml, 30 min; polymer treatment, 30 min desorption in water after 30 min adsorption in 1 mg/ml polymer solution). ( $\blacksquare$ ), before protein adsorption; ( $\hatched$ ),  $n = 3$ .

treating the LDPE surfaces pre-adsorbed with human albumin in the copolymer solutions. The protein nitrogen signal from XPS analysis of the surface before and after the polymer solution treatment was compared. Figure 10 shows the removal properties of pre-adsorbed proteins by the polymers (PEO mol wt 1900, polymer Nos. 1-11). Relative adsorbed amount of protein was determined as follows:

$$\text{Relative adsorbed amount of protein} = (n\% \text{ after polymer treatment}) / (n\% \text{ before polymer treatment})$$

Nitrogen atomic % decreased after the polymer treatment but it appeared that the comonomer composition did not have a significant effect.

Here we have some questions. Does the decrease in nitrogen atomic % really mean a decrease in adsorbed amount of protein after the polymer treatment? What is the mechanism for removal of pre-adsorbed protein by PEO-containing polymeric surfactants? Three cases are possible for the decrease in nitrogen atomic % after the polymer treatment, as seen in Figure 11. As the protein-bound surface is immersed in the polymeric surfactant solution, protein molecules can be exchanged with the polymer molecules if the polymer molecules interact more strongly with the hydrophobic surface than the pre-adsorbed protein molecules (a), or the highly mobile PEO chains of the polymer may penetrate into the protein bound on the surface and thereby remove the protein from the surface (b), or the polymer molecules will bind on to the protein surface (c). In the case of (c), the polymer will not work for protein removal, even though the protein nitrogen signal will be decreased. From the studies using  $^{125}\text{I}$ -labelled protein, we can distinguish cases (a) and (b) from case (c). Table 4 shows the results. If only the shielding (case (c)) is occurring, valid radioactivity from protein-labelling will not be changed before and after the polymer treatment. But as the adsorbed amount of protein calculated from the retained radioactivity after the polymer treatment decreased, as seen in Table 4, it can be said that some proteins are removed from the surface

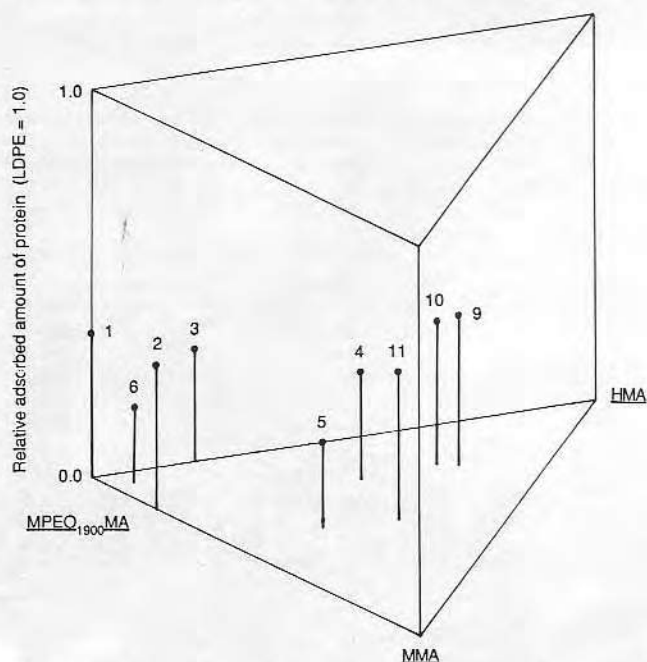


Figure 10 Relative adsorbed amount of human albumin on LDPE surface after the copolymer solution treatment (protein pre-adsorption, human albumin 1 mg/ml, 30 min; PEO mol wt 1900, polymer Nos. 1-11; polymer solution treatment, 1 mg/ml, 30 min)  $n = 3$ .

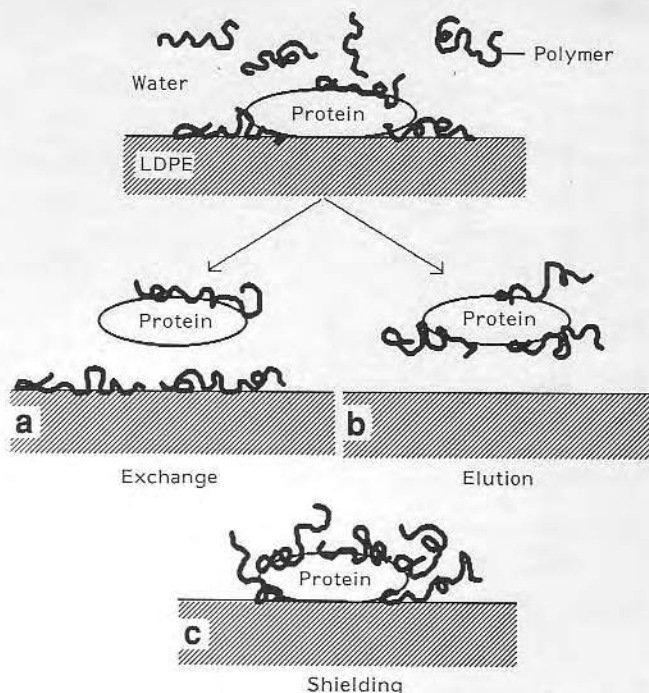


Figure 11 Possible mechanisms involved in removal of pre-adsorbed proteins by PEO-containing surfactants (XPS analysis and  $^{125}\text{I}$ -labelling of proteins or surfactants were used to distinguish between three possible mechanisms).

after the polymer treatment. Now we must distinguish between exchange (case (a)) and elution (case (b)).  $^{125}\text{I}$ -labelled polymers used for solution treatment may give an answer. If elution predominates, then the adsorbed amount of polymer after polymer solution treatment will be very small. If the adsorbed amount of polymers on the pure LDPE surface (Table 2) and the LDPE surface after the polymer solution treatment (Table 4) are compared, it can be seen that almost the same amount of the polymers are adsorbed in both two surfaces, which probably means the predominance of exchange (case (a)). However, the results from XPS analysis and  $^{125}\text{I}$ -labelling of protein and polymer in Table 4 suggest that all three cases, i.e. exchange, elution and shielding are actually involved, even though exchange and shielding appear to predominate.

### Comparison with commercial surfactants

The surface properties of the copolymers discussed in this paper, such as adsorption on LDPE surface, protein resistance and removal of pre-adsorbed proteins, are compared with those of some selected commercial surfactants containing PEO and PPO or PBO, from our previous studies<sup>17-18</sup>.

Table 4 Comparison of the XPS and  $^{125}\text{I}$ -labelling results for removal of pre-adsorbed protein<sup>a</sup> by the copolymer treatment<sup>b</sup>

Polymer no.	MW <sub>PEO</sub>	Nitrogen atomic % from protein	$\mu\text{g}/\text{cm}^2$ from protein	$\mu\text{g}/\text{cm}^2$ from polymer
Pure LDPE		10.4 $\pm$ 3.3	0.45 $\pm$ 0.08	
17	1900	3.3	0.27	0.25
18	1900	3.1	0.27	0.22
19	1900	4.1	0.29	0.40
20	4000	3.2	0.23	0.19
21	4000	3.5	0.25	0.23
22	4000	3.6	0.20	0.15

<sup>a</sup>Protein pre-adsorption; human albumin 1 mg/ml, 30 min.

<sup>b</sup>Polymer solution treatment; 1 mg/ml, 30 min.

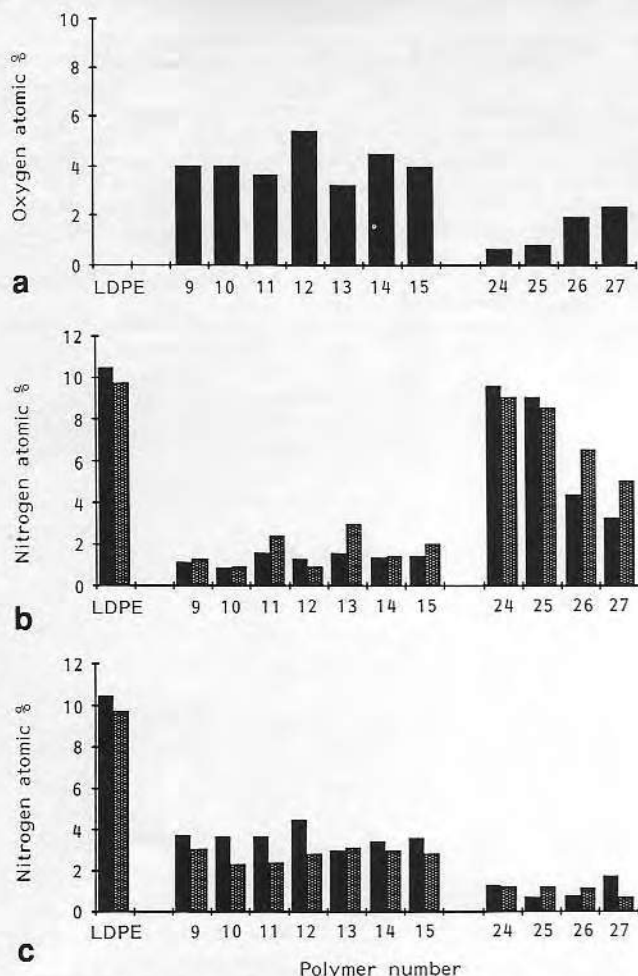


Figure 12 Comparison of surface properties between the synthesized copolymers and selected commercial surfactants containing PEO and PPO or PBO (polymer Nos. 24-27, commercial surfactants; polymer No. 24, PEO<sub>13</sub>-PPO<sub>30</sub>-PEO<sub>13</sub> triblock; polymer No. 25, PEO<sub>13</sub>-PBO<sub>25</sub>-PEO<sub>13</sub> triblock; polymer No. 26, star-like 4 PEO<sub>26</sub> and 4 PPO<sub>29</sub> block; polymer No. 27, condensed polymer of PEO<sub>13</sub>-PPO<sub>30</sub>-PEO<sub>13</sub>,  $n = 3$  for copolymers synthesized;  $n = 3-5$  for commercial surfactants)<sup>17,19</sup>. (a) adsorbed amount of polymers on LDPE surface; (b) protein resistance of polymer-treated LDPE surfaces; (c) removal properties of pre-adsorbed protein on LDPE surface by polymer solution treatment (■, albumin 1 mg/ml adsorption; ▨, plasma 1% adsorption).

As seen in Figure 12, the copolymers synthesized show much better protein (albumin and plasma) resistance than the commercial block surfactants, probably due to larger amount of adsorption and longer PEO chains, whilst the commercial block surfactants show much better removal properties of pre-adsorbed proteins than the copolymers synthesized, even though their molecular weights and PEO chain lengths are much shorter than our synthesized copolymers. This means that exchange of proteins with the commercial surfactant at LDPE surface may not be the predominant mechanism for removal of pre-adsorbed proteins. Perhaps the short PEO blocks of the commercial surfactants can penetrate more effectively into the protein molecule bound on the surface and thereby elute the adsorbed proteins.

## ACKNOWLEDGEMENTS

This study was funded by the Center for Biopolymers at Interfaces (CBI), University of Utah. We thank Dr Shoji Nagaoka (Toray, Kanagawa, Japan) for gifts of the macromonomer samples, BASF-Wyandotte (Wyandotte, MI, USA)

and ICI (Cleveland, UK) for gifts of the surfactant samples and for technical information and the National Institutes of Health, Devices and Technology Branch, (NHLBI) for the LDPE samples.

## REFERENCES

- 1 Bailey, F.E. and Koleske, J.V., *Poly(Ethylene Oxide)*, Academic Press, New York, USA, 1976, p. 29
- 2 Merrill, E.W. and Salzman, E.W., Polyethylene oxide as a biomaterial, *ASAIO J.* 1983, **6**, 60-64
- 3 Kjellander, R. and Florin, E., Water structure and changes in thermal stability of the system poly(ethylene oxide)-water, *J. Chem. Soc. Faraday Trans. 1*, 1981, **77**, 2053-2077
- 4 Bailey, F.E. and Callard, R.W., Thermodynamic parameters of poly(ethylene oxide) in aqueous solution, *J. Applied Polymer Sci.* 1959, **1**, 373-379
- 5 Narten, A.H., Liquid water: Atom pair correlation functions from neutron and X-ray diffraction, *J. Chem. Phys.* 1972, **56**, 5681-5687
- 6 Andrade, J.D., Nagaoka, S., Cooper, S., Okano, T. and Kim, S.W., Surfaces and blood compatibility: Current hypotheses, *ASAIO J.* 1987, **10**, 75-84
- 7 Atha, D.H. and Ingham, K.C., Mechanism of precipitation of proteins by polyethylene glycols: Analysis in terms of excluded volume, *J. Biol. Chem.* 1981, **256**, 12108-12117
- 8 Hermans, J., Excluded-volume theory of polymer-protein interactions based on polymer chain statistics, *J. Chem. Phys.* 1982, **77**, 2193-2203
- 9 Knoll, D. and Hermans, J., Polymer-protein interactions comparison experiments and excluded volume theory, *J. Chem. Phys.* 1983, **258**, 5710-5715
- 10 Andrade, J.D., Interfacial phenomena and biomaterials, *Med. Instr.* 1973, **7**, 110-120
- 11 Coleman, D.L., Gregonis, D.E. and Andrade, J.D., Blood-materials interactions: the minimum interfacial free energy and the optimum polar/apolar ratio hypotheses, *J. Biomed. Mater. Res.* 1982, **16**, 381-398
- 12 Merrill, E.W., Salzman, E.W., Wan, S., Mahmud, N., Kushner, L., Lindon, J.N. and Curme, J., Platelet-compatible hydrophilic segmented polyurethanes from polyethylene glycols and cyclohexane diisocyanate, *Trans. ASAIO* 1982, **28**, 482-486
- 13 Hiatt, C.W., Shelokov, A., Rosenthal, E.J. and Galimore, J.M., Treatment of controlled pore glass with poly(ethylene oxide) to prevent adsorption of rabies virus, *J. Chromatography* 1971, **56**, 362-364
- 14 Hawk, G.L., Cameron, J.A. and Dufault, L.B., Chromatography of biological materials on polyethylene glycol treated controlled-pore glass, *Preparative Biochem.* 1972, **2**, 193-203
- 15 Gregonis, D.E., Buerger, D.E., Van Wagenen, R.A., Hunter, S.K. and Andrade, J.D., Poly(ethylene glycol) surfaces to minimize protein adsorption, in *Trans. Second World Congress on Biomaterials*, 1984, p. 266 Society for Biomaterials, Birmingham, AL, USA
- 16 Winters, S., Immobilized heparin via a long chain poly(ethylene oxide) spacer for protein and platelet compatibility, Ph.D. Thesis, University of Utah, 1986
- 17 Lee, J.H. and Andrade, J.D., Surface properties of aqueous PEO/PPO block copolymer surfactants, in *Polymer Surface Dynamics*, (Ed. J.D. Andrade), Plenum Press, New York, USA, 1988, pp. 119-136
- 18 Lee, J.H., Kopecek, J. and Andrade, J.D., Surface properties of aqueous PEO-containing block copolymer surfactants: Protein-resistant surfaces, *Polymeric Mater. Sci. Eng.* (Div. of ACS), 1987, **57**, 613-617
- 19 Lee, J.H., Kopecek, J. and Andrade, J.D., Protein-resistant surfaces prepared by PEO-containing block copolymer surfactants, *J. Biomed. Mater. Res.* 1989, **23**, 351-368
- 20 Thurow, H. and Geisen, K., Stabilization of dissolved proteins against denaturation at hydrophobic interfaces, *Diabetologia*, 1984, **27**, 212-218
- 21 Chuang, H.Y.K., King, W.F. and Mason, R.G., Interaction of plasma proteins with artificial surfaces: Protein adsorption isotherms, *J. Lab. Clin. Med.* 1978, **92**, 483-496
- 22 Tuszynski, G.P., Knight, L., Piperno, J.R. and Walsh, P.N., A rapid method for removal of [<sup>125</sup>I] iodine following iodination of protein solutions, *Anal. Biochem.* 1980, **106**, 118-122
- 23 Andrade, J.D., X-ray photoelectron spectroscopy, in *Surface and Interfacial Aspects of Biomedical Polymers Vol. 1, Surface Chemistry and Physics*, (Ed. J.D. Andrade), Plenum Press, New York, USA, 1985, p. 105-195



- 24 Gnanou, Y. and Lutz, P., The ability of macromonomers to copolymerize: A critical review with the new developments, *Makromol. Chem.* 1989, **190**, 577-588
- 25 Hamaide, T., Revillon, A. and Guyot, A., Reactivite de macromeres du polyoxyethylene en copolymerisation radicalaire, *Eur. Polym. J.* 1984, **20**, 855-861
- 26 Tsukahara, Y., Tanaka, M. and Yamashita, Y., On the copolymerization reactivity of macromonomers, *Polymer J.* 1987, **19**, 1121-1125
- 27 Ulbrich, K., Konak, C., Tuzar, Z. and Kopecek, J., Solution properties of drug carriers based on poly [N-(2-hydroxypropyl)methacrylamide] containing biodegradable bonds, *Makromol. Chem.* 1987, **188**, 1261-1272
- 28 Duncan, R., Cable, H.C., Rejmanova, P., Kopecek, J. and Lloyd, J.B., Tyrosinamide residues enhance pinocytic capture of N-(2-hydroxypropyl)methacrylamide copolymers, *Biochem. Biophys. Acta.* 1984, **799**, 1-8
- 29 Kronberg, B., Sjoblom, E., Ehrenborg, L., Stenius, P. and Wesslen, B., Surface activity and stability properties of polymethylmethacrylate-G-polyethylene oxide polymers, *Polymer Preprints*, 1985, **26**, 236-238
- 30 Clunie, J.S. and Ingram, B.T., *Adsorption from Solution at the Solid/Liquid Interface*, (Eds. G.D. Parfitt and C.H. Rochester), Academic Press, New York, USA, 1983, Ch. 3
- 31 Furlong, D.N. and Aston, J.R., Adsorption of polyoxyethyl-ated nonionic phenols, *Colloids and Surfaces* 1982, **4**, 121-129
- 32 Corkill, J.M., Goodman, J.F. and Tate, J.R., Adsorption of alkyl sulphanylalkanols on Graphon, *Trans. Faraday Soc.* 1967, **67**, 2264-2269
- 33 Rosen, M.J., *Surfactants and Interfacial Phenomena*, Wiley-Interscience, New York, USA, 1978, Ch. 1 and 5
- 34 Kayes, J.B. and Rawlins, D.A., Adsorption characteristics of certain polyoxyethylene-polyoxypropylene block copolymers on polystyrene latex, *Colloid and Polymer Sci.* 1979, **257**, 622-629

## BLOOD COMPATIBILITY OF POLYETHYLENE OXIDE SURFACES

JIN HO LEE, HAI BANG LEE\*† and JOSEPH D. ANDRADE‡

*Department of Macromolecular Science, Han Nam University, 133 Ojeong Dong, Daedeog Ku, Taejeon 300-791, Korea*

*†Biomaterials Laboratory, Korea Research Institute of Chemical Technology, P.O. Box 107, Yuseong, Taejeon 305-343, Korea*

*‡Department of Bioengineering, University of Utah, Salt Lake City, Utah 84112, U.S.A.*

### CONTENTS

1. Introduction	1043
2. Solution properties of PEO in water	1045
2.1. General features	1045
2.2. Solubility and molecular structure of PEO in water	1047
2.3. Solubility vs temperature	1048
2.4. Mobility	1049
2.5. Heat and entropy of dilution	1050
2.6. Comparison with some other polymers	1050
2.6.1. Comparison of solubility with other polyethers	1050
2.6.2. Comparison of thermodynamic parameters with other water-soluble polymers	1052
3. Possible mechanisms for protein resistance of PEO surfaces	1056
3.1. Interfacial free energy	1056
3.2. Steric stabilization effect	1056
3.3. Relationship with solution properties	1058
4. Approaches to prepare PEO surfaces and their blood compatibility	1060
4.1. Bulk modification	1060
4.2. Physical adsorption	1062
4.3. Covalent grafting	1064
4.4. Graft copolymerization	1067
4.5. Other surface modifications	1070
5. Conclusions	1071
References	1073

### 1. INTRODUCTION

Knowledge of the interfacial interaction of polymers with plasma proteins and blood is important in establishing polymer blood compatibility. The interaction of plasma proteins and blood with polymers has been studied by many research groups. It is known that proteins are complex macromolecules with molecular weights ranging from thousands to millions (Fig. 1) and they adsorb at practically all interfaces during the first few minutes of blood or biological fluids exposure.<sup>1,2</sup> Generally the adsorption

\*To whom correspondence should be addressed

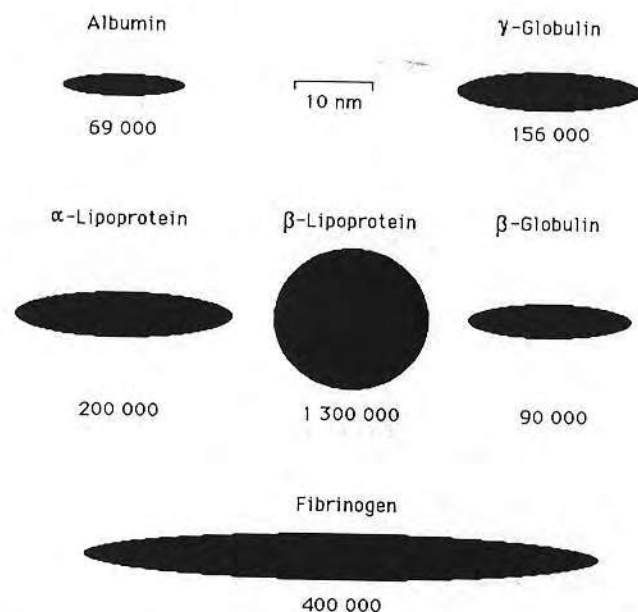


Fig. 1. Molecular weights and shapes (schematic) of some plasma proteins (from ref. 1).

process results in the activation of coagulation and subsequent thrombus formation.<sup>1-5</sup> There have been various efforts at minimizing or eliminating protein adsorption. Surfaces which show minimal protein adsorption may be important in many applications, not only for blood-contacting implant devices but also for other areas, such as membranes for separation processes, biosensors, chromatographic supports, contact lenses, blood and protein storage applications, etc.

Although a substantial amount of work on the improvement of blood compatibility of polymeric materials has been carried out, the results are still not very conclusive. This is partly due to the fact that the precise relationship between the nature of a surface and blood compatibility and the mechanisms of surface-induced thrombosis have not been completely elucidated.<sup>6-12</sup>

It seems that surfaces which non-specifically repel all proteins are desirable to minimize surface contact activation. This implies that the combined energies for attraction such as van der Waals attractions, electrostatic attractions, entropic attractions (i.e., hydrophobic bonding) and hydrogen bonding of the surfaces with proteins should be smaller than entropic and hydration repulsions due to thermal motion of flexible molecular chains and solvent molecules. Such surfaces can be prepared by immobilizing neutral, hydrophilic polymers. Among hydrophilic polymers, a particularly effective polymer for 'protein-resistant' (or blood-compatible) surfaces appears to be polyethylene oxide (PEO), due to its unique solution and surface properties in water.

In this article, we review the solution properties of PEO in water, because we are concerned only with water as a solvent (biological fluids or blood are aqueous solutions). We expect that the unique solution properties of PEO in water are closely related to the protein resistance of PEO surfaces. We compare PEO with polyethers having structural similarities and with other water-soluble polymers to figure out why PEO is particularly effective for protein resistance. There are many factors involved in PEO's passivity, including those related to its solution properties in water. We discuss possible mechanisms for protein resistance of PEO surfaces.

PEO surfaces have been prepared by many different methods. A number of research groups including our own have demonstrated greatly decreased adsorption of plasma and other proteins on PEO surfaces. We review approaches to prepare PEO surfaces and their experimental results in reducing protein adsorption and platelet adhesion.

## 2. SOLUTION PROPERTIES OF PEO IN WATER

### 2.1. General Features

Polyethylene oxide (PEO) is a crystalline, thermoplastic polymer. It is an uncharged polyether with the chemical formula,  $\text{H}-(\text{OCH}_2\text{CH}_2)_n-\text{OH}$ , which is the simplest structure of water-soluble polymers. Unlike most polymer systems, PEO is commercially available in an extraordinarily wide range of molecular weights from 200 to several million or more. The lower-molecular-weight members of this series, with chain lengths up to about 150, are known as polyethylene glycols (PEG).<sup>13</sup> The higher members of the series are known as polyethylene oxides or as polyoxyethylenes. In this article, we will call all these classes of compounds 'PEO' regardless of their molecular weights. The properties of PEO differ greatly because of the large differences in molecular weight, as seen in Table 1.

By X-ray analysis,<sup>14</sup> it is known that the PEO molecule in the crystalline state has a helical conformation which contains two turns in a fibre identity period (unit length of

Table 1. Properties of polyethylene oxides with different molecular weight<sup>13</sup>

Properties	200	400	Number-average molecular weight				6000	20,000
			600	1000	4000			
Specific gravity (20/20°C)	1.125	1.130	1.130	—	1.204	—	—	—
Melting point (°C)	—	4–8	20–25	37–40	53–56	60–63	50–55	—
Viscosity (cst, 100°C)	4.3	7.3	10.5	17.4	75–85	700–900	—	—
Heat of fusion (J/g)	—	151	146	155	180	192	172	—
Refractive index ( $n_D$ , 25°C)	1.460	1.467	1.469	—	—	—	—	—
Surface tension (dyn/cm)	44.5	44.5	44.5	—	—	—	—	—



Table 2. Structures and properties of polyethers with general formula  $\text{HO}[-(\text{CH}_2)_m-\text{O}]_n\text{H}^{14}$ 

	1	2	3	4	8
Polymer	Polymethylene oxide $(-\text{CH}_2\text{O}-)_n$	Polyethylene oxide $(-\text{CH}_2\text{CH}_2\text{O}-)_n$	Polytrimethylene oxide $(-\text{CH}_2\text{CH}_2\text{CH}_2\text{O}-)_n$	Polytetramethylene oxide $(-\text{CH}_2\text{CH}_2\text{CH}_2\text{CH}_2\text{O}-)_n$	Polymethylene (polyethylene) $(-\text{CH}_2-)_n$
structural formula					
melting point (°C)	180	60	34	36	137
density (g/cm <sup>3</sup> )	1.40–1.51	1.15–1.26		1.08–1.18	0.92–1.00
hardness	Hard	Soft	Soft	Soft	Medium
molecular structure	9 <sub>5</sub> helix	7 <sub>2</sub> helix	Planar zigzag	Planar zigzag	Planar zigzag
crystal structure†	Trigonal $a = 4.46 \text{ \AA}$ $c = 17.3 \text{ \AA}$	Monoclinic $a = 8.16 \text{ \AA}$ $b = 12.99 \text{ \AA}$ $c = 19.3 \text{ \AA}$ $\beta = 126^\circ 5'$		Monoclinic $a = 5.48 \text{ \AA}$ $b = 8.73 \text{ \AA}$ $c = 12.1 \text{ \AA}$ $\beta = 134^\circ 12'$	Orthorhombic $a = 7.40 \text{ \AA}$ $b = 4.93 \text{ \AA}$ $c = 2.534 \text{ \AA}$
	$N = 1$	$N = 4$		$N = 2$	$N = 2$

c, fibre axis; N, number of molecular chains in a unit cell.

c-axis) of 19.3 Å. The crystallographic unit cell contains four molecular chains and is monoclinic with  $a = 8.16 \text{ \AA}$ ,  $b = 12.99 \text{ \AA}$ ,  $c = 19.30 \text{ \AA}$ , and  $\beta = 126^\circ 5'$ . Table 2 summarizes the structures and properties of a series of polyethers with a general formula,  $\text{HO}[-(\text{CH}_2)_m-\text{O}]_n\text{H}$ . A more detailed structure analysis is, however, not possible by X-ray methods alone. Information concerning the conformation of the PEO chain in the crystalline and molten states as well as in solution has been obtained through analyses of infrared (IR),<sup>15–17</sup> Raman,<sup>18–21</sup> and NMR spectra.<sup>15,22–28</sup> In the crystalline state, IR and Raman analyses agree with the conformational assignment to internal rotation about the O–CH<sub>2</sub>, CH<sub>2</sub>–CH<sub>2</sub>, and CH<sub>2</sub>–O bonds of *trans*, *gauche*, *trans*, respectively. In the molten state, the conformation becomes somewhat disordered.<sup>16–18</sup> This disordering is noted principally by the appearance of a considerable fraction of *trans*, *trans*, *trans* conformations. In water, the PEO chain retains to a large degree the *trans*, *gauche*, *trans* sequence and helical conformation of the crystalline state, as evidenced from IR spectra,<sup>16</sup> Raman spectra,<sup>18</sup> NMR spectra,<sup>15,16</sup> and calorimetry.<sup>29</sup>

In comparison with all other water-soluble polymers, PEO is unique in its linearity of structure, non-ionic character and water solubility. This linear, relatively non-polar structure displays a high degree of polymer–solvent interaction in water, which is observed in the development of structural viscosity to an unusual degree.<sup>30–34</sup> PEO has many interesting properties; however, our main concern in this section is its unique solution behavior in water.

## 2.2. Solubility and Molecular Structure of PEO in Water

At room temperature, PEO is completely miscible with water in all proportions for all degrees of polymerization.<sup>13</sup> The water solubility of PEO is unlimited, at least up to temperatures slightly below 100°C. In contrast to the complete water solubility of PEO, closely related polymers such as polymethylene oxide, polytrimethylene oxide, polyacetaldehyde and polypropylene oxide are water-insoluble under ordinary conditions (Table 3).

Table 3. Structures and solubilities of polyethers.<sup>13,31,35</sup>

Polymer	Structural unit	Solubility in water at room temperature
Polymethylene oxide	$-\text{CH}_2\text{O}-$	No
Polyethylene oxide	$-\text{CH}_2-\text{CH}_2-\text{O}-$	Yes
Polytrimethylene oxide	$-\text{CH}_2-\text{CH}_2-\text{CH}_2-\text{O}-$	No
Polyacetaldehyde	$-\text{CH}-\text{O}-$	No
Polypropylene oxide	$\begin{array}{c}   \\ \text{CH}_3 \\ -\text{CH}-\text{CH}_2-\text{O}- \\   \\ \text{CH}_3 \end{array}$	Partially†

Why is PEO miscible in all proportions with water at room temperature, while other polyethers are not? It seems to be related to hydration of the ether oxygens in a manner which is apparently unique to the PEO structure.<sup>31,36,37</sup> Water is a highly structured liquid, with hydrogen bonds linking individual molecules to each other. The precise arrangement about each molecule is not known, but the tetrahedral symmetry of the oxygen bond orbitals and the tetrahedral structure of ice suggest a locally tetrahedral arrangement of molecules in the liquid state also.<sup>38</sup> The highly connected network of tetrahedrally coordinated water molecules contains quite a large fraction of interstitial space, as established by X-ray and neutron diffraction.<sup>39</sup> This network is characterized by oxygen–oxygen distances of 2.85 Å between neighbours and 4.7 Å between next-nearest neighbours. Any arrangement of this type would be disrupted by a solute dissolved in water. Some hydrogen bonds would have to be broken; if the solute is polar, new hydrogen bonds between water and the solute would be formed.<sup>38</sup> Kjellander and Florin<sup>40,41</sup> have intensively studied the PEO–water system and suggested that the water solubility of PEO can be explained in terms of a good structural fit between the water and the polymer. They suggested that PEO, in contrast to the other polyethers, can be fitted into the tetrahedral water lattice so that all of the lattice points are occupied, either by a water or by an ether oxygen, i.e., the conformation of the polymer can be arranged so that both the distances of neighbouring and next-neighbouring oxygen atoms fulfil the requirements of the water lattice (see Section 2.6.1 for more discussion). The ethylene segments thus fill out voids in the spacious water structure and minimally perturb the structure of water itself.

### 2.3. Solubility vs Temperature

PEO exhibits an inverse solubility–temperature relationship.<sup>13,30,31,35,42</sup> One way of interpreting the inverse solubility–temperature relationship of PEO would be through a disordering of ‘hydration shells’ that exist about the polymer molecule at low temperatures.<sup>40,41,43–45</sup> These hydration shells correspond to a layer of highly oriented water which would surround the polymer in aqueous solution. The coupling between the polymer and water gives rise to enhanced structuring of the water that is close to the polymer chain and this makes it necessary to distinguish between water in the hydration shell of PEO and in the bulk solution. The hydration shell water is characterized by both lower entropy and enthalpy than the bulk water.<sup>41</sup> Thus, such a structure formation is entropically unfavourable, but this contribution to the free energy is overcome by the decrease in enthalpy on the increased structuring of the water and the binding to PEO.<sup>40,41</sup> Thus, PEO is water-soluble. The good fit between PEO and the water structure probably makes the enthalpy contribution significantly large. When the temperature is raised, the hydration shell is gradually broken down due to thermal motion. This means that the difference in properties between bulk and shell water decreases. Since the structure does not break down sufficiently rapidly when the temperature is raised, the unfavourable entropy contribution dominates and the system phase-separates, decreasing the extent of the enhanced structure (see refs 40 and 41 for detailed discussion). The phase separation or precipitation temperature depends on the polymer concentration.<sup>13</sup> For very dilute solutions ( $\leq 0.2\%$

polymer), the precipitation is observed as a cloud point. For slightly more concentrated solutions ( $\geq 0.5\%$  polymer), the polymer precipitates as a gel. At even higher temperatures, when the structure has largely been broken down, the unfavourable entropy contribution is diminished.<sup>40,41</sup> The system is then completely miscible again, provided the temperature is not high enough to cause destruction of the polymer.

Doolittle<sup>46</sup> tried to interpret the inverse solubility–temperature relationships of high-polymer–solvent systems. Solvophilic and solvophobic influences are considered to be reflected in the heat and entropy of dilution factors of the polymer–solvent interaction parameters. Thus the temperature dependence of the solubility is such that the solvent becomes a non-solvent at a critical temperature. In PEO, the hydrophobic and hydrophilic character is provided by the alternate ethylene units (hydrophobic) and oxygens (hydrophilic) of the polymer chain. If the inverse solubility–temperature phenomenon is to be interpreted as a hydrophilic–hydrophobic balance in the polymer system, increasing the hydrophobic character of the polymer should result in a lowering of the polymer precipitation temperature. Bailey and Callard<sup>31</sup> used copolymers of ethylene oxide and propylene oxide to test this prediction. They showed that the precipitation temperature, at a given polymer concentration, decreases linearly with increasing propylene oxide content.

### 2.4. Mobility

The dynamic properties of a polymer depend on the probable polymer conformations and the transition probabilities. The presence of bulky groups attached to the backbone will introduce steric hindrances and reduce the mobility of polymer segments. The dynamic behaviour of PEO in water has been studied by nuclear magnetic relaxation,<sup>9,47–50</sup> electron spin resonance,<sup>49</sup> and the measurement of dynamic moduli.<sup>51</sup> PEO, an uncharged polymer without bulky side groups, appears to be very flexible compared with polymers with bulky groups (steric hindrance) or polyelectrolytes such as polymethacrylic acid (steric and electrostatic hindrances).

The dielectric behaviour of PEO has been studied to elucidate polymer chain flexibility and polar bond interactions.<sup>13,52</sup> Davies *et al.*<sup>53</sup> found from dipole relaxation studies that there is a marked freedom of reorientation in PEO. They suggested that the carbon–oxygen linkage acts as a ball-and-socket joint, making the average freely moving unit little more than a single monomeric unit.

Breen *et al.*<sup>47</sup> studied the molecular weight dependence of the relaxation rates of PEO from NMR. They utilized dilute aqueous solutions of PEO to minimize polymer–polymer interactions. They suggested that the molecular weight dependence is caused by end group contributions and in addition by overall tumbling (small molecules). They also suggested that the position dependence of the relaxation rates along the chain disappears after some distance from the end and then the relaxation rate becomes the polymer relaxation rate. For long polymer chains, the contribution of end group dynamics to the relaxation rate will be insignificant. They failed to observe any end group effects in <sup>1</sup>H-relaxation rates when the PEO chain length was  $>100$ . It has also been reported that the segmental motions of PEO are independent of chain length when the chain length is greater than about 100<sup>54</sup> or about 130.<sup>55–57</sup>



Nagaoka *et al.*<sup>9</sup> also studied different PEO chains (attached on a surface) in a hydrated state using NMR spectroscopy. They related the linewidth of the peak <sup>13</sup>C NMR signal to the PEO chains. They found that increasing the PEO chain length to 100 decreases the width of the signal peak, indicating increased mobility.

## 2.5. Heat and Entropy of Dilution

The heat and entropy of dilution of PEO in water have been studied from the temperature dependence of the intrinsic viscosity,<sup>31,58</sup> vapour pressure and heat of mixing experiments,<sup>59</sup> and calorimetry.<sup>29,60–64</sup> It was calculated that both the heat of dilution and the entropy of dilution of PEO in water are negative. Negative values for these parameters imply a high degree of polymer–solvent interaction and orientation of solvent with respect to the polymer chain.<sup>58</sup>

Maron and Filisko<sup>29,64</sup> used a microcalorimeter to measure the heats of dilution and solution of PEO in water and organic solvents. They found from the organic solvent data that the heat of fusion or lattice energy of the sample is independent of the solution concentration or the solvent used. However, there was a difference in the behaviour of PEO between water and the organic solvents which was attributed to the difference in the conformation of the polymer in organic solvents and in water. PEO in organic solvents exists as a random coil, whereas in water its conformation is helical. It was shown that the interconversion of the random coil to the helix involves a heat evolution (164.4 J of heat per gram of polymer) and suggested that this heat evolution (or helix formation) probably accounts for the fact that PEO is water-soluble in contrast to polymethylene oxide and polypropylene oxide.

Lakhanpal *et al.*<sup>61–63</sup> also measured the heats of solution of PEO in organic solvents and water and obtained similar results to those of Maron and Filisko; their values were independent of the nature of the solvent used other than water. The anomalous behaviour of PEO in water was explained by the authors as a result of strong interactions via hydrogen bonds of the water molecules with the ether oxygens in the polymer chains.

## 2.6. Comparison with Some Other Polymers

### 2.6.1. Comparison of Solubility with Other Polyethers

As suggested in Section 2.2, the difference between PEO and the water-insoluble polyethers (see Table 3) may be that the latter do not satisfy the structural fit to allow a mainly unstrained coupling to a continuous tetrahedrally coordinated network of water (oxygen–oxygen distances of 2.85 Å between neighbours and 4.7 Å between next-nearest neighbours of the lattice) around the polymer chains. PEO can be nicely fitted into this type of water lattice without distortion of the lattice so that all of the lattice points are occupied, either by a water or by an ether oxygen, i.e., the conformation of PEO can be arranged so that both the distances of neighbouring and next-neighbouring oxygen atoms fulfil the requirements of the water lattice and the ethylene segments fill out voids in the spacious water structure.<sup>40</sup>

Consider polypropylene oxide (PPO). When PPO is introduced into water, it develops a hydration shell with an enhanced structuring of water as evidenced by the negative entropy and enthalpy of mixing.<sup>40,61,62</sup> Despite the fact that PPO has the same backbone structure as PEO, an optimal water structure cannot be formed, since the methyl groups of PPO constitute a steric hindrance. The strain of the water structure leads to a smaller hydrogen bond energy than in the case of PEO. That is the reason why PPO is partially soluble in water for only oligomers. The smaller hydrogen bond energy due to the strain of water lattice also leads to a lower precipitation temperature.<sup>40,63</sup> This suggestion is in accord with the fact that some copolymers of PEO and PPO are water-soluble but have a lower precipitation temperature than PEO.<sup>66</sup> As the proportion of PPO increases, this temperature decreases.<sup>31</sup> When the methyl groups along the chain become more numerous, it would be expected that the strain in the water structure would increase, making the heat of mixing less negative and lowering the precipitation temperature.

In the case of polymethylene oxide (PMO), the distance between neighbouring oxygens seems too short to be accommodated in a water structure.<sup>40</sup> It is in fact rather striking that PMO is not water-soluble, although it has a higher oxygen/carbon ratio than PEO and does not have any side groups to cause steric hindrance. Thus, the distance between neighbouring oxygens in the polyether and steric hindrance are both important factors for the solubility of polyethers in water.

Polyacetaldehyde has practically the same oxygen–oxygen distance as PMO (see Table 3 for its structure). In an amorphous form it is freely soluble in many organic solvents but is insoluble in water.<sup>66,67</sup> It also has too short a distance between neighbouring oxygens to be accommodated in the water structure and has a side group which affords steric hindrance.

Table 4. Thermodynamic parameters for polymer–water interactions

Water-soluble polymer	$\chi^{\dagger}$ (Temp. °C, [ref.])	$A_2 \times 10^4$ (cm <sup>3</sup> mol/g <sup>2</sup> ) (Temp. °C, $MW \times 10^{-4}$ , [ref.])	$\sigma$ (Temp. °C, [ref.])
PEO	0.45 (27, [74]) 0.44 (23, [75]) 0.41–0.42 (–, [76])	30.4–116 (25, 1.09–80, [74]) 62 (25, 1.01 [74]) 30.5–36.4 (25, 0.37–0.89, [70])	1.38 ± 0.06 (20, [74]) 1.95 (–, [72])
PAA	–	–	–
PMAA	1.36 (40, [77])	–	–
PAAm	0.49 (30, [78]) 0.47 (30, [79])	1.8 (25, 140, [74]) 0.64 (25, 470, [74]) 4.9–5.4 (25, 110–200, [74])	2.36 (30, [72]) 2.72 ± 0.10 (30, [74]) 2.36 (30, [74])
PMAAm	–	0.29 (25, 32, [74])	–
PVA	0.49–0.50 (–, [80]) 0.49 (30, [81])	3.9–5.2 (30, 18–19.6, [75]) 0.82–4.5 (–, –, [72])	1.87 (–, [72]) 2.04 ± 0.1 (30, [74])
PVP	0.58 (25, [82]) 0.49 (30, [83])	3.4 (25, 2.45–3.79, [74]) 2.5–64.7 (25, 1.95–93.3, [74])	2.55 (–, [72])

<sup>†</sup> Values for sufficiently dilute solutions.



### 2.6.2. Comparison of Thermodynamic Parameters with Other Water-Soluble Polymers

Common synthetic polymers that are soluble in water at normal temperatures are as follows (Fig. 2):

polyethylene oxide (PEO), polyacrylic acid (PAA), polymethacrylic acid (PMAA), polyacrylamide (PAAm), polymethacrylamide (PMAAm), polyvinyl alcohol (PVA), and polyvinylpyrrolidone (PVP).

Table 4 summarizes some thermodynamic parameters involved in polymer–water interactions. Of these,  $\chi$ , called the polymer–solvent or Flory–Huggins interaction parameter, is a measure of the interaction between a given solvent and a given polymer. It is a free-energy parameter and a temperature-dependent quantity. By Flory–Huggins theory,<sup>36,68</sup> the free-energy change of mixing of liquid and polymer to form a

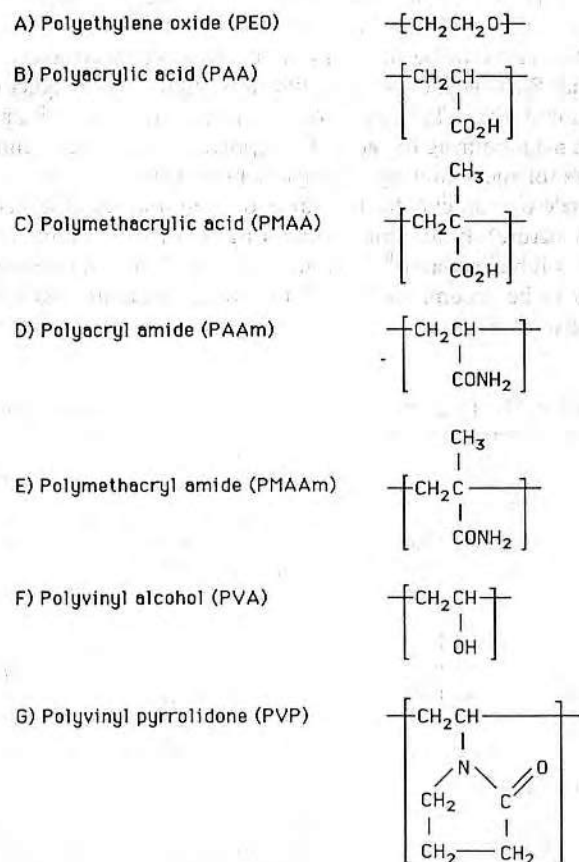


Fig. 2. Structures of common water-soluble synthetic polymers.

solution ( $\Delta G_M$ ) is defined as shown below. This assumes that the polymer is completely amorphous and sufficiently large and that  $\Delta G_M$  originates in the replacement of some of the contacts between like species in the pure liquids with contacts between unlike species in the solution:

$$\Delta G_M = \Delta H_M - T\Delta S_M \quad (1)$$

$$\Delta H_M = RT\chi n_1 v_2 \quad (2)$$

$$\Delta S_M = -R(n_1 \ln v_1 + n_2 \ln v_2) \quad (3)$$

and thus,

$$\Delta G_M = RT(n_1 \ln v_1 + n_2 \ln v_2 + RT\chi n_1 v_2) \quad (4)$$

where  $\Delta H_M$  is the heat of mixing,  $\Delta S_M$  is the configurational entropy of mixing,  $R$  is the universal gas constant,  $T$  is the temperature,  $n_1, n_2$  are the moles of solvent and polymer, respectively, and  $v_1, v_2$  are the volume fractions of solvent and polymer, respectively.

The polymer–solvent interaction parameter  $\chi$  characterizes the interaction energy per mole of solvent divided by  $RT$  for a specific solvent–polymer system. Since  $v_1$  and  $v_2$  are the volume fractions, the two logarithmic terms on the right-hand side of eq. (4) are always negative. This allows the value of  $\chi$  to be positive (up to 0.5, in fact) while still allowing for complete miscibility ( $\Delta G_M$  is still negative). Considering the effect of molecular weight, for a given mass of polymer and of solvent, the term  $n_2 \ln v_2$  will become less negative with increasing molecular weight, finally becoming zero in the limit of infinite molecular weight. Thus a higher molecular weight for the polymer makes for a less favourable free-energy contribution for the mixing process, leading to the well-recognized inverse relation between the solubility of a polymer and its molecular weight. From eq. (2), a positive value of  $\chi$  corresponds to a positive value for the contribution  $\Delta H_M$ , which thus disfavors mixing, while the converse is also true. In the great majority of cases, experimental values for  $\chi$  are positive. Values of  $\chi$  up to 0.5 are found for systems showing complete miscibility, while for  $\chi > 0.5$  the systems are characterized by only limited miscibility, with higher values of  $\chi$  corresponding to decreasing extent of interaction of the two components. There are various methods for the determination of  $\chi$ ,<sup>69</sup> such as equilibrium swelling, osmometry, vapour pressure measurement, sedimentation, viscosity measurement, optical studies and inverse gas chromatography.

In Table 4,  $A_2$  is the second virial coefficient, which is a direct characteristic of intermolecular interactions between a solvent and a polymer, or between polymers in a solvent.  $A_2$  can be determined by different methods,<sup>77</sup> such as osmometry, ebulliometry (based on the difference between the boiling temperature of a solution and the boiling temperature of the pure solvent), cryoscopy (based on the difference between the freezing temperature of a solution and the freezing temperature of the pure solvent) and light-scattering. These are expressed as follows:

osmometry

$$\pi/C = RT/M_n + A_2C + A_3C^2 + \dots \quad (5)$$

$$A_2 = (\rho_s/\rho_p^2 M_s)(1/2 - \chi) \quad (6)$$

ebulliometry

$$\Delta T_b/C = K_e/M_n + A_2C + A_3C^2 + \dots \quad (7)$$

$$A_2 = (RT^2/\rho_p^2\Delta H_s)(1/2 - \chi) \quad (8)$$

cryoscopy

$$\Delta T_m/C = K_c/M_n + A_2C + A_3C^2 + \dots \quad (9)$$

$$A_2 = (RT^2/\rho_p^2\Delta H_s)(1/2 - \chi) \quad (10)$$

light-scattering

$$KC/R_\theta = 1/M_w P_\theta + 2A_2C + \dots \quad (11)$$

$$A_2 = (\rho_s/\rho_p^2 M_s)(1/2 - \chi) \quad (12)$$

where  $\pi$  is the osmotic pressure,  $C$  is the solution concentration,  $M_n$  is the number-average molecular weight,  $A_2$  and  $A_3$  are the second and third virial coefficients, respectively,  $\rho_s$  is the density of the solvent,  $\rho_p$  is the density of the polymer,  $M_s$  is the molecular weight of the solvent,  $\Delta T_b$  is the boiling point elevation,  $K_e$  is the ebullioscopic constant,  $\Delta H_s$  is the heat of solvent evaporation in ebulliometry or fusion in cryoscopy,  $\Delta T_m$  is the depression of the melting point,  $K_c$  is the cryoscopic constant,  $K$  is a constant,  $R_\theta$  is the Rayleigh ratio,  $M_w$  is the weight-average molecular weight and  $P_\theta$  is the scattering factor.

In all cases  $A_2$  is expressed as a function of  $(1/2 - \chi)$ . The units of  $A_2$  depend on the way in which it is expressed. The sign of  $A_2$  is important. A positive second virial coefficient indicates association between polymer and solvent molecules or repulsive interactions between polymer molecules in a solvent such as excluded-volume effects or repulsive electrostatic effects.<sup>70</sup> A negative second virial coefficient indicates attractive two-polymer molecular interactions, such as hydrophobic or attractive electrostatic effects. Negative  $A_2$  is common for highly charged macromolecules such as proteins, which associate quite easily. On the other hand,  $A_2$  for non-ionic polymers should always be positive, due to excluded-volume considerations (excluded volume is generally defined as the effective volume of a solution that, strictly for steric reasons, is not available to molecules or particles as the result of the introduction of another molecule or particle<sup>71</sup>). For polymer-solvent interactions, a general rule for positive values of  $A_2$  is that

- (1) for good solvents,  $A_2$  is high,
- (2) for poor solvents,  $A_2$  is low,
- (3) at  $A_2 = 0$ , the polymer behaves thermodynamically ideally (i.e., no polymer-solvent interaction).

$A_2$  is dependent on the temperature and the molecular weight of the polymer.

In Table 4,  $\sigma$  is the steric factor or stiffness parameter characterizing the flexibility of a polymer chain in a solvent.<sup>72</sup> The flexibility of polymer chains depends primarily on the ease of rotation around the bonds of the main chain, which in turn is directly influenced by the nature of the side groups. The steric factor is defined as follows:<sup>73,74</sup>

$$\sigma = (\langle r^2 \rangle_0 / \langle r^2 \rangle_{of})^{1/2} \quad (13)$$

where  $\langle r^2 \rangle_0$  is an unperturbed mean-square end-to-end distance of a linear chain molecule in solution and can be determined by limiting viscosity number measurements, light-scattering and small-angle X-ray scattering,<sup>69</sup>  $\langle r^2 \rangle_{of}$  is a mean-square end-to-end distance of a freely rotating chain. The freely rotating state is a hypothetical state of the chain in which the bond angle restrictions are retained, but the steric hindrances to internal rotation are released. The value of  $\langle r^2 \rangle_{of}$  can be readily calculated from the given basic structure of the chain. For instance, if the chain consists of only one kind of bond of length,  $l$ , we obtain

$$\langle r^2 \rangle_{of} = nl^2[(1 + \cos \theta)/(1 - \cos \theta)] \quad (14)$$

where  $n$  is the number of bonds and  $\theta$  is a supplement of the valence bond angle (for more discussion, see ref. 73). Since in a real polymer chain some hindrance to free rotation is invariably present, the steric factor is always greater than 1, the more so, the lower the ease of rotation about the bonds of the main chain, i.e., the lower the chain flexibility.

As seen in Table 4, PEO shows lowest values of  $\chi$  among the water-soluble synthetic polymers, which means complete miscibility of PEO with water ( $\chi < 0.5$ ). The anomalous behaviour of PEO in water is explained as a result of strong interaction via hydrogen bonds of water molecules with the ether oxygens of the polymer chains.<sup>61-63</sup> PEO shows much higher values of  $A_2$  than other water-soluble polymers, which means that PEO is highly interactive with water (water is a better solvent for PEO than for other water-soluble polymers) and PEO chains are highly repulsive towards each other in water. Flory<sup>68</sup> suggested, by his 'dilute solution' treatment, that  $A_2$  can be regarded as expressing the volumes mutually excluded by neighbouring polymer molecules (i.e., excluded volumes). Thus, PEO in water will have a larger excluded volume than other water-soluble polymers. The  $\sigma$  values of PEO are also lower than other water-soluble polymers, which is considered as verification of the flexibility of the PEO chains. Higher  $\sigma$  values of PAAm or PVP may be due to bigger side groups which restrict chain flexibility.

Molecular motions on a timescale in the range between pico- ( $10^{-12}$ ) and micro- ( $10^{-6}$ ) seconds can be investigated by NMR. The dynamic behaviour of polymers in aqueous solution generally shows motional components in this range, which is characterized by correlation times (or reorientation times). Nuclear magnetic relaxation is driven by the modulations of local nuclear interactions, e.g.,  $^1\text{H}$ - $^{13}\text{C}$  dipolar coupling and C-D quadrupolar coupling. The chain segment mobility, responsible for the modulation of the coupling, depends on the flexibility of the polymer chain. The correlation time ( $\tau_c$ ) is regarded as the average time that the molecule requires to rotate through an angle of 1 rad.<sup>84,85</sup> In the solid state, where motion is hindered,  $\tau_c$  is very large. The local dynamics of polymers in aqueous solutions depend on the concentration and molecular weight of the polymer. The concentration dependence is caused by polymer-polymer interactions, whereas in the concentration-independent range the polymer dynamics is mainly determined intramolecularly and by solvent-polymer interactions. Molecular weight dependence is caused by end group contributions.<sup>47</sup> Molecular weight dependence of the relaxation is not observed, in the case of PEO, when the chain length is greater than about 100.<sup>47,54</sup>



In the pure liquid at room temperature, water molecules tumble about with a mean  $\tau_c$  of about  $2.5-10 \times 10^{-12}$  s ( $2.5-10$  ps).<sup>86,87</sup> The data available on  $\tau_c$  for polymers in aqueous solution are scarce and different conditions have been used. Breen *et al.*<sup>47</sup> determined  $\tau_c$  for PEO in  $D_2O$  solution at  $25^\circ\text{C}$ . They used dilute solutions of PEO to avoid polymer-polymer interactions. They found that  $\tau_c$  values for PEO are in the range  $15-100$  ps depending on the conditions used and are 30 times smaller than found for PMMA,<sup>48</sup> illustrating the high flexibility of the PEO chain. Lang *et al.*<sup>49</sup> compared  $\tau_c$  of PEO in dilute solutions, determined by NMR and electron spin resonance. They obtained similar values of  $\tau_c$  for PEO in various solvents to those of Breen *et al.*<sup>47</sup> and suggested that both methods indicate the highly flexible nature of this polymer.

### 3. POSSIBLE MECHANISMS FOR PROTEIN RESISTANCE OF PEO SURFACES

There are many possible factors involved in the protein-resistant character of PEO surfaces in aqueous solution. This section will discuss which mechanisms are involved and how the unique solution properties of PEO in water are related to PEO's passivity.

#### 3.1. Interfacial Free Energy

One possible explanation of PEO's passivity may involve its minimum interfacial free energy with water.<sup>88-90</sup> The basic concept of the minimal interfacial free-energy hypothesis is that as the interfacial free energy approaches zero, the driving force for protein adsorption decreases. Thus, non-specific protein adsorption should not occur and proteins at or near a low interfacial energy interface will not feel any greater effects from the surface than they do from the bulk solution.

Interfacial free energies ( $\gamma_{sw}$ ) of various materials have been calculated based on contact angle measurements.<sup>89-91</sup> Although those calculations involved several assumptions, the PEO-water interface showed very low interfacial free energies, and thus low driving forces for protein adsorption. However, other non-ionic water-soluble polymers also have very low interfacial free energies. Although their protein adsorption tendencies are small, these materials appear to be more interactive than PEO surfaces. This means that other factors are involved in PEO's passivity.

#### 3.2. Steric Stabilization Effect

It is well known by colloid scientists that spontaneous aggregation of colloid particles may be prevented by coating with non-ionic polymers. When two surfaces with adsorbed polymer layers approach each other at distances of separation of less than twice the thickness of the adsorbed layer, interaction of the two layers takes place. The degree of stabilization can be defined quantitatively in terms of the energy change occurring on the interaction of the adsorbed layers. The Gibbs free energy change,  $\Delta G$ , of the overlap interaction of the adsorbed layers is expressed as

$$\Delta G = \Delta H - T\Delta S \quad (15)$$

where  $\Delta H$  and  $\Delta S$  are enthalpy and entropy change, respectively. If  $\Delta G$  is positive on the overlap of the adsorbed layers, a repulsive force,  $\Delta F_R$ , between the surfaces is generated ( $\Delta F_R = \partial\Delta G/\partial x > 0$ , where  $x$  is the separation distance between the surfaces), and stabilization will result. If  $\Delta G$  is negative, an attractive force,  $\Delta F_A$  ( $\Delta F_A < 0$ ), is generated, and flocculation or coagulation will result. Under isothermal conditions, the stability is then a function of the enthalpy change ( $\Delta H$ ) and the entropy change ( $\Delta S$ ).

Many theories for explaining steric stabilization have been proposed, and many theoretical equations for calculating the energy change with the overlap of the adsorption layer have been devised.<sup>92-106</sup> Steric stabilization may be classified roughly into two major categories. The first is a volume restriction effect<sup>98,99,101</sup> (also called entropic stabilization,<sup>94</sup> elastic term,<sup>103</sup> or configurational entropy loss<sup>102</sup>), associated with the reduction in the total number of conformations available to the adsorbed polymer on the approach of a second surface. The second category is an excluded-volume effect<sup>92,102,107-110</sup> (also called osmotic pressure repulsion<sup>94,98,99</sup> or heat-mixing repulsion<sup>103</sup>), associated with changes in the mixing of polymer segments-solvent molecules as the second surface approaches.

In the volume restriction or entropic stabilization theory, it is assumed that a second surface approaching the adsorbed layer is impenetrable. Thus, the adsorbed layer is compressed and the polymer segments contained in the interaction region lose configurational entropy. This causes the polymer segments to occupy fewer possible configurations in the compressed state than in the uncompressed state. This reduction in entropy increases  $\Delta G$ , producing the net effect of repulsion between the surfaces. In this theory, the enthalpic interaction between the adsorbed layers is neglected so that  $\Delta G = -T\Delta S$ .

In contrast, the excluded-volume or osmotic pressure repulsion theory assumes that the adsorbed layers of two surfaces can overlap each other when they approach. In this model, the polymer segments are in contact, and this contact is reduced as a result of the contact between the segments in the overlapped region which results in the enthalpy of mixing,  $\Delta H_M$ . As a result of the increase in the segment concentration in the overlap region, there is also a reduction in the configurational entropy of the adsorbed molecules,  $\Delta S_M$ . Thus, the total free energy change,  $\Delta G_M$ , due to overlap of the adsorbed layers is expressed as both an enthalpic change and an entropic change:

$$\Delta G_M = \Delta H_M - T\Delta S_M \quad (16)$$

The excluded-volume theory has been developed in detail for the PEO case.<sup>92,107,108</sup>

Figure 3 shows schematically the interactions between two surfaces with adsorbed polymer layers. Three cases can be considered, depending on the separation distance between the two surfaces.<sup>105</sup>

(1)  $D > 2L$  (large surface separation): there is no change in available polymer conformations due to the interaction between the surfaces.

(2)  $L < D < 2L$  (interpenetration domain):<sup>111</sup> due to the local increase in polymer concentration, the number of available conformations decreases in the interpenetration region. Further, the free energy of each conformation may be altered since some



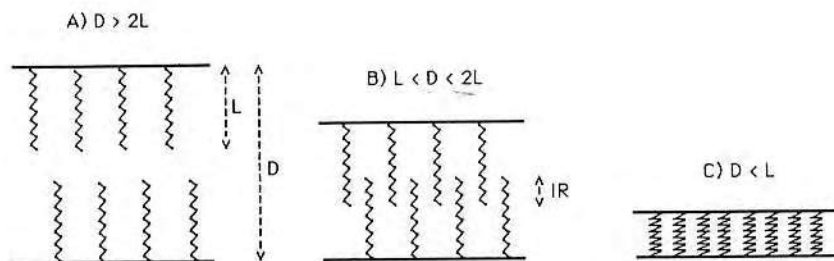


Fig. 3. Schematic diagram showing interactions between two surfaces with adsorbed polymer layers ( $L$ , thickness of adsorbed polymer layer;  $D$ , distance between two surfaces;  $IR$ , interpenetration region).

solvent-polymer interactions may be replaced with polymer-polymer interactions. The total free energy change may thus be positive or negative. The latter situation is expected to occur if the liquid phase is a poor solvent for surface-bound polymers.

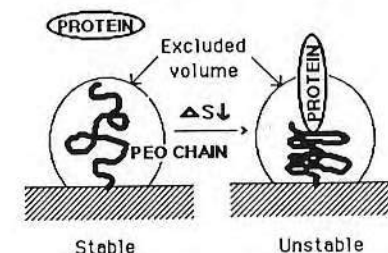
(3)  $D < L$  (interpenetration + compression domain).<sup>111</sup> two physical events may be present. First, the number of available conformations of polymer molecules decreases since the free space is reduced (volume restriction effect). This is expected to result in an increase in the total free energy proportional to the number of polymer chains. Second, the number of allowed conformations decreases further due to the local increase of polymer molecules, as described above in (2) (excluded-volume or osmotic pressure effect). The concentration change experienced by a given polymer molecule is proportional to the polymer surface concentration on the neighbouring surface; hence the total free energy change is expected to be proportional to the square of the segment density.

Now a question may arise. Steric stabilization is a general repulsion phenomenon for neutral, hydrophilic polymers in water. Thus, any water-soluble non-ionic polymers attached on a surface will have steric stabilization and protein-resistant effects. Why then is PEO particularly effective as a steric stabilizer and thus as a protein repeller in an aqueous system? To answer this, we should consider the solution properties of PEO in water, which are unique among polymers.

### 3.3. Relationship with Solution Properties

As discussed in Section 2, only PEO shows complete water solubility among the related polyethers, probably because PEO segments nicely fit in the water structure without any distortion of water lattices and minimize the tendency for hydrophobic interactions. The hydrophilicity and unique solubility properties of PEO produce surfaces that are in a liquid-like state with the polymer chains exhibiting considerable flexibility or mobility.<sup>13,40,112</sup> PEO is the most flexible in water among common non-ionic water-soluble polymers because it does not have bulky side groups in its structure and thus will not be hindered sterically in water (compare structures in Fig. 2 and steric factors in Table 4). It appears that the PEO molecule has a large excluded volume in

#### A) Steric Stabilization Effect



#### B) Chain Mobility

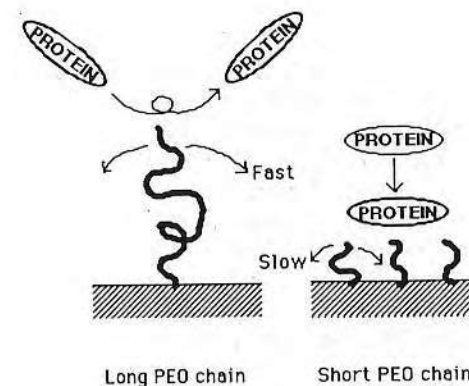


Fig. 4. Basic mechanisms involved in protein resistance of PEO surfaces (from ref. 113).

water, as evidenced by the high values of second virial coefficient (or low values of polymer-solvent interaction parameter, Table 4).

PEO surfaces in water with rapidly moving hydrated PEO chains and a large excluded volume tend to repel protein molecules which approach the surface.<sup>92,107,108,113</sup> Figure 4 schematically represents the interactions between proteins and PEO chains attached on a surface. Figure 4A indicates the steric stabilization (volume restriction or excluded volume) effect. The repulsive forces by the adsorbed PEO chain are generated by the loss of possible chain conformations, as the volume available to the adsorbed chains is reduced between approaching surfaces. As discussed in Section 2, PEO shows a large excluded volume in water and thus is very effective for steric repulsion. Figure 4B indicates the effect of the surface mobility of the PEO chains. For an irreversible adhesion, proteins should be in contact with a foreign surface more than a certain measure of time. PEO shows high mobility and hydration in water, as already discussed. Rapidly moving hydrated PEO chains on a

surface will effectively prevent stagnation of the proteins on the surface, probably because the contact time is shortened.<sup>113</sup> The mobility of the hydrated PEO chains increases with their chain length up to about 100,<sup>47,54,113</sup> hence the long PEO chains are supposed to suppress the adsorption of proteins more effectively than shorter chains.

#### 4. APPROACHES TO PREPARE PEO SURFACES AND THEIR BLOOD COMPATIBILITY

##### 4.1. Bulk Modification

Bulk polymers containing PEO have been prepared by block copolymerization (physical or reversible PEO networks) and crosslinking (covalent PEO networks).

Many studies of PEO-containing block copolymers have been reported.<sup>112,114-127</sup> The networks containing PEO can be created by evaporation of a solvent or by cooling from the molten state. Lyman<sup>114</sup> prepared PEO-polyethylene terephthalate (PET) block copolymers for application as dialysis membranes. He extended his work to include segmented polyurethanes (PU).<sup>128</sup> Merrill and Salzman<sup>112</sup> studied PEO-polybutylene terephthalate (PBT) block copolymers in a bead column and reported very low platelet retention. Furasawa *et al.*<sup>115</sup> and Grainger *et al.*<sup>116-118</sup> studied PEO and polystyrene (PS) block copolymers and reported minimal levels of *in vitro* plasma protein adsorption. Vulic *et al.*<sup>119-121</sup> prepared PS-PEO-heparin block copolymers to improve the blood compatibility. Grainger *et al.*<sup>122-124</sup> also prepared polydimethyl siloxane (PDMS)-PEO-heparin block copolymers and correlated platelet adhesion and extent of platelet release to assess the efficacy of these block copolymers as blood-compatible materials or coatings.

The segmented PU has been the most commonly studied of PEO-based materials.<sup>128,129-148</sup> Brash and coworkers<sup>129,130,136,137,147</sup> carried out plasma protein adsorption on segmented PU containing polyethers as the soft segment and showed that the segmented PU containing PEO as the polyether is significantly less adsorptive than those using PPO. Goodman *et al.*<sup>137,138</sup> showed that platelet spreading and activation on PU containing PEO as the soft segment are minimal in comparison with PU based on other macroglycols. Da Costa *et al.*<sup>131,132</sup> and Merrill *et al.*<sup>133-135</sup> studied the effect of the soft segment component on platelet adhesion. *In vitro* tests revealed that PEO-containing PU adsorbs lower levels of thrombin and far fewer platelets than those composed of PPO or polytetramethylene oxide (PTMO). Platelet retention was further reduced as the molecular weight of PEO increased. However, these *in vitro* studies may not correlate directly with *in vivo* experiments. Grasel and Cooper,<sup>136</sup> Lelah *et al.*,<sup>139</sup> Takahara *et al.*,<sup>140</sup> Okkema *et al.*<sup>141</sup> and Silver *et al.*<sup>142-144</sup> reported some controversial results from their *ex vivo* shunt experiments.

PEO-containing block copolymers and PU are promising biomaterials, but may have limited blood compatibility since significant levels of the hard non-PEO phase, which is usually highly thrombogenic, can appear on the surface.<sup>149,150</sup> Also, PEO does not exist as pendant chains and is attached by both ends to the copolymer segments. Thus, chain mobility is restricted.

Several studies of PEO networks or hydrogels have been reported.<sup>112,149-161</sup> In these systems, one component of a polymer network usually consists of large PEO chains end-linked by small junctional units to provide enhanced PEO chain mobility and thereby improved PEO surface coverage. A covalent homonetwork of PEO was created by irradiating a concentrated solution of PEO in water to ionizing radiation.<sup>112</sup> Radiolysis of water forms hydroxyl and hydrogen radicals. These species attack the PEO chains and thus a PEO hydrogel is produced. Covalent homonetworks of PEO<sup>152,153,161</sup> and networks of PEO-alginate<sup>154</sup> and PEO-polyepoxy siloxane<sup>149,155</sup> were prepared for biomedical applications. Chaikof *et al.*<sup>149</sup> prepared interpenetrating polymer networks (IPN) of long PEO chain and PDMS containing variations of PEO content and molecular weight. They reported a low level of platelet adhesion on those surfaces. Chaikof *et al.*<sup>160</sup> also observed the opposite result with the similar IPN of short PEO chain (*MW* 2000): enhanced deposition of platelets and fibrinogen. Verdon *et al.*<sup>150</sup> prepared PEO-PDMS hydrogels similar to those of Chaikof *et al.* and observed a low level of platelet deposition even on the gel with short PEO chain (*MW* 2000) and progressively lower levels of platelet deposition with increasing PEO content. PEO-containing networks of crosslinked epoxy resins,<sup>156</sup> polyacrylamide<sup>157,158</sup> and polyacrylic acid<sup>159</sup> have also been reported.

Recently, photocrosslinkable hydrogels based on PEO have been reported.<sup>151,162-167</sup> Nathan *et al.*<sup>162,163</sup> and Vyavahare and Kohn<sup>164</sup> developed polyether urethanes based on the copolymerization of PEO and lysine [poly(PEO-Lys)]. The wide range of functional groups made it possible to attach antibiotic drugs and anticancer agents to the polymer backbones using both degradable and non-degradable linkages. The poly(PEO-Lys) derivatives containing acrylate or methacrylate pendant chains could be crosslinked by exposure to UV irradiation. They reported that the resulting hydrogels are transparent, highly swollen membranes with significant mechanical strengths. Sawhney *et al.*<sup>165,166</sup> prepared photopolymerizable and biodegradable block copolymers consisting of PEO and polylactic acid or polyglycolic acid with terminal acrylate groups. These block copolymers, photopolymerized *in vivo* in direct contact with the tissues by exposure to UV light, appeared to form an adherent hydrogel barrier that is highly effective in reducing postoperative adhesions. Pathak *et al.*<sup>167</sup> also prepared hydrogels via rapid photopolymerization of PEO-based macromers (PEO diacrylates and multiacrylates of various molecular weights) in direct contact with cells and tissue.

Nagaoka and coworkers<sup>9,113,168,169</sup> prepared hydrogels containing methoxy PEO monomethacrylates with pendant PEO chains of various chain lengths and investigated their interactions with blood components. They found that plasma protein adsorption and platelet adhesion onto these hydrogels decreased significantly with increases in PEO chain length, up to around 100.

Other bulk modifications to prepare PEO surfaces include PEO-PPO blends. Bots *et al.*<sup>170-174</sup> prepared crosslinked blends of PEO and PPO using UV irradiation for use as small-diameter vascular prostheses. They reported that these crosslinked blends show good blood compatibility due to an enrichment of PEO on the surface and good mechanical properties comparable to natural blood vessels.

Bulk modification to produce PEO surfaces offers an advantage over PEO coatings

or surface treatments for some applications, in that they are composed of PEO throughout the bulk and surface of the material. These materials retain their biocompatibility even when subjected to surface abrasion or erosion.<sup>151</sup> However, the mechanical properties of PEO networks or hydrogels are sometimes not strong enough for biomedical applications.<sup>175</sup> Immobilization of PEO or its derivatives on to the surface of a polymeric substrate with high mechanical strength has been attempted to generate a PEO surface, mainly by physical adsorption, covalent grafting, and graft copolymerization.

#### 4.2. Physical Adsorption

PEO surfaces have been prepared by physical adsorption of PEO onto existing substrates.<sup>176–182</sup> Only high-molecular-weight PEO ( $MW > 100,000$ ) can be effectively adsorbed on hydrophobic surfaces. The adsorbed high-molecular-weight PEO may be expected to have loops and free ends projecting into the aqueous phase, consistent with most models of polymer adsorption at interfaces. Chromatographic supports and membranes used for the separation of proteins, cells and viruses have been treated by physical adsorption of high-molecular-weight PEO. Physically adsorbed PEO homopolymers, however, could be displaced by other macromolecules which have higher affinity for the surface. Many proteins and cells in the blood can easily displace physically adsorbed PEO from the surface.

We prepared PEO surfaces by physical adsorption of various PEO-containing amphiphilic copolymers onto hydrophobic low-density polyethylene (LDPE) films (Fig. 5).<sup>183–188</sup> Adsorption of PEO-containing block copolymers would be more stable than that of PEO homopolymers, as the hydrophobic segments provide hydrophobic adsorption forces or anchor points to common hydrophobic medical materials, while the hydrophilic PEO chains can be extended into the bulk aqueous solution to provide a PEO surface with relatively free mobility.<sup>189–196</sup> This approach may provide a simple and effective means for producing PEO surfaces as protein-resistant surfaces if the copolymers can be adsorbed strongly on to the surfaces. In a study on adsorption of commercially available PEO-PPO or PEO-polybutylene oxide (PBO) block copolymers with different structures at the hydrophobic solid–water interface (Fig. 5A–C), we observed that adsorbed amount of the copolymer increases with increasing concentration and decreasing PEO chain length. The stability of adsorbed copolymer molecules on hydrophobic surfaces was highly dependent on the structure (tri-, star-like, or alternate block) of the copolymers and on the nature of the hydrophobic segment (PPO or PBO). Albumin resistance was highly dependent on the adsorbed amount of the copolymers and on the PEO chain mobility. From this study, however, we observed that PPO or PBO are not strongly hydrophobic due to the presence of their ether oxygens. Also PPO or PBO blocks should have limited chain length ( $n < 30$ ) to prevent self-aggregation in aqueous solution, resulting in weak bonding of the copolymer molecules on the surface. To overcome these limitations, we synthesized copolymers of alkyl methacrylates with methoxy PEO methacrylates. The long hydrophobic polymethyl methacrylate (PMMA) backbone and alkyl side chains of

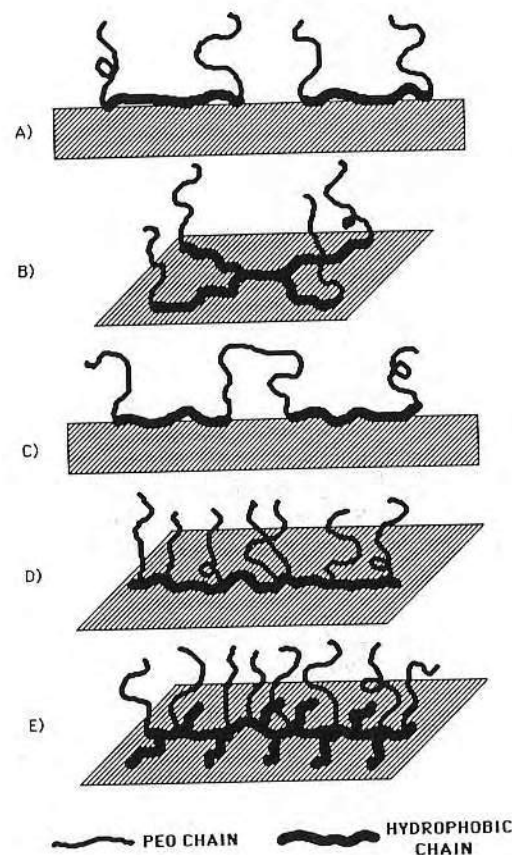


Fig. 5. Types of PEO-containing amphiphilic copolymers and expected conformation of the copolymers at the water–hydrophobic solid interface: (A) PEO–PPO–PEO or PEO–PBO–PEO triblock copolymers; (B) star-like copolymers with 4 PPO and 4 PEO blocks; (C) alternate PEO–PPO block copolymers; (D) methacrylate copolymers with PMMA backbone and PEO side chains; (E) methacrylate copolymers with PMMA backbone, alkyl and PEO side chains (from refs 183 and 184).

these copolymers provided stable adsorption on a hydrophobic surface (Fig. 5D and E). The PEO surfaces prepared by the adsorption of the synthesized PEO-grafted copolymers ( $MW$  of PEO 1900 and 4000) showed efficient protein (albumin and plasma)-resistant character.

Several research groups<sup>117,192,197–217</sup> have also prepared PEO surfaces using PEO-containing amphiphilic block copolymers. Lee *et al.*<sup>197</sup> and Kayes and Rawlins<sup>192</sup> prepared stable PEO surfaces on polystyrene (PS) latex particles or beads using PEO–PPO triblock copolymers with longer hydrophobic PPO segments and showed



minimized protein adsorption. Tan *et al.*<sup>198,199</sup> also modified PS latex nanoparticles by PEO-PPO block copolymers and showed minimized interactions with blood components and prolonged blood circulation in rats. Illum and coworkers<sup>200–203</sup> reported the influence of PEO-PPO block copolymers as surface modifiers on macrophage uptake and organ distribution of PS particles. Broomhaar *et al.*<sup>204</sup> showed that the avoidance of macrophage uptake can be achieved by the adsorption of PEO-PPO block copolymers onto PS microspheres. Bridgett *et al.*<sup>205</sup> and Humphries *et al.*<sup>206,207</sup> reported reduced bacterial adhesion to PS surfaces coated with PEO-PPO block copolymers. Owens *et al.*<sup>208</sup> coated octadecyldimethylsilane-treated glass beads with a PEO-PPO-PEO triblock copolymer with longer PEO chains and observed inhibited cell adhesion. Amiji *et al.*<sup>209,210</sup> used different PEO-PPO-PEO triblock copolymers with varying chain lengths of PEO and PPO and showed that the copolymers containing a minimum of 56 PO residues and 19 EO residues are sufficient to repel proteins and platelets. Gingell *et al.*<sup>211,212</sup> prepared PEO surfaces on octadecyldimethylsilane-treated glass beads using PEO-PBO triblock copolymers with long PEO and PBO blocks and showed that these block copolymers can totally inhibit platelet adhesion and spreading. Grainger *et al.*<sup>117</sup> prepared PEO surfaces on glass beads using PEO-PS block copolymers. Maechling-Strasser *et al.*<sup>213</sup> prepared glass and silica beads adsorbed with poly(*N*-acetyleneimine)-PEO-poly(*N*-acetyleneimine) block copolymer to obtain steric exclusion chromatography supports which are non-adsorbent for proteins.

Another method of preparing PEO surfaces involves Langmuir-Blodgett (LB) deposition of PEO block copolymers such as a PEO-poly( $\gamma$ -benzyl-L-glutamate) copolymer.<sup>218</sup> It was reported that a LB film consisting of PEO-poly( $\gamma$ -benzyl-L-glutamate) copolymers results in high-quality monomolecular assemblies displaying high degrees of structural order. Platelet adhesion onto the LB film and solvent-cast film were compared.

The adsorption of PEO-containing amphiphilic copolymers onto hydrophobic surfaces provides the simplest method of preparing PEO surfaces for the prevention of protein adsorption and platelet adhesion. This method has numerous biomedical application areas, including chromatographic supports, contact lenses, catheters and more complicated medical devices, due to its simplicity and non-specificity. A main disadvantage with this approach, however, is that the immobilized polymers do not permanently remain on the surface.

#### 4.3. Covalent Grafting

Covalent grafting of PEO or PEO derivatives to substrates is the most effective way of creating a permanent PEO surface. Several techniques have been used to attach PEO covalently to surfaces. These include direct coupling techniques which lead to surfaces containing pendant PEO chains.<sup>219–245</sup> The direct coupling methods employ PEO molecules which have first been derivatized using a reactive coupling agent. The activated PEO then reacts with a functional group on the surface. Akizawa *et al.*<sup>219</sup> and Kishida *et al.*<sup>220</sup> coupled methoxy PEO with a terminal carboxyl group to form an

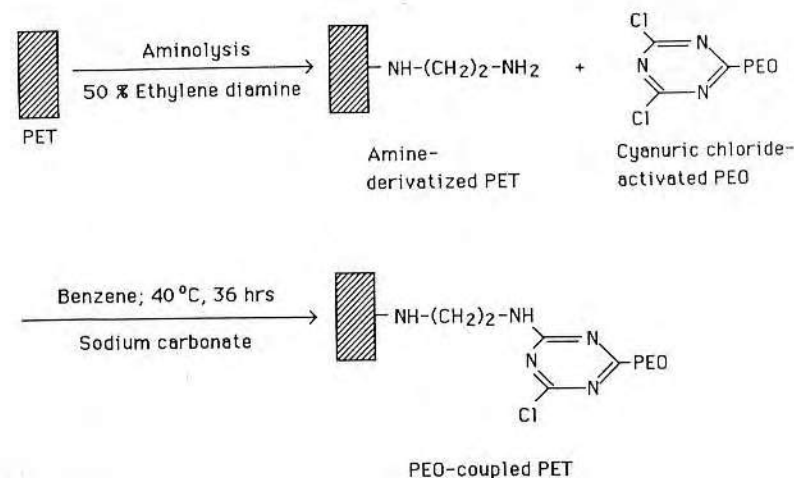


Fig. 6. Covalent grafting reaction of cyanuric chloride-activated PEO to an amine-derivatized PET film surface (from ref. 221).

ester linkage with the hydroxyl groups of cellulose dialysis membranes. They observed improved dialysis efficiency and blood compatibility with PEO grafting. Desai and Hubbell<sup>221,222</sup> grafted cyanuric chloride-activated PEO to amine-derivatized PET surfaces (Fig. 6). They observed about a 50% decrease in plasma protein adsorption and more than 90% decrease in platelet adhesion using PEO (*MW* 18,500 and 100,000)-grafted surfaces. Bergstrom *et al.*<sup>223,224</sup> covalently bound linear PEO and branched PEO with four arms to PS and showed that fibrinogen adsorption is significantly reduced by coating PS with either linear or branched PEO of *MW* 1500–20,000. Sefton and coworkers<sup>225–227</sup> immobilized PEO onto glutaraldehyde-crosslinked PVA hydrogel via either an aldehyde or an isocyanate group. They reported that the PEO-immobilized hydrogel reduces albumin adsorption and platelet adhesion on the surface. Kiss *et al.*<sup>228</sup> prepared densely packed PEO surfaces by grafting PEO onto PE and mica substrates. Monofunctional PEO-aldehyde was coupled by means of reductive amination to primary and secondary amino groups of polyethylene imine (PEI) adsorbed on oxidized PE and mica.<sup>229</sup> The adsorption of plasma proteins to these PEO surfaces was studied by means of ellipsometry and ESCA. Kim and coworkers<sup>230–240</sup> grafted PEO onto segmented PU surfaces via isocyanate groups and the PEO was further coupled with heparin.<sup>241</sup> Both ends of PEO were derivatized with diisocyanate functional groups by reacting toluene 2,4-diisocyanate (TDI) and PEO. The isocyanate-derivatized PEO molecules were then grafted onto a segmented PU surface through a reaction between the urethane urea and the terminal isocyanate groups of isocyanate-derivatized PEO. The other synthetic scheme to obtain PEO-grafted PU surfaces involves the coupling of hexamethylene diisocyanate (HMDI) to segmented PU. The free isocyanate groups

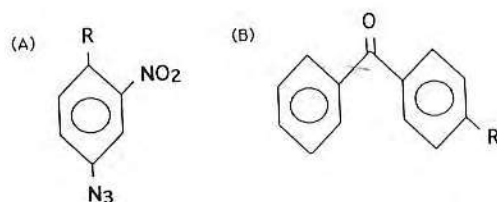


Fig. 7. Two basic types of photoreactive reagent: (A) aromatic azide; (B) substituted BP (R, attachment site for polymers to be coupled) (from ref. 246).

attached to PU were then coupled through a condensation reaction to terminal hydroxyl end groups on PEO molecules to obtain a PEO-grafted PU surface. The PEO-grafted PU was again coupled with HMDI to introduce reactive isocyanate groups. The PEO-grafted PU surfaces were finally coupled to heparin functional groups ( $-OH$  or  $-NH_2$ ). It was shown that the PEO-grafted surfaces have enhanced *in vitro*, *ex vivo* and *in vivo* blood compatibility. Han *et al.*<sup>242–245</sup> also grafted PEO onto PU surfaces via isocyanate groups and further sulfonated the terminal hydroxyl groups of the grafted PEO by propane sulfone. They obtained similar results to Kim and coworkers.

The chemical coupling method is possible only if the surface has chemically active functional groups which can react with PEO derivatives. This limits the application of this technique to certain biomaterials. In addition, the grafting procedures can be very complicated and are often time-consuming.

For inert surfaces without any functional groups, such as PE, polypropylene (PP) and polytetrafluoroethylene (PTFE), PEO grafting is possible only when the surface is premodified with reactive functional groups. However, grafting by use of UV or  $\gamma$  irradiation may not require premodification of the polymer surface.

For photochemical surface modification, two basic types of photoreactive reagents – aromatic azide and substituted benzophenone (BP) – have commonly been used (Fig. 7).<sup>246</sup> Upon UV irradiation, the aromatic azide undergoes an irreversible photolysis with generation of nitrogen gas and a highly reactive nitrene intermediate. This nitrene intermediate is capable of addition to carbon–carbon double bonds to form aziridine ring systems and of direct insertion into carbon–hydrogen bonds to form secondary amines. BP undergoes photochemical excitation with the initial formation of an excited singlet state, which can then undergo intersystem crossing to a triplet state. This highly reactive intermediate is then capable of insertion into carbon–hydrogen bonds by abstraction of a hydrogen atom from the polymer surface, followed by collapse of the resulting radical pair to form a new carbon–carbon bond.<sup>247</sup> Either reaction event results in a covalent coupling process that is relatively independent of the chemical composition of the surface. This permits the modification of a wide variety of medical device materials.

Allmer *et al.*<sup>248</sup> covalently coupled PEO chains to a glycidyl methacrylate (GMA)-bound PE surface. PE films were pregrafted with GMA by UV-irradiating the film in the presence of GMA. PEO chains were then attached to the GMA-grafted surface through reaction with

the epoxy groups. It was observed that the adsorption of transferrin onto this PEO-grafted surface was sufficiently reduced as compared with a pure PE surface. Tseng and Park<sup>249</sup> synthesized PEO–phenyl azide for photo-induced grafting to various polymeric substrates. They showed that platelet adhesion decreases by 95% on PEO-grafted dimethyldichlorosilane (DDS)-treated glass as compared with that on control DDS glass. Nakayama and Matsuda<sup>250</sup> grafted a cinnamated PEO onto a polycinnamate-coated PET film by exposure to UV light. They observed minimal cell adhesion on such a surface. Brinkman *et al.*<sup>251,252</sup> prepared a network of PEO immobilized on segmented PU substrates. The PU substrates were dipped in a solution of PEO in the presence of dicumyl peroxide (DCP). After drying, the PEO–DCP-coated substrates were UV<sup>251</sup> or heat-treated<sup>252</sup> to prepare PEO-immobilized surfaces. Platelet deposition with tubing in a capillary flow system was investigated, and it was found that on surfaces modified with high-molecular-weight PEO (180,000) such deposition is almost absent.

High-energy  $\gamma$  or electron beam irradiation has also been used to graft PEO to various substrates by generating free radicals on the surfaces.<sup>253–255</sup> Amiji and Park<sup>255</sup> grafted PEO–PPO–PEO block copolymers to DDS glass by  $\gamma$ -irradiation. They reported that effective grafting is achieved when the copolymer-adsorbed DDS glass is exposed to  $\gamma$ -irradiation in the presence of an aqueous buffer. Platelet adhesion decreased by 85% on the PEO block copolymer-grafted DDS glass as compared with that on control DDS glass. Gamma irradiation may be effective to graft PEO on polymer substrates; however, irradiation at high doses may alter the bulk properties of some polymers such as polypropylene (PP).

Plasma glow discharge techniques have also been used to graft PEO onto polymeric substrates.<sup>256–261</sup> Gombotz *et al.*<sup>256,257</sup> coupled *bis*-amino PEO to cyanuric chloride-activated PET films. Prior to PEO immobilization, amino groups were introduced on to the PET films by exposing them to an allylamine plasma glow discharge. The amino groups on the PET film were next activated with cyanuric chloride and then reacted with *bis*-amino PEO. It was found that the adsorption of albumin and fibrinogen decreases with increasing molecular weight of immobilized PEO. Wang and Hsiue<sup>258</sup> prepared PAA-grafted PE films by plasma glow discharge and then covalently immobilized *bis*-amino PEO onto the PAA-grafted surface by a chemical reaction using a coupling agent, 1-cyclohexyl-3-(2-morpholinoethyl) carbodiimide metho-*p*-toluenesulfonate (CMC). Sheu *et al.* introduced a method of grafting PEO-containing block copolymers, alkyl PEO block copolymers<sup>259,260</sup> and PEO–PPO–PEO triblock copolymers,<sup>261</sup> by exposing the adsorbed copolymers to plasma glow discharge (Fig. 8). A large reduction of fibrinogen adsorption on the PEO-grafted LDPE surfaces was observed for the high-PEO-content copolymers.

#### 4.4. Graft Copolymerization

Polymer surfaces modified by graft copolymerization carry several macromolecular chains which are covalently attached to the polymer substrates. Modifying the polymer surfaces by graft copolymerization of monomer is made possible by utilizing



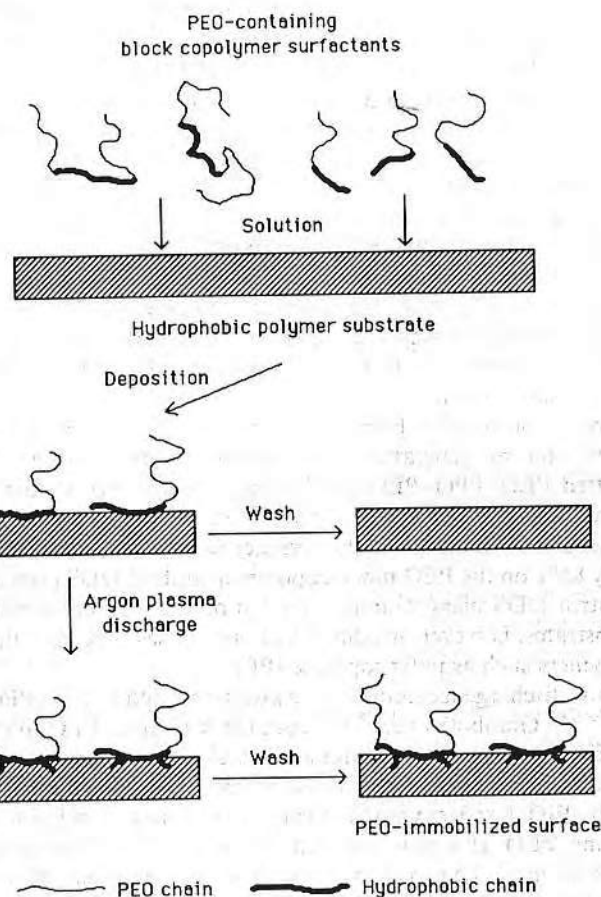


Fig. 8. Schematic diagram showing argon plasma discharge treatment for the immobilization of PEO-containing block copolymers (from ref. 261).

initiating species like free radicals or peroxides which are generated on polymer substrates by UV, high-energy  $\gamma$  irradiation, plasma discharge or corona discharge. Methoxy PEO monomethacrylate macromers are commonly used to prepare this type of PEO surface.

Mori *et al.*<sup>169</sup> prepared PEO surfaces by photo-induced grafting of methoxy PEO methacrylates with PEOs of different molecular weights to a poly(vinyl chloride) (PVC) surface in the presence of dithiocarbamate (DTC). PVC was reacted with sodium *N,N*-dithiocarbamate to introduce DTC groups, which are necessary for photo-induced graft copolymerization. Then methoxy PEO methacrylates with PEO chains of various chain lengths as side chains were graft-copolymerized to PVC

containing DTC groups, using UV irradiation. It was found that plasma protein adsorption and platelet adhesion significantly decrease on PEO-grafted surfaces with increasing PEO chain lengths up to 100 EO residues. Brinkman *et al.*<sup>251</sup> have also studied photo-induced graft copolymerization of the same macromer onto PU surfaces in the presence of DCP. Platelet deposition on PU surfaces grafted with methoxy PEO 400 methacrylate was almost absent. Golander *et al.*<sup>262</sup> prepared PEO surfaces by the photopolymerization of monoacrylated PEO onto PVC and sulfated PE in the presence of hexanediol diacrylate. They found exceptionally low degrees of protein adsorption on these PEO surfaces.

A number of research groups have carried out radiation<sup>263–267</sup> or plasma-induced<sup>175,268</sup> graft copolymerization to improve blood compatibility of polymeric materials. These graft copolymerizations employ the pre-irradiation technique. The active species for polymerization (free radicals or peroxides) are separately generated prior to polymerization of the monomer. In the case of plasma-induced graft copolymerization, free radicals would directly initiate graft copolymerization if the polymeric material subjected to plasma is not exposed to an oxygen-containing atmosphere prior to polymerization. On the other hand, graft copolymerization is initiated following decomposition of peroxides, i.e., if the substrate polymer is irradiated in air or is immediately exposed to air once irradiation has occurred.<sup>258</sup> Sun *et al.*<sup>263,264</sup> prepared PEO surfaces by radiation-induced graft copolymerization of methoxy PEO methacrylates onto silastic films by the radiation technique in the presence of  $\text{Cu}^+$  ions to prevent homopolymer gelation. About 70% decrease in fibrinogen adsorption was observed when the number of EO residues of the grafted PEO was 100.

Plasma exposure generates initiating species for polymerization only in the surface region of the exposed substrate polymer. Chinn *et al.*<sup>268</sup> modified PET and PS surfaces with a plasma discharge of ethylene oxide for the purpose of cell culture. Fujimoto *et al.*<sup>175</sup> prepared PEO surfaces by graft copolymerization of methoxy PEO methacrylates onto PU films using a plasma discharge technique. They treated PU films with argon plasma to introduce peroxides on the surface. The film was then reacted with an aqueous methoxy PEO methacrylate solution in a nitrogen gas atmosphere at an elevated temperature to allow the peroxides on the surface to thermally decompose and initiate the graft copolymerization of the macromer. It was observed that the PEO-grafted PU surface shows reduced protein adsorption *in vitro* and reduced platelet adhesion *in vitro* and *ex vivo*. It was suggested that the optimum graft density suppressing the protein adsorption is as low as  $5 \mu\text{g}/\text{cm}^2$ .

We prepared 'PEO gradient surfaces' where the surface density of the grafted PEO chains is changed gradually along the sample length (Fig. 9).<sup>269</sup> The PEO gradient surfaces were produced on the PE films by a corona discharge treatment with gradually increasing power (Fig. 10) followed by graft copolymerization of PEO monomethacrylates (Fig. 11). By the corona discharge treatment, peroxides are formed on polymer surfaces. The peroxide groups produced on the PE surface increased gradually with an increase in the corona power.<sup>270</sup> The peroxides act as initiators for graft copolymerization. The density of the PEO chains grafted onto the PE surface increased gradually due to the peroxides with gradually increasing surface density, as



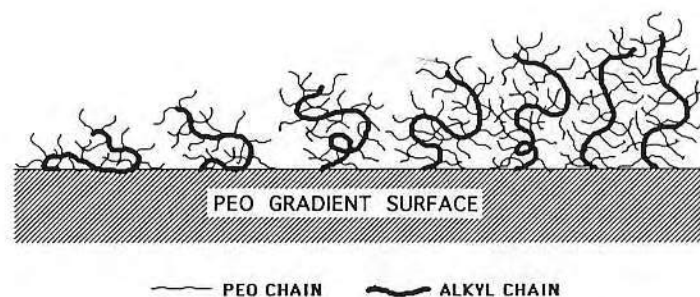


Fig. 9. Schematic diagram showing a PEO gradient surface.

seen in Fig. 9. The corona discharge treatment is a simpler and more practical method than the plasma discharge method because polymer sheets are directly treated in air at atmospheric pressure within a few seconds, whereas the plasma discharge method is carried out under vacuum. We found that plasma protein adsorption and platelet adhesion on the PEO gradient surfaces are gradually reduced by increasing the PEO chain length and the PEO surface density.

#### 4.5. Other Surface Modifications

Polymer substrates have also been modified with PEO by surface entrapment techniques. Desai and Hubbell<sup>271</sup> developed a technique to incorporate PEO onto the surfaces of various base polymer substrates. The technique involved immersing the polymeric material to be modified in a liquid that is a mutual solvent for the polymer substrate and PEO. They suggested that the interface between the substrate and the liquid begins to swell and results in loosening of the polymer network on the surface of

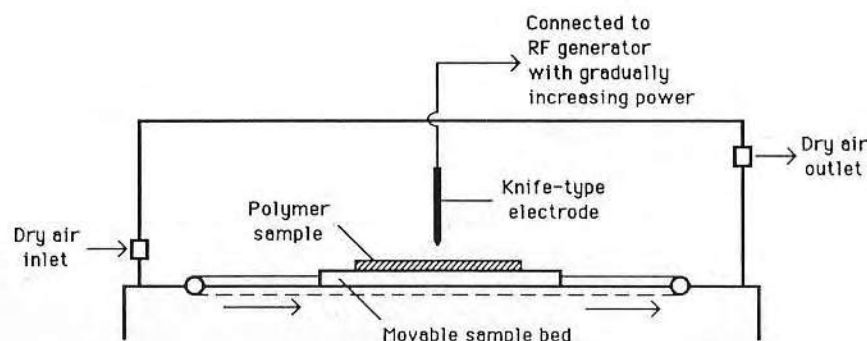


Fig. 10. Schematic diagram showing corona discharge apparatus for the preparation of gradient surfaces (from ref. 270).

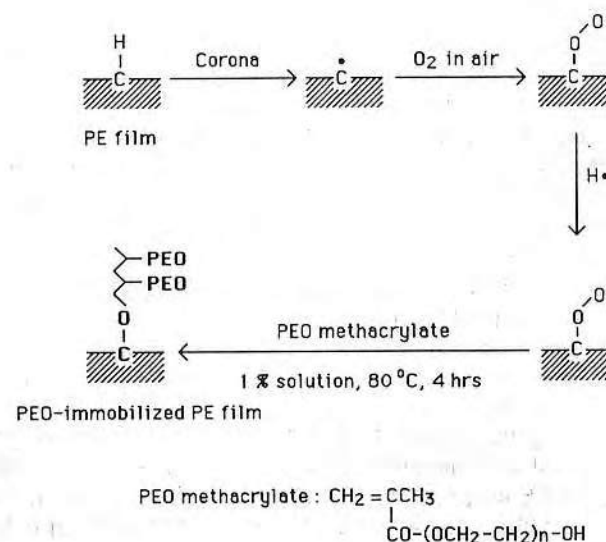


Fig. 11. Possible mechanism for the formation of PEO gradient surfaces by corona discharge treatment followed by graft copolymerization of PEO monomethacrylates.

the base polymer substrate. Thus the PEO molecules are free to diffuse into the semidissolved interface. After some time the system is quenched with water, which is a non-solvent for the polymer substrate but is mutually soluble with the immersion solvent, resulting in collapse of the swollen interface, entrapping the PEO chains within the base polymer network. It was found from protein adsorption studies, fibroblast adhesion assays and whole blood perfusions over these PEO-entrapped polymer surfaces that the surface modified with PEO 18,500 is very effective in reducing the tested biological interactions. A similar technique has been studied by Ruckenstein and coworkers<sup>272-274</sup> using PEO-containing block copolymers.

Wesslen and coworkers<sup>275,276</sup> modified segmented PU surfaces through the use of PEO-containing block copolymers as additives. They showed that adsorption of fibrinogen is significantly reduced by the additives to levels similar to those obtained for PU surfaces grafted with PEO.

## 5. CONCLUSIONS

In this article, we have reviewed the unique solution properties of PEO in water, factors involved in PEO's passivity, which is closely related to its solution properties in water, and various techniques to prepare PEO surfaces.

It appears that PEO in water has rapid motions and a large excluded volume compared with the less water-soluble or insoluble polyethers and other water-soluble synthetic polymers. As we consider the structures of the polyethers (see Table 3) and

water-soluble synthetic polymers (see Fig. 2), we can expect that PEO will be the most flexible in water among those polymers because it does not have bulky side groups attached to the backbone and is uncharged. Thus, PEO segments will not be sterically hindered in water and will be highly mobile (see Table 4). PEO molecules are highly interactive with water, as evidenced by the high values of the second virial coefficient or low values of the polymer-solvent interaction parameter. However, PEO molecules will minimally perturb the structure of water itself because they will nicely fill out water lattice points (by oxygen atoms) and voids in the water structure (by ethylene segments) without distortion of water lattices if the suggestion by Kjellander and Florin<sup>40,41</sup> is true. Other polyethers or water-soluble polymers will distort water structure due to the unsuitable distances of neighbouring and next-neighbouring ether oxygen atoms or bulky side groups.

We considered interfacial free energies, steric stabilization effects, and solution properties as the main factors for protein resistance of the surfaces with adsorbed polymer layers. Among the water-soluble polymers, PEO is particularly effective for protein resistance, probably due to a combination of factors such as minimum interfacial free energies with water and the unique solution properties in water, such as almost unlimited solubility, good structural fit between PEO and water, high mobility, large excluded volume, and hydrophilicity.

Direct and quantitative evidence for repulsion between two PEO surfaces has been studied by Klein and Luckham,<sup>277,278</sup> and Claesson and Golander<sup>279</sup> using the curved mica surface force apparatus developed by Israelachvili *et al.*<sup>280,281</sup> Measurements of interactions between two protein-coated surfaces<sup>282,283</sup> and between PEO and protein-coated surfaces using this apparatus are in progress by several groups to understand the interaction behaviour of proteins with PEO. There are many forces involved in interactions between a PEO surface and proteins. For protein resistance, repulsive forces by the combined factors for PEO's passivity (discussed in this article) should be larger than attractive forces such as van der Waals forces between the surface and proteins or between the PEO chains and proteins, hydrophobic forces between the surface and proteins or between the ethylene segments of the PEO chains and proteins, and hydrogen bonding of the ether oxygens of the PEO chains with proteins.

PEO surfaces have been prepared by bulk modifications such as block copolymerization and crosslinking to produce PEO networks. Bulk modification to produce PEO surfaces may be promising for some applications if the material is composed of PEO throughout. However, the mechanical properties of PEO networks or hydrogels are not good enough for many applications. Also PEO does not usually exist as pendant chains and is attached by both ends to the copolymer segments. Thus PEO chain mobility is restricted. Immobilization of PEO or its derivatives onto the surface of polymeric substrates with high mechanical strengths has been attempted by many research groups.

PEO surfaces have been prepared by physical adsorption of high-molecular-weight PEO or various PEO-containing amphiphilic copolymers onto hydrophobic polymeric substrates. This approach may provide a simple, rapid and effective means of producing PEO surfaces, if the PEO-containing copolymers can be adsorbed strongly onto the

surfaces. However, the immobilized polymers do not permanently remain on the surface.

Covalent grafting of PEO or PEO derivatives to polymeric substrates is the most effective way of creating a permanent PEO surface. Several techniques have been used to attach PEO covalently to surfaces. These include direct chemical coupling of PEO derivatives onto substrates. However, this method is possible only if the surface has chemically active functional groups which can react with PEO derivatives. This limits the application of this technique to certain biomaterials. In addition, the coupling procedures are usually very complicated and time-consuming. For inert surfaces without any functional groups, PEO grafting has been carried out using UV irradiation, high-energy  $\gamma$  irradiation and plasma glow discharge. Other covalent PEO grafting methods includes graft copolymerization of PEO-containing macromers on polymer substrates. The polymer substrates are pre-irradiated using UV irradiation, high-energy  $\gamma$  irradiation, plasma glow discharge or corona discharge to produce active species on the surface prior to polymerization of the macromer.

Many newer approaches are being attempted to prepare stable and effective PEO surfaces by simple and rapid means. If we can find an effective way to produce PEO surfaces simply and non-specifically on various polymeric materials, it will be very promising for a host of biomedical applications.

## REFERENCES

1. Ch. Weiss, *Human Physiology* (R. F. Schmidt and G. Thews Eds.), Ch. 16, Springer-Verlag, Berlin (1983).
2. L. Vroman, *Blood*, Natural History Press, New York (1967).
3. R. F. A. Zwaal and H. C. Hemker (Eds.), *Blood Coagulation*, Elsevier, Amsterdam (1986).
4. A. L. Bloom, *Haemostasis* **20** (Suppl. 1), 14 (1990).
5. J. M. Courtney, N. M. K. Lamba, S. Sundaram and C. D. Forbes, *Biomaterials* **15**, 737 (1994).
6. A. S. Hoffman, *Biomaterials: Interfacial Phenomena and Applications* (S. L. Cooper and N. A. Peppas Eds.), p. 3, Adv. Chem. Ser. 199, American Chemical Society, Washington, DC (1982).
7. L. L. Hench and E. C. Ethridge, *Biomaterials: An Interfacial Approach*, Academic Press, New York (1981).
8. S. W. Kim and J. Feijen, *CRC Critical Reviews in Biocompatibility*, Vol. 1, p. 215, CRC Press, Boca Raton, FL (1985).
9. J. D. Andrade, S. Nagaoka, S. Cooper, T. Okano and S. W. Kim, *ASAIO J.* **10**, 75 (1987).
10. Y. Ikada, *Polymers in Medicine* (K. Dusek Ed.), p. 103, Springer-Verlag, Berlin (1984).
11. M. Amiji and K. Park, *J. Biomater. Sci., Polym. Ed.* **4**, 217 (1993).
12. Y. Ikada, *Biomaterials* **15**, 725 (1995).
13. F. E. Bailey and J. Y. Koleske, *Poly(ethylene oxide)*, Academic Press, New York (1976).
14. H. Tadokoro, Y. Chatani, T. Yoshihara, S. Tahara and S. Murahashi, *Makromol. Chem.* **73**, 109 (1964).
15. K. J. Liu and J. L. Parsons, *Macromolecules* **2**, 529 (1969).
16. H. Matsuura and T. Miyazawa, *Bull. Chem. Soc. Japan* **41**, 1798 (1968).
17. H. Matsuura and T. Miyazawa, *J. Polym. Sci., Polym. Phys.* **7**, 1735 (1969).
18. J. L. Koenig and A. C. Angood, *J. Polym. Sci., Polym. Phys.* **8**, 1787 (1970).
19. E. F. Oleiniki and N. S. Enikolopyan, *J. Polym. Sci., Part C* **16**, 3677 (1968).
20. J. F. Rabolt, K. W. Johnson and R. N. Zitter, *J. Chem. Phys.* **61**, 504 (1974).
21. J. R. Bartlett and R. P. Cooney, *J. Chem. Soc., Faraday Trans. 1* **82**, 597 (1986).
22. H. F. Olf and A. Peterlin, *Makromol. Chem.* **104**, 135 (1967).
23. T. M. Connor and K. A. Mclauchlan, *J. Phys. Chem.* **69**, 1888 (1965).
24. K. J. Liu, *Macromolecules* **1**, 213 (1968).
25. K. J. Liu, *Macromolecules* **1**, 308 (1968).

26. K. L. Liu and J. E. Anderson, *Macromolecules* **2**, 235 (1969).
27. K. L. Liu and R. Ullman, *J. Chem. Phys.* **48**, 1158 (1968).
28. K. Matsuzaki and H. Ito, *J. Polym. Sci., Polym. Phys.* **12**, 2507 (1974).
29. S. H. Maron and F. E. Filisko, *J. Macromol. Sci., Phys.* **B6**, 79 (1972).
30. F. E. Bailey, G. M. Powell and K. L. Smith, *Ind. Eng. Chem.* **50**, 8 (1958).
31. F. E. Bailey and R. W. Callard, *J. Appl. Polym. Sci.* **1**, 56 (1959).
32. P. Gregory and M. B. Huglin, *Makromol. Chem.* **187**, 1745 (1986).
33. B. Chew and A. Couper, *J. Chem. Soc., Faraday Trans. I* **72**, 382 (1976).
34. A. Teramoto, S. Kusamizu, H. Tanaka, Y. Murakami and H. Fujita, *Makromol. Chem.* **90**, 78 (1966).
35. P. Molyneux, *Water-soluble Synthetic Polymers: Properties and Behavior*, Vol. 1, CRC Press, Boca Raton, FL (1983).
36. P. Molyneux, *Water, A Comprehensive Treatise*, Vol. 4, *Aqueous Solutions of Amphiphiles and Macromolecules* (F. Franks Ed.), Ch. 7, Plenum Press, New York (1975).
37. M. J. Blandamer, M. F. Fox, E. Powell and J. W. Stafford, *Makromol. Chem.* **124**, 222 (1969).
38. C. Tanford, *The Hydrophobic Effect: Formation of Micelles and Biological Membranes*, 2nd Ed., Ch. 4 and 5, Wiley-Interscience, New York (1980).
39. A. H. Narten, *J. Chem. Phys.* **56**, 5681 (1972).
40. R. Kjellander and E. Florin, *J. Chem. Soc., Faraday Trans. I* **77**, 2053 (1981).
41. E. Florin, Ph. D. Thesis, Royal Institute of Technology, Stockholm, Sweden (1983).
42. S. Bluestone, J. E. Mark and P. J. Flory, *Macromolecules* **7**, 325 (1974).
43. J. D. Bernal and R. H. Fowler, *J. Chem. Phys.* **1**, 515 (1933).
44. H. I. Frank and M. W. Evans, *J. Chem. Phys.* **13**, 507 (1945).
45. G. Nemethy and H. A. Scheraga, *J. Chem. Phys.* **36**, 3401 (1962).
46. A. K. Doolittle, *The Technology of Solvents and Plasticizers*, Ch. 14, Wiley, New York (1954).
47. J. Breen, D. van Duijn, J. de Bleijser and J. C. Leyte, *Ber. Bunsenges. Phys. Chem.* **90**, 1112 (1986).
48. C. W. R. Mulder, J. Schrieffer and J. C. Leyte, *J. Phys. Chem.* **89**, 475 (1985).
49. M. C. Lang, F. Laupretre, C. Noel and L. Monnerie, *J. Chem. Soc., Faraday Trans. II* **75**, 349 (1979).
50. T. W. N. Bieze, J. R. van der Maarel, C. D. Eisenbach and J. C. Leyte, *Macromolecules* **27**, 1355 (1994).
51. A. Eshuis and P. F. Mijnlief, *Polymer* **27**, 1951 (1986).
52. F. E. Bailey and J. V. Koleske, *Nonionic Surfactants* (M. J. Schick Ed.), Ch. 23, Dekker, New York (1967).
53. M. Davies, G. Williams and G. D. Loveduck, *Z. Electrochem.* **64**, 575 (1960).
54. G. G. Hammes and P. B. Roberts, *J. Am. Chem. Soc.* **90**, 7119 (1968).
55. K. J. Liu and R. Ullman, *J. Chem. Phys.* **48**, 1158 (1968).
56. P. Tormala, H. Lattila and J. J. Lindberg, *Polymer* **14**, 481 (1973).
57. D. Braun and P. Tormala, *Makromol. Chem.* **179**, 1025 (1978).
58. F. E. Bailey and R. W. Callard, *J. Appl. Polym. Sci.* **1**, 373 (1959).
59. G. M. Malcolm and J. S. Rowlinson, *Trans. Faraday Soc.* **53**, 921 (1957).
60. A. Kagemoto, S. Murikami and R. Fujishiro, *Makromol. Chem.* **105**, 154 (1967).
61. M. L. Lakhanpal, H. G. Singh, H. Singh and S. C. Sharma, *Indian J. Chem.* **6**, 95 (1968).
62. M. L. Lakhanpal, V. Kapoor, R. K. Sharma and S. C. Sharma, *Indian J. Chem.* **4**, 59 (1966).
63. M. L. Lakhanpal, L. Moti and R. K. Sharma, *Indian J. Chem.* **3**, 547 (1965).
64. S. H. Maron and F. E. Filisko, *J. Macromol. Sci.* **B6**, 57 (1972).
65. L. S. Sandell and D. A. I. Goring, *Makromol. Chem.* **138**, 77 (1970).
66. N. G. Gaylord (Ed.), *Polyethers*, Wiley-Interscience, New York (1963).
67. J. Furukawa and T. Saegusa, *Polymerization of Aldehydes and Oxides*, Wiley-Interscience, New York (1963).
68. P. J. Flory, *Principles of Polymer Chemistry*, Ch. 12, Cornell University Press, New York (1953).
69. J. F. Rabek, *Experimental Methods in Polymer Chemistry*, Ch. 2, Wiley-Interscience, New York (1980).
70. R. S. King, H. W. Blanch and J. M. Prausnitz, *AIChE J.* **34**, 1585 (1988).
71. J. Hermans, *J. Chem. Phys.* **77**, 2193 (1982).
72. E. A. Bekturov and Z. Kh. Bakauova, *Synthetic Water-soluble Polymers in Solution*, Ch. 3, Huthig and Wepf, Basel (1986).
73. P. J. Flory, *Principles of Polymer Chemistry*, Ch. 14, Cornell University Press, New York (1953).
74. J. Brandrup and E. H. Immergut (Eds.), *Polymer Handbook*, 3rd edn., Wiley-Interscience, New York (1988).
75. L. W. Nichol, A. G. Ogston and B. N. Preston, *Biochem. J.* **102**, 407 (1967).
76. E. Edmond and A. G. Ogston, *Biochem. J.* **109**, 569 (1968).
77. B. Katchman and A. D. McLaren, *J. Am. Chem. Soc.* **73**, 2124 (1951).
78. G. S. Misra and S. N. Bhattacharya, *Eur. Polym. J.* **15**, 125 (1979).
79. W. Stockmayer and M. Fixman, *J. Polym. Sci., Part C* **1**, 137 (1963).
80. N. A. Peppas and E. W. Merrill, *J. Polym. Sci.* **14**, 459 (1976).
81. V. J. Klenin, O. V. Klenina, B. I. Shvartsburd and S. Y. Frenkel, *J. Polym. Sci., Polym. Symp.* **44**, 131 (1974).
82. M. Dole and I. L. Faller, *J. Am. Chem. Soc.* **72**, 414 (1950).
83. L. C. Cerny, T. E. Helminiak and J. F. Meier, *J. Polym. Sci.* **44**, 539 (1960).
84. J. F. Rabek, *Experimental Methods in Polymer Chemistry*, Ch. 20, Wiley-Interscience, New York (1980).
85. M. L. Martin, J. J. Delpuech and G. J. Martin, *Practical NMR Spectroscopy*, Heyden & Son, London (1980).
86. J. N. Israelachvili, *Intermolecular and Surface Forces*, p. 44, Academic Press, London (1985).
87. D. D. Ely, M. J. Hey and B. L. Winteringham, *J. Solution Chem.* **5**, 787 (1976).
88. J. D. Andrade, *Medical Instrum.* **7**, 110 (1973).
89. D. L. Coleman, D. E. Gregonis and J. D. Andrade, *J. Biomed. Mater. Res.* **16**, 381 (1982).
90. D. L. Coleman, Ph. D. Thesis, University of Utah, Salt Lake City (1980).
91. J. D. Andrade, R. N. King, D. E. Gregonis and D. L. Coleman, *J. Polym. Sci., Polym. Symp.* **66**, 383 (1979).
92. J. Hermans, *J. Chem. Phys.* **77**, 2193 (1982).
93. D. H. Napper, *Polymeric Stabilization of Colloidal Dispersions*, Academic Press, London (1983).
94. T. Sato and R. Ruch, *Stabilization of Colloid Dispersions by Polymer Adsorption*, Ch. 3, Dekker, New York (1980).
95. R. H. Ottewill, *Nonionic Surfactants* (M. J. Schick Ed.), Ch. 19, Dekker, New York (1967).
96. E. J. Clayfield and E. C. Lumb, *J. Colloid Interface Sci.* **22**, 269 (1966).
97. D. J. Meier, *J. Phys. Chem.* **71**, 1861 (1967).
98. F. Th. Hesselink, *J. Phys. Chem.* **75**, 65 (1971).
99. F. Th. Hesselink, A. Vrij and J. Th. G. Overbeek, *J. Phys. Chem.* **75**, 2094 (1971).
100. J. W. Dobbie, R. Evans, D. V. Gibson, J. B. Smitham and D. H. Napper, *J. Colloid Interface Sci.* **45**, 557 (1973).
101. D. W. J. Osmond, B. Vincent and F. A. Waite, *Colloid Polym. Sci.* **253**, 676 (1975).
102. A. K. Dolan and S. F. Edwards, *Proc. R. Soc. London A* **343**, 427 (1975).
103. D. H. Napper, *J. Colloid Interface Sci.* **58**, 390 (1977).
104. B. Vincent, P. E. Luckham and F. A. Waite, *J. Colloid Interface Sci.* **73**, 508 (1980).
105. P. Bongrand, C. Capo and R. Depieds, *Prog. Surface Sci.* **12**, 217 (1982).
106. P. Bongrand and G. I. Bell, *Cell Surface Dynamics: Concepts and Models* (A. S. Perelson, C. DeLisi and F. W. Wiegel Eds.), Ch. 14, Dekker, New York (1984).
107. D. H. Atha and K. C. Ingham, *J. Biol. Chem.* **256**, 12108 (1981).
108. D. Knoll and J. Hermans, *J. Biol. Chem.* **258**, 5710 (1983).
109. N. G. Maroudas, *Nature* **254**, 695 (1975).
110. Th. F. Tadros, *The Effect of Polymers on Dispersion Properties* (Th. F. Tadros, Ed.), p. 1, Academic Press, New York (1982).
111. J. B. Smithsam, R. Evans and D. H. Napper, *J. Chem. Soc., Faraday Trans.* **71**, 285 (1975).
112. E. W. Merrill and E. W. Salzman, *ASAIO J.* **6**, 60 (1983).
113. S. Nagaoka, Y. Mori, H. Takiuchi, K. Yokota, H. Tanzawa and S. Nishimi, *Polymers as Biomaterials* (S. W. Shalaby, A. S. Hoffman, B. D. Ratner and T. A. Horbett Eds.), p. 361, Plenum Press, New York (1984).
114. D. J. Lyman, *Trans. ASAIO* **10**, 17 (1964).
115. K. Furasawa, Y. Shimura, K. Otobe, K. Atsumi and K. Tasuda, *Ronbushu Kobushu* **4**, 309 (1977).
116. D. W. Grainger, T. Okano and S. W. Kim, *Advances in Biomedical Polymers* (C. G. Gebelbein Ed.), p. 229, Plenum Press, New York (1987).
117. D. W. Grainger, C. Nojiri, T. Okano and S. W. Kim, *J. Biomed. Mater. Res.* **23**, 979 (1989).
118. D. W. Grainger, T. Okano and S. W. Kim, *J. Colloid Interface Sci.* **132**, 161 (1989).



119. I. Vulic, T. Okano, S. W. Kim and J. Feijen, *Biomaterials and Clinical Applications 7* (A. Pizzoferrato, P. G. Marchetti, A. Ravaglioli and A. J. C. Lee Eds.), p. 491, Elsevier, Amsterdam (1987).
120. I. Vulic, T. Okano, S. W. Kim and J. Feijen, *J. Polym. Sci., Polym. Chem.* **26**, 381 (1988).
121. I. Vulic, A. J. B. Loman, J. Feijen, T. Okano and S. W. Kim, *J. Polym. Sci., Polym. Chem.* **28**, 1693 (1990).
122. D. W. Grainger, S. W. Kim and J. Feijen, *J. Biomed. Mater. Res.* **22**, 231 (1988).
123. D. W. Grainger, K. Knutson, S. W. Kim and J. Feijen, *J. Biomed. Mater. Res.* **24**, 403 (1990).
124. D. W. Grainger, T. Okano, S. W. Kim, D. G. Castner, B. D. Ratner, D. Brigg and Y. K. Sung, *J. Biomed. Mater. Res.* **24**, 547 (1990).
125. T. Okano, M. Urano, N. Sugiyama, M. Shimada, I. Shinohara, K. Kataika and Y. Sakurai, *J. Biomed. Mater. Res.* **20**, 1035 (1986).
126. D. K. Gilding and A. M. Reed, *Polymer* **20**, 1454 (1979).
127. S. K. Hunter, D. E. Gregonis, D. L. Coleman, B. Hanover, R. L. Stephen and S. C. Jacobsen, *Trans. ASAI0* **29**, 250 (1983).
128. D. J. Lyman, *J. Biomed. Mater. Res.* **1**, 17 (1967).
129. S. J. Whicher and J. L. Brash, *J. Biomed. Mater. Res.* **12**, 181 (1978).
130. J. L. Brash and S. Uniyal, *J. Polym. Sci.* **66**, 377 (1979).
131. V. Sa da Costa, D. Brier-Russell, G. Trudell, D. F. Waugh, E. W. Salzman and E. W. Merrill, *J. Colloid Interface Sci.* **76**, 594 (1980).
132. V. Sa da Costa, D. Brier-Russell, E. W. Salzman and E. W. Merrill, *J. Colloid Interface Sci.* **80**, 445 (1981).
133. E. W. Merrill, E. W. Salzman, V. Sa da Costa, D. Brier-Russell, A. Dincer, P. Pape and J. N. Linton, *Adv. Chem. Ser.* **199**, 35 (1982).
134. E. W. Merrill, V. Sa da Costa, E. W. Salzman, D. Brier-Russell, L. Kushner, D. F. Waugh, G. Trudel, S. Stopper and V. Vitale, *Adv. Chem. Ser.* **199**, 95 (1982).
135. E. W. Merrill, E. W. Salzman, S. Wan, N. Mahmud, L. Kushner, J. N. Linton and J. Curme, *Trans. ASAI0* **28**, 482 (1982).
136. T. G. Grasel and S. L. Cooper, *Biomaterials* **7**, 315 (1987).
137. S. L. Goodman, M. D. Lelah, L. K. Lambrecht, S. L. Cooper and R. M. Albrecht, *Scanning Electron Microsc.* **1**, 379 (1984).
138. S. L. Goodman, T. G. Grasel, S. L. Cooper and R. M. Albrecht, *J. Biomed. Mater. Res.* **23**, 105 (1989).
139. M. D. Lelah, T. G. Grasel, J. A. Pierce and S. L. Cooper, *J. Biomed. Mater. Res.* **20**, 433 (1986).
140. A. Takahara, A. Z. Okkema, A. J. Coury and S. L. Cooper, *Biomaterials* **12**, 324 (1991).
141. A. Z. Okkema, T. G. Grasel, R. J. Zdrahala, D. D. Solomon and S. L. Cooper, *J. Biomater. Sci., Polym. Ed.* **1**, 43 (1989).
142. J. H. Silver, K. B. Lewis, B. D. Ratner and S. L. Cooper, *J. Biomed. Mater. Res.* **27**, 735 (1993).
143. J. H. Silver, J. W. Marchant and S. L. Cooper, *J. Biomed. Mater. Res.* **27**, 1443 (1993).
144. J. H. Silver, C. W. Myers, F. Lim and S. L. Cooper, *Biomaterials* **15**, 695 (1994).
145. Y. Ito and Y. Imanish, *CRC Critical Reviews in Biocompatibility*, Vol. 5, p. 45, CRC Press, Boca Raton, FL (1989).
146. D. J. Fabrizio-Homan and S. L. Cooper, *J. Biomater. Sci., Polym. Ed.* **3**, 27 (1991).
147. J. L. Brash, S. Uniyal and Q. Samak, *Trans. ASAI0* **20**, 69 (1974).
148. S. Niu, T. Matsuda and T. Oka, *Trans. ASAI0* **36**, M164 (1990).
149. E. L. Chaikof, E. W. Merrill, J. E. Coleman, K. Ramberg, R. J. Connolly and A. D. Callow, *AIChE J.* **36**, 994 (1990).
150. S. L. Verdon, E. L. Chaikof, J. E. Coleman, L. L. Hayes, R. J. Connolly, K. Ramberg, E. W. Merrill and A. D. Callow, *Scanning Microsc.* **4**, 341 (1990).
151. P. D. Drumheller and J. A. Hubbell, *J. Polym. Sci., Polym. Chem.* **32**, 2715 (1994).
152. C. P. Pathak, A. S. Sawhney and J. A. Hubbell, *Polymer Preprints* **33**, 65 (1992).
153. A. Nathan, D. Bolikal, N. Vyavahara, S. Zalipsky and J. Kohn, *Macromolecules* **25**, 4476 (1992).
154. N. P. Desai, A. Sojomihardjo, P. A. Sandford and P. Soon-Shiong, *Trans. Soc. Biomaterials* **16**, 206 (1993).
155. E. L. Chaikof and E. W. Merrill, *New Polym. Mater.* **2**, 125 (1990).
156. X. Peng, Y. Song, Y. Qi, S. Wu, L. Li and D. Chen, *Chinese J. Polym. Sci.* **8**, 342 (1990).
157. K. Mukae, Y. H. Bae, T. Okano and S. W. Kim, *Polymer J.* **22**, 250 (1990).
158. Y. H. Bae, T. Okano and S. W. Kim, *Makromol. Chem., Rapid Commun.* **9**, 185 (1988).
159. S. Nishi and T. Kotaka, *Polymer J.* **21**, 393 (1989).
160. E. L. Chaikof, E. W. Merrill, A. D. Callow, R. J. Connolly, S. L. Verdon and K. Ramsberg, *J. Biomed. Mater. Res.* **26**, 1163 (1992).
161. N. B. Graham, N. E. Nwachuku and D. J. Walsh, *Polymer* **23**, 1345 (1982).
162. A. Nathan, S. Zalipsky and J. Kohn, *Polymer Preprints* **31**, 213 (1990).
163. A. Nathan, S. Zalipsky, S. I. Ertel, S. N. Agathos, M. L. Yarmush and J. Kohn, *Bioconj. Chem.* **4**, 54 (1993).
164. N. Vyavahare and J. Kohn, *J. Polym. Sci., Polym. Chem.* **32**, 1271 (1994).
165. A. S. Sawhney, C. P. Pathak, J. J. van Rensberg, R. C. Dunn and J. A. Hubbell, *J. Biomed. Mater. Res.* **28**, 831 (1994).
166. A. S. Sawhney, C. P. Pathak and J. A. Hubbell, *Macromolecules* **26**, 581 (1993).
167. C. P. Pathak, A. S. Sawhney and J. A. Hubbell, *J. Am. Chem. Soc.* **114**, 8311 (1992).
168. S. Nagaoka and A. Nakao, *Biomaterials* **11**, 119 (1990).
169. Y. Mori, S. Nagaoka, H. Takiuchi, T. Kikuchi, N. Noguchi, H. Tanzawa and Y. Noishiki, *Trans. ASAI0* **28**, 459 (1982).
170. J. G. F. Bots, L. Van der Does and A. Bantjes, *Biomaterials* **7**, 393 (1986).
171. J. G. F. Bots, L. van der Does and A. Bantjes, *Polym. Sci. Technol.* **34**, 223 (1986).
172. J. G. F. Bots, L. van der Does and A. Bantjes, *Biological and Biomechanical Performance of Biomaterials* (P. Christel, A. Meunier and A. J. C. Lee Eds.) p. 189, Elsevier, Amsterdam (1986).
173. J. G. F. Bots, L. van der Does and A. Bantjes, *Dev. Hematol. Immunol.* **14**, 277 (1986).
174. J. G. Bots, L. van der Does and A. Bantjes, *Br. Polym. J.* **19**, 527 (1987).
175. K. Fujimoto, H. Inoue and Y. Ikada, *J. Biomed. Mater. Res.* **27**, 1559 (1993).
176. C. W. Hiatt, A. Shelokov, E. J. Rosenthal and J. M. Galimore, *J. Chromatogr.* **56**, 362 (1971).
177. G. L. Hawk, J. A. Cameron and L. B. Dufault, *Prep. Biochem.* **2**, 193 (1972).
178. T. Kato, K. Nakamura, M. Kawaguchi and A. Takahashi, *Polymer J.* **13**, 1037 (1981).
179. J. N. George, *Blood* **40**, 862 (1972).
180. W. Wasiewski, M. J. Fasco, B. M. Martin, T. C. Detwiler and J. W. Fenton, *Thrombo. Res.* **8**, 881 (1976).
181. Y. L. Cheng, S. A. Darst and C. R. Robertson, *J. Colloid Interface Sci.* **118**, 212 (1987).
182. D. H. Randerson and J. A. Taylor, *Plasmapheresis, New Trends in Therapeutic Applications* (Y. Nose, P. S. Malchesky and J. W. Smith Eds.), p. 69, ISAO Press, Cleveland, OH (1983).
183. J. H. Lee, J. Kopecek and J. D. Andrade, *J. Biomed. Mater. Res.* **23**, 351 (1989).
184. J. H. Lee, P. Kopeckova, J. Kopecek and J. D. Andrade, *Biomaterials* **11**, 455 (1990).
185. J. D. Andrade, J. Kopecek and J. H. Lee, *U.S. Pat.* 5,075,400 (1991).
186. J. H. Lee, Ph. D. Thesis, University of Utah, Salt Lake City (1988).
187. J. H. Lee, J. Kopecek and J. D. Andrade, *Polym. Mater. Sci. Eng.* **57**, 613 (1987).
188. J. H. Lee, P. Kopeckova, J. Zhang, J. Kopecek and J. D. Andrade, *Polym. Mater. Sci. Eng.* **59**, 234 (1988).
189. J. H. Lee and J. D. Andrade, *Polymer Surface Dynamics* (J. D. Andrade Ed.), p. 119, Plenum Press, New York (1988).
190. S. I. Jeon, J. H. Lee, J. D. Andrade and P. G. De Gennes, *J. Colloid Interface Sci.* **142**, 149 (1991).
191. S. I. Jeon and J. D. Andrade, *J. Colloid Interface Sci.* **142**, 159 (1991).
192. J. B. Kayes and D. A. Rawlins, *Colloid Polym. Sci.* **257**, 622 (1979).
193. H. Thurow and K. Geisen, *Diabetologia* **27**, 212 (1984).
194. J. S. Clunie and B. T. Ingram, *Adsorption from Solution at the Solid/Liquid Interface* (G. D. Parfitt and C. H. Rochester Eds.), p. 105, Academic Press, New York (1983).
195. B. Kronberg, E. Sjoblom, L. Ehrenborg, P. Stenius and B. Wesslen, *Polymer Preprints* **26**, 236 (1985).
196. D. N. Furlong and J. R. Aston, *Colloids Surf.* **4**, 121 (1982).
197. J. Lee, P. A. Martic and J. S. Tan, *J. Colloid Interface Sci.* **131**, 252 (1989).
198. J. S. Tan and P. A. Martic, *J. Colloid Interface Sci.* **136**, 415 (1990).
199. J. S. Tan, D. E. Butterfield, C. L. Voycheck, K. D. Caldwell and J. T. Li, *Biomaterials* **14**, 823 (1993).
200. L. Illum, L. O. Jacobsen, R. H. Muller, E. Mak and S. S. Davis, *Biomaterials* **8**, 113 (1987).
201. S. S. Davis, S. J. Douglas, L. Illum, P. D. Jones, E. Mak and R. H. Muller, *Targeting of Drugs with Synthetic Systems* (G. Gregoriadis, J. Senior and G. Poste Eds.), p. 123, Plenum Press, New York (1985).

202. S. S. Davis and L. Illum, *Biomaterials* **9**, 111 (1988).
203. L. Illum and S. S. Davis, *FEBS Lett.* **167**, 79 (1984).
204. W. Breemhaar, E. Brinkman, D. J. Ellens, T. Beugeling and A. Bantjes, *Biomaterials* **5**, 269 (1984).
205. M. J. Bridgett, M. C. Davies and S. P. Denyer, *Biomaterials* **13**, 411 (1992).
206. M. Humphries, J. F. Jaworzyn and J. B. Cantwell, *FEMS Microbiol. Ecol.* **38**, 299 (1988).
207. M. Humphries, J. F. Jaworzyn, J. B. Cantwell and A. Eakin, *FEMS Microbiol. Lett.* **42**, 91 (1987).
208. N. F. Owens, D. Gingell and P. R. Rutter, *J. Cell Sci.* **87**, 667 (1987).
209. M. Amiji, H. Park and K. Park, *Trans. Soc. Biomater.* **14**, 41 (1991).
210. M. Amiji and K. Park, *Biomaterials* **13**, 682 (1992).
211. D. Gingell and N. Owens, *J. Biomed. Mater. Res.* **28**, 491 (1994).
212. D. Gingell, N. Owens, P. Hodge, C. V. Nicholas and R. O'Dell, *J. Biomed. Mater. Res.* **28**, 505 (1994).
213. C. Macchling-Strasser, Ph. Dejardin, J. C. Galin, A. Schmitt, V. Housse-Ferrari, B. Seville, J. N. Mulvihill and J. P. Cazenave, *J. Biomed. Mater. Res.* **23**, 1385 (1989).
214. G. E. Kenny and C. L. Dunsmoor, *Israel J. Med. Sci.* **23**, 732 (1987).
215. A. Gardas and A. Lewartowska, *J. Immunol. Methods* **106**, 251 (1989).
216. G. R. Harper, M. C. Davies, S. S. Davis, Th. F. Tadros, D. C. Taylor, M. P. Irving and J. A. Waters, *Biomaterials* **12**, 695 (1991).
217. J. E. O'Mullane, C. J. Davison, K. Petrak and E. Tomlinson, *Biomaterials* **9**, 203 (1988).
218. C. S. Cho, T. Takayama, M. Kunou and T. Akaiki, *J. Biomed. Mater. Res.* **24**, 1369 (1994).
219. T. Akizawa, T. Kino, S. Koshikawa, Y. Ikada, A. Kishida, M. Yamashita and K. Imamura, *Trans. ASAI* **35**, 333 (1989).
220. A. Kishida, K. Mishima, E. Corrette, H. Konishi and Y. Ikada, *Biomaterials* **13**, 113 (1992).
221. N. P. Desai and J. A. Hubbell, *J. Biomed. Mater. Res.* **25**, 829 (1991).
222. N. P. Desai and J. A. Hubbell, *Polym. Mater. Sci. Eng.* **62**, 731 (1990).
223. K. Bergstrom, K. Holmberg, A. Safran, A. S. Hoffman, M. J. Edgell, B. A. Hovanes and J. M. Harris, *J. Biomed. Mater. Res.* **26**, 779 (1992).
224. K. Bergstrom, E. Osterberg, K. Holmberg, A. S. Hoffman, T. P. Schuman, A. Kozlowski and J. M. Harris, *J. Biomater. Sci., Polym. Ed.* **6**, 123 (1994).
225. M. V. Sefton, G. Llanos and W. E. Ip, *Polym. Mater. Sci. Eng.* **62**, 741 (1990).
226. G. R. Llanos and M. V. Sefton, *J. Biomed. Mater. Res.* **27**, 1383 (1993).
227. G. R. Llanos and M. V. Sefton, *Macromolecules* **24**, 6065 (1991).
228. E. Kiss, C. G. Golander and J. C. Eriksson, *Prog. Colloid Polym. Sci.* **74**, 113 (1987).
229. C. G. Golander and J. C. Eriksson, *J. Colloid Interface Sci.* **119**, 38 (1987).
230. C. Nojiri, K. D. Park, T. Okano and S. W. Kim, *Trans. ASAI* **35**, 357 (1989).
231. C. Nojiri, T. Okano, H. A. Jacobs, K. D. Park, S. F. Mohammad, D. B. Olsen and S. W. Kim, *J. Biomed. Mater. Res.* **24**, 1151 (1990).
232. K. D. Park, A. Z. Piao, H. Jacobs, T. Okano and S. W. Kim, *J. Polym. Sci., Polym. Chem.* **29**, 1725 (1991).
233. S. W. Kim, H. Jacobs, J. Y. Lin, C. Nojiri and T. Okano, *Ann. N. Y. Acad. Sci.* **516**, 116 (1988).
234. C. Nojiri, T. Okano, H. Koyanagi, S. Nakahama, K. D. Park and S. W. Kim, *J. Biomater. Sci., Polym. Ed.* **4**, 75 (1992).
235. S. C. Lin, H. A. Jacobs and S. W. Kim, *J. Biomed. Mater. Res.* **25**, 791 (1991).
236. K. D. Park, W. G. Kim, H. Jacobs, T. Okano and S. W. Kim, *J. Biomed. Mater. Res.* **26**, 1151 (1992).
237. K. D. Park, T. Okano, C. Nojiri and S. W. Kim, *J. Biomed. Mater. Res.* **22**, 977 (1991).
238. C. Nojiri, T. Okano, K. D. Park and S. W. Kim, *Trans. ASAI* **34**, 386 (1988).
239. C. Nojiri, T. Okano, K. D. Park and S. W. Kim, *Trans. ASAI* **35**, 357 (1989).
240. C. Nojiri, K. D. Park, D. W. Grainger, H. Jacobs, T. Okano, H. Koyanagi and S. W. Kim, *Trans. ASAI* **36**, M168 (1990).
241. D. D. Solomon, C. W. McGary and V. J. Pascarella, *U. S. Pat.* 4,521,564 (1985).
242. D. K. Han, K. D. Park, K. D. Ahn, S. Y. Jeong and Y. H. Kim, *J. Biomed. Mater. Res., Appl. Biomater.* **23**, 87 (1989).
243. D. K. Han, S. Y. Jeong and Y. H. Kim, *J. Biomed. Mater. Res., Appl. Biomater.* **23**, 211 (1989).
244. D. K. Han, S. Y. Jeong, Y. H. Kim, B. G. Min and H. I. Cho, *J. Biomed. Mater. Res.* **25**, 561 (1991).
245. D. K. Han, K. D. Park, S. Y. Jeong, Y. H. Kim, U. Y. Kim and B. G. Min, *J. Biomed. Mater. Res.* **27**, 1063 (1993).
246. R. A. Amos and P. E. Guire, *Trans. Soc. Biomater.* **14**, 175 (1991).
247. S. G. Dunkirk, S. L. Gregg, L. W. Duran, J. D. Monfils, J. E. Haapala, J. A. Marcy, D. L. Clapper, R. A. Amos and P. E. Guire, *J. Biomater. Appl.* **6**, 131 (1991).
248. K. Allmer, J. Hilborn, P. H. Larsson, A. Hult and B. Ranby, *J. Polym. Sci., Polym. Chem.* **28**, 173 (1990).
249. Y. C. Tseng and K. Park, *J. Biomed. Mater. Res.* **26**, 373 (1992).
250. Y. Nakayama and T. Matsuda, *J. Polym. Sci., Polym. Chem.* **31**, 3299 (1993).
251. E. Brinkman, A. Poot, L. van der Does and A. Bantjes, *Biomaterials* **11**, 200 (1990).
252. E. Brinkman, A. Poot, T. Beugeling, L. van der Does and A. Bantjes, *Int. J. Artif. Organs* **12**, 390 (1989).
253. D. O. Hummel, *J. Polym. Sci., Polym. Symp.* **67**, 169 (1980).
254. A. S. Hoffman, *Adv. Polym. Sci.* **57**, 141 (1984).
255. M. Amiji and K. Park, *J. Colloid Interface Sci.* **155**, 251 (1993).
256. W. R. Gombotz, W. Guanghui, T. A. Horbett and A. S. Hoffman, *J. Biomed. Mater. Res.* **25**, 1547 (1991).
257. W. R. Gombotz, W. Guanghui and A. S. Hoffman, *J. Appl. Polym. Sci.* **37**, 91 (1989).
258. C. C. Wang and G. H. Hsiue, *J. Polym. Sci., Polym. Chem.* **31**, 2601 (1993).
259. M. S. Sheu and A. S. Hoffman, *Polymer Preprints* **32**, 239 (1991).
260. M. S. Sheu, A. S. Hoffman, J. G. A. Terlingen and J. Feijen, *Clinical Materials* **13**, 41 (1993).
261. M. S. Sheu, A. S. Hoffman and J. Feijen, *J. Adhesion Sci. Technol.* **6**, 995 (1992).
262. C. G. Golander, S. Jonsson, T. Vladkova, P. Stenius and J. C. Eriksson, *Colloids Surf.* **21**, 149 (1986).
263. Y. H. Sun, W. R. Gombotz and A. S. Hoffman, *J. Bioactive Compat. Polym.* **1**, 316 (1986).
264. Y. H. Sun, W. R. Gombotz and A. S. Hoffman, *Polymer Preprints* **28**, 282 (1987).
265. B. D. Ratner and A. S. Hoffman, *Synthetic Biomedical Polymers: Concepts and Practice* (M. Szycher and W. J. Robinson Eds), p. 133, Technomic, Westport, CT (1980).
266. B. Jansen and G. Ellinghorst, *J. Biomed. Mater. Res.* **19**, 1085 (1985).
267. Y. Ikada, M. Suzuki, M. Taniguchi, H. Iwata, W. Taki, H. Miyake and H. Handa, *Radiat. Phys. Chem.* **18**, 1207 (1981).
268. J. A. Chinn, T. A. Horbett, B. D. Ratner, M. B. Schway, Y. Haque and S. D. Hauschka, *J. Colloid Interface Sci.* **127**, 67 (1989).
269. J. H. Lee, B. J. Jeong and G. S. Khang, *Trans. Soc. Biomater.* **18**, 146 (1995).
270. J. H. Lee, H. G. Kim, G. S. Khang, H. B. Lee and M. S. Jhon, *J. Colloid Interface Sci.* **151**, 563 (1992).
271. N. P. Desai and J. A. Hubbell, *Biomaterials* **12**, 144 (1991).
272. E. Ruckenstein and D. B. Chung, *J. Colloid Interface Sci.* **123**, 170 (1988).
273. J. H. Chen and E. Ruckenstein, *J. Colloid Interface Sci.* **132**, 100 (1991).
274. J. H. Chen and E. Ruckenstein, *J. Colloid Interface Sci.* **142**, 544 (1991).
275. B. Wesslen, M. Kober, C. Freij-Larsson, A. Ljungh and M. Paulsson, *Biomaterials* **15**, 278 (1994).
276. M. Kober and B. Wesslen, *J. Polym. Sci., Polym. Chem.* **30**, 1061 (1992).
277. J. Klein and P. Luckham, *Nature* **300**, 429 (1982).
278. J. Klein and P. Luckham, *Macromolecules* **17**, 1041 (1984).
279. P. M. Claesson and C. G. Golander, *J. Colloid Interface Sci.* **117**, 366 (1987).
280. J. N. Israelachvili and G. E. Adams, *J. Chem. Soc., Faraday Trans. I* **74**, 975 (1978).
281. J. N. Israelachvili, R. K. Tandon and L. R. White, *J. Colloid Interface Sci.* **78**, 430 (1980).
282. J. Klein and P. F. Luckham, *Colloids Surf.* **10**, 65 (1984).
283. E. Perez and J. E. Proust, *J. Colloid Interface Sci.* **118**, 182 (1987).



Jin Ho Lee, Jindrich Kopecek and Joseph Andrade

Department of Materials Science and Engineering, University of Utah, Salt Lake City, Utah 84112

**Abstract:** Polyethylene oxide (PEO)-containing nonionic polymer surfactants were studied as a possible means to produce PEO-rich surfaces by a simple solution treatment of common hydrophobic medical materials. Surface tension and adsorption properties of PEO/polypropylene oxide (PPO) and PEO/polybutylene oxide (PBO) block copolymer surfactants were investigated for this purpose, using the Wilhelmy plate technique and X-ray photoelectron spectroscopy (XPS). The protein-resistant character of the surfaces coated with surfactant were also evaluated by XPS.

## INTRODUCTION

PEO surfaces are becoming recognized as exhibiting low protein adsorption and low cell adhesion characteristics. The hydrophilicity and unique solubility properties of PEO produces surfaces that are in a liquid-like state with the polymer chains exhibiting considerable flexibility or mobility (Refs. 1,2). In our previous work (Ref. 3), surface tensions of aqueous PEO-PPO-PEO triblock and related surfactant solutions, and adsorption properties of those surfactants on dimethyl dichloro silane (DDSi)-coated glass surfaces, which are strongly hydrophobic, were investigated. In this paper, we present the surface properties of the PEO-PBO-PEO triblock surfactants at the air/water interface by measuring surface tension and compare them with those of PEO-PPO-PEO triblock surfactants (Ref. 3). The adsorption properties of the surfactants having different structure on hydrophobic polymer substrates (low density polyethylene, N.I.H. reference material) were investigated using XPS. Protein-resistant character of the polymer surfaces coated with surfactant by a simple solution treatment were also evaluated by XPS.

## RESULTS AND DISCUSSION

The surface tensions of aqueous surfactant solutions were measured by the Wilhelmy plate method (Ref. 3) using clean, hydrophilic glass slides. The surfactants used were soluble in water at room temperature (20°C) for the concentration range used (10<sup>-4</sup> mg/ml to 10.0 mg/ml). PEO-PBO-PEO triblock surfactants show good surface tension reduction in aqueous solution as the concentration increases (Fig. 1). As the

PROC. POLYMERIC MATLS SCI ENGRG, DIV. 4 ACS,  
57 (1987) 613

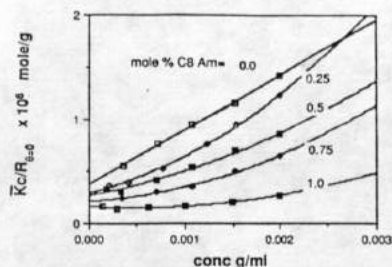


Fig. 3. The light scattering data extrapolated to zero scattering angle as a function of polymer concentration at different amounts of incorporated hydrophobe.

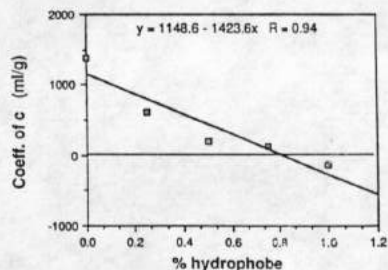


Fig. 4. The coefficient of c for the light scattering results as a function of the % hydrophobe.

612

molecular weight of PBO decreases and the content of EO decreases, the surface tension reduction increased more sharply. Reduction of surface tension is one of the most commonly measured properties of surfactants in aqueous solution. It depends directly on the replacement of molecules of water at the air/water interface by molecules of surfactant (Ref. 4). We expect the hydrophobic PBO or PPO segments predominate at the air/water interface while the more hydrophilic PEO segments tend to extend into the aqueous phase. The increase in surface tension reduction with concentration is indicative of the amount of the surfactant adsorbed at the air/water interface. The surface tensions of PEO-PBO-PEO triblock surfactants were compared with those of PEO-PPO-PEO surfactants in Fig. 2. As the concentration increases, the surface tensions of PEO-PBO-PEO surfactants decreased more sharply. This means

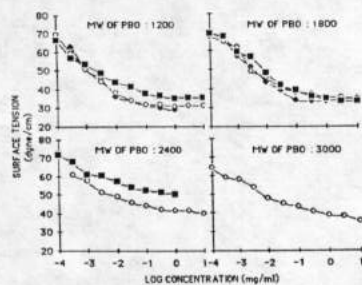


Fig. 1. Surface tension-log concentration plots of the PEO-PBO-PEO triblock surfactant solutions. (EO %: +, 40; o, 60; \*, 80)

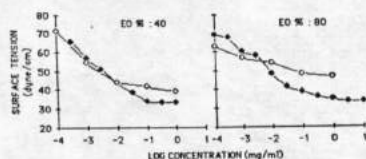


Fig. 2. Comparison of surface tensions of PEO-PBO-PEO triblock surfactants with PEO-PPO-PEO triblock surfactants. (+, PEO-PBO-PEO; o, PEO-PPO-PEO; MW of PBO, 1800; MW of PPO, 1750)

614

that the PEO molecules are more adsorbed at the air/water interface and produce a more hydrophobic surface than the PPO surfactants. Surfactants having different structures, PEO-PPO-PEO triblock, PEO-PBO-PEO triblock, alternate PEO/PPO block (condensation product of PEO-PPO-PEO triblock) and a star-like polymer containing 4 PPO and 4 PEO blocks are compared in Fig. 3. Different values of surface tension are observed, even though the polymers have similar PBO or PPO chain lengths (n=25 for PBO, and 29 or 30 for PPO) and the same PEO content (40 wt%) (A-D in Fig. 3). The same surfactants were adsorbed onto LDPE in aqueous solution, and relative amount of adsorption was measured by XPS. The oxygen to carbon atomic ratio was used as an indicator of the amount of the surfactant adsorbed as LDPE does not show any oxygen peaks. From E-H in Fig. 3, we can see that the adsorption is highly structure dependent. We assume that the surfactant molecules are physically adsorbed on the hydrophobic LDPE surface, probably via hydrophobic interactions of the PBO or PPO blocks with the surface. The PEO chains of the surfactant will be extended into aqueous solution, where they are expected to be highly mobile. The star-like block copolymer and especially the alternate block copolymer appear much more effective for stable adsorption onto the LDPE than triblocks, probably due to a greater amount of hydrophobic binding sites of those blocks, which can be adsorbed more strongly. PEO-PBO-PEO triblock surfactant shows unstable adsorption. This phenomena can possibly be explained by aggregation of the molecule in aqueous solution, i.e. PBO blocks show more a hydrophobic character than PPO blocks, as evidenced by their lower surface tension values (compare A and B in Fig. 3), which means a higher possibility to self-aggregate in aqueous solution. Such an intermolecular aggregate or micelle is expected to have a large portion of PEO segment at the aqueous interface. If this type of aggregate is adsorbed on the hydrophobic surface, it will be readily desorbed. From the literature (Ref. 5), it is suggested that PPO chains longer than n=30 lead to a ball structure in aqueous solution. PBO chains, on the other hand, probably form the ball-like structure at n=25.

The protein-resistant character of LDPE surfaces pre-adsorbed with star-like block and alternate block surfactants was also evaluated by XPS. We compared the nitrogen to carbon atomic ratio of the surfactant-treated surface with that of untreated LDPE surface (I and J in Fig. 3). The amount of adsorbed protein (human serum albumin, HSA) on the surfactant-treated surfaces significantly decreased, compared with the untreated surface. A possible explanation for this relates to PEO's relatively unique solution properties and its molecular conformation in aqueous solution (Refs. 6,7). In addition, a volume restriction effect can be considered. It is thought that a repulsive force exists due to a loss of configurational entropy of the surface bound PEO when a protein approaches the PEO surface (Ref. 8). There is also an osmotic

615



repulsion component due to polymer chain interpenetration (Ref. 8). It appears that PEO surfaces in water are particularly effective in exhibiting rapid motions (Ref. 9) and a large excluded volume, thereby actively minimizing the adsorption of proteins. As seen in I and J of Fig. 3, the star-like block surfactant at high concentration shows a protein repulsion effect similar to that of the alternate block surfactant, even though its adsorbed amount on LDPE was very small (compare G and H in Fig. 3). This result suggests that the mobility of PEO chains is an important factor for protein repulsion because the star-like block has tail-type PEO chains which are more mobile than the loop chain present in the alternate block copolymer.

Work on other novel polymeric surfactants is in progress.

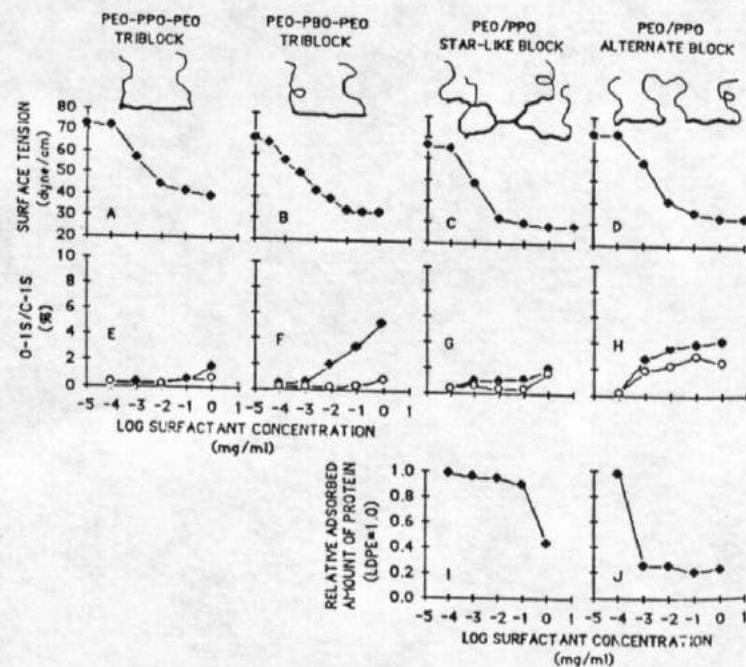


Fig. 3. Surfactants with different structure. (PPO chain length, 29-30; PBO chain length, 25; PEO wt %, 40; —, PPO or PBO; —, PEO) A-D) Surface tensions of the surfactant in aqueous solution. E-H) Adsorbed amount of the surfactants on LDPE (—•—, 30min adsorption; —○—, 30min desorption after 30min adsorption). I, J) Adsorption of HSA (30min in 1mg/ml in PBS buffer solution (PH=7.4)) on the surfactant-treated surfaces.

## ACKNOWLEDGEMENT

We thank BASF-Wyandotte and ICI for gifts of the surfactant samples and for technical information.

## REFERENCES

- (1) E. W. Merrill and E. W. Salzman, *ASAIO J.*, **6**, 60 (1983)
- (2) S. Nagaoka, Y. Mori, H. Takiuchi, K. Tanzawa and S. Nishiumi, *Polymer Preprints*, **24**, 67 (1983)
- (3) J. H. Lee and J. D. Andrade, "Surface Properties of Aqueous PEO/PPO Block Copolymer Surfactants," *Polymer Surface Dynamics*, J. D. Andrade, ed., Plenum Press, New York, in press (1987)
- (4) M. J. Rosen, *Surfactants and Interfacial Phenomena*, Chap. 1 and 5, Wiley-Interscience, New York (1978)
- (5) H. Thurow and K. Geisen, *Diabetologia*, **27**, 212 (1984)
- (6) F. E. Bailey Jr. and J. Y. Koleske, *Poly (Ethylene Oxide)*, Academic Press, London (1976)
- (7) M. J. Schick, ed., *Nonionic Surfactants*, Marcel Dekker, New York (1966)
- (8) Th. F. Tadros, ed., *The Effect of Polymers on Dispersion Properties*, P. 1-38, Academic Press, London (1982)
- (9) S. Nagaoka, Y. Mori, H. Takiuchi, K. Yokota, H. Tanzawa and S. Nishiumi, "Interaction between Blood Components and Hydrogels with Poly (Oxyethylene) Chains," *Polymers as Biomaterials*, S. W. Shalaby, A. S. Hoffman, B. D. Ratner and T. A. Horbett, ed., P. 361-374, Plenum Press, New York (1984)